The role of IQGAP3 in triple negative breast cancer

Pipili, Aikaterini

Awarding institution:
King's College London

The role of IQGAP3 in triple negative breast cancer

Aikaterini Pipili

2017

A thesis submitted to fulfil the requirements for the degree of Doctor of Philosophy

Division of Cancer Studies

King's College London

Declaration of Authorship

Aikaterini Pipili

Acknowledgements

This thesis is dedicated to my dear late uncle (uncoulinos mou) who passed away during the first year of my PhD after two years of fighting lung cancer. Your memory kept me from giving up more times that I can count and keeps making me want to do better. There hasn't been a day that I haven't wished I could speak to you, see you smile and hear your soothing words. I can't think of a greater victory than knowing you would be proud of me right now. I miss you, always.

I would like to express my deepest gratitude and appreciation to my supervisor Dr Claire Wells. You are an inspiration for all the women in science aspiring to combine a successful academic career with a family life. You have always made me see my work from a fresh angle; as I have often said, everything makes more sense after 5 minutes of talking to you. Thank you for all your support, particularly during my writing up time.

Special thanks go to past members of the Wells lab Dr Nicole Nicholas, Dr Fahim Ismail and Dr Nouf Babteen for all their help as well as their valued friendship. You made the first years of my PhD very enjoyable and you were all missed when you left the lab. I can't even imagine reaching this stage without Dr(!) Mario De Piano, Maddie Gale, Dr Kiruthikah Thillai and Hoyin Lam. I can easily write another thesis on how I much I valued the endless (bad) jokes, the inappropriate questions, the medical reassurance, the meetings in the City, the cakes, the good lasagna, the right way of eating sushi, the friendship, the support. I wouldn't change anything - not even the extra weight. I am grateful to Dr Stephanie Koo and Mirella Georgouli for all the help, chats, and encouragement and for making the office an enjoyable place. I would also like to thank Dr Michaela Lesjak, Dr Jez Carlton, Dr Yolanda Olmos and Dr Steve Terry for their help, kindness and technical advice. I would like to acknowledge the help I received from my second supervisor Professor Andrew Tutt and members of his team Dr Pierfrancesco Marra, Dr Rebecca Marlow and Dr Fara Braso-Maristany.

I would have never made it to this stage without my favourite person, Alex. Thank you for putting up with me, for being the only light in times of darkness and for pointing out my accomplishments when I could only see my shortcomings. I am truly lucky to have you in my life. I am also grateful to my beloved cousin Alexis who took care of me (and my healthy appetite for good wine) during my final year. Life is always better when you are on the floor above or around the corner. Special thanks also go to my best friend Ioanna, 'the salad' and the Heath for the cathartic Tuesdays.

I would finally like to express my endless gratitude to my family; my mum and dad, aunty and granny. Thank you for your love, support and for believing in me when I didn't believe in myself. Mamsis - I am sorry they don't give out PhDs for amazing mums. Thank you for being just that even when I am far from being an amazing daughter. I couldn't have done it without you.

Finally, to my health anxiety – I could have easily done it without you making everything more difficult. I hope the completion of this thesis marks the end of you too. Good riddance!

Abstract

Triple negative breast cancer refers to a spectrum of breast tumours which are characterised by the lack of overexpressing hormone or HER2 receptors. These tumours present as high grade and tend to have reduced progression free survival rates because of their aggressive and metastatic behaviour. The lack of targeted therapies for triple negative breast cancer also contributes to the observed poor outcomes.

During a genetic profiling screen of aggressive breast tumours, mRNA levels of IQGAP3 were specifically found to be upregulated in triple negative tumours compared to other types of the disease and normal tissue samples. IQGAP3 is the most recently discovered member of the IQGAP family of scaffold proteins. Even though IQGAP1 is a well described effector for the Rho GTPases and has also been heavily associated with tumourigenesis and cancer cell motility, far less is known about IQGAP3. The aim of this project was to investigate the role of IQGAP3 in triple negative breast cancer cell behaviour. At first, IQGAP3 was found to be expressed across a panel of triple negative cell lines. Modulating expression levels of IQGAP3 conferred morphological changes, disrupted cell migration and inhibited the ability of cells to form specialised invasive adhesion structures, termed invadopodia. Reduced expression of IQGAP3 disrupted RhoA activity and actomyosin contractility. IQGAP3 was also found to interact with PAK6 and Filamin-A; proteins already associated with the regulation of cell morphology. Indeed, PAK6 overexpression rescued the IQGAP3 depletion phenotype. IQGAP domains have previously been suggested to have potential therapeutic value thus IQGAP3 could be a promising candidate to target in order to inhibit metastasis in triple negative breast cancer.

Contents

List of Figures

List of Tables

Abbreviations

2D	2-Dimensional
3D	3-Dimensional
ABD	Actin binding domain
AID	Auto-inhibitory domain
ALK	Anaplastic lymphoma kinase
APC	Adenomatous polyposis coli
APS	Ammonium persulfate
AR	Androgen receptor
Arp2/3	Actin-related proteins 2/3
ATP	Adenosine triphosphate
BM	Basement membrane
BSA	Bovine serum albumin
Cdc42	Cell division control protein -42
CRIB	Cdc42/Rac interactive binding region
c-Src	Cellular Src
DAPI	4,6-diamidino-2-phenylindole
DMEM	Dulbecco's Modified Eagle Medium
DMSO	Dimethyl sulfoxide
DNA	Deoxyribonucleic acid
DTT	Dithiolthreiol
E. coli	*Escherichia coli*
ECL	Enhance chemiluminescence
ECM	Extracellular matrix
EDTA	Ethylenediaminetetraacetic acid
EGF	Epidermal growth factor
EMT	Epithelial to mesenchymal transition
ER	Oestrogen receptor

ERK1	Extracellular receptor kinase 1
ERK2	Extracellular receptor kinase 2
F-actin	Filamentous actin
FAK	Focal adhesion kinase
FBS	Foetal bovine serum
FGFR	Fibroblast
FRET	Fluorescence resonance energy transfer
GAPDH	Glyceraldehyde 3-phosphate dehydrogenase
GAP	GTPase activating protein
GBD	GTPase binding domain
GEF	Guanine nucleotide exchange factor
GDI	GDP dissociation inhibitor
GTP	Guanosine triphosphate
HCC	Hepatocellular carcinoma
HEPES	4-(2-hydroxyethyl)-1-piperazineethanesulfonic acid
HER2	Human epidermal growth factor receptor 2
HCl	Hydrochloric acid
HGF	Hepatocyte growth factor
IGFR	Insulin-like growth factor 1 receptor
IP	Immunoprecipitation
IQGAP	IQ motif containing GAP
kDa	Kilodaltons
LB agar	Luria-Bertani agar
LB broth	Luria-Bertani broth
LIMK	LIM kinase
LPA	Lysophosphatidic acid
MAPK	Mitogen-activated protein kinase
mDia	Diaphanous related formin
$MgCl_2$	Magnesium chloride
MLC	Myosin light chain
MLCK	Myosin light chain kinase

MMP	Matrix metalloproteinase
MP	Myosin light chain phosphatase
mRNA	Messenger RNA
MTT	3-(4,5-Dimethylthiazol-2-yl)-2,5-Diphenyltetrazolium Bromide
Na_3VO4_4	Sodium orthovandate
NaCl	Sodium chloride
NAF	Sodium fluoride
Nck1	Non-catalytic region of tyrosine kinase adaptor protein 2
NF-κB	Nuclear transcription factor B
PAKs	p21 activated kinases
PBS	Phosphate buffered saline
PFA	Paraformaldehyde
PI3K	Phosphatidylinositol-3 kinase
PIP5-K	Phosphatidylinositol-4-phosphate 5- kinase
PIP2	Phosphatidylinositol 4,5-bisphosphate
PIX	PAK interacting exchange factor
PMSF	Phenylmethylsulfonylfluoride
PR	Progesterone receptor
PP1B	Protein phosphatase 1B
Rac1	Ras-related C3 botulinum toxin substrate 1
RhoA	Ras homolog gene family, member A
RPMI-1640	Roswell Park Memorial Institute-1640
RNA	Ribonucleic acid
ROCK	Rho-associated, coiled-coil containing protein kinase 1
RTK	Receptor tyrosine kinase
SCAR/WAVE	Suppressor of cAMP receptor/WASP verprolin-homologous
SDS-PAGE	Sodium dodecyl sulphate polyacrylamide gel electrophoresis
SEM	Standard error of the mean
shRNA	Short hairpin ribonucleic acid
siRNA	Short interfering ribonucleic acid
TEMED	Tetramethylethylenediamine

TGFβ1	Transforming growth factor beta 1
Tks5	Tyrosine kinase substrate 5
TNBC	Triple negative breast cancer
TRITC	Tetramethylrhodamine isothiocyanate
VEGF	Vascular endothelial growth factor
WASP	Wiskott-aldrich syndrome protein
WIP	WASP interacting protein

Chapter 1

Introduction

Chapter 1 Introduction

1.1 Breast cancer

Breast cancer is one of the most commonly diagnosed types of cancer which despite medical advances in the recent years, represents one of the leading causes of cancer related deaths among women (Jemal et al., 2010). The 5 year relative survival rate is almost 100% for early stage tumour but dramatically drops to 21% for stage IV patients highlighting the fact that early stage tumours can be adequately treated while the management of late stage diagnoses remains challenging (Hayat et al., 2007). A combination of genetic and environmental factors influence the development of breast cancer including mutations on the BRCA1 and BRCA genes, increasing age, obesity, alcohol and oral contraceptives (Rojas and Stuckey, 2016). Breast cancer is widely recognised as a very heterogeneous disease with distinct subtypes characterised by specific molecular markers and clinical outcomes (Hirata et al., 2014). Tumours marked by increased expression of oestrogen (ER) and progesterone (PR) receptors have a more differentiated appearance and are thought to be hormonally regulated as they respond better to drugs targeting hormone receptors such as Tamoxifen (Althuis et al., 2004). Amplification of the human epidermal growth factor 2 (HER2) receptor is found in up to 30% of breast tumours and it is associated with aggressive disease and poor clinical outcomes (Hirata et al., 2014). Nonetheless, the development of targeted therapies such as the monoclonal antibody Trastuzumab and tyrosine kinase inhibitor Lapatinid have significantly improved outcomes (Hirata et al., 2014). Tumours lacking hormone and HER2 receptors are grouped under the disease spectrum known as triple negative breast cancer (TNBC) (Foulkes et al., 2010).

1.1.1 Triple negative breast cancer

Triple negative tumours exhibit mutations on the TP53 gene as well as on BRCA1 which normally functions as a DNA repair effector (Anders and Carey, 2009). TNBC tumours tend to have a less differentiated appearance largely presenting as grade 3 upon diagnosis. TNBC is also most commonly diagnosed among non-Caucasian ethnic groups, such as women of African origin, while retaining a highly proliferative and metastatic phenotype (Anders and Carey, 2009). In fact, TNBC patients show reduced progression-free and overall survival rates 3 years after initial diagnosis with the brain and visceral organs becoming the primary targets of metastatic disease (Anders and Carey, 2009).

Gene expression analysis of triple negative tumours showed that 6 TNBC subtypes can be identified (Lehmann et al., 2011). The major subtype of TNBC which also exhibits the highest mitotic potential is known as basal-like and is characterised by the expression of distinct cytokeratins found on the basal myoepithelium of the normal breast and in most cases the overexpression of the EGF receptor (Nielsen et al., 2004). Interestingly, Lehmann et al., separated the basal-like tumours that make the 70% of all triple negative tumours into basal-like 1 and basal-like 2 (Lehmann et al., 2011). Basal-like 1 type tumours highly express genes related to DNA replication and cell cycle while basal-like 2 tumours particularly express growth factor signalling pathways such as the EGF pathway (Lehmann et al., 2011). Another significant type is the mesenchymal-like which is also divided into mesenchymal and mesenchymal stem-like subtypes. The former exhibits elevated expression of genes related to cell motility such as Rho GTPases and pathways such as the TGFβ and ALK pathways (Lehmann et al., 2011). Meanwhile, the mesenchymal stem cell-like type also incorporates growth factor signalling, low expression of claudins and a phenotype consistent to that of stem cells with low proliferation and low CD24 expression (Lehmann et al., 2011).

However, as reviewed by Reis-Filho and Tutt, micro-array based expression profiling revealed that 15 to 54% of basal-like tumours express ER, PR or HER2 receptors (Reis-Filho and Tutt, 2008) . This implies that basal-like cancers are not necessarily synonymous to TNBC despite their observed similarity and thus attention should be given in the context of therapeutically treating these two entities (Reis-Filho and Tutt, 2008). Given that triple negative tumours are characterised by compromised DNA repair due to the BRCA1 mutations, platinum-based chemotherapy is usually the first choice of treatment (Hudis and Gianni, 2011). At the same time, highly proliferative tumours such as basal-like could benefit from anti-mitotic agents such as taxanes (Lehmann et al., 2011). Stagg and Allard reviewed the importance of lymphocytic infiltrate in some triple negative tumours and its association with clinical outcomes and argued that emerging immunotherapeutic approaches could benefit some patients (Stagg and Allard, 2013). However, they also stress the fact that given the heterogeneity of the disease only a fraction of patients will benefit from a single given approach (Stagg and Allard, 2013). Consequently, current TNBC patients cannot benefit from targeted therapy, which further contributes to the observed poor outcomes (Hudis and Gianni, 2011).

1.1.2 Tumour metastasis

The diagnosis of metastatic disease is the leading cause of cancer mortality (Jemal et al., 2010) . Metastasis means that cells from the primary tumour have managed to invade the surrounding tissue of the tumour by degrading the extracellular matrix, intravasate into the vascular system, avoid immune surveillance, extravasate and finally colonise distant organs as reviewed by Valastyan and Weinberg (Valastyan and Weinberg, 2011), **(figure 1.1)**. This involves the coordination of dramatic changes in cellular behaviour including the acquisition of a motile and invasive phenotype, cell survival in non-permissive environments such as the vasculature and proliferation at distant sites. Hence, there are several stages of metastasis that can be potentially therapeutically targeted and thus understanding the molecular mechanisms behind each stage is crucial (Palmer et al., 2011).

Epithelial to mesenchymal transition (EMT) has been associated with the onset of metastasis. Loss of E-cadherin and apicobasal cell polarity are early events regulated by EMT inducers such as SNAIL, TWIST and TGFβ signalling (Thiery et al., 2009). Extracellular signals such as epidermal growth factor (EGF), hepatocyte growth factor (HGF) Insulin-Like growth factor 1 (IGF1) have also been shown to induce a mesenchymal phenotype characterised by a front to rear polarity which is established by the activity of the Rho GTPases (Lamouille et al., 2014). In order to escape from the primary tumour, cells must penetrate the basement membrane which is achieved by secreting matrix metalloproteases (Kessenbrock et al., 2010), **(figure 1.1)**. Cells can adopt different modes of invasion; one of which is the formation of actin rich protrusions capable of secreting MMPs, known as invadopodia (Friedl and Alexander, 2011; Lohmer et al., 2014). Indeed, inhibition of MMPs has been shown to prevent invasion in animal models (Kessenbrock et al., 2010) while increased expression of MMP9 was found in aggressive HER2 positive and triple negative breast tumours and correlated with higher rates of metastasis (Yousef et al., 2014). However, MMPs also act as signalling mediators in physiological processes which can explain why MMP inhibitors failed to improve clinical outcomes in human clinical trials (Kessenbrock et al., 2010). Once outside the BM, cancer cells interact with the tumour supporting stroma which contains a variety of cells including macrophages, adipocytes and endothelial cells that provide further environmental cues promoting an invasive behaviour (Valastyan and Weinberg, 2011), **(figure 1.1)**.

Metastatic tropism refers to the cross-talk between tumour cells and distant organ sites that create a permissive environment for tumour cells to colonise those organs (Lorusso and Rüegg, 2012).

For example, hormonally regulated breast tumour cells preferentially metastasize to the bone where they hijack molecular signals normally regulating bone remodelling and ensure their survival and proliferation (Lorusso and Rüegg, 2012). However, triple negative tumours exhibit a different organ metastatic tropism than the hormonally influenced tumours as they are more likely to spread rapidly to visceral organs including the lungs and liver (Dent et al., 2009).

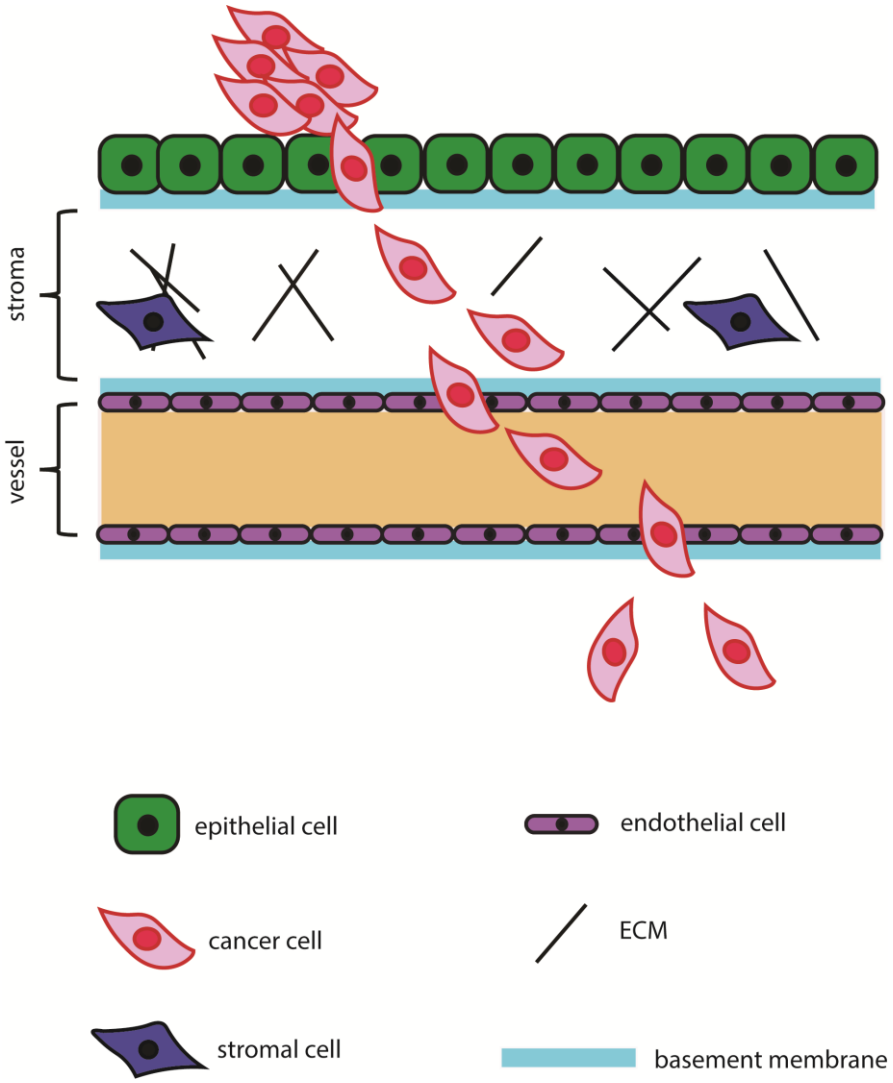

Figure 1.1 Schematic of the metastatic cascade. Cells from the primary tumour acquire the ability to breach the basement membrane and escape into the surrounding stromal tissue. From there, some of these cells intravasate into the lymphatics or vasculature through which they can travel, extravasate and colonise distant sites thereby forming metastases.

1.2 The significance of cancer cell motility

One of the most important hallmarks in cancer progression and metastasis is tumour cells acquiring the ability to move and travel through the vasculature or the lymphatics in order to colonise distant organs (Friedl and Wolf, 2003). The first step to cell movement is the ability of the cell to alter its morphology and engage with the extracellular environment resulting in a polarised shape (Lauffenburger and Horwitz, 1996).

1.2.1 Actin organisation

Changes in cell morphology are mediated by the dynamic actin cytoskeleton. Actin filaments are polymers of monomeric actin forming a double stranded helix with characteristic barbed and pointed ends (Blanchoin et al., 2014; Pollard, 1986). Polymerisation is dependent on the concentration of the available actin monomers and occurs more favourably at the barded end of the filament followed by hydrolysis of ATP coupled to the actin monomer subunits (Pollard, 1986). Regulatory proteins controlling the assembly and disassembly of actin filaments create the architectural structures of the actin cytoskeleton that provide shape and movement features. For example, cross-linking of actin filaments dictate cell shape and provide structural rigidity while branching actin networks enable the formation of lamellipodia and forward movement (Blanchoin et al., 2014). Parallel actin filaments are observed in filopodia, which are finger-like structures known to sense the extracellular environment (Mattila and Lappalainen, 2008). Furthermore, stress fibres are bundles of cross-linked actin filaments with crucial functionality in migrating cells (Kassianidou and Kumar, 2015). Stress fibres link the cell with the extracellular matrix via focal adhesions and also provide the structural basis for the maturation of focal complexes into focal adhesions ultimately acting as mechanosensing structures and enabling directional cell migration (Burridge and Wittchen, 2013; Kassianidou and Kumar, 2015). Furthermore, anti-parallel actin bundles provide the base for the contractile unit together with non-muscle myosin II (NMMII) (Kassianidou and Kumar, 2015). NMMII is made of two heavy chains, 2 regulatory light chains and 2 essential light chains (Vicente-Manzanares et al., 2009). The heavy chains of NMMII hold ATPase activity and can also bind filamentous actin while the essential light chains provide structural stability to the heavy chains (Vicente-Manzanares et al., 2009). Phosphorylation of the regulatory light chains on Ser19 creates the necessary conformational change that allows the

formation of myosin filaments and enhances hydrolysis of ATP (Vicente-Manzanares et al., 2009). Ultimately, myosin thick filaments slide towards the barbed end of actin filaments with opposite polarity thereby inducing tension and contractility (Kassianidou and Kumar, 2015; Murrell et al., 2015). Importantly, myosin IIB activity is enriched in ventral stress fibres at the cell rear contributing to front to back polarity and tail retraction in migrating cells (Kassianidou and Kumar, 2015; Vicente-Manzanares et al., 2008).

1.2.2 Models of cell migration

The extracellular environment is a crucial influencing factor leading to differential results depending on whether cell migration is considered in 2D and 3D *in vitro* studies, or intravital *in vivo* studies thus making the study of cell migration challenging and complex (Clark and Vignjevic, 2015). Nonetheless, studies in 2D cell migration have provided much of our understanding regarding cell motility while the main mechanisms have also been confirmed in 3D; for example forward cell extension is defined by the same molecular and structural characteristics both in 2D and 3D (Petrie and Yamada, 2012). Cells migrate either individually or collectively **(figure 1.2)**; individual cell migration has been studied extensively but interestingly the significance of collective cell migration has been highlighted at the invasive front of breast tumours in organoid systems where invading leader cells were reported to express E-cadherin and other basal epithelial markers (Cheung et al., 2013). Additionally, intravital imaging of MDA-MB-231 and low passage primary breast cancer cells revealed that these cells migrated as multi-cellular streams and that this particular mode of invasion was associated with increased intravasation and circulating tumour cells in the blood vessels of a mouse model (Patsialou et al., 2013). Multi-cellular streaming is an intermediate mode of migration which involves cells migrating in a single line while forming short-lived cell junctions **(figure 1.2)**, (Friedl et al., 2012).

Cell migration is also classified according to the shape of migrating cells as well as their engagement with the extracellular matrix (Friedl and Wolf, 2010). Mesenchymal migration is adopted by cells extending a pseudopod that gradually lead to lamellipodia dynamics and an elongated morphology **(figure 1.2)**. The protrusion then engages with the extracellular matrix forming strong focal adhesions that create high traction forces pulling on the surrounding matrix (Friedl, 2004). Large focal adhesions have a slower turnover rate and are thus associated with slower cell speed (Friedl, 2004). Localised pericellular proteolysis mediated by MT1-MMP behind the leading protrusion realigns the extracellular matrix and reduces cell stress during forward

moving as it creates paths of least resistance (Friedl and Wolf, 2009). Focalised matrix degradation together with cell body contraction mediates the forward pulling of the cell body and finally cell tail retraction ultimately achieving cell displacement (Friedl and Wolf, 2010, 2009). In fact, when colon cancer L-10 cells migrate collectively, the front leader cells adopt a mesenchymal mode of migration and locally degrade the matrix which in turn provides migration tracks for the following cells which retain cell-cell junctions (Friedl, 2004).

Amoeboid migration is adopted by rounded bleb forming cells lacking stress fibres and mature focal adhesions **(figure 1.2)**. Cell contractility resulting from the activation of myosin light chain induces an increase in the intracellular hydrostatic pressure which in turn can locally disrupt the actin cytoskeleton and allow cytosolic content to form blebs against the plasma membrane (Lämmermann and Sixt, 2009). Amoeboid cell movement is thus not mediated by actin polymerisation and the generation of traction forces; rather by a propulsive mechanism driven by actomyosin contractility (Fackler and Grosse, 2008). Nonetheless, amoeboid melanoma cells have been shown to secrete high levels of MMPs such as MMP9 and MMP13 suggesting that matrix degradation is important in the amoeboid mode of migration as well (Orgaz et al., 2014). Furthermore, the lack of engagement with the surrounding matrix makes the amoeboid movement type much faster than the mesenchymal one (Lämmermann and Sixt, 2009). The morphology of migrating cells depends on a number of factors concerning the extracellular matrix like its dimension and rigidity as well as the expression of adhesive and proteolytic determinants (Friedl and Wolf, 2010). Increased matrix stiffness signals via integrins and promotes cell elongation and the formation of focal adhesions (Friedl and Wolf, 2010). Contrary to rigid environments, soft matrices like the lymphatics and vasculature allow cells to squeeze through and thus promote the amoeboid mode of migration (Krakhmal et al., 2015). Cell confinement mediated by the pores in the surrounding matrix also support an elongated morphology while larger gaps promote a rounded morphology (Friedl and Wolf, 2010). Ultimately, the ability of cells to modulate their morphology according to the extracellular micro-environment is referred to as cell plasticity. This is a crucial feature maintained by cancer cells as it allows them to survive and migrate through structurally heterogeneous tissues (Friedl and Alexander, 2011). Breast cancer cells have been shown to exhibit the ability to modulate their morphology based on the extracellular environment. For example, triple negative MDA-MB-231 and BT-549 cells grown in laminin rich extracellular matrix cluster together and form elongated projections via which they keep in contact (Kenny et al., 2007). However, MDA-MB-231 cells invaded a 3D matrigel matrix while displaying a rounded

morphology and high contractility at the cell rear as indicated by the microbeads displacement and the accumulation of pMLC (Poincloux et al., 2011). Breast cancer cell invasion has been associated with amoeboid movement; oestrogen receptors of ER positive tumour cells are lost at the invasive front as well as lymph metastases. Additionally, loss of ER induced loss of vinculin which in turn increased actomyosin contractility and amoeboid migration in MCF7 cells (Gao et al., 2017). Furthermore, MTLn3E cells overlaid with a collagen gel were able to invade by distorting the matrix. The observed matrix deformation was reported to be independent of protease activity and was mediated by generating contractile force induced by ROCK and myosin light chain activation (Wyckoff et al., 2006). Interestingly, different factors modulating RhoA activity have been reported to dictate cell plasticity in breast cancer cells; Net1 is a RhoA GEF necessary for the induction of amoeboid invasion of MDA-MB-231 cells in matrigel (Carr et al., 2013) while E3 ubiquitin ligase Smurf1 degrades RhoA thereby allowing the formation of lamellipodia and promoting mesenchymal migration (Sahai et al., 2007).

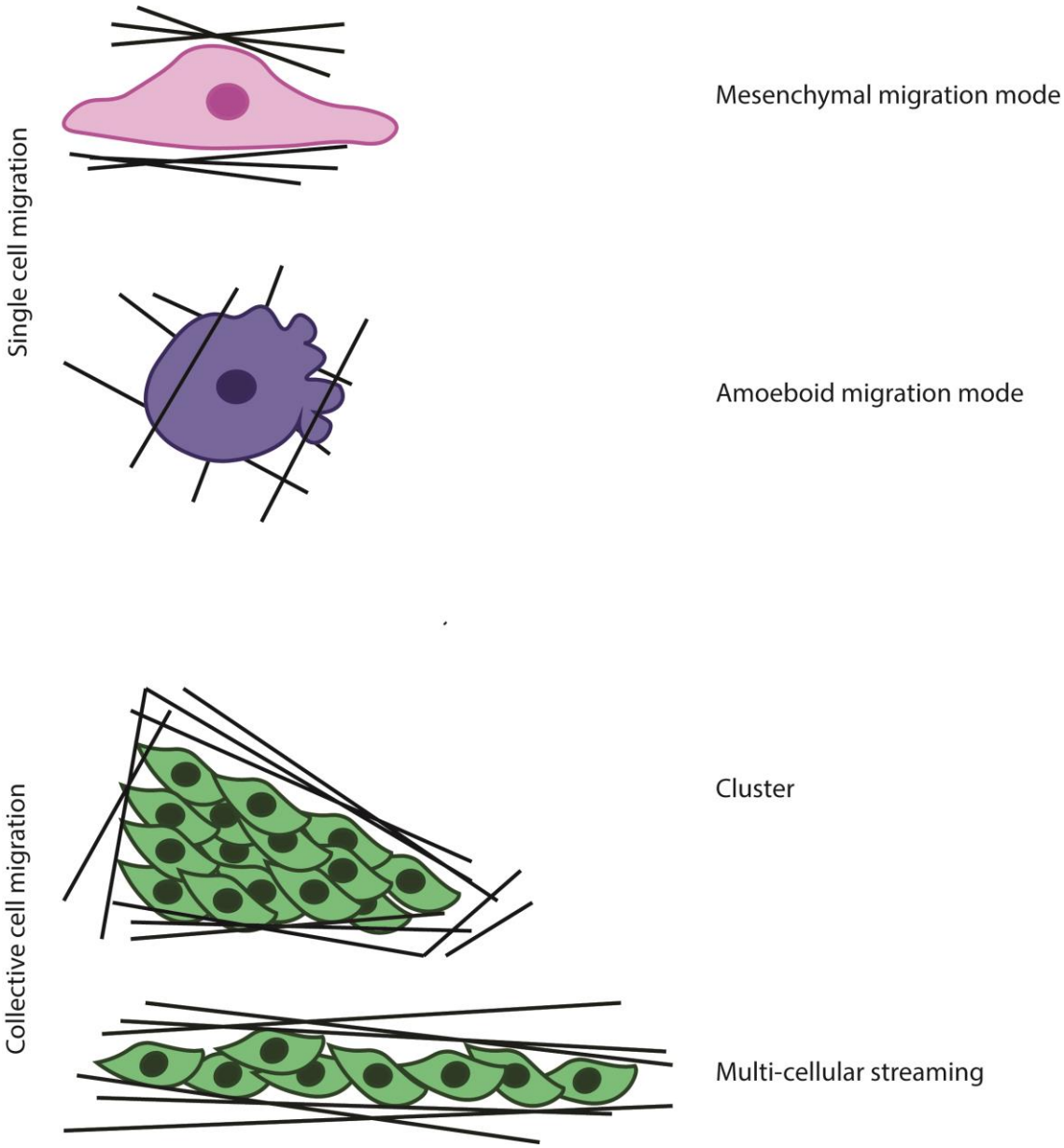

Figure 1.2 Modes of cell migration. Cells can either migrate individually or collectively. In individual cell migration, cells can either adopt a mesenchymal or an amoeboid mode. Mesenchymal migration is characterised by an elongated morphology and matrix degradation while the amoeboid type is mainly driven by high contractility resulting in a rounded blebby cell morphology. In collective cell migration cells can either migrate in clusters or in streams where cells form a line while maintaining transient contacts.

.

1.2.3 Invadopodia: A special protrusion in mediating metastasis

Extracellular matrix degradation and invasion is a crucial part of the metastatic cascade (Valastyan and Weinberg, 2011). Twist is a well characterised transcriptional factor promoting metastasis. Twist has been shown to upregulate expression of platelet derived growth factor receptor α (PDGFRα) which in turn stimulates Src activity ultimately resulting in the formation of actin rich membrane protrusions which can target the secretion of MMPs and degrade the extracellular matrix in human mammary epithelial HMLE cells(Eckert et al., 2011), **(figure 1.3)**. These structures are known as invadopodia and have been implicated in the local invasion, intravasation and metastasis of breast cancer cells to the lung (Eckert et al., 2011; Gligorijevic et al., 2012). In fact, recent advances in intravital microscopy have also allowed the visualisation of extravasating MDA-MB-231LN cells extending invadopodia into the extravascular stroma of the chorioallantoic membrane (CAM) of the chicken embryo (Leong et al., 2014).

Invadopodia are complex structures incorporating adhesion proteins, actin binding proteins, metalloproteases with Rho GTPases and their effectors contributing to their dynamic formation and activity (Murphy and Courtneidge, 2011).

Extracellular signals stimulate the formation of invadopodia via the activation of plasma membrane receptors initiating signalling cascades (Hoshino et al., 2013). In breast cancer cells activation of EGFR, Met and TGFβ receptors has been shown to induce formation of invadopodia (Mandal et al., 2008; Rajadurai et al., 2012; Yamaguchi et al., 2005). Similar results have been reported for head and neck squamous carcinoma cells when VEGF becomes activated (Lucas et al., 2010). Activation of these signalling cascades meet at stimulating a set of kinases, particularly Src but also ERK and PAKs that induce the formation of invadopodia (Foxall et al., 2016). Src phosphorylates various substrates including cortactin and Tks5 which constitute hallmark elements of invadopodia formation (Murphy and Courtneidge, 2011), **(figure 1.3)**. Tks5 is an adaptor protein shown to be crucial for invadopodia formation by specifically localising early and marking invadopodia sites as well as acting as a scaffold for other invadopodia elements such as cortactin (Crimaldi et al., 2009; Murphy and Courtneidge, 2011; Seals et al., 2005). PAK1 mediated phosphorylation of cortactin Ser113 has been shown to be important for invadopodia formation and activity (Ayala et al., 2008). Src phosphorylation of cortactin as well as active Cdc42 stimulate the Arp2/3 complex via N-WASP and WIP ultimately initiating actin polymerisation (Murphy and Courtneidge, 2011; Tehrani et al., 2007). Apart from the activation of the Arp2/3 complex, ERK induced cortactin phosphorylation on tyrosine residues (tyr421) releases cofilin

and enables its actin filament severing activity thereby also contributing to actin polymerisation and the elongation of the invadopodium protrusion (Oser et al., 2009), **(figure 1.3)**. Ultimately, the invadopodia core consists of branched actin filaments at the base of the protrusion while unbranched actin bundles mediated by the actions of mDia and fascin, are responsible for invadopodia elongation and are observed closer to the tip of the protrusion (Schoumacher et al., 2010). Furthermore, inactivation of cofilin activity by cortactin which is once again able to sequester cofilin upon dephosphorylation is required for the stabilisation of invadopodia structures (Oser et al., 2009). Additionally, spatial regulation of RhoC activity by p190RhoGEF and p190RhoGAP also regulates cofilin activity via ROCK and LIMK **(see section 1.3.1)**; RhoC remains active around the protrusion, ultimately inactivating cofilin and therefore restricting the direction of the elongating protrusion (Bravo-Cordero et al., 2011). Cross-linking proteins such as Filamin-A **(see section 1.3.5)** and fascin have also been reported to localise at invadopodia promoting stability (Li et al., 2010; Takkunen et al., 2010).

Invadopodia maturation ultimately involves the targeting and secretion of metalloproteases (MMPs). Cortactin once again appears crucial for the secretion of MMP2 and MMP9 as well as the presentation of MT1-MMP on the tip of the invadopodia protrusion (Clark et al., 2007) , **(figure 1.3)**. Interestingly, the association of cortactin to MT1-MMP endosomes is facilitated by MT1-MMP tyrosine phosphorylation by LIMK (Lagoutte et al., 2016). Meanwhile, atypical PKC phosphorylates cortactin on MT1-MMP late endosomes facilitating trafficking in triple negative breast cancer cells (Rossé et al., 2014). Interestingly, under the influence of Cdc42 and RhoA, IQGAP1 **(see section 1.3.2.1)** interacts with components of the exocyst complex to regulate the accumulation of MT1-MMP at invadopodia ultimately potentiating matrix degradation (Sakurai-Yageta et al., 2008).

Moreover, little is known regarding the dissolution of invadopodia but recently Rac1 induced PAK1 was reported to phosphorylate cortactin which lead to cortactin becoming detached from the actin rich structure ultimately marking the turnover of invadopodia in breast cancer cells (Moshfegh et al., 2015). Additionally, phosphorylation of the actin cross-linking protein AFAP-110 on Ser 277 has also been reported to be important for the turnover of the protrusion (Foxall et al., 2016). Finally, even though a wide range of regulatory elements within the invadopodia life-cycle have been identified, what determines the spatio-temporal regulation of their activity remains largely unknown. Nonetheless, invadopodia formation has been proposed as a promising target to

prevent metastasis ultimately suggesting that inhibiting invadopodia could be beneficial in treating triple negative breast cancer (Murphy and Courtneidge, 2011).

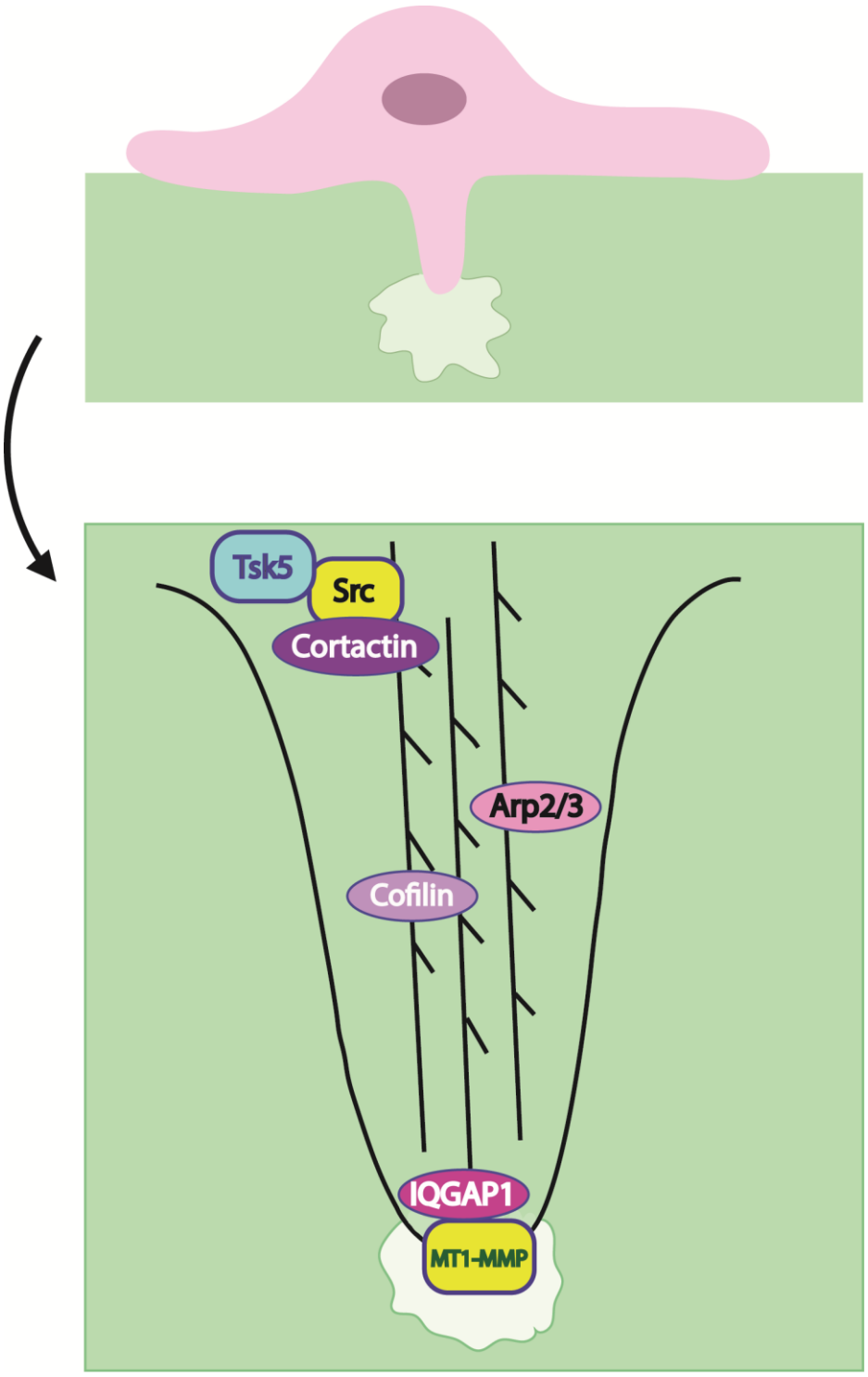

Figure 1.3 Invadopodia components. Cancer cells are able to form protrusions that secrete metalloproteases degrading the extracellular matrix. The formation of the protrusion is induced by extracellular signals that converge on kinases such as Src, a master regulator of invadopodia. Src phosphorylates major invadopodia components Tsk5 and cortactin that are crucial for invadopodia formation and elongation. Actin polymerisation is induced by activated Arp2/3 complex and supported by the severing activity of cofilin. Once the actin rich protrusion is stabilised, the presentation of MT1-MMP mediated by IQGAP1 as well as the secretion of other MMPs, degrade the surrounding extracellular matrix.

1.3 Rho GTPase pathways and cell migration

1.3.1 The Rho GTPases

The Rho GTPases are key regulators of cytoskeletal dynamics and cell motility, enabling the architectural variability observed in actin structures like invadopodia and creating a series of morphological changes during cell migration (Ridley et al., 2003; Spuul et al., 2014).The most prominent and well-studied members of the family are Rho, Rac and Cdc42 which cycle from an inactive GDP bound form to an active GTP bound form thanks to guanine-nucleotide exchange factors (GEFs) and back to an inactive GDP bound one due to the hydrolysing activity of GTPases activating proteins (GAPs) (Ridley, 2001), **(figure 1.4)**. Another mechanism via which the activity of Rho GTPases is prevented is via GDP dissociation inhibitors (GDIs) which sequester GDP bound Rho GTPases thereby preventing GEF activity and also bind GTP bound Rho GTPases and prevent them from activating their effectors (DerMardirossian and Bokoch, 2005), **(figure 1.4)**.

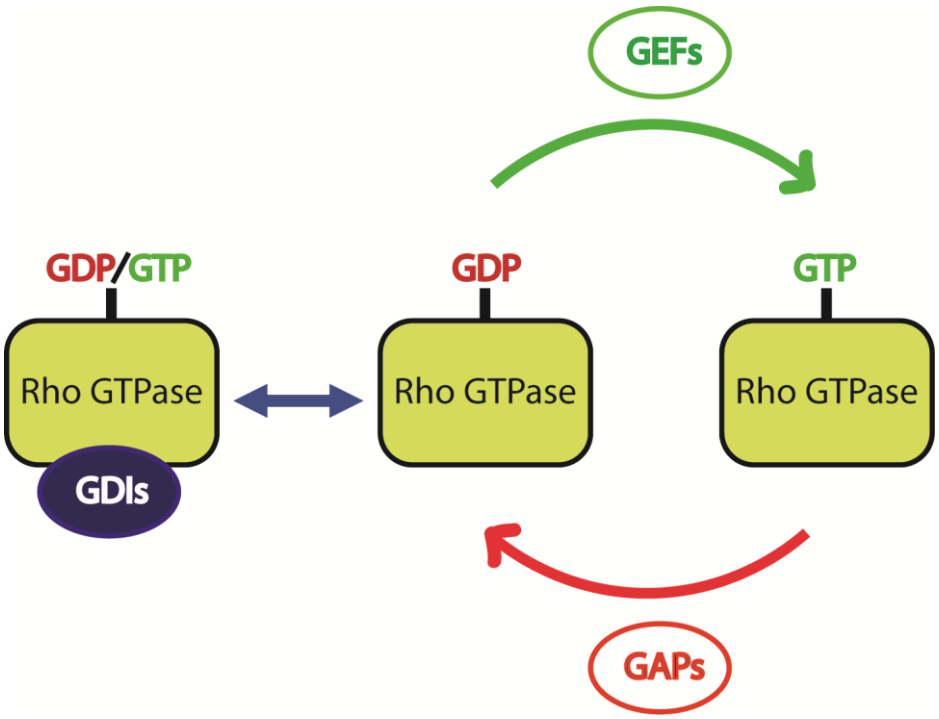

Figure 1.4 Regulation of Rho GTPase activity. Inactive GDP bound Rho GTPases become activated by GEFs and cycle back to an inactivated form by GAPs. GDIs sequester inactive Rho GTPases from activation sites and also bind active Rho GTPases preventing downstream effects.

The Rho GTPases have well characterised roles in controlling cytoskeletal dynamics and cellular architecture. Rac1 induces the extension of the lamellipodium at the early stages of cell migration by activating Arp2/3 which is a protein complex whose actin nucleating action creates actin filaments on the sides of pre-existing ones thereby resulting in a branching actin filament network at the leading cell edge (Ridley et al., 1992; Ridley, 2001), **(figure 1.5)**. Cdc42 is responsible for the establishment of cell polarity (Etienne-Manneville and Hall, 2001; Vega and Ridley, 2008) as well as the formation of actin rich filopodia which are dynamic structures that could be dictating directional migration by sensing the surrounding space as reviewed (Mattila and Lappalainen, 2008; Ridley, 2001), **(figure 1.5)**. After the forward extension of the front part of the cell, focal complexes are formed in response to Rac providing preliminary attachments with the ECM (Rottner et al., 1999). These immature focal complexes develop into focal adhesions with the downregulation of Rac and activation of Rho (Nobes and Hall, 1995; Ridley and Hall, 1992; Rottner et al., 1999). Rac has also been shown to induce the expression of MMP2, MMP9 and MT1-MMP ultimately contributing to the focalised matrix degradation that creates paths of least resistance in order for the cell to move forward (Friedl and Wolf, 2009; Parri and Chiarugi, 2010). Rho regulates actin contractility via ROCK which induces myosin light chain (MLC) phosphorylation by directly phosphorylating MLC and inhibiting MLC phosphatase (Fukata et al., 2001; Parri and Chiarugi, 2010). Additionally, Rho is responsible for the formation of actin stress fibres which attach onto focal adhesions ultimately providing rigidity and tension (Chrzanowska-Wodnicka and Burridge, 1996; Ridley and Hall, 1992), **(figure 1.5)**. The dynamic turnover of focal adhesions is equally important for efficient cell migration as together with contractility, it allows the cell body to follow the extended front edge of the cell (Ridley, 2001). Once again Rac activates PAK which in turn interacts with paxillin and induces the structural dissolution of focal adhesions (Ridley, 2001; Zhao et al., 2000). Meanwhile, Rho activity and cell contractility is also required for cell tail retraction as detachment of the cell rear is disrupted upon loss of Rho activity (Parri and Chiarugi, 2010; Sun et al., 2013), **(figure 1.5)**. The tightly regulated activity of the Rho GTPases is also required during the invadopodia lifecycle; Cdc42 and RhoA have been associated with invadopodia formation and elongation respectively (Spuul et al., 2014) while both are thought to be important for matrix degradation (Sakurai-Yageta et al., 2008). Additionally, Rac1 has been reported to regulate the dissolution and turnover of invadopodia (Moshfegh et al., 2015).

While there are distinct roles attributed to Rho GTPases, the cross-talk between them as well as the spatiotemporal regulation of their activity is just as important in ensuring effective cell migration. To begin with, Cdc42 has been shown to activate Rac and induce focal complexes in Swiss 3T3 cells, suggesting a synergistic relationship between Rac1 and Cdc42 (Nobes and Hall, 1995). In agreement with this is the fact that both Rac1 and Cdc42 induce actin polymerisation by activating the Arp2/3 complex via the actin nucleators SCAR/WAVE and N-WASP respectively **(figure 1.5)**, (Ma et al., 1998; Olson and Sahai, 2009). Meanwhile, an antagonistic relationship between Rac and Rho is widely accepted. In fact, a bistable relationship has been described between Rac1 and RhoA activity with inhibition of PAK influencing the switch between the two steady states and ultimately conferring changes in migration and morphology (Byrne et al., 2016). Additionally, mathematical modelling supported by *in vitro* work have suggested that the activation state of MEK creates a feedback loop that determines the localised activity of Rac1 or RhoA; the Sos1 – Eps8 – Abi1 complex is responsible for relaying the inhibition of MEK which in turn promotes Rac1 activity and suppression of RhoA (Hetmanski et al., 2016a, 2016b). Furthermore, cell plasticity in melanoma cells has been also shown to be regulated by shifts between Rac1 and RhoA activity; Rac activity induced by DOCK3, a Rac GEF, is needed for the mesenchymal mode of migration while ROCK downregulates Rac activity via ARHGAP22 a Rac GAP ultimately promoting the amoeboid type of migration in A375M2 cells (Sanz-Moreno et al., 2007). Ultimately, the fine spatiotemporal regulation of the Rho GTPases by their respective GEFs and GAPs controls efficient cell migration and morphology (Byrne et al., 2016). Nonetheless, once activated, the Rho GTPases signal via multiple effectors that potentiate Rho GTPase activity and control cytoskeletal dynamics.

The primary consequence of Rac and Cdc42 is actin polymerisation during the extension phase of lamellipodia and filopodia respectively (Ridley, 2001). Rac signals via IRSp53 and WAVE to activate Arp2/3 while Cdc42 achieves Arp2/3 activation via WASP (Ridley, 2001), **(figure 1.5)**. This cascade creates a branching architecture in the extending actin cytoskeleton as Arp2/3 is favouring the addition actin filaments on the side of pre-existing ones (Mullins et al., 1998; Ridley, 2001). Apart from directly inducing actin polymerisation Rac1 influences cytoskeletal dynamics by binding to phosphatidylinositol-4-phosphate 5-kinase (PIP 5-kinase) which synthesizes phosphatidylinositol-4,5-bisphosphate (PIP2), that in turn removes capping proteins such as gelsolin from the barbed end of actin filaments ultimately encouraging actin polymerisation (Tolias et al., 2000), **(figure 1.5)**. Moreover, Rho primarily acts via ROCK to influence phosphorylation of

MLC and induce actomyosin contractility; either by directly phosphorylating MLC or by inhibiting MLC phosphatase (MP) (Amano et al., 1996; Katoh et al., 2001; Kimura et al., 1996). ROCK together with mDia induce the formation of stress fibres (Ridley, 1999; Tominaga et al., 2000). Activated ROCK can also phosphorylate LIMK ultimately inhibiting cofilin and stabilising stress fibres (Ohashi et al., 2000; Ridley, 2001), **(figure 1.5)**. The signalling networks influencing Rho GTPase activity involve multiple kinases and other regulatory elements; this thesis is going to focus primarily on the IQGAP family of scaffold proteins but also on p21-activated kinases (PAKs) as well as Filamin-A **(figure 1.5)**.

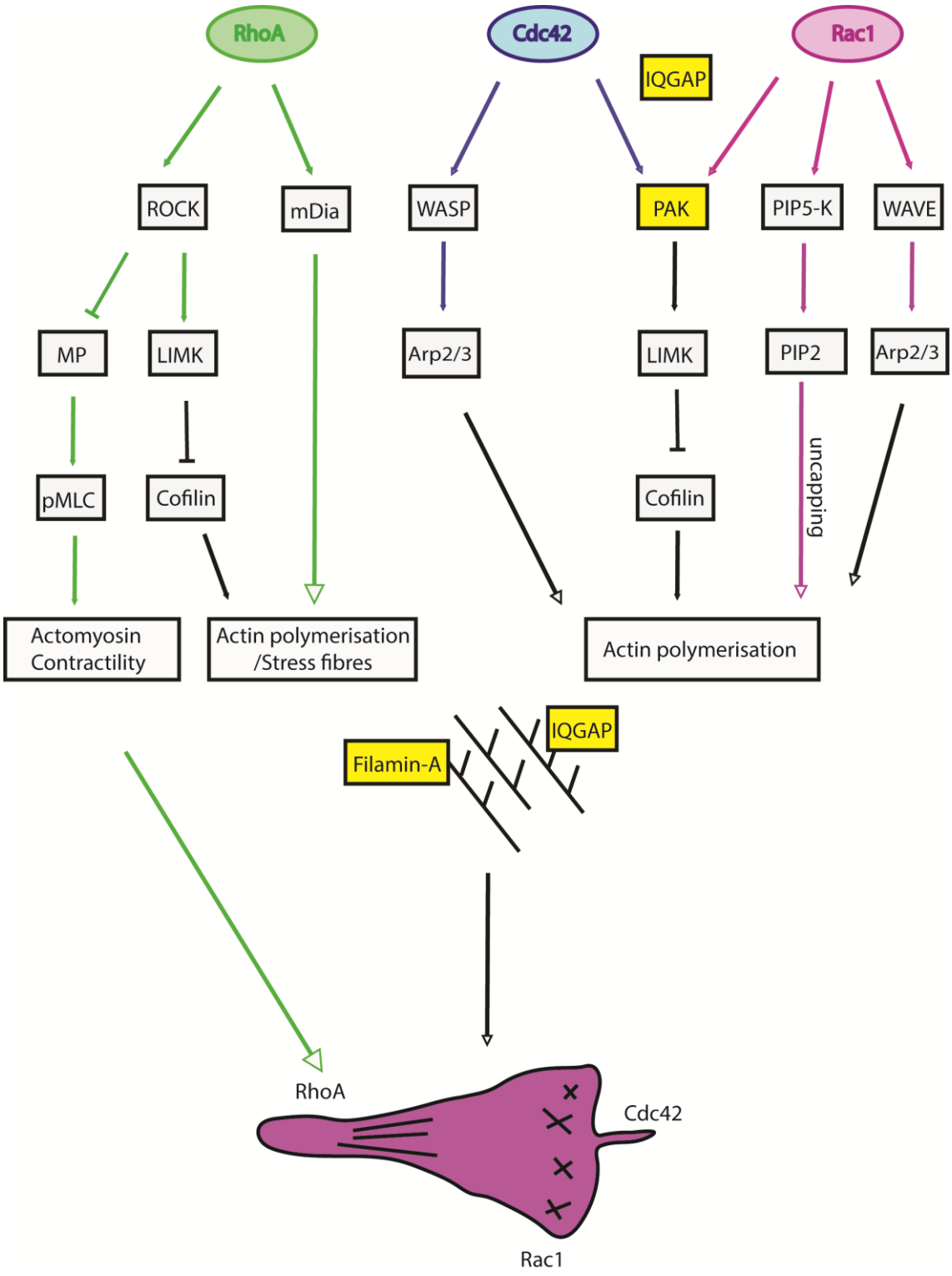

Figure 1.5 Rho GTPase effectors regulate cytoskeletal dynamics. Rac1 and Cdc42 regulate membrane protrusions by activating the Arp2/3 complex and inducing actin polymerisation. They also signal via PAK and LIMK to inactivate cofilin and inhibit actin depolymerisation. Another mechanism promoting actin polymerisation is the uncapping of actin filaments induced by the Rac1 – PIPK-5 – PIP2 signalling pathway. Regulatory proteins support these processes either by scaffolding or cross-linking. RhoA induces the formation of stress fibres via mDia but also by signalling via ROCK and LIMK. RhoA also induced actomyosin contractility by activating MLC via ROCK. Ultimately, Rac1 and Cdc42 are primarily active at the cell front regulating the formation of lamellipodia and filopodia respectively while RhoA regulates cell contractility and cell rear retraction.

1.3.2 IQGAP family of scaffold proteins

The IQGAP family of scaffold proteins has received a lot of attention as Rac1 and Cdc42 effectors (Briggs and Sacks, 2003). IQGAP1 was the first member of the family to be discovered and was initially shown to interact with activated Rac1 and Cdc42 **(figure 1.5)** and becoming enriched at COS7 cell areas with membrane ruffling as well cell junctions of MDCK cells (Kuroda et al., 1996). Since then, IQGAP1 has been implicated in various cytoskeletal processes including directional cell migration, cell adhesion and cell polarity while another two IQGAP members, IQGAP2 and IQGAP3 have also been identified sharing some functionality but also harbouring unique properties (Smith et al., 2015).

Recently, a genetic profiling screen based on approximately 200 tumours that was performed at the Breast Cancer Now Unit of Guy's Hospital and King's College London (de Rinaldis et al., 2013) revealed that IQGAP3 is upregulated in TNBC compared to other classes of breast cancer and normal breast tissue **(figure 1.6)**.

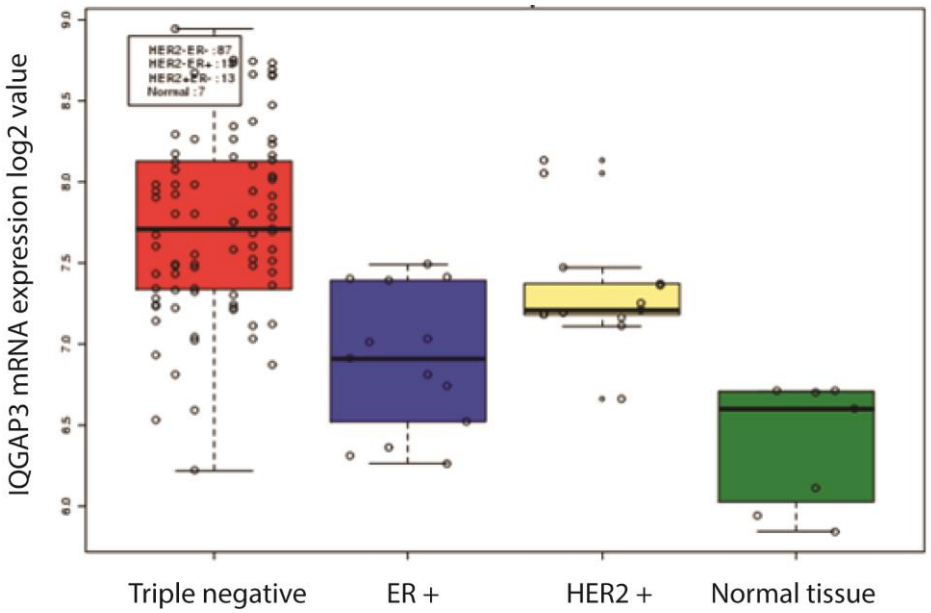

Figure 1.6 IQGAP3 mRNA levels in breast tumours. mRNA profiling was performed on a cohort of approximately 200 invasive breast tumours from patients treated at Guy's hospital between 1979-2007 (de Rinaldis et al., 2013). IQGAP3 mRNA levels were found to be upregulated in triple negative tumours compared to hormonally regulated tumours, tumours over-expressing HER2 as well as normal tissue samples. This information and schematic used was kindly offered by Professor Andrew Tutt and colleagues from the Breast Cancer Now Unit of Guy's Hospital.

IQGAPs exhibit significant sequence homology and comparable structures (White et al., 2009). The structural domains shared by IQGAPs allow them to harbour multiple interacting partners and exhibit varied properties (Smith et al., 2015), **(figure 1.7)**. Studies on IQGAP1 have expanded our knowledge on the function of IQGAP domains. At the N-terminus IQGAPs have a calponin homology domain (CHD) that has the potential to maintain a high affinity interaction with the actin cytoskeleton but also bind calmodulin and Ca^{2+}(Ho et al., 1999; Smith et al., 2015). Towards the middle of the protein sequence, IQGAPs have an IQ region containing 4 IQ motifs; these IQ domains interact with calcium and calmodulin, myosin essential light chain (essential MLC) and S100B (Pathmanathan et al., 2011). This region also mediates interactions with EGFR and MEK (Smith et al., 2015) and is also responsible for IQGAP1 homo-dimerisation (Ren et al., 2005). IQGAPs have a WW domain which has been shown to interact with ERK (Roy et al., 2004). Even though WW domains are known to interact with proline rich sequences, ERK lacks a proline rich motif while the interaction is mediated via a region of the WW domain other than the WW motif (Smith et al., 2015). Towards the C-terminus of IQGAPs there is a GAP related domain (GRD) which binds the Rho family members Rac1 and Cdc42 maintaining their active GTP bound state (Ho et al., 1999; Smith et al., 2015). Despite the name and homology with GAPs, the catalytic arginine finger normally seen in GAPs is replaced by a threonine residue in the GRD which abolishes the hydrolytic activity of the domain without disrupting binding to Ras (Kurella et al., 2009). This explains why IQGAPs can maintain the activated state of the Rho GTPases. Finally, a RasGAP C-terminal domain has been described as unique to IQGAPs and is known to mediate a variety of interactions for example with E-cadherin, APC and CLIP-170 (Abel et al., 2015), **(figure 1.7)**. Despite their observed homology, IQGAPs have different expression patterns. IQGAP1 is ubiquitously expressed while IQGAP2 and IQGAP3 are much more tissue restricted (White et al., 2009). IQGAP2 is primarily expressed in the liver but has also been found in the salivary glands, thyroid, stomach, kidneys, testis, prostate and platelets while IQGAP3 is expressed in the brain, lung, small intestine, colon and testis (White et al., 2009). The observed difference in expression across different tissues might suggest that despite their high homology, IQGAPs possess differential functionality (White et al., 2009).

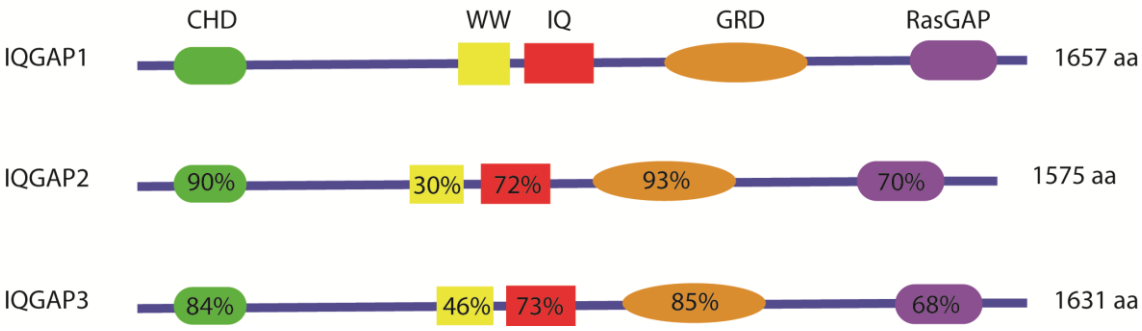

Figure 1.7 Schematic domain structure of IQGAP proteins. Starting from the N-terminus IQGAPs share homologous domains; a calponin homology domain (CHD), a WW domain, an IQ domain containing 4 IQ motifs, a GAP related domain and a C-terminus RasGAP domain that is unique to IQGAPs. Percentages indicate the amino acid identity of IQGAP2 and IQGAP3 domains compared to the equivalent domains of IQGAP1. Percentages were obtained from (White et al**.,** 2009).

1.3.2.1 IQGAP1

IQGAP1 has been associated with multiple cellular processes by interacting with more than 130 binding partners thanks to its multifunctional domains (Hedman et al., 2015). Initially it was observed to bind the actin cytoskeleton and active Cdc42 and Rac1 but not RhoA in a Ca2+/calmodulin dependent manner thereby acting as a cross-linking protein and scaffold in regulating the actin cytoskeleton (Bashour et al., 1997; Ho et al., 1999; Kuroda et al., 1996). The interaction of IQGAP1 with the Rho GTPases has been extensively described; recently it was proposed that the GRD domain interacts with Rac1 and Cdc42 with different affinities while the RasGAP-CT is also important in mediating the interaction of IQGAP1 with the Rho GTPases (Nouri et al., 2017). Additionally, the regions on IQGAP1 interacting with Rac1 and Cdc42 are overlapping but not identical (Nouri et al., 2017). In fact, IQGAP1 has been shown to maintain the active state of Cdc42 by inhibiting its GTPase activity (Swart-Mataraza et al., 2002). IQGAP1 mediated regulation of Rac1 appears to be more complex as it has been shown to promote Rac1 mediated migration in glioma cells (Hu et al., 2009) while promoting Rac1 deactivation by interacting with RacGAP1 in U-2OS osteosarcoma cells (Jacquemet et al., 2013). Since then, IQGAP1 has also been reported to bind GTP bound prenylated RhoA (Casteel et al., 2012).

In addition, IQGAP1 has been implicated in cell polarisation as it has been reported to bind CLIP-170 which in turns interacts with elongating microtubules at the cell periphery (Fukata et al., 2001; Parri and Chiarugi, 2010). This interaction allows a complex between CLIP-170, IQGAP1 and activated Rac1/Cdc42 to be formed which in turn recruits elongating microtubules towards the leading cell edge of Vero cells ultimately implicating IQGAP1 in cell polarisation (Fukata et al., 2001). The implication of IQGAP1 in directional cell migration was further confirmed when Choi *et al.,* also showed that IQGAP1 is localised close to the leading edge of MDA-MB-231 cells (Choi et al., 2013). This localisation is mediated by the type Iγ phosphatidylinositol 4-phosphate 5-kinase (PIPKIγ) recruiting IQGAP1 at the leading edge where IQGAP1 is also able to bind Phosphatidylinositol 4,5 bisphosphate (PIP2) (Choi et al., 2013). The interaction between IQGAP1 and PIP2 confers the necessary conformational change that triggers IQGAP1 to activate key actin polymerisation regulators N-WASP and Arp2/3 complex. Loss of the interaction between IQGAP1 and PIP2 leads to subsequent loss of a single leading edge and thus directional migration (Choi et al., 2013).

Additionally, IQGAP1 is also involved in cell adhesion as it was found that calmodulin regulates the association of IQGAP1 with e-cadherin thus disrupting cell junctions in MCF7 cells (Li et al., 1999). Furthermore, the interaction between IQGAP1 and PAK6 induced cell dissociation in colony forming prostate cancer DU-145 cells upon HGF stimulation (Fram et al., 2014).

Moreover, IQGAP1 also acts as a scaffold for the mitogen activated kinase cascade (MAPK) cascade potentially becoming implicated in many biological functions such as cell proliferation and differentiation (Brown and Sacks, 2006). Indeed, IQGAP1 has been found to selectively bind KRAS. This interaction did not depend on the activity status of the kinase or the ability of KRAS to bind its downstream effectors. Furthermore, overexpression of IQGAP1 in pancreatic cells enhanced the interaction of a gain of function KRASV12 with BRaf as well as the activation of ERK (Matsunaga et al., 2014). IQGAP1 was reported to bind ERK2 via a sequence within its WW domain other than the actual WW motif. This binding facilitated ERK2 activation upon epidermal growth factor (EGF) stimulation (Roy et al., 2004). Interestingly, both overexpression and depletion of IQGAP1 attenuated EGF induced ERK activation (Roy et al., 2004). Since then, it has been argued that the IQ domain of IQGAP1 is more important in mediating the interaction with ERK1/2(Bardwell et al., 2017). Moreover, IQGAP1 is necessary for ERK and Akt phosphorylation during cardiac function and remodelling in response to prolonged pressure overload (Sbroggiò et al., 2011). Additionally, overexpression of IQGAP1 increased Akt phosphorylation in IQGAP1 null MEFs ultimately suggesting that IQGAP1 is also important for the PI3K-Akt signalling cascade (Choi et al., 2016). Based on the effect of modulating IQGAP1 levels on ERK and Akt activation, it has been suggested that levels of IQGAP1 might dictate which signalling pathway it is going to scaffold to ensure survival (Choi and Anderson, 2017).

1.3.2.2 IQGAP2

IQGAP2 was identified soon after IQGAP1 displaying 62% homology to its predecessor sharing the same domains while also interacting with Rac1 and Cdc42 without displaying GTPase activity (Brill et al., 1996). Interestingly, IQGAP2 appears to be the only IQGAP able to interact with GDP bound Rac1 and Cdc42 (Brill et al., 1996). Nonetheless, despite the early discovery of IQGAP2, far less is known about IQGAP2 than IQGAP1. The human testis specific splice IQGAP2 variant has been reported to have 3 IQ motifs instead of 4 (Wang et al., 2009). In platelets, IQGAP2 localises diffusely in the cytoplasm whereas upon thrombin stimulation IQGAP2 associates with

Arp2/3 and acts as a scaffold for cytoskeletal dynamics ultimately localising at filopodia (Schmidt et al., 2003). Interestingly, this interaction is regulated by GTP bound Rac1 and not Cd42 (Schmidt et al., 2003). Additionally, IQGAP2 interacts with and mediates the effects of activated RhoG in NIH3T3 cells (Wennerberg et al., 2002). Furthermore, IQGAP1 and IQGAP2 appeared to have different localisation in the gastric epithelium with IQGAP1 localising in the cortex of chief and neck mucous cells while IQGAP2 localised in the nuclei and cell contacts in isolated rabbit gastric glands (Chew et al., 1998). IQGAP2 has also been found in a complex with c-AMP dependent protein kinase (PKA) and Protein kinase A-anchoring protein 220 (AKAP-220). The formation of this complex enables the PKA induced phosphorylation of IQGAP2 on Thr 716 which in turn supports the interaction of IQGAP2 with Rac1-GTP and induced membrane ruffling (Logue et al., 2011).

1.3.2.3 IQGAP3

When IQGAP3 was identified as a member of the IQGAP family, it was also found to act as a scaffold for Rho GTPases Rac1 and Cdc42 thereby controlling the remodelling of the actin cytoskeleton (Wang et al., 2007), **(figure 1.8)**. The interaction of IQGAP3 with the Rho GTPases is not as extensively investigated as the one of IQGAP1 even though the C-terminus of IQGAP3 containing the GRD interacted with both Rac1 and Cdc42 (Wang et al., 2007). Additionally, IQGAP3 and not IQGAP1 appeared to induce neurite outgrowth in PC12 cells and axonal elongation in primary hippocampal neurons (Wang et al., 2007). This observation not only reinforced the role of IQGAP3 in contributing to cytoskeletal dynamics, it also validated the fact that despite the high homology shared by IQGAP1 and IQGAP3, these two IQGAPs could also harbour unique functionality. Consistent with this, IQGAP3 was found to specifically localise in actively proliferating transit amplifying cells within the crypts of murine small intestine tissue samples (Nojima et al., 2008). IQGAP3 expression was also diminished in cultured Eph4 cells after they reached confluency and stopped proliferating. Additionally, ectopic expression of IQGAP3 in quiescent NIH-3T3 cells induced expression of Ki67, suggesting that IQGAP3 can induce cell cycle re-entry (Nojima et al., 2008). Indeed, IQGAP3 was uniquely found to regulate proliferation by binding GTP-bound Ras thereby activating ERK2 ultimately proving that IQGAP3 also acts as a scaffold for the MAPK cascade (Nojima et al., 2008), (**figure 1.8**).

IQGAP3 was also reported to be involved in cell migration as loss of IQGAP3 expression decreased clustering of Adenomatous polyposis coli (APC) at the leading cell edge of PC12 cells (Caro-Gonzalez et al., 2012). Upon activation by ERK2 phosphorylation, APC dissociates from actin and binds the elongating microtubules during cell extension thereby contributing to cell migration (Caro-Gonzalez et al., 2012). Loss of IQGAP3 might thus be interfering with the ERK induced APC phosphorylation that promotes APC clustering at the cell front (Caro-Gonzalez et al., 2012). Furthermore, even though IQGAP1 and IQGAP2 were shown to localise in specific structures during zebra-fish development, IQGAP3 was found to be present in proliferating areas irrespective of specific tissues. Morpholinos targeting IQGAP3 mRNA were used to inhibit IQGAP3 expression in zebra-fish embryos. IQGAP3 depletion inhibited cell proliferation and migration during zebra-fish development as shown by the position and number of IQGAP3 depleted cells at 24 hours post fertilisation (Fang et al., 2015). Additionally, Yang *et al.,* demonstrated that IQGAP3 inhibited the migration, invasion and proliferation abilities of the lung cancer cell line A549. This study also suggested that IQGAP3 elicits its proliferation promoting effects by binding to ERK1 upon EGF stimulation and facilitating its activation (Yang et al., 2014), **(figure 1.8)**. However, the mechanism via which IQGAP3 might be contributing to lung cancer cell migration remains unknown. In addition to proliferation, IQGAP3 has also been reported to be involved in cytokinesis; even though both IQGAP1 and IQGAP3 appear to affect cytokinesis only IQGAP3 was shown to specifically interact with anillin regulating the localisation of RhoA and pMLC to the furrow (Adachi et al., 2014), **(figure 1.8)**. The unique properties of IQGAP3 in proliferation and cytokinesis further reinforce the notion that despite the similarity shared by IQGAPs, each member of the family can still maintain unique functionality. Interestingly, even though all IQGAPs have been reported to bind Rac1 and Cdc42, their association with Rho appears to be more complex. It has been widely reported that IQGAPs do not directly interact with Rho (Adachi et al., 2014; Wang et al., 2007; White et al., 2009). Nonetheless, IQGAP1 was recently reported to interact with GTP bound prenylated RhoA (Casteel et al., 2012). Consequently, the potential interaction between IQGAP3 and Rho needs to be further investigated.

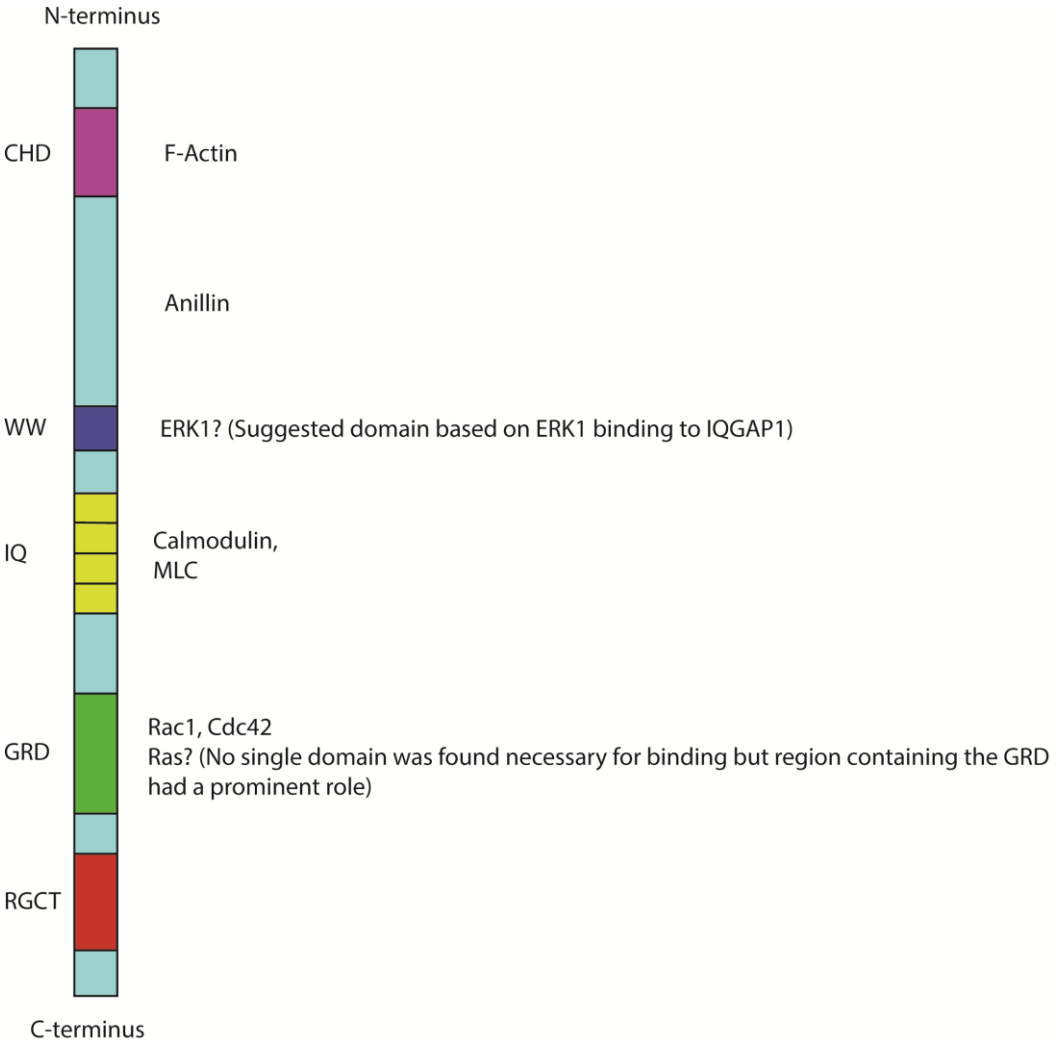

Figure 1.8 Schematic of known IQGAP3 binding partners. F-actin interacts with the calponin homology domain (CHD). Anillin binding was localised in the region containing the CHD and the WW domain. The location of ERK1 binding on IQGAP3 was not explored but ERK1 has been shown to interact with the WW and the IQ domains of IQGAP1. Rac1 and Cdc42 interact with the GAP related domain. Finally, no single domain was found necessary for Ras binding as Ras interacted with all the IQGAP3 domain mutants; however, the region containing the GRD appeared to have a prominent role in mediating the interaction.

1.3.3 IQGAPs in cancer

IQGAPs have been associated with neoplasia in various studies. In fact IQGAP1 mRNA levels are upregulated in various malignancies including colorectal, head and neck, breast, lung and liver cancers (White et al., 2009). This may come as no surprise given the implication of IQGAP1 with cell migration, invasion and adhesion as well as its scaffolding activity for the MAPK cascade, a pathway heavily associated with tumourigenesis (Hedman et al., 2015; White et al., 2009). In fact, after IQGAP1 was identified as a key regulator of H-Ras targeted tumourigenesis, it was suggested that the WW peptide of IQGAP1 could be therapeutically significant. This was supported by the fact that when it was systemically administered in a mouse model of pancreatic cancer, the WW peptide inhibited tumour growth and significantly increased survival rates (Jameson et al., 2013). Additionally, high levels of both IQGAP1 and IQGAP3 are required to drive squamous cell carcinoma in an *in vivo* xenograft skin model while the expression of the IQ domain in Ras driven organotypic tissues are substantially less proliferative disordered and invasive and display reduced p-ERK staining (Monteleon et al., 2015). Interestingly, in this study the WW domain did not exhibit any anti-tumourigenic effects (Monteleon et al., 2015). IQGAP1 is also important in invadopodia mediated matrix degradation by targeting MT1-MMP at the tip of the protrusions in MDA-MB-231 cells (Sakurai-Yageta et al., 2008).

While IQGAP2 is mainly expressed in the liver, IQGAP2 deficient mice develop hepatocellular carcinoma which is also accompanied by overexpression of IQGAP1 and loss of membrane E-cadherin (Schmidt et al., 2008). In fact, mice deficient for both IQGAP1 and IQGAP2 had a decreased incidence of hepatocellular carcinoma and improved survival suggesting that the malignant phenotype resulting from loss of IQGAP2 is dependent on IQGAP1 (Schmidt et al., 2008). These results together with the fact that decreased IQGAP2 expression is marked in gastric and prostate cancers support the notion of IQGAP2 being a tumour suppressor in spite of the tumorigenic activity of IQGAP1 (Smith et al., 2015).

IQGAP3 has also become increasingly associated with malignancy. IQGAP3 mRNA levels have been found to be upregulated in lung tumours where it is believed to drive tumourigenesis by interacting with ERK1 and promoting proliferation migration and invasion in A-549 lung cancer cells (Yang et al., 2014). Additionally, IQGAP3 expression was found to be increased in the plasma of hepatocellular carcinoma patients and also correlated with tumour size hence its value as a prognostic marker is now starting to be considered (Qian et al., 2016). IQGAP3 could also

be acting as an oncogene in pancreatic cancer as mRNA levels of IQGAP3 were also upregulated in pancreatic tumours while depleting IQGAP3 in BXPC-3 and SW1990 pancreatic cancer cell lines (Xu et al., 2016). Finally, IQGAP3 protein and mRNA expression has been shown to be increased in breast tumours compared to samples of adjacent normal tissue (Hu et al., 2016). In contrast to the mRNA screen based on the Guy's Hospital tissue sample cohort (de Rinaldis et al., 2013), **(figure 1.6)** this study found that levels of IQGAP3 were higher in HER2 positive cells compared to the triple negative MDA-MB-231 cells (Hu et al., 2016). Hence this study did not focus on triple negative breast cancer. IQGAP3 depletion in ZR-75-30 and BT474 breast cancer cells reduced their proliferation, migration and invasion capacities. Interestingly, IQGAP3 depletion also reduced expression of pERK1/2 and Twist (Hu et al., 2016). Nonetheless, the exact mechanism via which IQGAP3 is implicated in breast cancer cell migration was not investigated. Furthermore, despite the defined role of IQGAP1 in invadopodia activity, it is not known whether IQGAP3 maintains such role. This thesis will thus give particular attention in investigating a potential implication of IQGAP3 in invadopodia dynamics.

1.3.4 The p21- activated kinases

Some of the better characterised effectors of the Rho GTPases are the p21 activated kinases (PAKs); a family of Serine/Threonine kinases implicated in multiple cellular processes through that capacity (King et al., 2014). Indeed, PAKs are involved with cell growth and proliferation, as well as with the regulation of cytoskeletal dynamics thus controlling cell morphology, migration and invasion (King et al., 2014; Rane and Minden, 2014). There are 6 PAK isoforms that are separated in 2 groups based on their sequence and structural homology; group I consists of PAK1-3 while group II consists of PAK4-6 (King et al., 2014). The two groups display some key structural and regulatory differences (Arias-Romero and Chernoff, 2008). All PAKs have a regulatory and a catalytic domain **(figure 1.9)**. At the N-terminus of group I PAKs, the GTPase binding domain (GBD) can be found. The GBD also contains some over-lapping sequences with an auto-inhibitory domain (AID) that is crucial for the activation state of the kinase (Arias-Romero and Chernoff, 2008; Bokoch, 2003). Other regulatory components include proline rich regions that act as substrates for interacting partners with Src homology 3 (SH3) domains (Bokoch, 2003; Rane and Minden, 2014). The catalytic kinase domain lies at the C-terminus of all PAKs (King et al., 2014), **(figure 1.9).** In their inactivated state, group I PAKs exist as homo-dimers as the AID binds the kinase domain inhibiting its catalytic activity. This translates to the fact that group I PAKs

have low basal activity. Binding of either Rac1 or Cdc42 induces a conformational change that releases the kinase domain from its inhibited state (Bokoch, 2003; Zenke et al., 1999). This in turn allows PAK1 to auto-phosphorylate at various sites including Thr 423 within the catalytic domain that maximises its enzymatic ability. Even after the dissociation of the activator Rho GTPase, PAK1 remains active to relay downstream effects (Bokoch, 2003; Zenke et al., 1999).

The first N-terminal proline rich region interacts with the adaptor protein Nck (Bokoch et al., 1996) while the second proline rich region binds Growth Factor Receptor-bound protein 2 (Grb2) (Puto et al., 2003), **(figure 1.9)**. Both interactions are enhanced upon growth factor receptor stimulation suggesting that PAK1 can translocate to the plasma membrane (Arias-Romero and Chernoff, 2008; Bokoch et al., 1996; Puto et al., 2003). Another proline rich region mediates the interaction of group I PAKs with PIX which is a Rac1 and Cdc42 GEF that recruits PAK1 to Rac1 and Cdc42 induced focal complexes in Hela cells (Manser et al., 1998), **(figure 1.9)**. These proline rich domains might also serve as binding regions to the WW domain of IQGAPs (Hedman et al., 2015).

Even though group II PAKs also contain an N-terminal GBD and C-terminal kinase domain, there are district differences in their structure and regulation **(figure 1.9)**. Group II PAKs preferentially interact with Cdc42 while induction of their kinase activity is not dependent on the interaction with Cdc42 (Arias-Romero and Chernoff, 2008). Initially only PAK5 was reported to harbour a recognised AID functioning like the one observed in PAK1 (Ching et al., 2003). Nonetheless, work on the N-terminus of PAK4 has identified a conserved region across group II PAKs that could maintain the inactive state of the kinase and also reduce PAK6 activity (Ha et al., 2012). PAK4 also has a unique binding site within its C-terminus for β5 integrin; PAK4 mediated phosphorylation of β5 integrin is important for cell migration in CS-1 cells (Li et al., 2010; Takkunen et al., 2010).

PAK isoforms have differential expression distribution and a variety of different substrates implicating them in cytoskeletal dynamics, signal transduction, and gene transcription (Arias-Romero and Chernoff, 2008). This thesis will focus on PAK1 and PAK6.

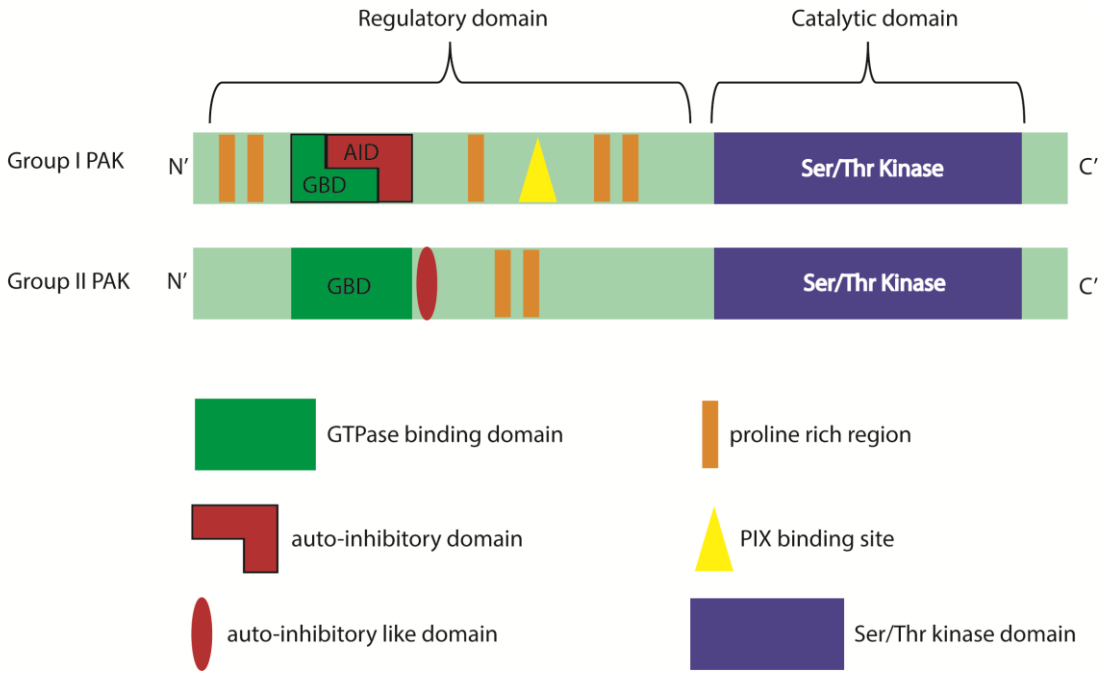

Figure 1.9 Schematic of PAK structure. All PAKs have an N-terminal regulatory domain and a C-terminal catalytic domain containing the Ser/Thr kinase region. In the regulatory Group I PAKs have a GTPase binding domain (GBD) that has overlapping sequence with the auto-inhibitory domain (AID). Group I PAKs also have several proline rich regions mediating interactions with SH3 domains. A binding site for PIX has also been identified. In group II PAKs there is no universally accepted AID, although putative auto-inhibitory regions adjacent to the GBD have been suggested.

1.3.4.1 PAK1

PAK1 was at first identified in the brain but was also detected in the spleen, lung and testis (Arias-Romero and Chernoff, 2008; Manser et al., 1994). Active PAK1 is heavily involved in cytoskeletal dynamics downstream of Rac1 and Cdc42 and localises at the membrane ruffles, cell protrusions and periphery of migrating cells (Parrini, 2012). PAK1 has also been shown to phenocopy Cdc42 in Swiss 3T3 cells in inducing filopodia suggesting that it might also influence cytoskeletal dynamics downstream of Cdc42 (Sells et al., 1997). Activated PAK1 interacts and phosphorylates LIMK on Thr 508 which confers Rac1 induced membrane ruffling in BHK cells by inhibiting cofilin mediated actin depolymerisation (Edwards et al., 1999). PAK1 also phosphorylates paxillin at Ser 273 and promotes GIT1 binding to paxillin as well as targets the complex of GIT1-PIX-PAK1 at the leading edge of CHO-K1 cells ultimately enhancing Rac induced protrusion and focal adhesion turnover (Nayal et al., 2006). Consistent with this, inhibition of PAK1 reduced actin flow within the lamella, displaced myosin IIA and disrupted the architecture and turnover of focal adhesions in PtK1 cells (Delorme-Walker et al., 2011). However, Dart *et al*., reported that PAK1 depletion in MDA-MB-231 cells did not affect paxillin phosphorylation at Ser273 whereas PAK4 depletion reduced levels of S273 phosphorylation (Dart et al., 2015). At the same time, PAK1 has been shown to phosphorylate MLCK ultimately reducing active MLC and peripheral cell spreading in BHK-21 cells (Sanders et al., 1999). PAK1 also binds Filamin-A via its CRIB domain and phosphorylates Filamin-A on Ser 2152 which in turn confers membrane ruffles and lamellipodia in MCF7 and M2 cells. Interestingly, binding of Filamin-A on the CRIB domain of PAK1 induces kinase activity (Vadlamudi et al., 2002). Additionally PAK1 also signals via the MAPK cascade to control stability of lamellipodia in macrophages (Smith et al., 2008). Indeed PAK1 can phosphorylate both MEK1 and Raf1 (King et al., 2014).

PAK1 is implicated in multiple signalling pathways that promote malignancy. Indeed, PAK1 expression is upregulated in cancers of the breast, colon, kidney, prostate as well as melanoma, yet no activating mutations have been identified (Rane and Minden, 2014). Furthermore, depletion of PAK1 in prostate cancer PC3 cells inhibited transendothelial cell migration and tumour growth in mouse xenografts while expression of MMP9 was significantly reduced ultimately implicating PAK1 in prostate cancer microinvasion (Goc et al., 2013). Interestingly, PAK1 was found to be involved with invadopodia formation in melanoma cells (Nicholas et al.,

2016). PAK1 expression also correlated with colorectal cancer progression from normal tissue to lymph node metastasis (Carter et al., 2004). In fact PAK1 drives colon cancer DLD1 cell proliferation migration and survival through activation of ERK and Akt (Huynh et al., 2010). Moreover, PAK1 phosphorylates the oestrogen receptor (ER) on Ser 305 mediating its transactivation and thus regulating the expression of downstream gene targets such as the progesterone receptor (PR). Indeed, ectopic expression of constitutively active PAK1 in murine mammary glands during pregnancy and lactation led to mammary hyperplasia (Wang et al., 2002). These mice later displayed pre-malignant and malignant lesions which expressed high levels of phosphorylated MEK1/2 and p38MAPK (Wang et al., 2005). Additionally, phosphorylated PAK1 localised in the nuclei in cells of advanced tumours in the polyoma middle-T antigen transgenic mouse model of breast cancer suggesting that PAK1 transcriptional activity is involved in breast cancer tumourigenesis and progression (Wang et al., 2005). Localisation of PAK1 in the nucleus has also been linked with tamoxifen resistance in MCF7 cells (Holm et al., 2006). Ultimately, the use of PAK inhibitors in combination with standard taxane based chemotherapy was deemed as a promising therapeutic strategy for breast cancer (Ong et al., 2015).

1.3.4.2 PAK6

PAK6 was first identified as an androgen receptor (AR) binding partner in a yeast two hybrid screen. In fact, PAK6 bound to the ligand binding domain of AR and inhibited AR signalling (Yang et al., 2001). Soon after, PAK6 was also found to interact with ERα inhibiting ER induced transcription (Lee et al., 2002). The fact that PAK6 interacts and inhibits the downstream transcriptional activity of hormone receptors suggests that PAK6 could contribute to the development of hormonally independent tumours that are known to be aggressive (Schrantz et al., 2004).

A truncated C-terminal mutant of PAK6 displayed higher kinase activity than the full length protein consistent with the hypothesis that group II PAKs also possess an auto-inhibitory mechanism (Yang et al., 2001). PAK6 can be inhibited by p38 MAP kinase inhibitor SB203580 and increases with p38 MAP kinase upstream activator MKK6 suggesting that p38 MAP is involved in the regulation of PAK6 activity in HEK-293 cells (Kaur et al., 2005). PAK6 expression has been detected in the prostate, testis, brain, kidney and placenta (Jaffer and Chernoff, 2002; Yang et al., 2001). Additionally, PAK6 expression was reported in prostate and breast cancer cell lines including the PC3 and MDA-MB-231 cells while it was also increased in primary, metastatic and

recurrent prostate tumours compared to normal prostate epithelium (Kaur et al., 2008). Furthermore mass-spectrometry and immunoprecipitation assays confirmed that IQGAP1 and protein phosphatase 1B (PP1B) associate with PAK6 (Kaur et al., 2008). Indeed, PAK6 was shown to promote cell junction disassembly by associating with IQGAP1 and e-cadherin upon HGF stimulation in DU-145 cells (Fram et al., 2014). Additionally, similarly to PAK1, depletion of PAK6 also reduced MMP9 expression in PC3 cells (Goc et al., 2013). Furthermore, depletion of PAK6 expression induced a cell-cycle arrest at G2/M phase which was further enhanced by docetaxel in LAPC-4 and PC3 cells (Wen et al., 2009). This is an interesting observation as IQGAP3 depletion also inhibits cell proliferation in Eph4 cells (Nojima et al., 2008) and thus a potential synergy between PAK6 and IQGAP3 should be investigated. Inhibition of cell invasion *in vitro* as well as tumour growth *in vivo* induced by PAK6 depletion was also enhanced by docetaxel suggesting that this synergy could be exploited therapeutically (Wen et al., 2009). The clinical implication of PAK6 in prostate cancer is further supported by the fact that PAK6 depletion increased radiosensitivity of PC3 and DU-145 cells potentially because PAK6 is preventing apoptosis by phosphorylating BAD (Zhang et al., 2010). Nonetheless, despite the characterised role of PAK6 in prostate cancer, little is known about PAK6 in other settings such as breast cancer and whether inhibition of PAK6 would have an effect in breast tumour growth.

1.3.5 Filamin-A

The activity of the Rho GTPases is also regulated by Filamin-A (Stossel et al., 2001). Filamin-A is an actin filament binding and cross-linking protein that has been shown to influence the architecture and organisation of the actin cytoskeleton (Flanagan et al., 2001; Wang et al., 1975), **(figure 1.5)**. Filamin-A first acquired its name due to the fact that it was found to localise with actin filaments (Wang et al., 1975). There are 3 human Filamins (Filamin-A, B and C); all of them display actin-filament cross-linking activity while maintaining the capacity of attaching binding partners to the plasma membrane (van der Flier and Sonnenberg, 2001). Ultimately, through these features, filamins contribute to the complex cytoskeletal architecture adopted by migrating cells (Stossel et al., 2001).

Filamins are found as homo-dimers of large peptide chains that associate with each other via their C-termini. The actin binding domain (ABD) consisting of two calponin homology domains lies at the far N-terminus of each monomer and its similar to those found in other actin binding domains such as α-actinin and calponin (van der Flier and Sonnenberg, 2001). Following the

ABD, each filamin monomer contains 2 rod domains made of 24 anti-parallel β-sheets. These are interrupted by two calpain sensitive hinge domains (Nakamura et al., 2007; Stossel et al., 2001). The rod domains mediate the interactions with binding partners while the hinge domains contribute to the elasticity observed in the actin networks reconstituted *in vitro* (Gardel et al., 2006). Ultimately, dimerization results in a Y shape of the filamin dimer which enables the cross-linking activity of the protein (Nakamura et al., 2007), **(figure 1.10)**.

The association of Filamin-A with cytoskeletal dynamics already suggests that Filamin-A is important in cell migration. This is well characterised in M2 melanoma cells lacking Filamin-A expression compared to the M2 sub-line A7 that express Filamin-A. Indeed, M2 cells make unstable protrusions and blebs while displaying compromised migration. Unlike the M2 cells, Filamin-A reconstituted A7 cells displayed improved elasticity, protrusion stability and cell motility (Cunningham et al., 1992). Interestingly, similar levels of Arp2/3 were detected in both cell types further confirming the importance of Filamin-A in regulating cytoskeletal architecture and stability (Flanagan et al., 2001). Consistent with this, Filamin-A binds Rac1, Cdc42 and RhoA although the functional significance of these interactions is not well described (Ohta et al., 1999; Stossel et al., 2001). Filamin-A has been reported to mediate Rho activity during the retraction of the neutrophil neuropod by controlling the localisation of pMLC and RhoA (Sun et al., 2013). Filamin-A has also been implicated in the antagonistic cross-talk between Rac and Rho which was discussed earlier; Filamin-A is required for the ROCK induced FilGAP mediated Rac inactivation in melanoma A7 cells (Ohta et al., 2006).The role of Filamin-A is perhaps to provide spatial control of FilGAP in areas where it can be phosphorylated by ROCK and inactivate Rac (Ohta et al., 2006). Filamin-A has also been shown to interact with β1 integrin and vimentin thus regulating the cell surface expression of β1 integrin and cell spreading on collagen (MacPherson and Fagerholm, 2010). Furthermore, a complex of Filamin-A and IQGAP1 recruits RacGAP1 to β1 integrin active sites at the cell periphery to downregulate Rac1 and ensure directional cell migration (Jacquemet et al., 2013). These examples suggest that Filamin-A favours RhoA activity over Rac1 activity. Apart from supporting cytoskeletal architecture and stability Filamin-A also has mechanosensing properties. Filamin-A enables cells to adapt to mechanical force stresses by changing its conformation thereby revealing previously hidden interacting regions, ultimately allowing the integration of Filamin-A in further signalling pathways (Razinia et al., 2012). In fact, the interaction of Filamin-A with FilGAP has also been shown to prevent HEK-293 cells under mechanical stress from undergoing apoptosis (Shifrin et al., 2009).

Interestingly, apart from regulating cytoskeletal dynamics and cell shape Filamin-A has other functions. Indeed, Filamin-A is involved in DNA repair by interacting with BRCA1 in the nucleus of HCT116 cells (Velkova et al., 2010). Also, calpain induced cleavage yields C-terminal fragments that interact with the androgen receptor and translocate to the nucleus thereby disrupting AR signalling (Loy et al., 2003; Nakamura et al., 2011).

Given the implication of Filamin-A in cell migration, it may come as no surprise that Filamin-A is involved in human diseases including cancer (Yue et al., 2013). However, the role of Filamin-A in cancer progression is far from clear. Filamin-A is over-expressed in many cancers including the one of the breast, prostate, lung, colon as well as melanoma (Savoy and Ghosh, 2013). Cyclin D1 interacts and phosphorylates Filamin-A at Ser1459 and Ser2152 regulating Filamin-A mediated cell migration and invasion in MDA-MB-231 cells (Zhong et al., 2010). Additionally, Filamin-A is also phosphorylated by Akt at Ser2152 and drives arsenic induced cell migration in human bronchial epithelial cell line, BEAS-2B cells while Filamin-A expression has been associated with poor survival in lung cancer adenocarcinoma patients (Li et al., 2015). Meanwhile, nuclear Filamin-A was found in benign prostate tissue while cytoplasmic Filamin-A localisation was linked with prostate cancer progression and metastasis (Bedolla et al., 2009). Consequently, it has been argued that cytoplasmic Filamin-A promotes migration and metastasis while nuclear Filamin-A regulates transcription and inhibits tumour growth (Savoy and Ghosh, 2013). Consistent with its pro-metastatic activity Filamin-A has been found at invadopodia (Takkunen et al., 2010) and linked with IQGAP1 (Jacquemet et al., 2013). However, whether Filamin-A is associated with IQGAP3 remains unknown.

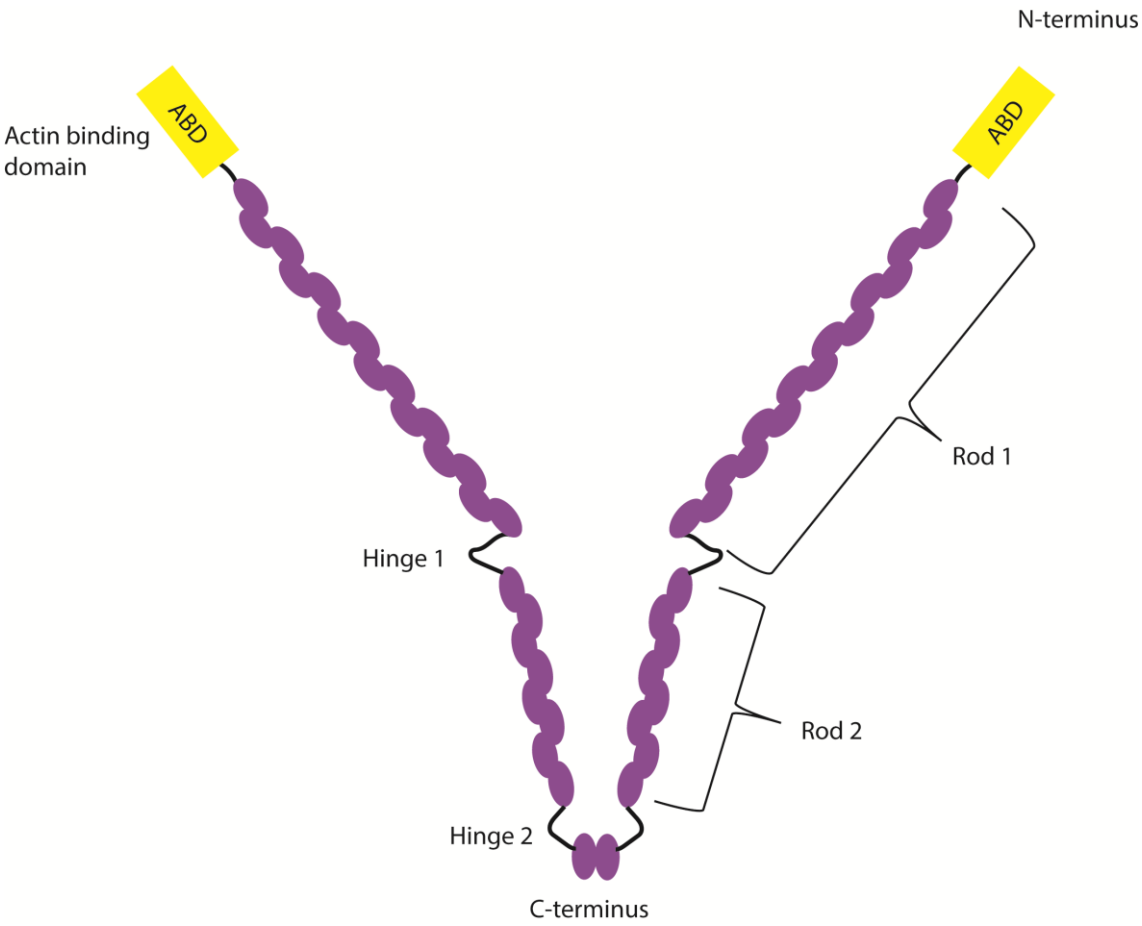

Figure 1.10 Schematic of Filamin-A structure. Filamin-A is a homo-dimer of 2 large monomers. At the N-terminus of each homo-dimer lies an actin binding domain (ABD). This is followed by 24 β-sheets that become interrupted by 2 hinge regions providing flexibility. Each monomer is thus separated in two rod domains. Dimerization occurs via the C-termini of the Filamin monomers.

1.4 Project Aims

The aim of the project was to investigate the role of IQGAP3 in triple negative breast cancer cells and to identify potential mechanisms via which IQGAP3 is involved in cell migration. Specific objectives comprised the following:

- Characterise the expression levels of IQGAP3 in a panel of triple negative breast cancer cell lines and identify the most suitable cell models to further this study.
- Assess the effect of modulating IQGAP3 expression in specific cell phenotypes such as cell morphology, random 2D migration and invadopodia activity.
- Identify IQGAP3 binding partners and explore their functional significance in the context of triple negative breast cancer cell behaviour.

Chapter 2

Materials and Methods

Chapter 2 : Materials and Methods

2.1 Materials

2.1.1 General materials

3-(4,5-Dimethylthiazol-2-yl)-2,5-Diphenyltetrazolium Bromide (MTT)	**Sigma-Aldrich, UK**
4-(2-hydroxyethyl)-1-piperazineethanesulfonic acid (HEPES)	**A&E Scientific**
4', 6-diamidino-2-phenylindole (DAPI)	**Sigma-Aldrich, UK**
Acrylamide (30%)	**Severn Biotech Ltd, UK**
Alexa Fluor® 488 Phalloidin	**Invitrogen, UK**
Agarose	**Invitrogen, UK**
Ammonium persulfate (APS)	**Sigma-Aldrich, UK**
Ampicillin	**Sigma-Aldrich, UK**
Aprotinin	**Sigma-Aldrich, UK**
Beta (β)- mercaptoethanol	**Sigma-Aldrich, UK**
Bovine serum albumin (BSA)	**VWR International, UK**
Bovine serum albumin (BSA)- Fatty acid free	**VWR International, UK**
Bromophenol blue	**Bio-Rad**
Calcium phosphate transfection kit	**Invitrogen, UK**
Cell dissociation buffer	**Sigma-Aldrich, UK**
Coverslips 13mm	**Scientific Laboratories Supplies**
DH5α™ competent Escherichia coli (E. coli) cells	**Invitrogen, UK**
Dimethyl sulfoxide (DMSO)	**Sigma-Aldrich, UK**
Dithiothreitol (DTT)	**Sigma-Aldrich, UK**
Dulbecco's Modified Eagle's Medium (DMEM)	**Sigma-Aldrich, UK**
Duolink® In Situ Detection Reagents Red	**Sigma-Aldrich, UK**
Enhanced chemiluminescence (ECL) Prime western blotting detection reagent	**GE Healthcare Life Sciences, UK**
Ethanol	**BDH Laboratory Supplies, UK**
Ethylenediaminetetraacetic acid (EDTA)	**Sigma-Aldrich, UK**
Fibronectin	**Sigma-Aldrich, UK**
FluorSave™ Reagent	**Calbiochem, UK**
Foetal bovine serum (FBS)	**GIBCO®, Invitrogen, UK**
Formaldehyde	**ThermoFisher Scientific, USA**
X-ray film	**Scientific Laboratory Supplies, UK**
Gateway® LR Clonase™ enzyme kit (including proteinase K)	**Invitrogen, UK**

Gelatin- Type A from porcine skin	**Sigma-Aldrich, UK**
GFP-TRAP	**ChromoTek, Germany**
Glutaraldehyde solution, Grade I, 25%	**Sigma-Aldrich, UK**
Glycerol	**Sigma-Aldrich, UK**
Glycine	**Sigma-Aldrich, UK**
HCl	**VWR International, UK**
HiPerfect transfection reagent	**Qiagen Ltd, UK**
Insulin solution, human	**Sigma-Aldrich, UK**
Kanamycin solution	**Sigma-Aldrich, UK**
Leupeptin	**Sigma-Aldrich, UK**
Lipofectamine 2000	**Invitrogen, UK**
Luria-Bertani agar (LB-agar)	**Sigma-Aldrich, UK**
Luria-Bertani broth (LB-broth) tablets	**Sigma-Aldrich, UK**
Methanol	**VWR International, UK**
Milk powder	**Marvel, UK**
NEB®-10 beta competent E.coli cells (high efficiency)	**New England Biolabs, UK**
Nitrocellulose membrane	**PerkinElmer, UK**
Nonidet™ P40 substitute (NP-40)	**Sigma-Aldrich, UK**
Nuclease-free water	**ThermoFisher Scientific, USA**
Oleoyl-L-α-lysophosphatidic acid sodium salt (LPA)	**Sigma-Aldrich, UK**
OptiMEM	**Invitrogen, UK**
Paraformaldehyde (PFA)	**Sigma-Aldrich, UK**
Penicillin-Streptomycin	**Sigma-Aldrich, UK**
Phalloidin CruzFluor™ 647 Conjugate	**Santa Cruz**
Phenylmethylsulfonylfluoride (PMSF)	**Sigma-Aldrich, UK**
Phosphate buffered saline (PBS) tablets	**Oxoid Limited, UK**
Dulbecco's PBS with Calcium and Magnesium	**GIBCO®, Invitrogen, UK**
Dulbecco's PBS without Calcium and Magnesium	**LONZA, UK**
Pierce™ ECL western blotting substrate	**ThermoFisher Scientific, USA**
Precision Plus Protein™ All Blue standards	**Bio-rad, UK**
Precision Plus Protein™ dual colour standards	**Bio-rad, UK**
Purelink® HiPure Plasmid Filter Maxi-prep kit	**Invitrogen, UK**
Puromycin	**Sigma-Aldrich, UK**
Rhodamine Phalloidin	**ThermoFisher Scientific, USA**
Rhodamine B Isothiocyanate	**Sigma-Aldrich, UK**

Roswell Park Memorial Institute (RPMI)-1640 medium	**Sigma-Aldrich, UK**
Slide-A-Lyzer® dialysis cassette	**ThermoFisher Scientific, USA**
Sodium borohydride	**Sigma-Aldrich,UK**
Sodium Chloride (NaCl)	**Sigma-Aldrich, UK**
Sodium dodecyl sulphate (SDS)	**Sigma-Aldrich, UK**
Sodium fluoride (NaF)	**Alfa Aesar, UK**
Sodium hydroxide (NaOH)	**Sigma-Aldrich, UK**
Sodium orthovanadate (Na3VO4)	**New England Biolabs, UK**
Sucrose	**Sigma-Aldrich, UK**
Tetramethylethylenediamine (TEMED)	**Sigma-Aldrich, UK**
Tris-base	**Sigma-Aldrich, UK**
Triton X-100	**VWR International, UK**
Tween® 20	**VWR International, UK**

Table 2-1 General reagents

2.1.2 Buffers

Blocking solution	5% w/v milk powder or 5% w/v BSA in Tris buffered saline (TBS)-Tween
GFP-Trap wash/dilution buffer	10 mM Tris-HCl pH 7.5, 150 mM NaCl, 5 mM EDTA
GFP-Trap Lysis buffer	10 mM Tris-HCl pH 7.5, 150 mM NaCl, 5 mM EDTA, 0.5% NP-40
Gel Sample buffer (2x)	100 mM Tris-HCl pH 6.8, 4% w/v SDS, 20% v/v glycerol, 2% β-mercaptoethanol, 0.2% w/v bromophenol blue.
Stripping buffer	25 mM Glycine pH 2, 1% w/v SDS
Protease inhibitor cocktail	1 mM DTT, 10 µg/ml leupeptin, 1 µg/ml aprotinin, 10 mM PMSF, 10 mM NaF, 1 mM Na3VO4
SDS-PAGE running buffer (10x)	250 mM Tris-base, 1.92 M Glycine, 1% w/v SDS
SDS-PAGE transfer buffer (10x)	250 mM Tris-base, 1.92 M Glycine.

TBS-Tween	25 mM Tris-HCl pH 7.6, 50 mM NaCl, 0.1% v/v Tween 20

Table 2-2 Buffers

2.1.3 Antibodies

Antibody	Species	Company	Dilution for IF	Dilution for WB
β-actin	Mouse	Sigma-Aldrich	-	1:5000
β-tubulin	Mouse	Sigma-Aldrich	-	1:5000
Cortactin	Mouse	Millipore (Upstate)	1:50	-
Filamin-A	Rabbit	Genetex	-	1:1000
GFP	Mouse	Roche	-	1:1000
IQGAP1	Rabbit	Cell Signalling Technology	-	1:1000
IQGAP3	Mouse	Abnova	-	1:500
IQGAP3	Rabbit	Sigma-Aldrich	1:50	1:500
Phospho – myosin light chain (Ser 19)	Rabbit	Cell Signalling Technology	-	1:1000
c-myc (9E10)	Mouse	Santa-Cruz	1:50	1:1000
Zyxin	Rabbit	Thermo Fisher Scientific	1:400	-

Table 2-3 Primary antibodies

Antibody	Species	Company	Dilution for IF	Dilution for WB
Alexa Fluor®488 anti-mouse	Goat	Invitrogen	1:400	-
Alexa Fluor®488 anti-rabbit	Goat	Invitrogen	1:400	-
Alexa Fluor®568 anti-rabbit	Goat	Invitrogen	1:400	-
Alexa Fluor®647 anti-mouse	Goat	Invitrogen	1:400	-
Alexa Fluor® Rhodamine Phalloidin		Invitrogen	1:1000	
Alexa Fluor® 488 Phalloidin		Invitrogen	1:300	
Phalloidin CruzFluor™ 647 Conjugate		Santa Cruz	1:300	
HRP conjugated anti-mouse	Goat	DAKO		1:2000
HRP conjugated anti-rabbit	Goat	DAKO		1:2000

Table 2-4 Secondary antibodies and Phalloidin stains

2.1.4 Oligonucleotide sequences

Primer	5'-3' sequence
IQGAP3 Forward	ATGGAGTGCTGCTGGCCAAG
AttB2 Reverse	TTGTACAAGAAAGCTGGG

Table 2-5 Sequencing primers

siRNA	5'-3' sequence	Company
Negative control (non-silencing)	AAUUCUCCGAACGUGUCACGU	Qiagen, UK
Silencer Select (s43270) IQGAP3 siRNA (**oligo 1**)	CAAUGAGGCUCUGGACAAA	Thermo Fisher Scientific
siGENOME IQGAP3 siRNA (D-009077-02-0002)(**oligo 2**)	CAAGAUGACUACAGGAUAU	Dharmacon

Table 2-6 siRNA sequences

2.1.5 Plasmids

Construct	Source
pcDNA-DEST47 GFP vector	Kind gift from Sans-Moreno lab, King's College London, UK
ORFEXPRESS™-Shuttle Clone GC-E2954-CF IQGAP3 entry vector	Genecopoeia, USA
pDEST™ HA vector	Invitrogen, UK
IQGAP3-GFP	Generated by author
IQGAP3-HA	Generated by author
IQGAP1-GFP	Claire Wells lab, King's College London, UK
IQGAP2-myc	Kind gift from Professor David Sacks, NIH
GFP alone	Claire Wells lab, King's College London, UK
PAK1-myc	Claire Wells lab, King's College London, UK
PAK6-myc	Claire Wells lab, King's College London, UK
PAK6-GFP	Claire Wells lab, King's College London, UK

Table 2-7 Plasmids

2.2 Methods

2.2.1 Generation of tagged IQGAP3 expression constructs

In order to make tagged IQGAP3 expression constructs, the Gateway™ Technology system was employed. To create GFP and HA tagged IQGAP3 constructs the IQGAP3 entry clone was transferred into the pcDNA-DEST47 GFP vector and pDEST™ HA vector respectively using the LR reaction. The entry clone was mixed with the respective destination vector and TE buffer and 2µl of LR Clonase enzyme II mix was added to each mix. The reactions were then incubated at 25°C for 1h. To terminate the reactions, 1 µl of Proteinase K was added and the mix was incubated at 37°C for 10 min. Each reaction was then used to transform chemically competent *E. coli* cells.

2.2.2 Transformation of *Escherichia coli* cells

NEB®-10 beta *E.coli* cells normally stored at -80°C were thawed on ice. 1 µl of the LR reaction mix or plasmid DNA was then added to the cells, without vigorous pipetting. The mixtures were then put on ice for 30 minutes. Bacteria were then transformed by heat shock. Tubes containing the bacteria and DNA were incubated at 42°C for 30 seconds and were then returned to ice for another 2 minutes. 500 µl of LB-broth were added to the transformed *E.coli* cells which were then shaken at 37°C for 1 hour at 225rpm. 100µl of the transformed bacteria were then spread onto LB-agar plates containing the appropriate antibiotic. Plates were then placed inverted in an incubator set at 37°C overnight. On the following day 3 colonies were picked and grown in LB broth supplemented with the appropriate selection antibiotic. A small fraction of the yielded culture was used to make a glycerol stock while the rest was used for DNA purification.

2.2.3 DNA plasmid purification

Plasmid DNA was isolated and purified from the grown *E.coli* cultures using the Invitrogen Purelink® HiPure Plasmid Filter Maxi-prep kit according to the manufacturers' protocol. The purified DNA was resuspended in TE buffer and the yielded DNA concentration was determined in ng/µl using a Nano-drop system. The newly made IQGAP3 expression constructs were sequenced by Europhin MWG Operon using an IQGAP3 forward primer and a reverse primer recognising the AttB2 sequence of the expression vector (**table 2-6**).

2.2.4 Culture of human cell lines

Human breast cancer MDA-MB-231 cells and Human Embryonic Kidney HEK293 cells were obtained from Claire Wells, King's College London and were grown in Dulbecco's modified Eagle's media (DMEM) supplemented with 10% v/v FBS and 1 mM penicillin-streptomycin. Human breast cancer cell lines HCC38, HCC1937 and HCC1143, MDA-MB-436 and MCF10A were obtained from the Breast Cancer Now Unit of King's College London. The HCC38, HCC1143 and HCC1937 cells were grown in Roswell Park Memorial Institute-1640 (RPMI-1640) media supplemented with 10% v/v FBS and 1 mM penicillin-streptomycin. The MDA-MB-436 cells were grown in RPMI-1640 supplemented with 10% v/v FBS, 1 mM penicillin-streptomycin, 10µg/ml human insulin and 16µg/ml Glutathione. The MCF10A cells were grown in DMEM/F12 supplemented with 5% FBS, 1mM penicillin-streptomycin 20µg/ml EGF, 800ng/ml hydrocortisone, 100ng/ml cholera toxin and 20µg/ml insulin. The BT-549 cells were obtained from Dr Phillippe Chavrier, Centre de Recherche Institut Curie and were grown in RPMI supplemented with 10% v/v FBS and 1 mM penicillin-streptomycin and 10µg/ml human insulin. All cell lines were maintained at 37°C in a humidified tissue culture incubator with 5% of atmospheric CO_2. Cells were passaged before confluency was reached. In order to passage cells, growth media were aspirated and cells were washed with Phosphate Buffered Saline (PBS). Cells were detached by incubating them with trypsin/EDTA for 5 min at 37°C. Following detachment, trypsin was deactivated by adding equal volumes of growth media and cells were pelleted by centrifugation at 1200 rpm for 5 minutes. The cell pellet was then resuspended in appropriate volumes and seeded in flasks or dishes at appropriate dilutions.

2.2.5 Freezing down and thawing out cells

In order to freeze cells down, cells were subjected to normal passaging but instead of re-suspending them in growth media, cells were split in cryovials containing 90% FBS, 10% DMSO solution. Sealed cryovials were then placed in a cryo-freezing container at -80°C to ensure freezing at a slow rate. Cells were later stored in a liquid nitrogen tank for long-term storage.

In order to thaw cells out, the cryovials were removed from liquid nitrogen and were thawed in a 37°C water bath. Growth media were added in the cell suspension to dilute the DMSO even further followed by a 5min centrifugation at 1200 rpm. Cells were then resuspended in fresh growth media and seeded in a t25 flask. Growth media were changed again the following day.

2.2.6 Acid or ethanol treatment of coverslips

For immunofluorescent staining experiments, 13 mm diameter round glass coverslips were submerged in a solution of 60% 1 M hydrochloric acid (HCl) and 40% of 70% ethanol. On the next day the mixture was discarded before dH2O was added and boiled. The coverslips were then rinsed six times with fresh dH2O and placed on paper to dry followed by being autoclaved.

For the invadopodia assay, coverslips were placed in petri dishes avoiding overlap and scratches. Coverslips were rocked in 70% ethanol for 30 min and then in 96% ethanol for further 30 min. Coverslips were then left to dry in the tissue culture hood and petri dishes were sealed with parafilm.

2.2.7 Fibronectin coating of cell plates or glass coverslips

Human fibronectin solution was diluted at a 10µg/ml concentration and added to the desired container at appropriate volumes followed by a 30 min incubation at 37°C. The fibronectin solution was then washed out twice with PBS followed by seeding the cells onto the coated surface.

2.2.8 Cell proliferation Assay

Cells were seeded in 96 well plates coated with fibronectin at a cell density of 1000 cells/ml in growth media. On the day of the assay and following two PBS washes, 50µl of methyl thiazolyldiphenyl tetrazolium bromide (MTT) diluted in serum free media (0.5mg/ml) were added to the cells and the plates were incubated at 37°C for 3 hours. The MTT was then aspirated and replaced with equal volumes of DMSO. The 540 nm absorbance was measured using an Alpha-fusion plate reader. Three technical replicates were included for each condition. The proliferation assay was performed 1, 2 and 4 days post cell seeding.

2.2.9 Transient transfection with the Lipofectamine 2000 reagent

MDA-MB-231 and BT-549 cells were seeded at 10^5 cells/ml and incubated overnight. On the following day, growth media were replaced with fresh media without antibiotics. The following transfection mixes were then prepared according to the size of the plate used.

	2cm tissue culture plate (2ml)	**10cm tissue culture plate (10 ml)**
Tube A	3µl of lipofectamine 200 100µl of OptiMEM media	15µl of lipofectamine 200 500µl of OptiMEM media
Tube B	3µg of DNA 100µl of OptiMEM media	15µg of DNA 500µl of OptiMEM media

Table 2-8 Lipofectamine 2000 transfection reaction mix.

After 5 minutes at room temperature, tube A mixture was added to tube B and were left to incubate for further 15 min at room temperature prior to being added to the cells. Cells were incubated with the transfection mix overnight. Subsequent experiments followed the following day or cells were left to recover with fresh media for another 24h.

2.2.10 Transient transfection with the Calcium Phosphate kit

HEK-293 cells were seeded at a 10^5 cells/ml density and were incubated overnight at 37°C. On the following day, media were changed 4 hours before transfection. Transfection mixes were prepared as described below:

	2 cm culture dish (2ml)	**10 cm culture dish (10ml)**
Tube A	6µl of 2.5M $CaCl_2$ 4µg DNA Make up to 60µl with sterile water	30µl of 2.5M $CaCl_2$ 20µg DNA Make up to 300µl with sterile water
Tube B	60 µl 2x Hepes buffered saline	300µl 2x Hepes buffered saline

Table 2-9 Calcium Phosphate kit transfection reaction mix.

Following the preparation of the reaction mix, contents of tube A were slowly added to tube B with aeration and left for 30 min at room temperature. The mixture was added to the cells drop-wise and cells were incubated overnight at 37°C. On the following day, cells were replenished with fresh media and were left for another 24 hours to recover.

2.2.11 Transient transfection with the Hiperfect reagent

Cells were seeded at $2x10^4$ cells/ml and were incubated overnight at 37°C. On the day of transfection, media were changed and 3µl of 20µM siRNA were added to 97µl optiMEM along with 10µl of the hiperfect reagent. The mixture was left for 15 min at room temperature before being added drop-wise to the cells resulting in a 30nM working siRNA concentration **(table 2-6)**. Cells were then incubated for appropriate time periods. Optimal IQGAP3 knockdown was achieved between 72h and 96h post transfection.

2.2.12 Lysophosphatidic Acid (LPA) treatment of cells

LPA sodium salt was dissolved in 0.1% fatty acid free BSA:PBS to achieve a 5mM stock solution. The mixture was placed in a water bath at 37°C for 1h in order for the LPA to be fully dissolved. The solution was then stored at 4°C. Prior to LPA treatment, cells were replenished with fresh growth media. The LPA stock solution was also put on the roller and brought to room temperature. 4µl of stock solution were added in each well to achieve a 10µM working solution. Cells were incubated with LPA for 30 min. A control well was included which was treated with 4µl of 0.1% fatty acid free BSA:PBS alone. Following incubation cells were washed with PBS and immediately fixed with 4% PFA.

2.2.13 Immunofluorescence

All immunofluorescent staining experiments were performed on cells seeded at appropriate density on fibronectin coated coverslips. On the day of immunofluorescent labelling, cells were washed 3 times with PBS and fixed with 4% PFA for 20 min. Following another 3 PBS washes, cells were permeabilised with 0.2% X-triton to break the cell membranes for 5 minutes. Following another 3 washes, coverslips were blocked with 5% FBS for 30 min and 3% BSA:PBS for another 30 min. Cells were then incubated with the primary antibody appropriately diluted in 3% BSA:PBS for 2 hours in the dark **(table 2-3)**. Once again, cells were washed 3 times with PBS. Secondary antibodies along with Phalloidin and DAPI were diluted appropriately in 3% BSA:PBS. Cells were

then incubated with the prepared mixture for 1h in the dark **(table 2-4)**. Coverslips were then washed twice in PBS and once in ddH_2O before being mounted on glass slides with the Fluorsave reagent. Coverslips were left in room temperature overnight and then stored at 4°C in the dark. Cells were imaged on an Olympus IX71 microscope using Image ProPlus AMS software.

2.2.14 Image processing and cell shape analysis

Cell images were loaded on ImageJ where cells were manually drawn around to determine the cell shape. Shape descriptive parameters such as cell area and relative circularity were obtained for each cell. A circularity value of 1 indicates a perfect circle. Cell elongation was evaluated by the relative elongation parameter which was calculated by subtracting the circularity value from 1. 90 cells over 3 independent experiments were included in shape analyses.

2.2.15 Proximity ligation assay (PLA)

The proximity ligation assay was performed using the Duolink® In Situ Detection Reagents Red based on the manufacturer's protocol. BT-549 cells over-expressing IQGAP3-HA alone or IQGAP3-HA together with PAK6-myc or PAK1-myc were used in this assay to assess the interaction between IQGAP3 and PAK1 as well as IQGAP3 and PAK6. The procedure of fluorescent staining was followed as normal up until the incubation with the primary antibodies; in this case all conditions were probed for IQGAP3 and myc with primary antibodies raised in rabbit and mouse respectively as the PLA protocol requires the use of antibodies of opposite species. After the incubation with the primary antibodies, cells were then washed twice with buffer A provided with kit. From then on, 60 µl open droplet reactions were used. All incubations were performed in a dark and well humidified environment at 37°C. Plus and Minus PLA probes were diluted 1:5 in 3% BSA:PBS-Tween and were allowed to mix for 20 min at room temperature. Mixtures were added onto cells and incubated for 1h followed by another two washes with buffer A. Ligase was then diluted by 1:40 in ligation stock and added onto cells for 30 min. Ligation events were then amplified by adding polymerase diluted by 1:80 in amplification stock for 1 hour and 40 min. Cells were then washed twice with buffer B and twice with 0.01% buffer B. Cells were then subsequently stained with phalloidin 488 for 1h, washed twice with PBS, once with ddH_2O and then left to dry. Coverslips were then inverted on mounting medium with DAPI and sealed with nail polish. After 10 min coverslips were stored at -20°C. In parallel to the PLA assay conventional immunofluorescent staining using secondary antibodies was also performed to

determine transfection efficiencies of IQGAP3-HA and myc tagged PAK1 and PAK6. The PLA signal of imaged cells was quantified using the particle analysis plugin of ImageJ. The cell area of each cell was also obtained and a ratio of PLA signal over cell area was calculated for each cell.

2.2.16 Preparation of TRITC conjugated gelatin

Gelatin was dissolved in 61 mM NaCl and 50 mM sodium borohydrite; pH was set at 9.3 and the mix was incubated for one hour at 37°C. 1.8mg rhodamine was then added to the gelatin and was mixed by rolling for 4 h in the dark at room temperature. The rhodamine-conjugated gelatin (TRITC-gelatin) was then filtered through a 0.45 µm filter and injected into a dialysis cassette and left to dialyse against PBS for 3 days with frequent changes of PBS. Dialysed TRITC-gelatin was then spun down at 4000 rpm for 2 min before mixing it with 1 g sucrose by rolling. 1ml aliquots were stored at 4°C in the dark.

2.2.17 Invadopodia assay

While working in the dark, ethanol-washed coverslips were then coated with 200µl of TRITC-gelatin solution and incubated for 10 min at room temperature. Coverslips were then fixed with 0.5% glutaraldehyde for 15 min before being washed with PBS. The coverslips were then quenched with 5 mg/ml of sodium borohydride in PBS for 3 min followed by 3 PBS washes. The TRITC-gelatin coated coverslips were then sterilised in 70% ethanol, left to dry and then incubated with DMEM for 1 h at 37°C. Cells to be tested on the invadopodia assay were dissociated with cell dissociation buffer before seeding them at 2×10^4 cells in 1 ml on each TRITC-gelatin coated coverslips. Cells were then incubated for appropriate time periods at 37°C and fixed with 4% PFA. Staining was performed as described above with Phalloidin 488 so that the actin cytoskeleton fluoresces green against the red gelatin. 150 cells over 3 independent experiments were imaged to determine % of cells with invadopodia capacity.

2.2.18 Random 2D migration assay

Cells were seeded at appropriate density on 10µg/ml coated wells of a 6 well plate. On the day of imaging, growth media were replaced with 3 ml of fresh media along with 60µl of HEPES buffer. The plates were sealed and imaged under the Olympus IX71 microscope using Image Pro Plus AMS software at 37°C. Cell images were taken every 5 min for 16 hours. Files were extracted,

saved as AVI and then loaded on the Manual tracking plugin of ImageJ to obtain the X and Y coordinates of each frame. Analysis was then performed on Mathematica using the Chemotaxis 6.0 notebooks developed in-house by Graham Dunn and Gareth E. Jones. At least 30 cells were tracked and analysed over 3 independent experiments.

2.2.19 Preparation of cell lysates

In order to check for protein expression, cell lysates were prepared preferably when cells reached approximately 80% confluency. Cells were washed twice with PBS followed by adding 2x gel sample buffer in appropriate volumes according to the size of the plate. Cells were then scraped off and pipetted into Eppendorf tubes. Lysates were then boiled for 5min and stored at -20°C.

2.2.20 Immunoprecipitation using the GFP trap

Cells were washed with ice cold PBS and scraped into Eppendorf tubes. The tubes were then centrifuged at 300x g for 3 minutes at 4°C followed by another 2 washes with ice cold PBS. Cells were then resuspended in GFP trap lysis buffer **(table 2-2)** containing the protease inhibitor cocktail. In the case of assessing interactions of over-expressed IQGAP3-GFP in HEK-293 cells, cell conditions were lysed in half the volume of lysis buffer and were subsequently mixed together. Lysates were left on ice for 30 min, mixing them every 10 min. In the meantime, the GFP trap beads were equilibrated by washing them 3 times with the GFP trap wash buffer **(table 2-2)**. Lysates were then centrifuged at 20,000 x g for 10 minutes at 4°C and their supernatants were mixed with the beads and placed on the rotor for 1h at 4°C. A small fraction of each lysate was kept to check for protein expression. Following rotation, the beads along with the trapped proteins were washed 3 times with the GFP wash buffer. 2x sample buffer was added to the washed beads and the beads were boiled for 10 min.

2.2.21 Gel electrophoresis and immunoblotting

Samples were boiled again prior to being subjected to gel electrophoresis. Lysates were loaded on 6.5%-12.5% gels and proteins were separated by sodium dodecyl sulphate polyacrylamide gel electrophoresis (SDS-PAGE) at 125V for 1.5h in 1x running buffer. Proteins were then blotted onto nitrocellulose membrane for 1-2 hours at 100V in 1x transfer buffer **(table 2-2)**. Blots were then blocked in TBST with either 5% w/v non-fat milk powder, or 5% w/v BSA for 1 hour at room temperature. Blocked membranes were then rolled overnight at 4°C in primary antibody diluted

appropriately in the same blocking solution **(table 2.3)**. Membranes were then washed 3 times for 10 min in TBST to wash off unbound primary antibody. Membranes were then rolled in appropriate dilution of secondary antibody in the appropriate blocking solution for 1h at room temperature **(table 2.4)**. Following that, membranes were washed in TBST as before and probed proteins were visualised using the Pierce enhance chemiluminscence (ECL) kit.

2.2.22 Stripping of nitrocellulose membranes

In cases where re-probing of membranes was required, membranes were rocked in mild stripping buffer twice for 15 min each time **(table 2-2)**. Membranes were subsequently washed with PBS for 5 minutes and were ready to be blocked and re-probed with the appropriate primary antibody as described above.

2.2.23 Densitometry

Densitometric analysis of protein bands was performed on ImageJ where each band was attributed a mean grey value according to its intensity. These values were normalised to the background noise as well as the loading control used in each experiment. In some experiments, values were also made relative to the control condition.

2.2.24 Statistical analysis

Statistical analysis was performed where it was required always using datasets generated from 3 independent experiments. Analysis involved one-way Analysis of Variance (ANOVA) followed by Tukey's post hoc testing or unpaired t-tests based on the experimental conditions. Statistical analysis was reached when $P \leq 0.05$. One star (*) indicates a P value ≤0.05, (**) indicate a P value ≤0.01, (***) indicate a P value ≤0.001. Error bars represent the standard error of the mean (SEM).

Chapter 3

Characterisation of triple negative breast cancer cell lines.

Chapter 3 : Characterisation of triple negative breast cancer cell lines

3.1 Introduction

This project originated from a tissue micro-array where mRNA levels of IQGAP3 (a scaffold protein involved in cytoskeletal dynamics) were found to be upregulated in triple negative tumours compared to other types of breast cancer and normal tissue (de Rinaldis et al., 2013), **(figure 1.6)**. The aggressive behaviour exhibited by triple negative tumours is largely attributed to their invasive and metastatic capacity (Anders and Carey, 2009). Tumour cells undergo extensive cytoskeletal rearrangements including changes in cell adhesion and polarity in order to become motile (Thompson et al., 2005). Consequently, cell morphology and cell migration are features that have been extensively studied in the context of cancer cell metastasis and will also be carefully considered in this chapter.

The invasive behaviour of triple negative tumours (Liedtke et al., 2008) led us to hypothesise that increased expression of IQGAP3 might be contributing to triple negative breast cancer cell motility and invasion. IQGAP3 is the third and most recently discovered member of the IQGAP family of scaffold proteins which are all involved in cytoskeletal dynamics by interacting with Rac1 and Cdc42 as well as the actin cytoskeleton (White et al., 2009). Despite their high homology and structural similarity, IQGAPs have distinct expression patterns; IQGAP1 appears to be ubiquitously expressed while the expression of IQGAP2 and IQGAP3 is much more tissue restricted with IQGAP3 primarily being found in the brain, lung, testis and the bowel (White et al., 2009). Their structural similarity suggests that IQGAPs could have overlapping activity but their expression pattern supports the possibility of unique functionality as well.

IQGAP1 being the first family member to be discovered is also the most extensively characterised (Smith et al., 2015). IQGAP1 has a well described role in biological processes such as cell migration and adhesion hence it is perhaps not surprising that this particular IQGAP has been found to be upregulated in multiple carcinomas (White et al., 2009). For example, IQGAP1 is reported to be involved in cell adhesion as the association of IQGAP1 to e-cadherin (which is normally antagonised by calmodulin) disrupts cell-cell junctions (Li et al., 1999). It is not known whether IQGAP3 plays a similar role in cell adhesion.

Additionally, IQGAP1 has been reported to localise at the leading cell edge where it promotes directional cell migration; IQGAP1 is found in a complex with CLIP-170 and activated Rac1/Cdc42

which in turn recruits elongating microtubules towards the leading cell edge of Vero cells ultimately implicating IQGAP1 in cell polarisation (Fukata et al., 2001). Furthermore, IQGAP1 is also able to bind Phosphatidylinositol 4, 5 bisphosphate (PIP_2); this interaction is crucial for the subsequent activation of Arp2/3 and the formation of a single leading cell edge (Choi et al., 2013). Meanwhile the role of IQGAP3 in cell migration is less well described; although IQGAP3 has also been reported to promote clustering of Adenomatous polyposis coli (APC) at the leading cell edge where it normally regulates the elongating microtubule network (Caro-Gonzalez et al., 2012). Moreover, IQGAP3 but not IQGAP1 induce neurite outgrowth in PC12 cells and axonal elongation in primary hippocampal neurons further supporting a role for IQGAP3 in the regulation of the actin cytoskeleton (Wang et al., 2007). Furthermore, IQGAP3 was reported to regulate the migration and invasion ability of A549 lung cancer cells by interacting with ERK1 upon EGF stimulation (Yang et al., 2014). Diminishing IQGAP3 in pancreatic cancer BXPC-3 and SW1990 cells also reduced their migration ability (Xu et al., 2016). Interestingly, increased expression of IQGAP3 was recently reported in metastatic lung adenocarcinomas and was also linked to poor prognosis (Wu et al., 2015).

Invasion is a crucial part of metastasis that allows tumour cells to escape from the primary tumour and enter the vasculature which then allows the colonisation of distant organs. Invasion has been shown to occur via multiple mechanisms; it can be contractility mediated and matrix degradation independent where pulling forces induce the forward movement of the cell in a 3D environment (Poincloux et al., 2011; Sahai and Marshall, 2003). Cell invasion can also be mediated via the formation of invadopodia (Leong et al., 2014).

Invadopodia are actin rich protrusions that secrete metalloproteases able to degrade the basement membrane (Murphy and Courtneidge, 2011). This mechanism of invasion has been shown to be employed by breast cancer cells both *in vitro* and *in vivo* (Hashim et al., 2013; Leong et al., 2014). It is already known that IQGAP1 binds components of the exocyst complex and facilitates the delivery of MT1-MMP to these protrusions (Sakurai-Yageta et al., 2008), but whether IQGAP3 contributes to invadopodia activity is unknown.

In contrast to IQGAP1 and IQGAP3 the function of IQGAP2 appears to be significantly different and unique. In fact, IQGAP2 is reported to have tumour suppressor properties as IQGAP2 deficient mice develop hepatocellular tumours which exhibit increased expression of IQGAP1(Schmidt et al., 2008). Deciphering the functional differences between IQGAP2 and the other members of the family in the context of cancer biology is thus perhaps more straightforward.

Ultimately, there is sufficient evidence suggesting that IQGAPs can have differential functionality despite their high homology (White et al., 2009). Consequently, the investigation of a specific role of IQGAP3 in triple negative breast cancer was undertaken.

3.2 Results

3.2.1 IQGAP expression

At the beginning of this study priority was given to the establishment of crucial research tools such as the validation of a specific IQGAP3 antibody as well as tagged IQGAP genetic constructs. An IQGAP1-GFP construct as well as an IQGAP1 antibody was previously validated in our lab (Fram et al., 2014). A myc-tagged IQGAP2 construct was acquired to have a complete panel of the IQGAP family. A gateway compatible IQGAP3 entry clone was acquired and cloned in GFP and HA tagged destination clones. The resulting constructs were validated by sequencing and western blotting. In order to achieve good protein levels HEK-293 cells were transfected with IQGAP1-GFP, IQGAP2-myc, IQGAP3-GFP and IQGAP3-HA. Cell lysates were probed with anti-GFP, anti-myc and anti-HA to confirm expression (**figure 3.1A**). Cell lysates were then probed with an IQGAP1 antibody which specifically detected IQGAP1 at 222kDa (195kDa is the expected size of IQGAP1 plus 27kDa which is the expected size of GFP) (**figure 3.1B**). The same lysates were then probed with a new commercially available IQGAP3 antibody. The chosen IQGAP3 antibody specifically detected IQGAP3-GFP at expected size of 212kDa (185kDa is the expected size of IQGAP3 plus 27kDa which is the expected size of GFP) (**figure 3.1C**).

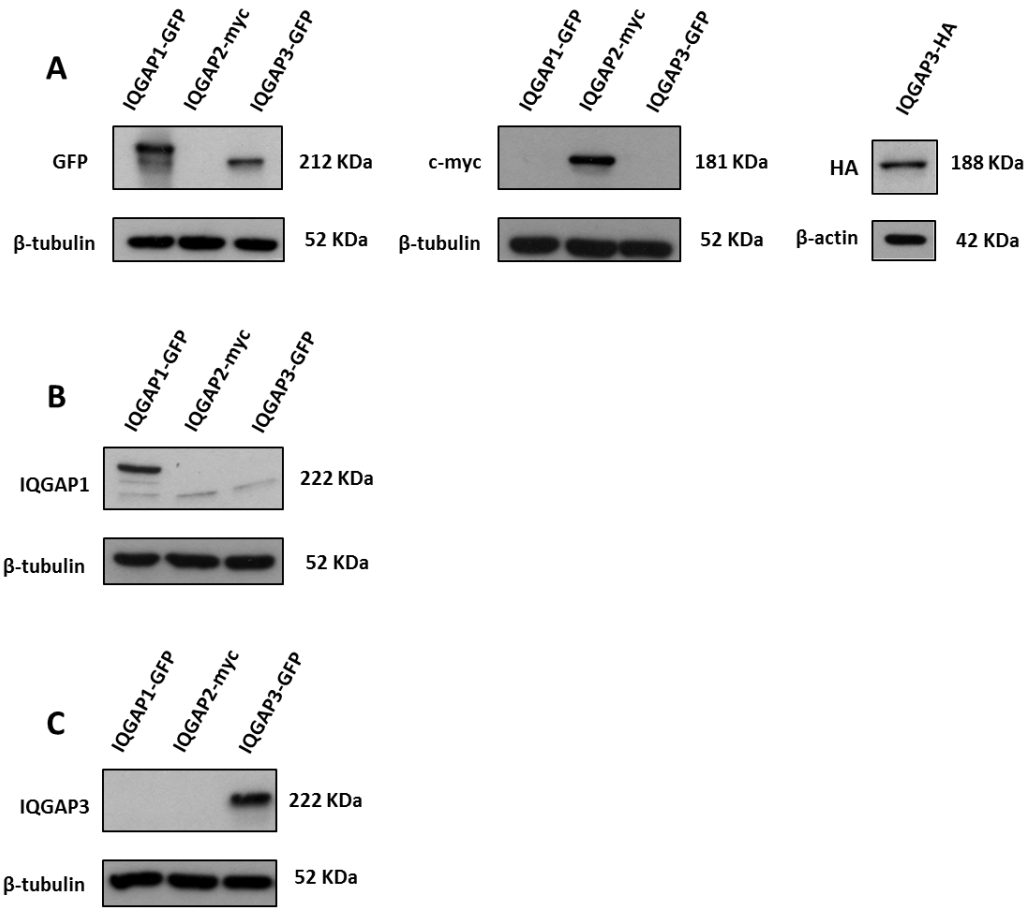

Figure 3.1 IQGAP constructs and antibody validation. HEK-293 cells were transfected with IQGAP1-GFP, IQGAP2-myc, IQGAP3-GFP and IQGAP3-HA respectively. (A) Cell lysates were probed for GFP c-myc and HA to confirm successful cloning and achieved transfection. (B) Cell lysates were probed for IQGAP1 to confirm IQGAP1 specificity. (C) Cell lysates were probed for IQGAP3 to check for IQGAP3 specificity. β-tubulin (52kDa) and β-actin (42kDa) were used as loading controls.

3.2.2 IQGAP3 expression in triple negative breast cancer cell lines

Evidence of IQGAP3 expression in breast cancer cell lines was obtained from a tissue micro-array measuring IQGAP3 mRNA levels (de Rinaldis et al., 2013). However, endogenous IQGAP3 expression across a panel of triple negative breast cancer lines has never been shown before. We thus sought to confirm endogenous protein expression of IQGAP3 and IQGAP1 for comparison across a panel of triple negative cell lines, considering the different expression patterns exhibited by IQGAPs (White et al., 2009). Probing for IQGAP2 was not performed taking into account that IQGAP2 has tumour suppressive properties (Schmidt et al., 2008) and thus it would be unlikely for it to drive triple negative breast cancer metastasis. The MCF10A cell line was included as a near normal representative (Soule et al., 1990).

Quantification of expression levels revealed that both IQGAP1 and IQGAP3 are expressed across the chosen cell line panel **(figures 3.2, 3.3)**. Interestingly, IQGAP3 levels are higher in the MB-231 cell line compared to those observed in the near normal MCF10A cells (Soule et al., 1990)**, (figure 3.2B)**. Additionally, apart from the HCC38 cells that exhibited the lowest IQGAP3 levels across the panel, the remaining triple negative lines trended towards having a higher IQGAP3 expression than the MCF10A cell line **(figure 3.2B)**.

Interestingly, IQGAP1 expression does not appear to follow the same trend across the cell line panel **(figure 3.3)**. In fact, no triple negative cell line was observed to have higher levels of IQGAP1 compared to the MCF10A cells.

Moreover, MB-231 cells, which had higher levels of IQGAP3 compared to MCF10A cells, are an established model for invasion studies (Holliday and Speirs, 2011). To further explore IQGAP3 expression in triple negative breast cancer, we compared MB-231, MCF10A and another line known to be used in invasion studies and particularly invadopodia assays; the BT-549 cell line (Monteiro et al., 2013; Moshfegh et al., 2015; Yamaguchi et al., 2011). Indeed, IQGAP3 expression of BT-549 cells sits between the one of MCF10A and MB-231 cells **(figure 3.4)**.

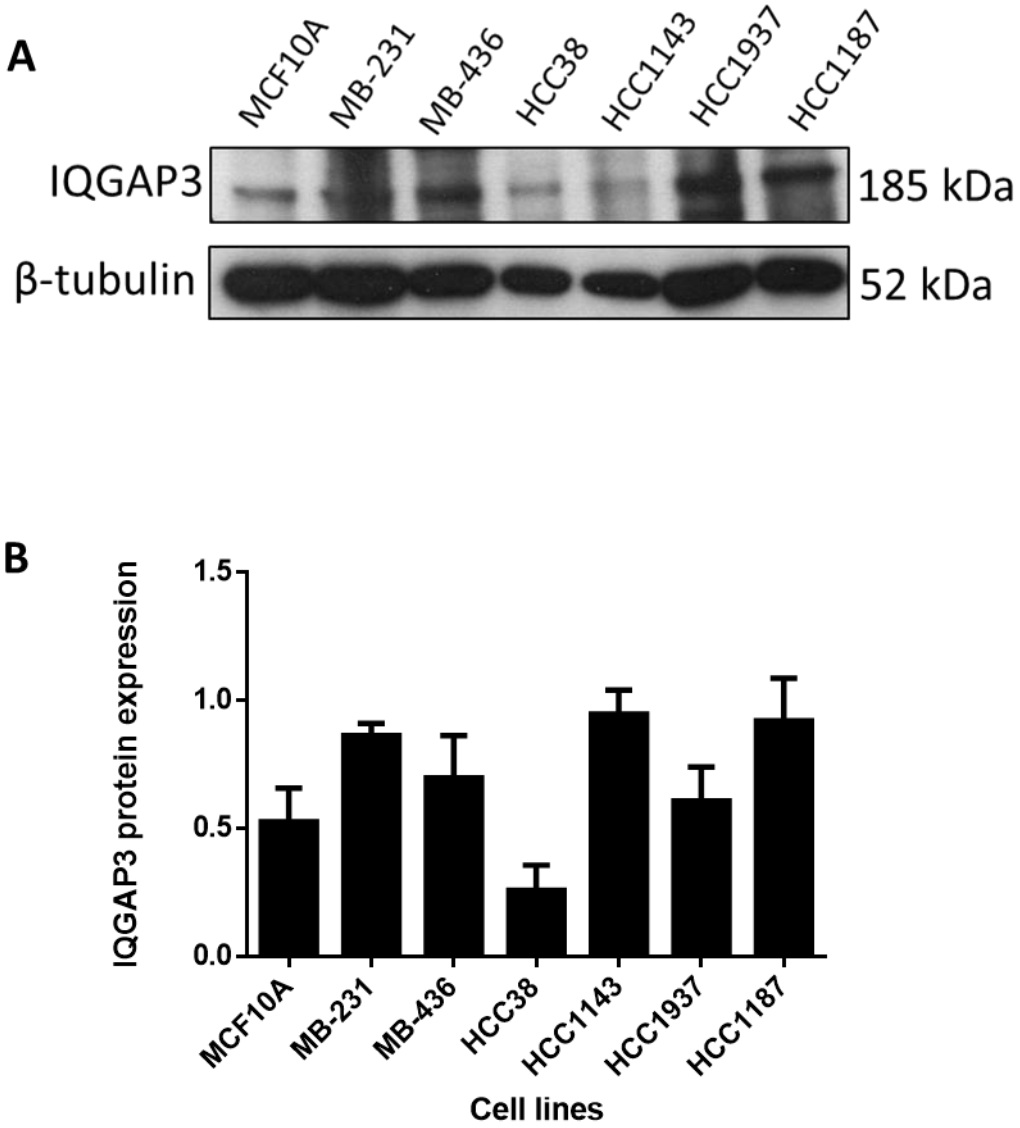

Figure 3.2 IQGAP3 expression in triple negative breast cancer cell lines. (A) Cell lysates of a panel of triple negative lines including the near normal representative MCF10A cell line were probed for IQGAP3 (Abnova, 185kDa). β-tubulin was used as a loading control (52kDa). (B) Expression levels were quantified by densitometric analysis on ImageJ and normalised against the loading control and background noise. Bars represent the mean normalised expression levels and error bars represent the SEM. (N=3)

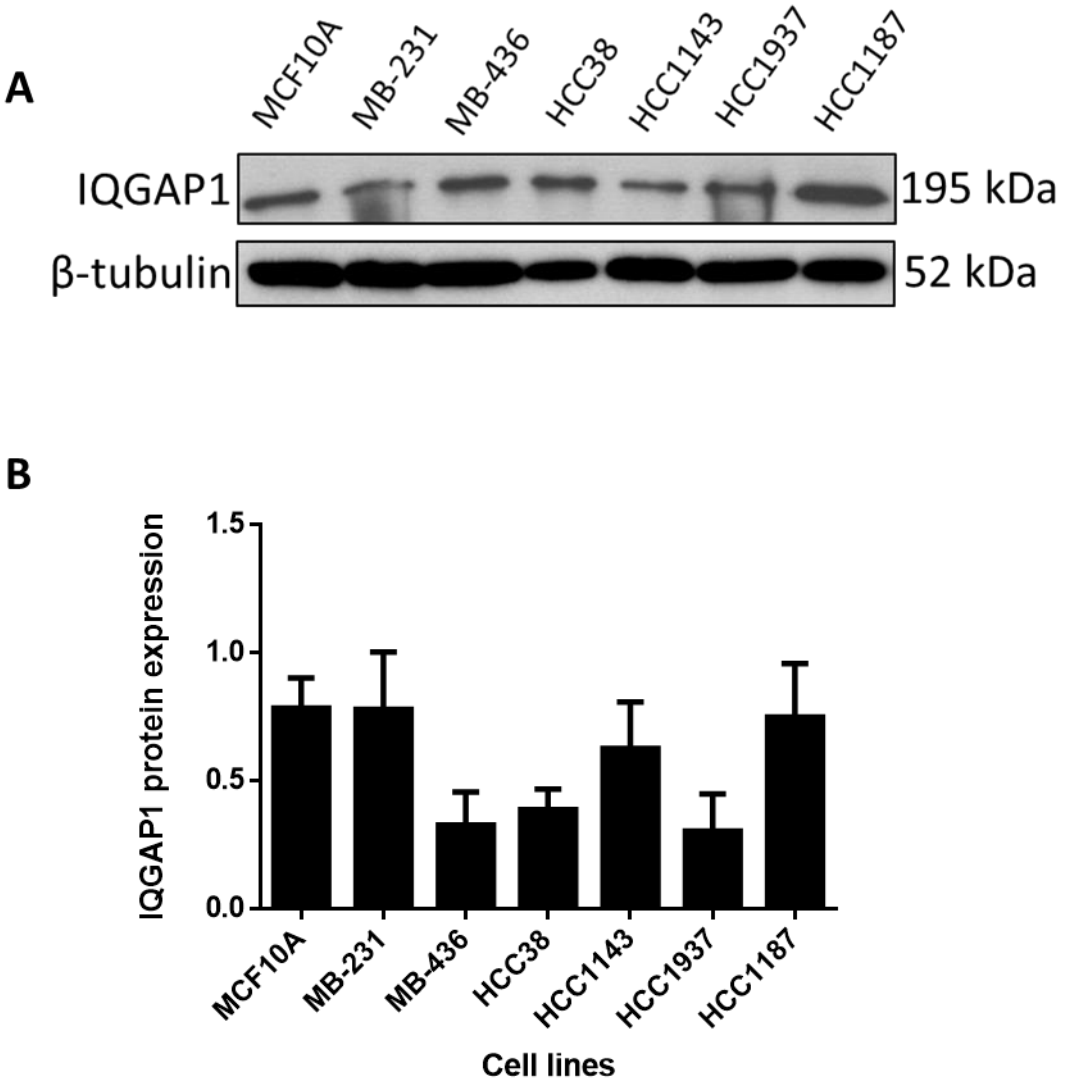

Figure 3.3 IQGAP1 expression in triple negative breast cancer cell lines. (A) Cell lysates of a panel of triple negative lines including the near normal representative MCF10A cell line were probed for IQGAP1 (195kDa). β-tubulin was used as a loading control (52kDa). (B) Expression levels were quantified by densitometric analysis on ImageJ and normalised against the loading control and background noise. Bars represent the mean normalised expression levels and error bars represent the SEM (N=3).

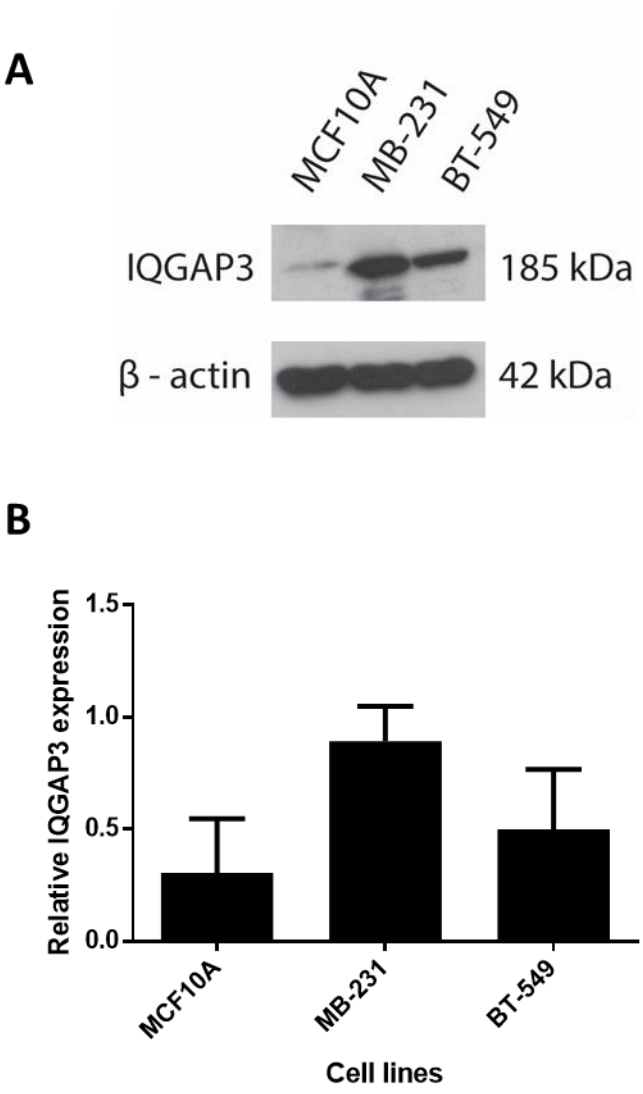

Figure 3.4 IQGAP3 expression. (A) Cell lysates of MCF10A, MB-231 and BT-549 cells were probed for IQGAP3 (Sigma, 185kDa). β-actin was used as a loading control (42kDa). (B) Expression levels were quantified by densitometric analysis on ImageJ and normalised against the loading control and background noise. Bars represent the mean normalised expression levels and error bars represent the SEM (N=3).

From the cell panel tested for IQGAP expression, the MB-231, BT-549, MB-436 and HCC38 were chosen to be further characterised in culture. This shortlisting of cell lines was decided based on reviewing published cell motility studies using triple negative cell lines, the observed IQGAP3 expression levels as well as personal communications advising on ease of cell culture. The MCF10A cell line was also cultured as a representative near normal cell line.

The MB-231, MB-436 and BT-549 cell lines fall under the mesenchymal-like category according to the TNBC subtypes classification published by (Lehmann et al., 2011). Interestingly, the mesenchymal-like cell lines appear to have increased expression of genes associated with cell motility such as the Rho pathway as well as genes associated with EMT (Lehmann et al., 2011). The basal-like type cell lines show increased expression of proliferation and DNA response associated genes such as the BRCA1 pathway (Lehmann et al., 2011).

The MB-231 and MB-436 cells are epithelial spindle shaped cells that were derived from pleural effusions of patients at M.D. Anderson Hospital and Tumour Institute in 1973 and 1976 respectively (Cailleau et al., 1978). The BT-549 is also a mesenchymal-like cell line derived from an invasive ductal carcinoma in 1978 (Littlewood-Evans et al., 1997). The HCC38 cell line is of epithelial origin and was derived from a primary breast ductal carcinoma in 1992 (Gazdar et al., 1998). The MCF10A cell line was derived from culturing fibrocystic breast tissue that was spontaneously immortalised (Soule et al., 1990).

The invadopodia making MB-231 cells has traditionally been regarded as an invasive cell line *in vivo* and *in vitro* which is consistent with the aggressive behaviour of triple negative breast cancer (Holliday and Speirs, 2011). The BT-549 cell line also has invadopodia making capacity and has also been successfully employed in xenograft studies (Tate et al., 2012). The MB-436 and HCC38 cells are also considered invasive given their ability to form tumours when injected orthotopically in immunocompromised mice (Iorns et al., 2012; Xu et al., 2015). However, MB-436 and HCC38 cells have not been previously reported to make invadopodia.

3.2.3 Cell morphology

Cell shape was primarily examined to check for particular morphological phenotypes that have been linked to cell invasion (Clark and Vignjevic, 2015). Cancer cells are normally in contact with extracellular matrix which involves a crucial part of the tumour microenvironment influencing cancer progression and metastasis (Bissell and Hines, 2011). Immunohistochemical analysis on primary breast tumour samples has in fact suggested that fibronectin expression correlates with poor prognosis and progression free survival (Bae et al., 2013). In order to examine cell morphology while trying to retain some aspects of the tumour microenvironment, cells were seeded on fibronectin coated glass coverslips and stained with TRITC phalloidin that stains the actin filaments as a marker of cell shape. Cell morphology features such as cell area and circularity were thus measured. The relative cell elongation parameter was obtained by subtracting the circularity value from 1.

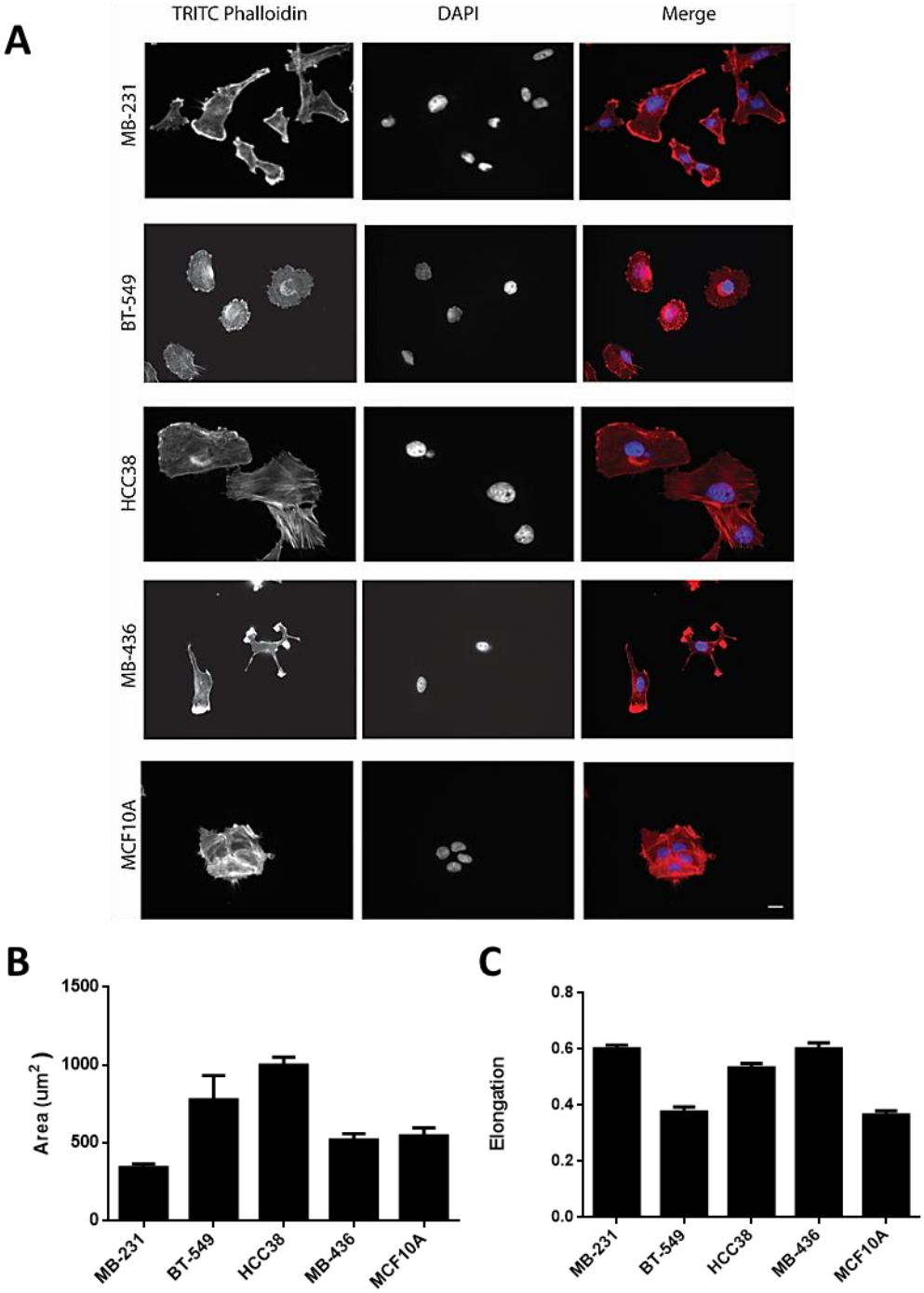

Figure 3.5 Cell morphology. (A) Cells were seeded on fibronectin coated coverslips. Cells were subsequently fixed and stained with TRITC Phalloidin (red) indicating the actin cytoskeleton and DAPI (blue) indicating the nuclei. Scale bar = 10µm. Cells were imaged and analysis was performed on ImageJ to obtain (B) the cell area and (C) elongation index. Analysis was performed on 30 cells per experiment. Bars represent the mean values and error bars represent the SEM (N=3).

The first observation that was made is that unlike the normal MCF10A cells, all the breast cancer cell lines that were evaluated grew as single cells while no colony forming capacity was observed (**figure 3.5A**). The absence of colony forming cells indicates the loss of ability to form cell-cell interactions. This is one of the primary characteristics of epithelial to mesenchymal transition (EMT) which is accompanied by loss of e-cadherin expression that normally maintains cell-cell junctions and tissue integrity (Thiery, 2002). This feature is consistent with the aggressive behaviour of triple negative breast cancer.

The cells were also evaluated in terms of other morphological features such as their area and elongation. In terms of their area, this feature varied a lot across the cell panel with the basal-like HCC38 cells appearing to have the largest cell area (**figure 3.5A, 3.5B**). The MB-231 and MB-436 which also express high levels of IQGAP3 **(figure 3.2B)** were shown to be the most elongated cells consistent with their mesenchymal phenotype (**figure 3.5C**) but also have small cell area **(figure 3.5B)**. Nonetheless, levels of IQGAP3 expression do not appear to strongly correlate with a particular morphological feature.

3.2.4 Random 2D migration

The migratory ability of the triple negative cell line panel was assessed by monitoring random cell movement on fibronectin coated plates (**figure 3.6**). Fibronectin is part of the interstitial ECM and influences cell behaviour by interacting with integrins (Huttenlocher and Horwitz, 2011) so once again it was considered to be a suitable matrix for this assay.

The MB-231 cell line is highly motile and has been widely used in both 2D and 3D migration assays (Holliday and Speirs, 2011). However, the migratory ability of the other cell lines chosen here has not been as extensively characterised.

Manual cell tracking and analysis on Mathematica revealed that all cancer cell lines tested were highly motile apart from the BT-549 cell line which exhibited lower mean cell speed (**figure 3.6**). Again, levels of IQGAP3 expression did not correlate with cell speed as high IQGAP3 expressing MB-231 and MB-436 cells have the same cell speed as low IQGAP3 expressing HCC38 cells (**figures 3.2B, 3.6B**).

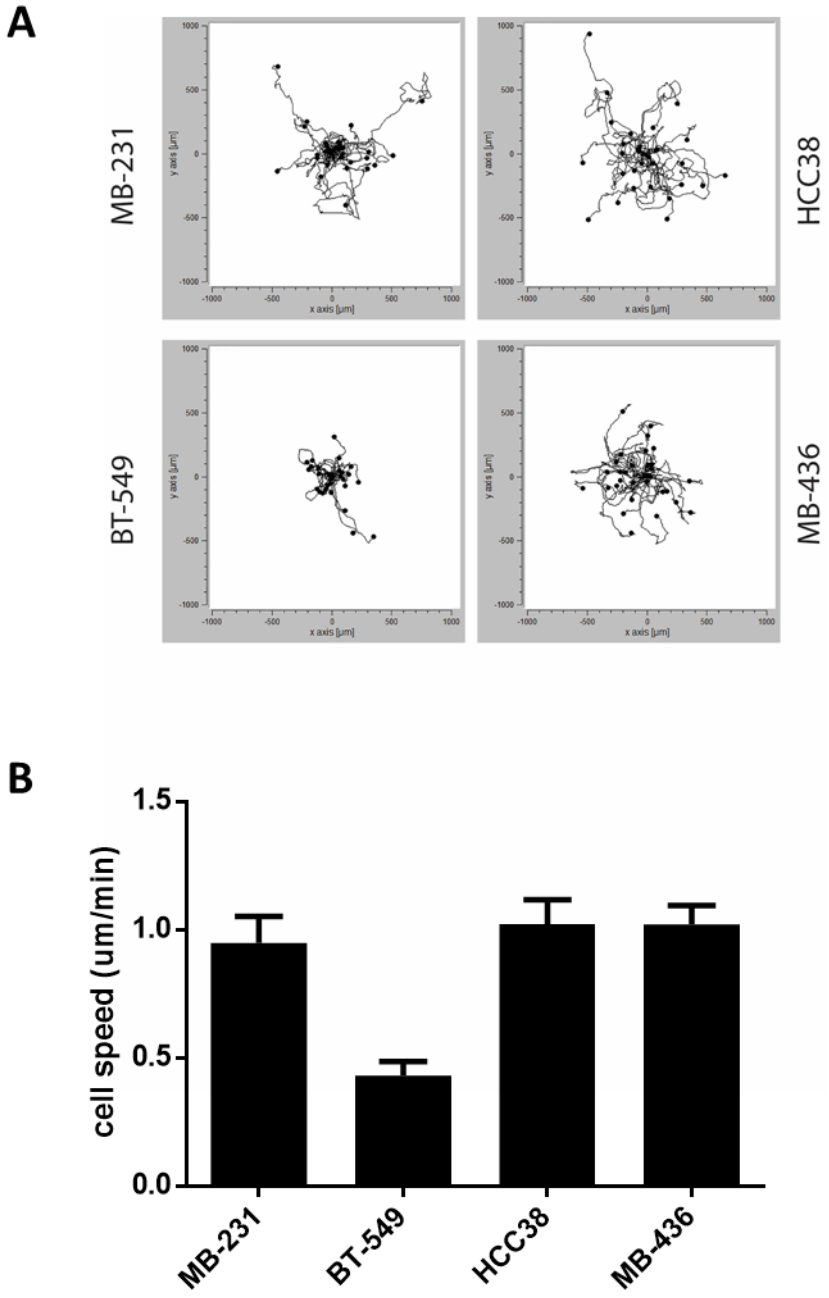

Figure 3.6 Random 2D migration on fibronectin. (A) Cell migration plots obtained on Mathematica after importing manual tracking data from ImageJ. (B) Quantification was performed on Mathematica. Bars represent the mean cell speed and error bars represent the SEM (N=3).

3.2.5 Invadopodia

Formation of invadopodia is considered indicative of invasive potential *in vitro* and *in vivo* (Eckert et al., 2011; Leong et al., 2014). We sought to examine the invasive potential of our cell lines knowing that MB-231 cells are widely used in invadopodia research (Mader et al., 2011) . In order to detect invadopodia formation *in vitro*, cells were seeded on glass coverslips previously coated with TRITC-conjugated gelatin. To allow invadopodia formation to occur cells were incubated at 37°C for 3h and were subsequently fixed with PFA and stained with Phalloidin 488 resulting in green stained cells over a red stained matrix (Hashim et al., 2013). Cells were considered able to make invadopodia when the actin puncta revealed by the phalloidin stain indicating the protrusive structure of invadopodia coincided with black holes in the red gelatin indicating matrix degradation (Hashim et al., 2013).

Out of the 4 cell lines that were subjected to the assay the HCC38 and MB-436 cells did not make any invadopodia (**figure 3.7**). Interestingly, reviewing the literature revealed that there is no published evidence of HCC38 or MB-436 cells being used in invadopodia assays. Together, these observations suggest that the HCC38 and MB-436 cells do not make invadopodia. As expected, the MB-231 cells exhibited definitive evidence of invadopodia formation and activity (**figure 3.7A, 3.7B**) which is consistent with their widespread use in invadopodia research. The BT-549 cells showed very little evidence of invadopodia presence at the 3h incubation as only a few very small invadopodia were detected. This observation suggested that the BT-549 cells might require longer incubations on the gelatin matrix to form active invadopodia. Further characterisation of the invadopodia capacity of the BT-549 cells was thus warranted.

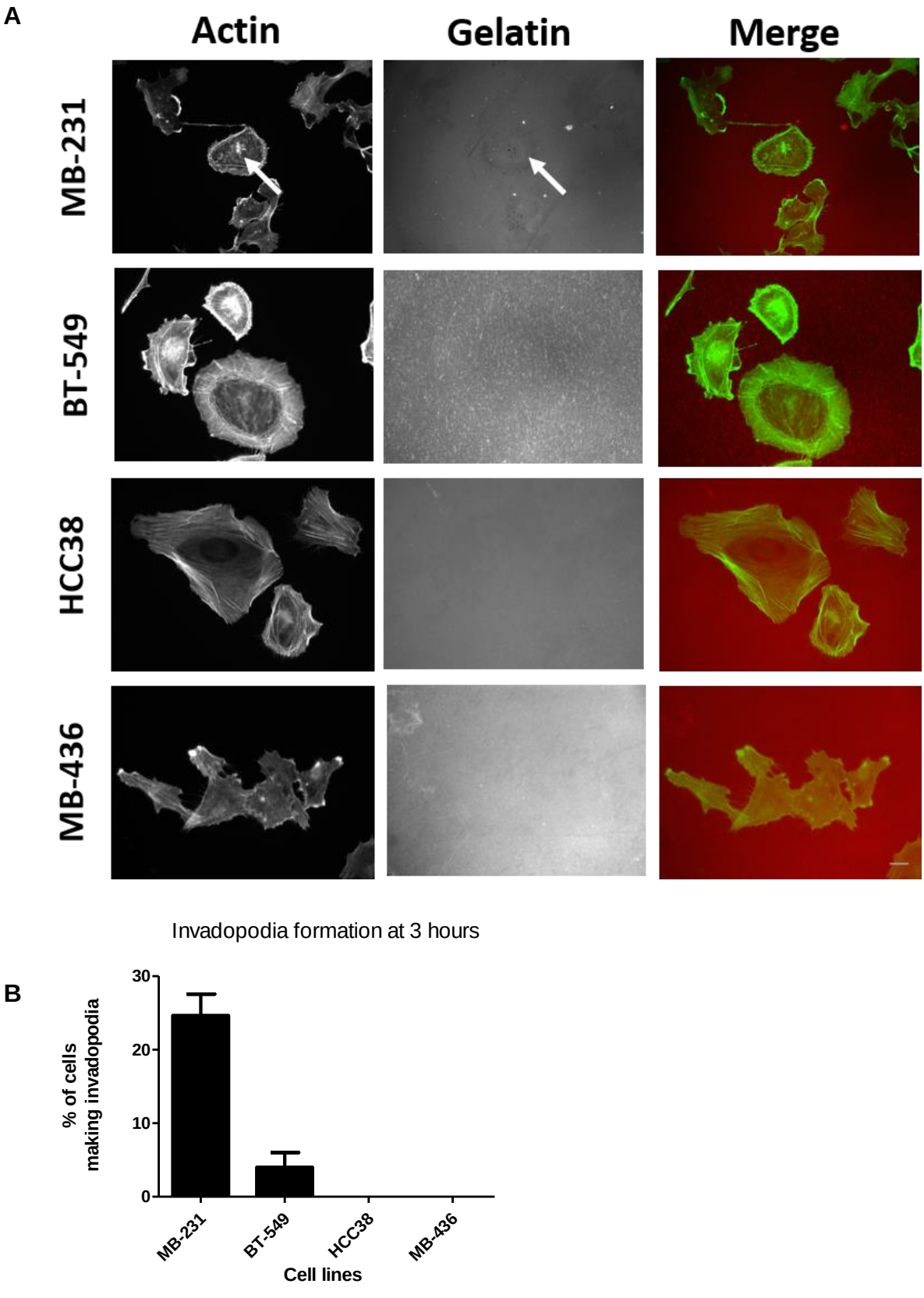

Figure 3.7 Invadopodia assay at 3h. (A) Cells were seeded on TRITC conjugated gelatin coated coverslips and incubated for 3h at 37°C. Coverslips were then fixed and stained with Phalloidin 488 (green) and cells were imaged. Scale bar corresponds to 10µm (B) Percentage of cells making invadopodia was determined for each individual experiment (N=3). Bars represent the mean percentage of cells making invadopodia and error bars represent the SEM.

3.2.6 Characterisation of invadopodia activity in the BT-549 cells

Previously published studies have proven the value of BT-549 cells in invadopodia research (Yamaguchi et al., 2011). This encouraged us to extend the characterisation of the BT-549 invadopodia capacity in longer incubations. The BT-549 cells were thus seeded on TRITC-gelatin coated coverslips and were fixed after 3, 6, 8 and 24 hours in order to more closely monitor invadopodia activity (**figure 3.8**).

Longer incubation periods in TRITC gelatin confirmed that the invadopodia making ability of BT-549 cells is substantially enhanced. In fact, if left for 24 hours post seeding, approximately 43% of the population is found positive for degradation competent invadopodia (**figure 3.8**). However, the resulting degradation was found unsuitably extensive covering a large part of the cell area. This would render potential degradation analyses difficult to carry out and thus the 24h time-point was rejected.

Meanwhile, the 6 and 8 hours of incubation periods recorded significant presence of mature invadopodia with well-defined degradation areas (**figure 3.8**). This was comparable to the invadopodia capacity of MB-231 cells (**figure 3.7B**) and therefore it was decided that an incubation time of 7h for BT-549 cells would be used for all subsequent invadopodia assays in the course of this study.

IQGAP3 expression does not correlate with invadopodia capacity across the triple negative cell line panel under characterisation (**figure 3.2B, 3.7**). Therefore, this particular experiment does not provide much insight as to whether IQGAP3 might be implicated in invadopodia dynamics. It should however be noted that high IQGAP1 expressing MB-231 cells make invadopodia as opposed to low IQGAP1 MB-436 and HCC38 (**figure 3.3B, 3.7**). This agrees with the well described role of IQGAP1 in the delivery of MT1-MMP upon invadopodia mediated matrix degradation (Sakurai-Yageta et al., 2008).

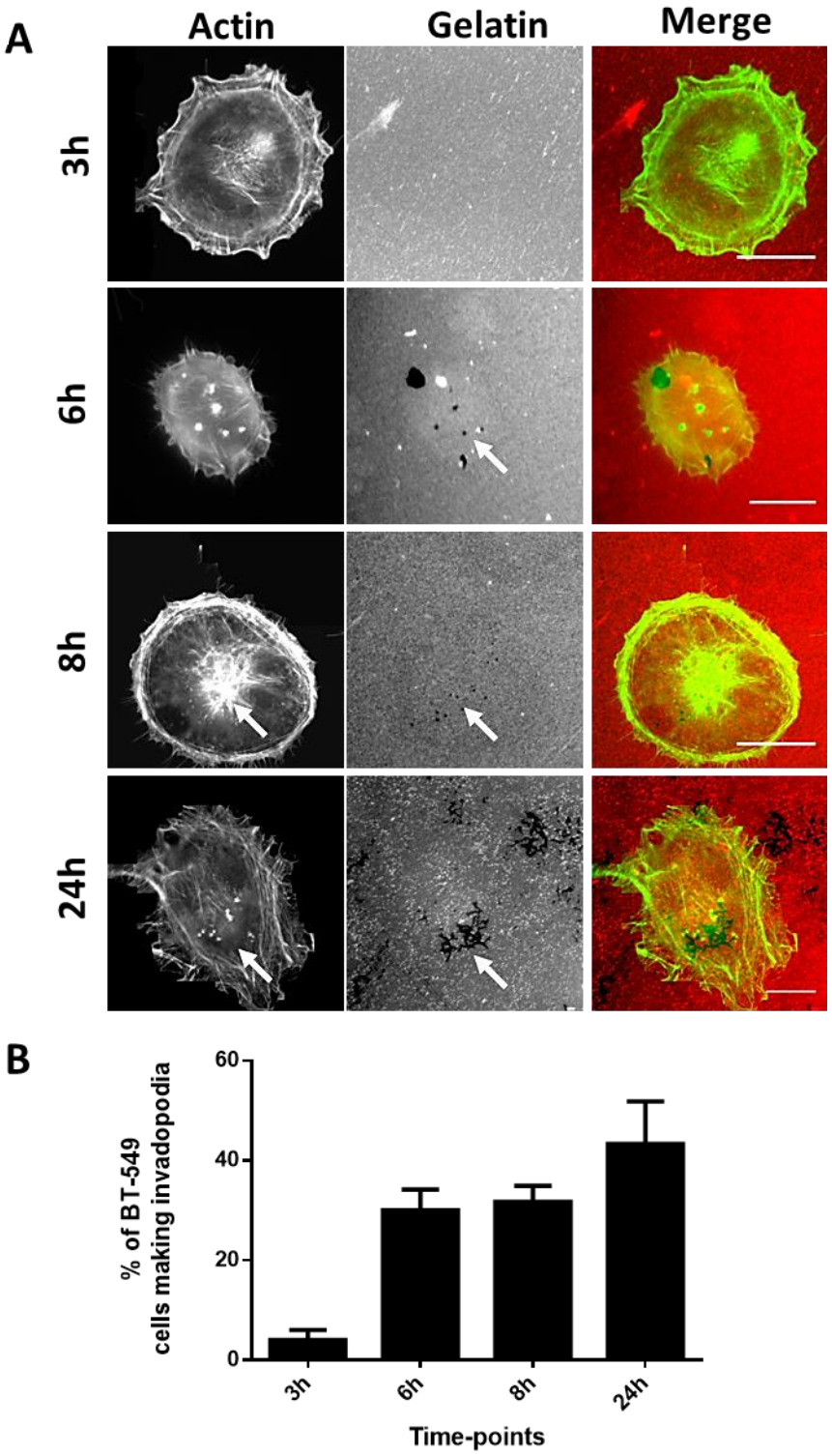

Figure 3.8 Invadopodia activity in BT-549 cells. (A) BT-549 cells were seeded on TRITC gelatin coated coverslips which were fixed after 3, 6, 8 and 24 hours respectively. Coverslips were fixed and stained with Phalloidin 488 (green) and cells were imaged. Scale bar corresponds to 10µm (B) Percentage of cells making invadopodia was determined for each individual experiment (N=3). Bars represent the mean percentage of cells making invadopodia and error bars represent the SEM.

3.2.7 Invadopodia and cell morphology

The *in vitro* invadopodia assay performed to assess the cells' ability to make invadopodia revealed that only a fraction of the cell population makes invadopodia. This means that a significant number of cells are not invading at any given time-point. Considering the relationship between invasion and cell morphology, we sought to characterise the cell shape features in cells exhibiting invadopodia compared to cells not exhibiting invadopodia. Morphological analysis revealed that both BT-549 and MB-231 cells having invadopodia capacity exhibited greater cell area than cells which did not have invadopodia capacity (**figures 3.9B, 3.10B**). Additionally, BT-549 cells with invadopodia were significantly rounder than their non-invasive counterpart (**figure 3.9C**). The same trend was observed in the MB-231 cells; however, it did not reach statistical significance perhaps because the MB-231 cells are generally more spindle shaped (**figures 3.5C, 3.10C**). These findings suggest that perhaps a spread and rounder cell morphology is more permissive of invadopodia activity.

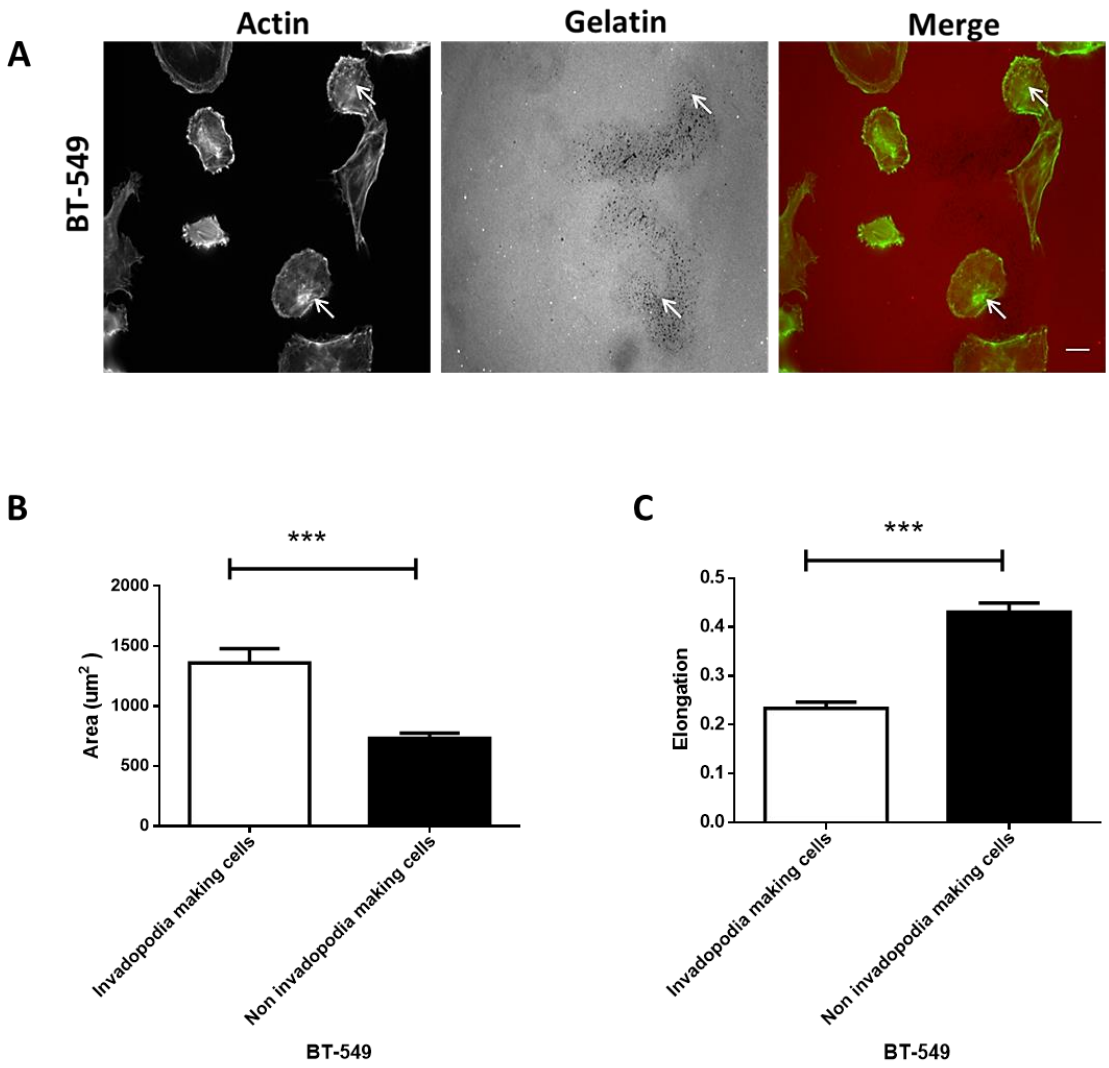

Figure 3.9 Relationship between invadopodia activity and cell morphology in BT-549 cells. (A) BT-549 cells were seeded on TRITC gelatin and were fixed and stained with Phalloidin 488 7 hours later. Cell images were obtained and morphological analysis was performed on 30 cells making invadopodia and 30 non invadopodia making cells. Scale corresponds to 10µm. (B) Bar charts show the cell area and (C) elongation measurements. Bars represent the mean values and error bars represent the SEM. Statistical analysis involved a t-test (***) = p≤ 0.001 (N=3).

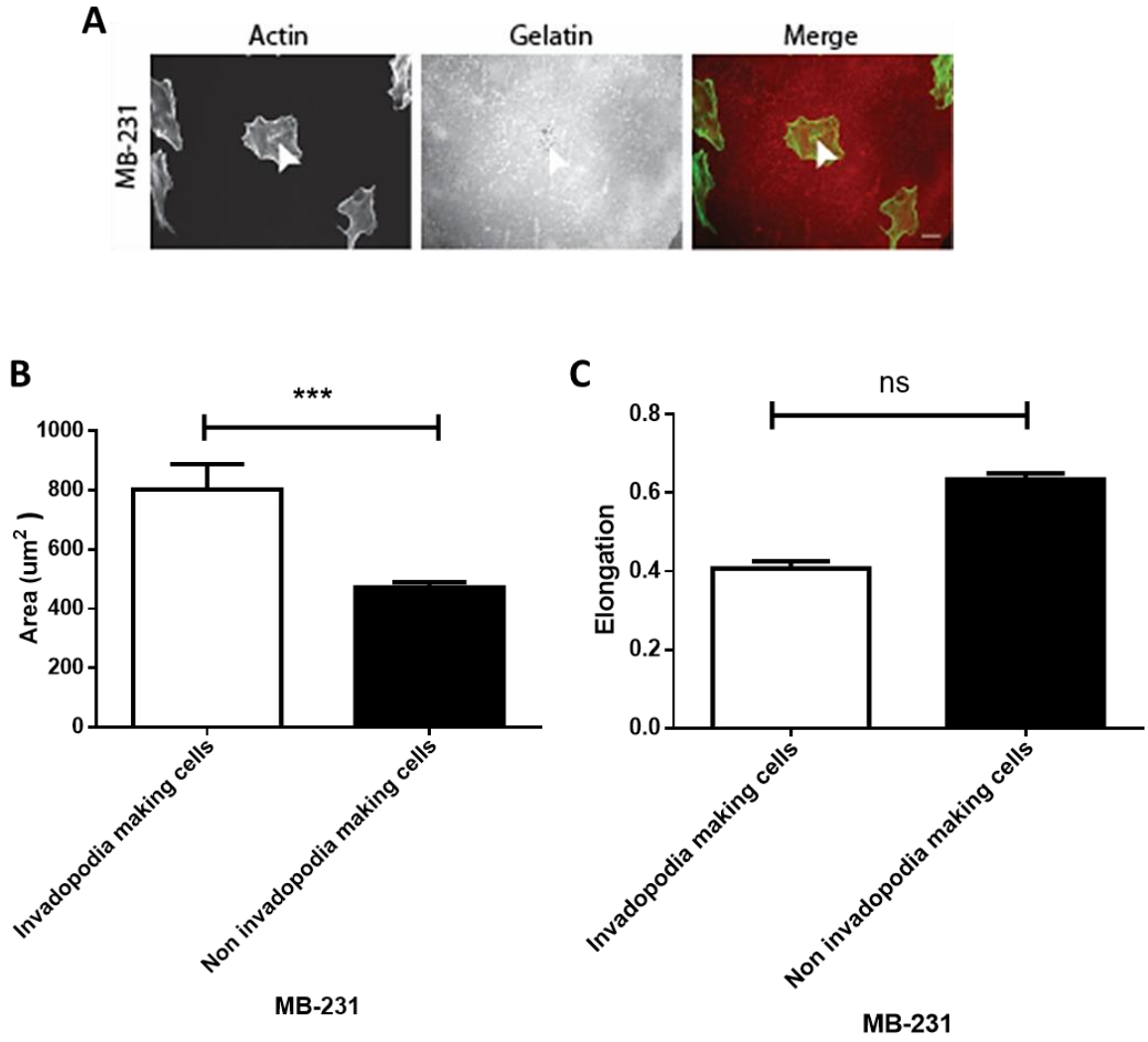

Figure 3.10 Relationship between invadopodia activity and cell morphology in MB-231 cells. (A) MB-231 cells were seeded on TRITC gelatin and were fixed and stained with Phalloidin 488 3 hours later. Cell images were obtained and morphological analysis was performed on 30 cells making invadopodia and 30 non invadopodia making cells. Scale corresponds to 10μm. Bar charts show (B) the cell area and (C) elongation measurements. Bars represent the mean values and error bars represent the SEM. Statistical analysis involved a t-test (***) = p≤ 0.001, ns means statistical significance was not reached (N=3).

3.2.8 Cell models

This study needed cell models baring features consistent with the aggressive behaviour exhibited by triple negative breast cancer. From the cell panel that was screened and characterised the MB-231 and BT-549 cell lines were deemed to be the most suitable since they were both motile and able to make invadopodia indicating an invasive behaviour. Additionally, the MB-231 cells trended towards having higher IQGAP3 expression, exhibited higher cell speed and a more elongated morphology than the BT-549 cells (**figure 3.4**). Using two lines that express different levels of IQGAP3 while exhibiting different morphological and migrational features was perceived as a positive feature for the progress of this project; especially when it comes to experiments involving the modulation of IQGAP3 expression levels in order to study its function.

3.3 Discussion

This chapter outlines the characterisation performed on a panel of triple negative breast cancer cell lines in terms of their IQGAP3 expression levels, morphology, random 2D migration and ability to make invadopodia. This characterisation was performed in order to choose the most suitable lines that would be used as the cell models for future study.

Having identified a specific IQGAP3 antibody we were able to progress previous mRNA studies to protein experiments. Western blotting revealed that IQGAP3 and IQGAP1 are expressed across the cell line panel tested including the normal MCF10A cells. Interestingly, IQGAP3 expression levels tended to be higher across the triple negative lines compared to MCF10A cells with the exception of the HCC38 cells (**figure 3.2**). In contrast to IQGAP3, this trend was not observed in the case of IQGAP1 as the near normal MCF10A cells were one of the high IQGAP1 expressing lines tested (**figure 3.3**). The expression pattern of IQGAP1 is perhaps not surprising as IQGAP1 has previously been reported as ubiquitously expressed across tissues (White et al., 2009). Nonetheless, the expression trend of IQGAP3 appeared promising and supported the hypothesis that IQGAPs can have differential functionality and activity despite their high structural similarity (White et al., 2009).

The triple negative cell lines that were further characterised all grew as single cells. The loss of junctions is an integral part of epithelial to mesenchymal transition (EMT) amongst other events such as cytoskeletal rearrangements, changes in polarity and upregulation of genes associated with the mesenchymal phenotype. These changes are translated into the formation of protrusive extensions allowing the acquisition of migratory and invasive capacity which eventually leads to the breach of the basement membrane (Lamouille et al., 2014). It is thus not surprising that cell lines representing aggressive triple negative tumours would share these traits.

Morphological characterisation confirmed the mesenchymal phenotype of the MB-231 and MB-436 cell lines considering they were found to be the most elongated lines. Mesenchymal cells have traditionally been regarded as the most aggressive fraction of the cell population found at leading edge of the invasive tumour (Kalluri and Weinberg, 2009). In spite of the motile and aggressive profile characterising mesenchymal cells, rounded cells can also have the capacity to move; the amoeboid movement type is characterised by a rounded morphology with blebs and prominent stress fibres as well as a fast and protrusive migration ability and has also been associated with breast cancer invasion (Cheung et al., 2013; Friedl and Wolf, 2010). Rho

signalling via ROCK drives amoeboid migration by inducing actomyosin contractility (Sahai and Marshall, 2003; Sanz-Moreno et al., 2011). In fact, the interplay of Rho and Rac can determine whether a cell will adopt a mesenchymal or amoeboid migration thus regulating cell plasticity (Sanz-Moreno et al., 2007). According to the Lehmann classification of triple negative breast cancer cell lines, MB-231, MB-436 and BT-549 fall into the mesenchymal stem like subtype whose genetic signature is enriched with upregulation of known EMT effectors such as components of the TGF-β and EGFR signalling pathways (Lehmann et al., 2011a). Interestingly, the very elongated MB-231 and MB-436 cells also had high IQGAP3 levels (**figures 3.2B, 3.5C**). IQGAP3 has been reported to be associated with directional migration by promoting APC clustering at the leading cell edge (Caro-Gonzalez et al., 2012) so perhaps this could contribute to the observed morphology. The role of IQGAP1 in polarity and cell migration is much better described (Choi et al., 2013; Fukata et al., 2001; Mataraza et al., 2007) ; however levels of IQGAP1 in MB-436 appear to be lower than those of the near normal MCF10A but also the aggressive MB-231 cells (**figure 3.3B**). Despite these observations there is no strong correlation of IQGAP expression and cell morphology across the cell line panel.

The study of random 2D migration revealed that all cell lines monitored by time-lapse microscopy were highly motile with the exception of BT-549 cells which were also motile but exhibited slower mean cell migration (**figure 3.6B**). The significantly slower cell speed exhibited by the BT-549 cells can be explained by potential differences in integrin expression. Along with their slower migration the BT-549 cells exhibited a very round morphology (**figure 3.5A, 3.5C**). Nonetheless, neither IQGAP1 nor IQGAP3 expression levels appear to correlate with the measured cell speeds across the cell line panel.

Particular attention has been given to the invadopodia mediated matrix invasion during this study. This was encouraged by the fact that the interaction of IQGAP1 with the exocyst complex has been shown to be crucial for the presentation of MT1-MMP at invadopodia sites (Sakurai-Yageta et al., 2008). Considering the high homology between the IQGAP family members, it was decided to consider the potential involvement of IQGAP3 in invadopodia dynamics. Our cell panel was thus screened for invadopodia formation ability.

Consistent with the current literature, only the MB-231 and BT-549 cells (both expressing higher levels of IQGAP3 than the MCF10A cells) could form invadopodia. MB-436 and HCC38 perhaps employ metalloprotease independent means of invasion as they have both been successfully employed in *in vitro* and *in vivo* invasion assays (Iida et al., 2012; Thompson et al., 1992).

However, the mode of invasion employed by these cell lines is not adequately characterised. Interestingly, the HCC38 and MB-436 cells exhibit low levels of IQGAP1 (**figure 3.3B**) which has been reported to be crucial for invadopodia mediated matrix degradation (Sakurai-Yageta et al., 2008).

Further analysis of cells making invadopodia showed that invadopodia capacity was associated with greater size and a rounder morphology (**figures 3.9, 3.10**). The relationship between morphology and invasion capacity is an ongoing matter of debate as multiple factors can influence both (Sahai and Marshall, 2003; Sanz-Moreno et al., 2007). The fact that there is no single mechanism of invasion has resulted in the investigation of cell plasticity which describes the ability of cancer cells to re-arrange their cytoskeleton and adopt different invasive mechanisms based on environmental cues (Friedl and Alexander, 2011). The cross-talk between Rac and Rho has been shown to regulate cell plasticity in melanoma and induce the switch between an amoeboid to a mesenchymal mode of migration (Sanz-Moreno et al., 2007). Migration of mesenchymal cells in 3D matrices is a result of a delicate synergy between adhesion and matrix proteolysis (Friedl and Wolf, 2009). In fact, work on HT-1080 fibrosarcoma and MB-231 3D cell migration suggests that areas of adhesion and matrix degradation are spatially distinct. Zones of matrix degradation were defined by the localisation of MT1-MMP and collagenolysis (Wolf et al., 2007). However, these studies did not measure invadopodia activity and thus it is difficult to determine how invadopodia are involved in cell migration and plasticity. It should also be noted that mechanisms governing migration can differ greatly between a 2D and a 3D environment given the more complex interaction with a 3D extracellular matrix (Friedl and Wolf, 2009). Nonetheless, our findings suggest that invadopodia capacity in triple negative breast cancer cell lines might be associated with cell spreading and hence one could argue that a cross-talk between invadopodia and cell adhesion does exist. In favour of this hypothesis are findings suggesting that β1 integrin activates tyrosine kinase Arg which in turn phosphorylates cortactin ultimately promoting invadopodia maturation (Beaty et al., 2013). However, FAK (a known focal adhesion turnover regulator) has been suggested to inhibit invadopodia formation (Chan et al., 2009).

3.4 Future work

The cell characterisation outlined in this chapter yielded the MB-231 and BT-549 cell lines as the most suitable cell models for this study. These cell lines were chosen because they are both motile, form mature invadopodia and express IQGAP3. It would be interesting to investigate the expression of EMT markers and known genetic traits involved in triple negative breast cancer in these cells. It should be noted that large scale studies adopt genetic approaches to identify high risk loci or frequently mutated genes (Lehmann et al., 2011). Even though this approach has proven to be very beneficial, the observed results are rarely validated at a protein level. This is crucial as potential changes observed at the genetic level may not necessarily translate to identical results at a protein level. Probing for markers such as p53, PI3K and components of the TGFβ signalling pathway such as SMADs and correlating their expression with the IQGAP3 levels observed might elucidate further signalling pathways that are active in triple negative breast cancer biogenesis.

The implication of invadopodia activity in triple negative breast cancer invasion could be reinforced by correlating the invasive capacity of the cell line panel in an *in vitro* invasion assay such as a trans-well 3D invasion assay. Further validation can involve subjecting our cell lines of interest in an *in vivo* invasion assay. The use of zebrafish embryos in invasion assays offers an inexpensive, reliable and fast readout of invasion. The assay involves injecting fluorescent cells in the yolk sac and monitoring their migration to the embryo tail (Eguiara et al., 2011). This migratory ability requires the breach of the yolk sac similarly to distant metastasis demanding the breach of the basement membrane. Breast cancer cell lines such as the MCF7 cells have been successfully used in this assay (Eguiara et al., 2011). In fact this assay could be used to determine the mode of migration employed by MB-436 and HCC38 cells. Therefore, the characterisation of the migratory behaviour of triple negative cell lines in this assay could benefit this study, expand our knowledge over cancer cell migration *in vivo* through direct and real-time visualisation and reduce the need to use mice.

Finally, to further investigate the relationship between invadopodia formation and cell spreading future experiments could compare focal adhesion formation between invadopodia making and non invadopodia making cell populations. This might elucidate potential variations in the focal adhesions number or maturity.

Chapter 4

Characterisation of IQGAP3 depletion and overexpression phenotypes

Chapter 4 : Characterisation of IQGAP3 depletion and overexpression phenotypes

4.1 Introduction

The observed high levels of IQGAP3 in MB-231 cells, which are known to be motile and invasive (Holliday and Speirs, 2011), prompted further investigation on the role of IQGAP3 in cell motility phenotypes. One of the most widely used research strategies in the study of protein function is the assessment of defined phenotypes of interest following the modulation of protein expression levels. This method has been widely employed in the field of cell motility while examining phenotypical readouts such as morphological features as well as migration and invasion capacity. Modulating the expression levels of IQGAP1 has delivered a plethora of data on IQGAP1 functions. The role of IQGAP1 in cell adhesion was further explored when E-cadherin was overexpressed in mouse fibroblasts and IQGAP1 was observed to accumulate in cell-cell junctions (Li et al., 1999). Over-expressing IQGAP1 in Swiss 3T3 cells revealed that IQGAP1 localises at the leading cell edge of migrating cells (Mataraza et al., 2003). Additionally, reducing IQGAP1 levels by both siRNA and stable retroviral systems in MCF7 cells resulted in reduced cell migration through an *in vitro* transwell system (Mataraza et al., 2003). Moreover, inhibition of IQGAP1 expression has also highlighted the importance of IQGAP1 in the directionality of cell migration; IQGAP1 is found in a complex with Filamin-A and RacGAP1 which supresses Rac1 and allows effective directional cell migration (Jacquemet et al., 2013). The importance of the IQGAP1 to PIP2 interaction in directional cell migration was also marked in IQGAP1 knockout MEFs which were transfected with a mutant IQGAP1 construct deficient of PIP2 binding. Disrupting the interaction of IQGAP1 with PIP2 led to a cell morphology characterised by multiple cell edges as well as loss of directionality in cell migration (Choi et al., 2013). Furthermore, overexpression of IQGAP1 in MB-231 cells revealed that IQGAP1 localises at invadopodia while IQGAP1 depletion reduced MT1-MMP accumulation and matrix degradation (Sakurai-Yageta et al., 2008).

Moreover, both overexpression and knockdown of IQGAP1 in MCF7 cells inhibited MEK and ERK activation upon EGF stimulation suggesting that the ability of IQGAP1 to act as a scaffold for the MAPK cascade is concentration dependent (Roy et al., 2005, 2004). Additionally, B-Raf kinase activity was hindered in IQGAP1 knockout MEFs as well as in siRNA mediated IQGAP1 knockdown 293H cells upon EGF stimulation (Ren et al., 2007). Overall, these studies have

marked the necessity of IQGAP1 scaffolding activity in the MAPK signalling cascade by modulating expression levels in various systems and by performing elegant immunoprecipitation experiments.

Nonetheless, the role of IQGAP3 is far less extensively described. The study that identified IQGAP3 as a novel IQGAP isoform reported that reducing IQGAP3 expression inhibited axonal elongation in neuronal cells. Interestingly, axonal elongation was not affected by IQGAP1 depletion (Wang et al., 2007). Perhaps the most striking finding on IQGAP3 function is that it regulates cell proliferation by activating ERK in a Ras dependent manner (Nojima et al., 2008). Indeed upon diminishing IQGAP3 expression in Eph4 cells cell proliferation was inhibited, levels of phosphorylated ERK were lost and active Ras was depleted. Meanwhile loss of IQGAP1 expression had no such effect (Nojima et al., 2008).

The implication of IQGAP3 in cell proliferation may inevitably prove problematic in experimental conditions where IQGAP3 expression is long-term inhibited. This becomes apparent in a study implicating IQGAP1 and IQGAP3 in normal skin homeostasis as well as squamous cell carcinoma tumourigenesis. In this study stable knockdown systems of different IQGAP levels are employed. Partial IQGAP3 depletion had no effect in primary keratinocyte proliferation, levels of phosphorylated ERK and levels of cyclin D1 while a near complete knockdown dramatically diminished all these features (Monteleon et al., 2015). From this study it can also be deduced that a very robust knockdown of IQGAP may be required to elicit phenotypical changes.

Furthermore, both IQGAP1 and IQGAP3 are reported to be implicated in cytokinesis as loss of either family member resulted in binucleated Hela cells (Adachi et al., 2014). Both IQGAPs are thought to regulate localisation of RhoA at the cleavage furrow. However, only IQGAP3 was shown to directly bind anillin and thus IQGAP3 was reported as the principal IQGAP to regulate RhoA localisation via anillin (Adachi et al., 2014). Nonetheless, the effect of IQGAP1 depletion in RhoA localisation was also prominent but was thought to be independent of anillin (Adachi et al., 2014). Consequently, IQGAP1 and IQGAP3 appear to work closely but still exhibit fine differences in functionality even in tightly regulated processes such as cytokinesis.

Furthermore, even though there are some reports implicating IQGAP3 in cancer cell motility by diminishing IQGAP3 in A549 lung cancer cells (Yang et al., 2014) and BXPC-3 and SW1990 pancreatic cancer cells (Xu et al., 2016), the available data is limited and the mechanism involved in largely unknown.

This chapter explores cellular phenotypes following modulation of IQGAP3 expression to identify possible molecular mechanisms through which IQGAP3 might promote triple negative breast cancer cell motility.

4.2 Results

4.2.1 Knockdown of IQGAP3 expression

In order to investigate the effect of reducing IQGAP3 expression on our phenotypes of interest, siRNA sequences that can effectively diminish IQGAP3 expression were validated. Two oligonucleotides were tested along with a negative siRNA control and a wild-type untransfected control by western blotting. Almost complete IQGAP3 depletion was achieved at 72 hours (3 days) post transfection and was maintained at 96h (4 days) by both oligonucleotides tested in MB-231 and BT-549 cells (**figures 4.1, 4.2**). As a result, assays investigating the effects of loss of IQGAP3 were performed within this time-frame.

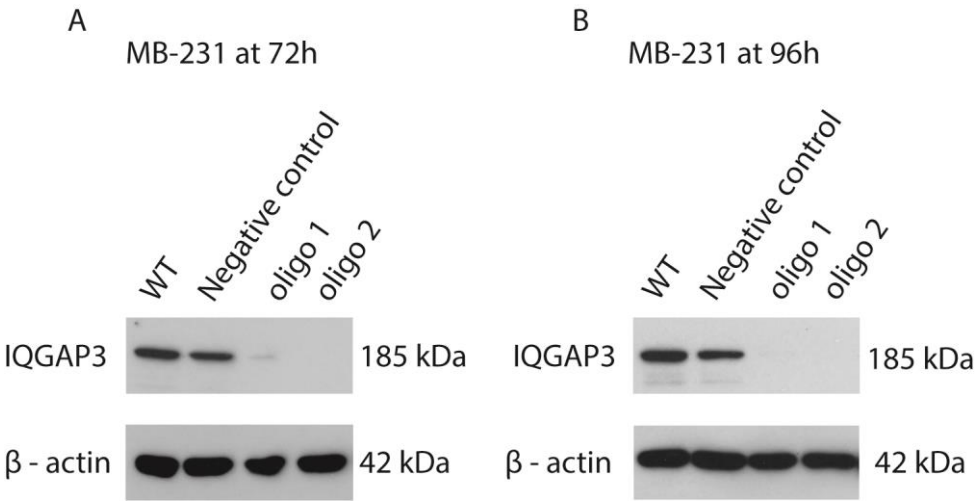

Figure 4.1 IQGAP3 knockdown in MB-231 cells. MB-231 cells were transfected with 2 siRNA oligonucleotides. A negative siRNA control as well as a wild-type sample were included in the assay. (A) Representative blot indicating diminished IQGAP3 expression conferred by both oligonucleotides tested 72h post transfection. β-actin was used as a loading control (N=3). (B) Representative blot indicating diminished IQGAP3 expression conferred by both oligonucleotides tested 96h post transfection. β-actin was used as a loading control (N=3).

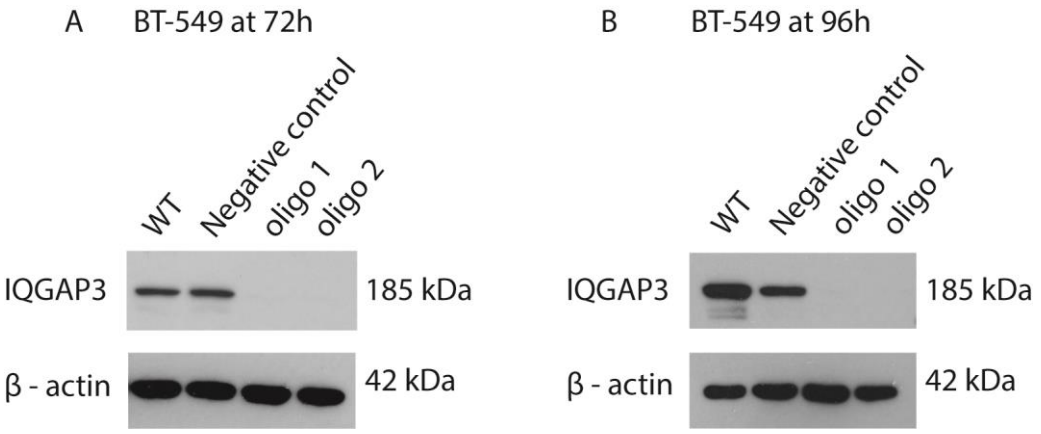

Figure 4.2 IQGAP3 knockdown in BT-549 cells. BT-549 cells were transfected with 2 siRNA oligonucleotides. A negative siRNA control as well as a wild-type sample were included in the assay. (A) Representative blot indicating diminished IQGAP3 expression conferred by both oligonucleotides tested 72h post transfection. β-actin was used as a loading control (N=3). (B) Representative blot indicating diminished IQGAP3 expression conferred by both oligonucleotides tested 96h post transfection. β-actin was used as a loading control (N=3).

4.2.2 Cell proliferation of IQGAP3 knockdown cells

After establishing two siRNA sequences that can effectively diminish IQGAP3 expression the effect of IQGAP3 depletion was assessed in cell proliferation; given that IQGAP3 has been reported to regulate this cellular process (Nojima et al., 2008). MTT assays were performed 2, 3 and 5 days post transfection and revealed that both oligonucleotides conferred a statistically significant reduction in cell proliferation in both MB-231 and BT-549 cells. This is consistent with previous studies reporting reduced proliferation in lung cancer, pancreatic cancer and her2 positive breast cancer cell lines (Hu et al., 2016.; Xu et al., 2016; Yang et al., 2014). The effect of IQGAP3 depletion in cell proliferation could potentially skew the analysis of migration and invasion experiments. Hence, the assays that were chosen to further this study were designed so that they are not influenced by cell proliferation.

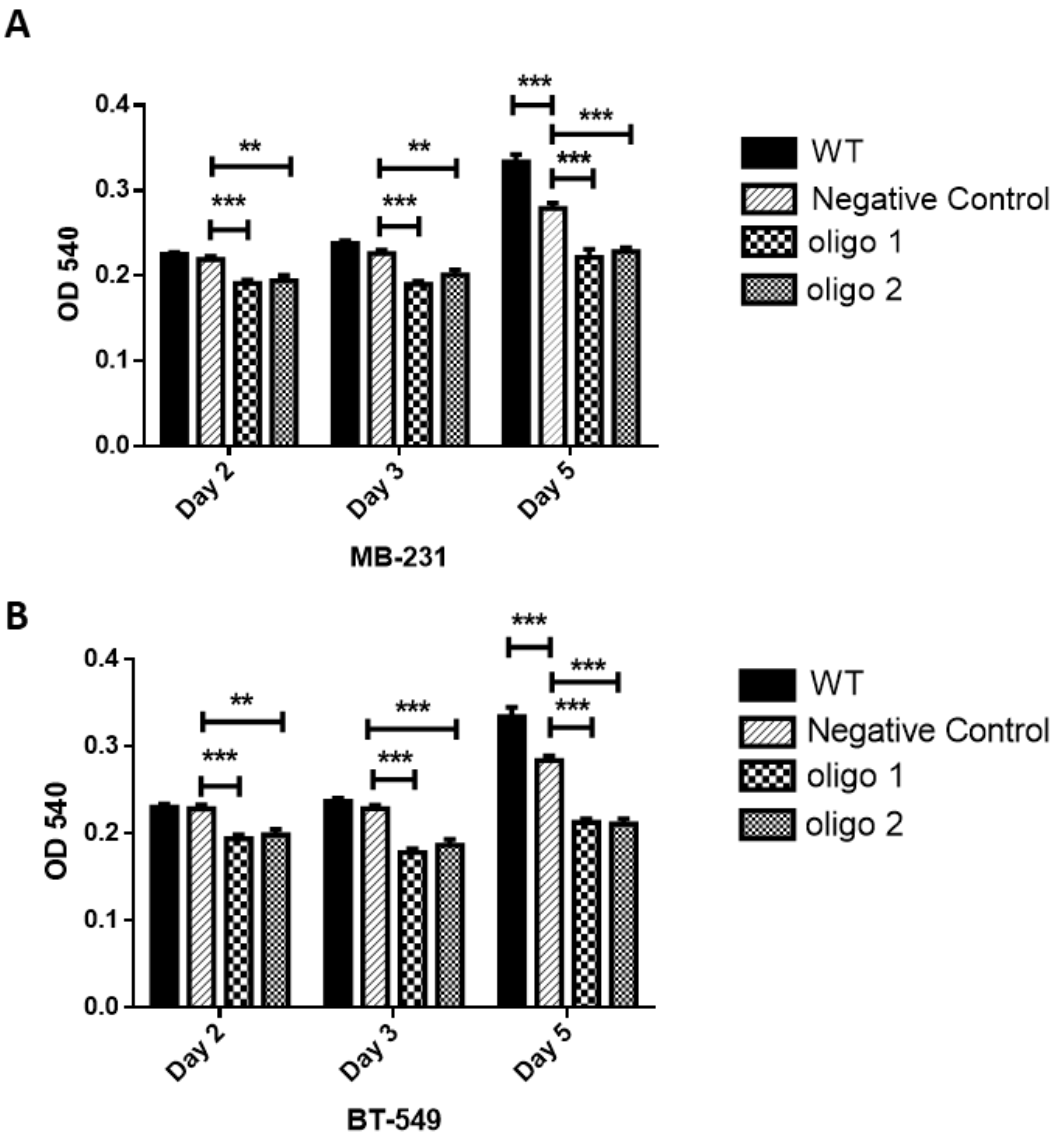

Figure 4.3 Cell proliferation in IQGAP3 depleted cells. (A) IQGAP3 knockdown cells as well as negative control and wild-type (A) MB-231 and (B) BT-549cells were subjected to an MTT assay 2, 3 and 5 days post transfection. Bars represent the mean absorbance values and error bars represent the SEM. Statistical analysis was performed using one way ANOVA followed by Tukey's post hoc testing. Comparisons between knockdown conditions and the negative control are indicated on the graph, (**) = $p \leq 0.01$, (***) = $p \leq 0.001$. There was no significant difference between the WT and the negative control conditions apart from Day 5 as indicated on the graph (N=3).

4.2.3 Cell morphology of IQGAP3 knockdown cells

Cell plasticity refers to the ability of cancer cell to alter their morphology and migrational properties depending on environmental cues of the tumour microenvironment (Friedl and Wolf, 2010). In fact, results on chapter 3 report that cells exhibiting invadopodia capacity are more rounded than the non-invasive population (**figure 3.9**). Potential changes in the morphology of triple negative breast cancer cells following IQGAP3 depletion could thus infer changes in their migratory and invasive ability. IQGAP3 depleted MB-231 and BT-549 cells were seeded on fibronectin coated coverslips. WT and cells transfected with negative siRNA control were included in the experiment. Cells were subsequently fixed and stained with TRITC phalloidin to mark the actin cytoskeleton 96h post transfection. Morphological analysis revealed that both oligonucleotides used to reduce IQGAP3 expression induced a hyper-elongated phenotype which was observed in both cell lines (**figures 4.4, 4.5**). The altered morphology following IQGAP3 depletion was thought to be accompanied by changes in the migratory ability of the affected cells considering the innate capacity of cancer cells to alter their shape and migration characteristics (Friedl and Wolf, 2010).

. .

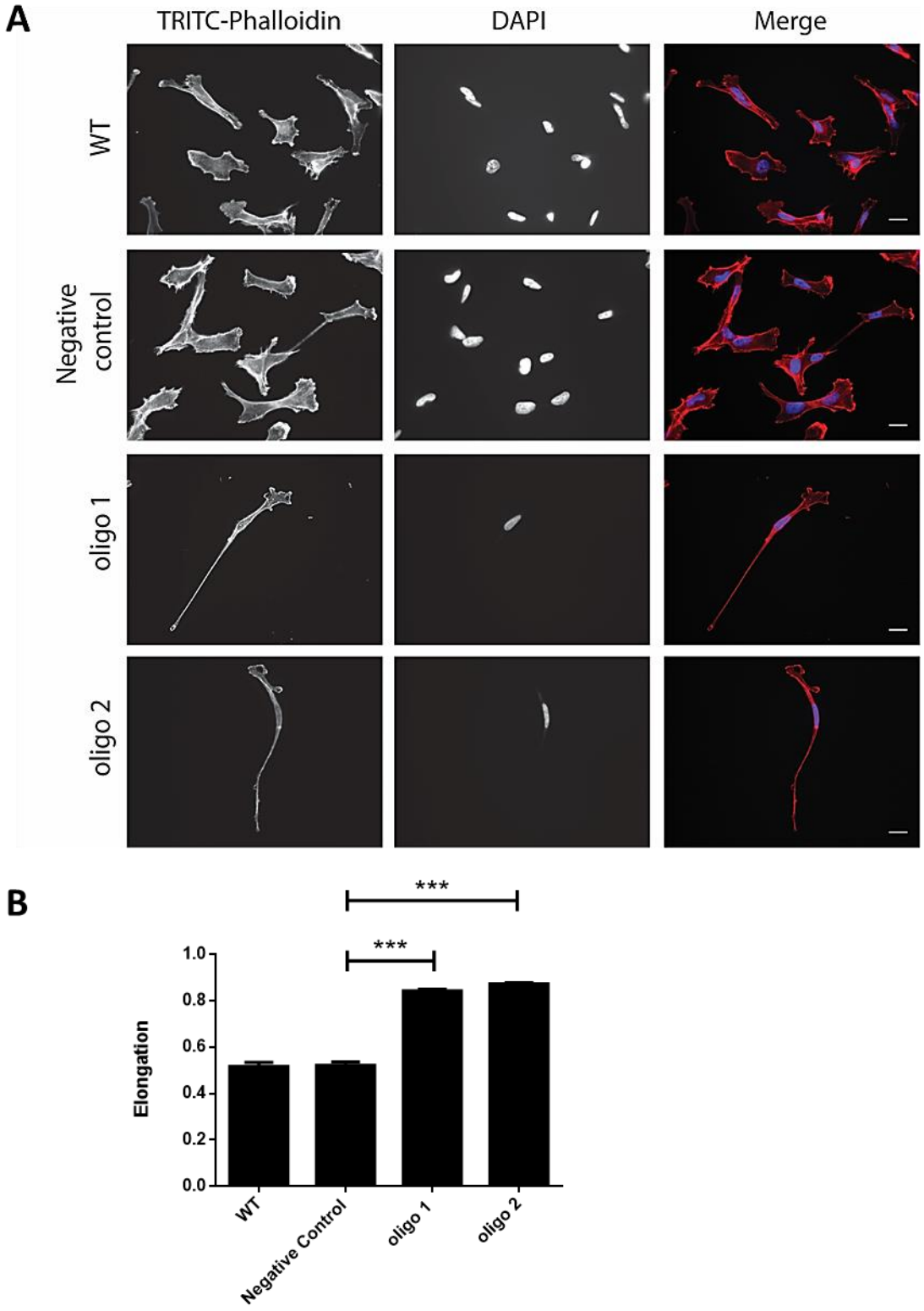

Figure 4.4 Morphology of IQGAP3 depleted MB-231 cells. (A) IQGAP3 knockdown and control MB-231 cells were seeded on fibronectin coated coverslips and were fixed 96h post transfection. Cells were then stained with TRITC phalloidin and DAPI. Imaged cells were subjected to morphological analysis on ImageJ. The scale bar corresponds to 10μm (B) Graphical representation indicating the elongation index of control and IQGAP3 knockdown cells. Bars represent the mean elongation values and error bars represent the SEM. Statistical analysis involved one way ANOVA followed by Tukey's post hoc testing. Comparisons between knockdown conditions and the negative control are indicated on the graph, (***) = $p \leq 0.001$. There was no significant difference between the WT and the negative control conditions (N=3).

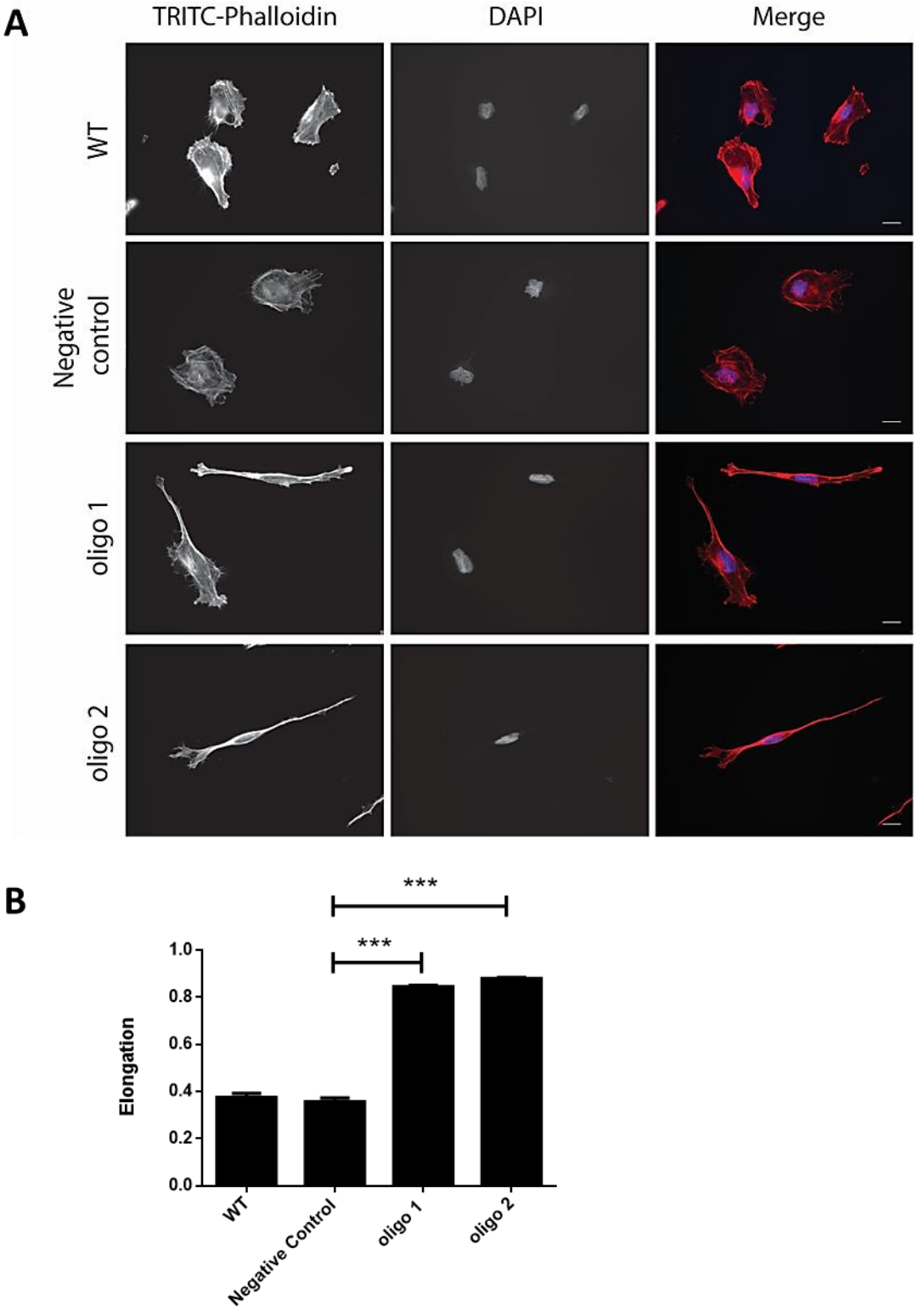

Figure 4.5 Morphology of IQGAP3 depleted BT-549 cells. (A) IQGAP3 knockdown and control BT-549 cells were seeded on fibronectin coated coverslips and were fixed 96h post transfection. Cells were then stained with TRITC phalloidin and DAPI. Imaged cells were subjected to morphological analysis on ImageJ. The scale bar corresponds to 10μm (B) Graphical representation indicating the elongation index of control and IQGAP3 knockdown cells. Bars represent the mean elongation values and error bars represent the SEM. Statistical analysis involved one way ANOVA followed by Tukey's post hoc testing. Comparisons between the knockdown conditions and the negative control are shown on the graph, (***) = $p \leq 0.001$. There was no significant difference between the WT and the negative control conditions. (N=3).

4.2.4 Random 2D migration of IQGAP3 knockdown cells

Having established that IQGAP3 knockdown induces an elongated phenotype in both MB-231 and BT-549 cells, (**figures 4.4, 4.5**) the ability of these cells to move on fibronectin was assessed. This approach also provided the opportunity to further examine the source of the observed elongated phenotype; whether it is a result of loss of tail retraction or over-extension of the leading edge. Control and knockdown cells seeded on fibronectin coated plates were monitored by time-lapse microscopy for up to 16 hours. The imaging experiment was performed within the time window where IQGAP3 knockdown is most efficient which is between 72 and 96 hours post transfection (**figures 4.1, 4.2**). Notably, the chosen migration assay is not impacted by changes in proliferation rate induced by IQGAP3 depletion (**figure 4.3**). Imaged cells were manually tracked on ImageJ and mean cell speed as well as statistical analysis were obtained in Mathematica Notebooks written by Professor Graham Dunn (Whale et al., 2012). Analysis showed that mean cell speed was significantly reduced in knockdown conditions compared to control in both MB-231 and BT-549 cells (**figures 4.6, 4.7**). Additionally, it was observed that IQGAP3 depleted cells were either unable to retract their tail and move forward or extended protrusions towards opposing directions ultimately restricting their total displacement. Reduced migration ability upon IQGAP3 depletion has been shown in lung cancer and pancreatic cancer cells (Xu et al., 2016; Yang et al., 2014). However, a significant morphological change alongside reduced migration properties has never been reported before suggesting that the underlying mechanism inducing these effects in the triple negative breast cancer cell lines tested might be unique.

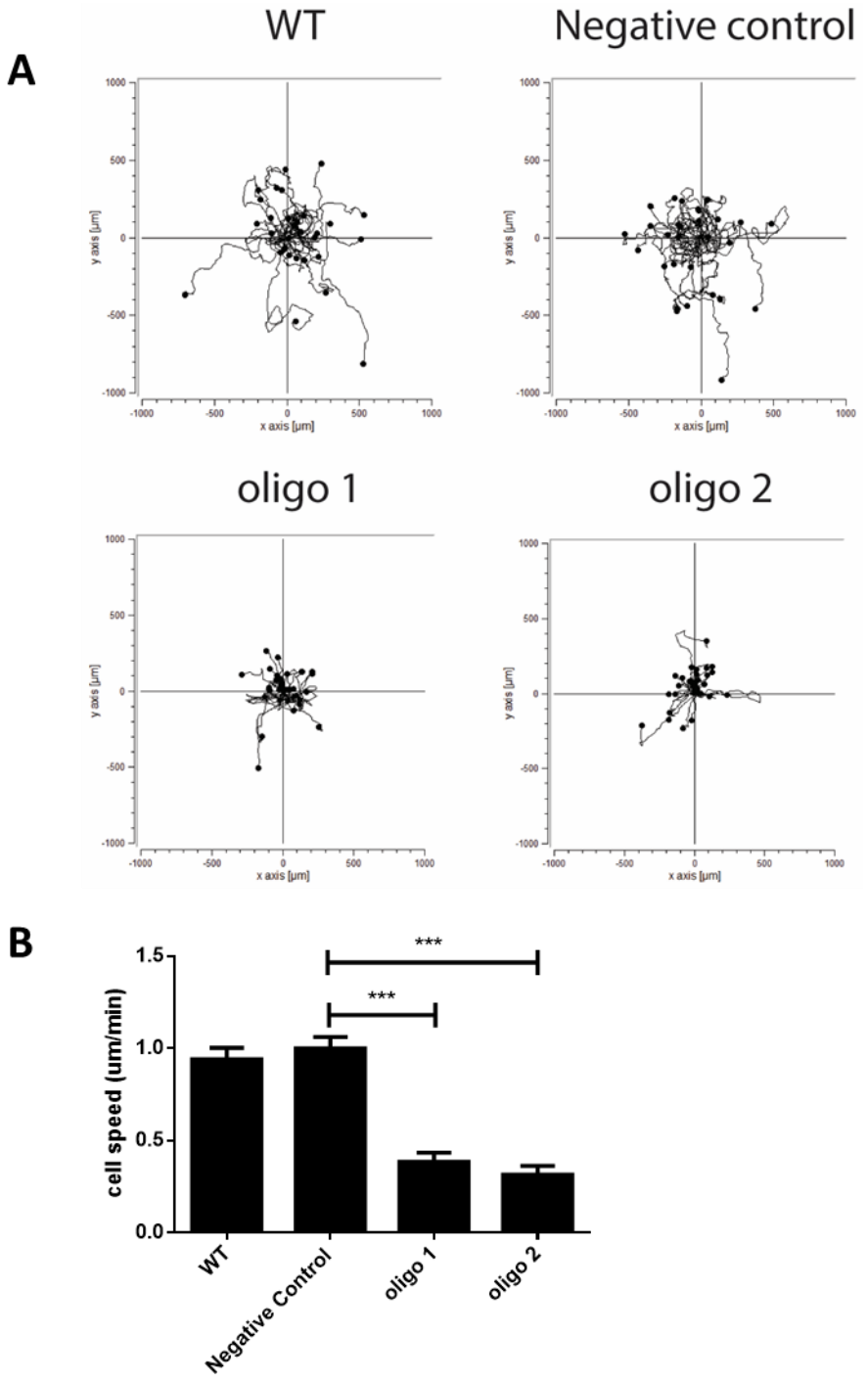

Figure 4.6 Random 2D migration of IQGAP3 depleted MB-231 cells. (A): Control and IQGAP3 knockdown MB-231 cells were seeded on fibronectin coated plates and monitored by time-lapse microscopy for 16 hours. Imaged cells were subsequently manually tracked on ImageJ, track plots, mean cell speed and SEM were obtained on Mathematica (B): Graphical representation of control and IQGAP3 knockdown cell speed. Bars represent the mean cell speed and error bars represent the SEM. Statistical analysis involved one way ANOVA followed by Tukey's post hoc testing. Comparisons between the knockdown conditions and the negative control are shown on the graph, (***) = $p \leq 0.001$. There was no significant difference between the WT and the negative control conditions. (N=3).

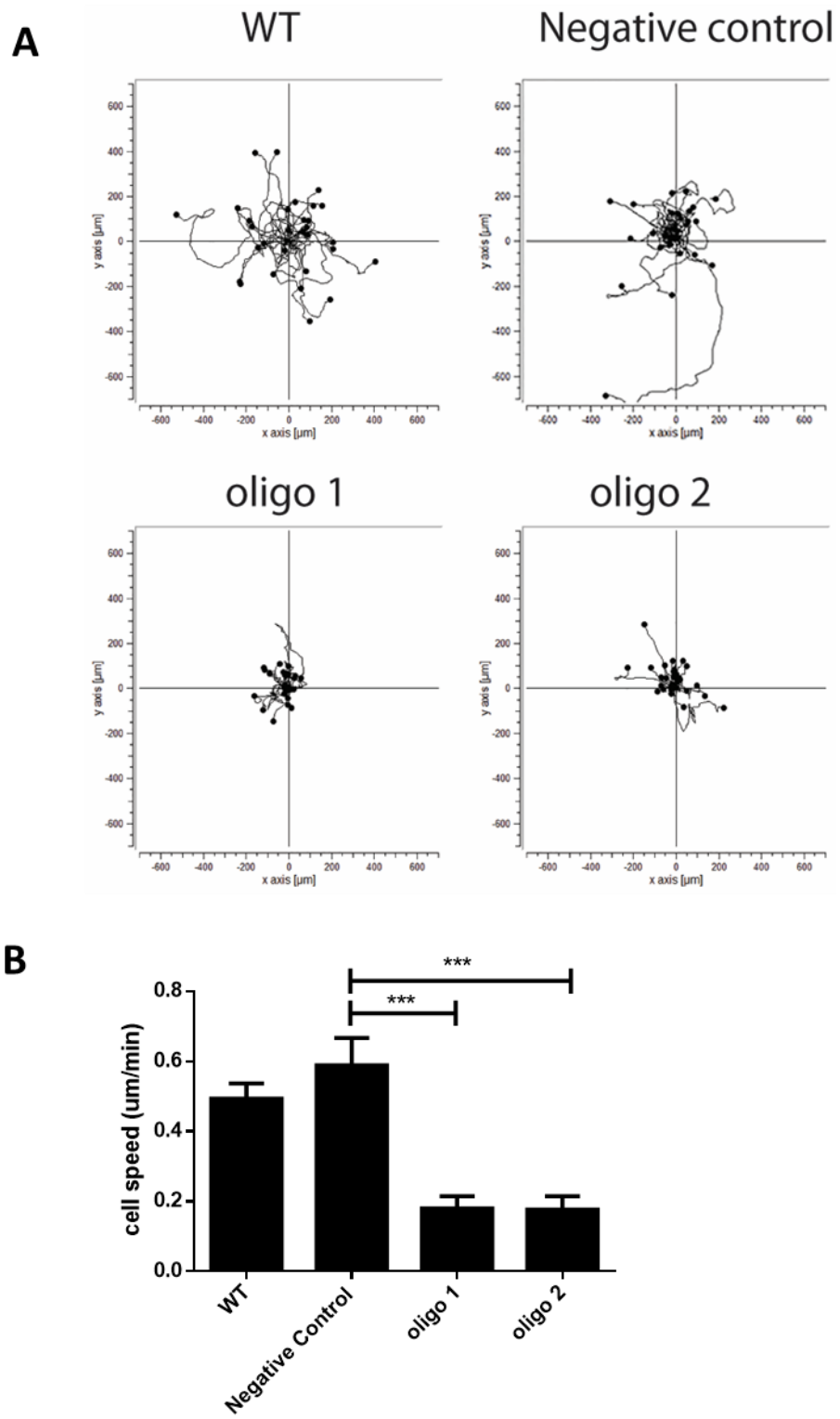

Figure 4.7 Random 2D migration of IQGAP3 depleted BT-549 cells. (A): Control and IQGAP3 knockdown BT-549 cells were seeded on fibronectin coated plates and monitored by time-lapse microscopy for 16 hours. Imaged cells were subsequently manually tracked on ImageJ, track plots, mean cell speed and SEM were obtained on Mathematica (B): Graphical representation of control and IQGAP3 knockdown cell speed. Bars represent the mean cell speed and error bars represent the SEM. Statistical analysis involved one way ANOVA followed by Tukey's post hoc testing. Comparisons between the knockdown conditions and the negative control are shown on the graph, (***) = $p \leq 0.001$. There was no significant difference between the WT and the negative control conditions. (N=3).

4.2.5 Focal adhesion formation in IQGAP3 knockdown cells

The reduced cell speed observed upon inhibiting IQGAP3 expression in MB-231 and BT-549 cells could be the result of impeded cell retraction and/or a change in cell adhesion dynamics. Indeed, cell adhesion is widely accepted as a crucial prerequisite for effective cell migration of mesenchymal cells (Huttenlocher and Horwitz, 2011). Focal adhesions act as “feet” that adhere firmly on the extracellular matrix while their dynamic formation and dissolution ensures forward moving (Ridley et al., 2003). RhoA regulates the formation of stress fibres and focal adhesions by inducing phosphorylation of myosin light chain and thus contractility (Chrzanowska-Wodnicka and Burridge, 1996; Ridley and Hall, 1992). Additionally, cell retraction is also under the regulation of Rho (Ridley, 2001). Consequently, we postulated that if diminished IQGAP3 was somehow interfering with Rho activity it would ultimately disrupt focal adhesion formation.

Zyxin is not found in nascent focal complexes but localises in mature focal adhesions in response to local retraction or arrested elongation of the leading cell edge (Zaidel-Bar et al., 2003). Additionally, even though the formation of nascent focal complexes is under the regulation of Rac, their progression into mature focal adhesions is under the regulation of Rho (Rottner et al., 1999). Interestingly, ROCK 1 depleted keratinocytes had very few zyxin positive focal adhesions whereas the formation of zyxin enriched focal adhesions was unaffected in ROCK 2 knockdown cells (Lock et al., 2012). Hence the available evidence suggested that impaired contractility might disrupt recruitment of zyxin and thus maturation of focal adhesions (Chrzanowska-Wodnicka and Burridge, 1996; Lock et al., 2012; Zaidel-Bar et al., 2003).

In order to test this hypothesis, control and IQGAP3 depleted MB-231 and BT-549 cells were seeded on fibronectin and fixed 96h post transfection. Cells were subsequently probed for zyxin and stained with phalloidin to indicate the actin cytoskeleton. Following imaging, control and knockdown cells were scored for mature focal adhesions based on their zyxin staining. Analysis revealed that formation of mature focal adhesions was significantly hindered in both triple negative lines tested upon loss of IQGAP3. Moreover, depletion of IQGAP3 led to very elongated triple negative breast cancer cells which were unable to form mature focal adhesions and move on fibronectin (**figures 4.4 – 4.9**). Even though reduced migration ability as a result of loss of IQGAP3 has been shown (Hu et al., 2016; Xu et al., 2016), a concurrent morphological and adhesion defect has not been reported before.

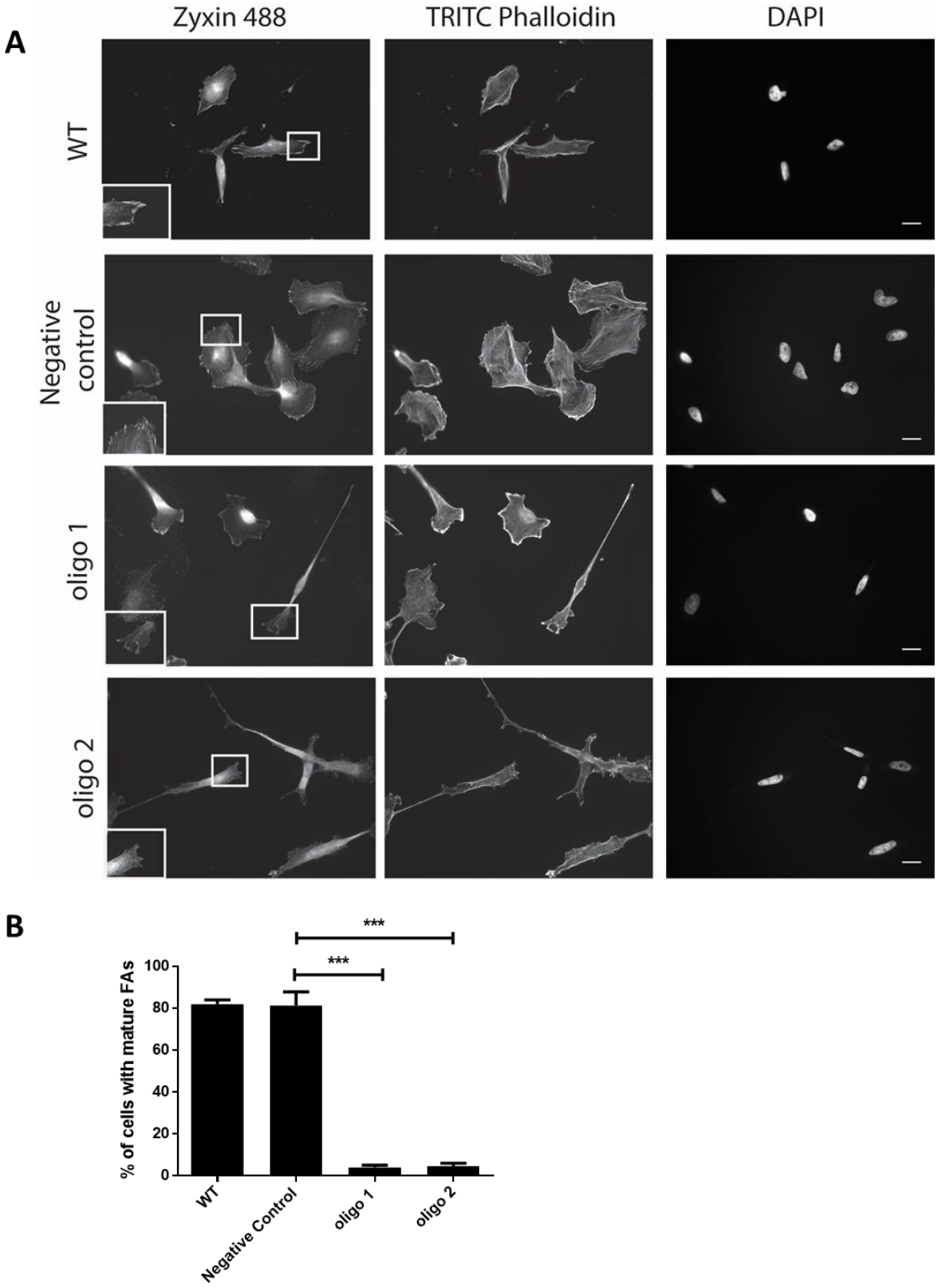

Figure 4.8 Formation of focal adhesions in IQGAP3 depleted MB-231 cells. (A): Control and IQGAP3 knockdown MB-231 cells were seeded on fibronectin and were fixed 96h post transfection. Scale bar corresponds to 10μm. Cells were stained for zyxin (1:400) and anti-rabbit 488 secondary antibody (1:600) as well as TRITC phalloidin. (B): Following imaging cells were scored for mature focal adhesions based on their zyxin staining. Bars represent the mean percentage of cells with focal adhesions and error bars represent the SEM. Statistical analysis involved one way ANOVA followed by Tukey's post hoc testing. Comparisons between the knockdown conditions and the negative control are shown on the graph, (***) = $p \leq 0.001$. There was no significant difference between the WT and the negative control conditions. (N=3).

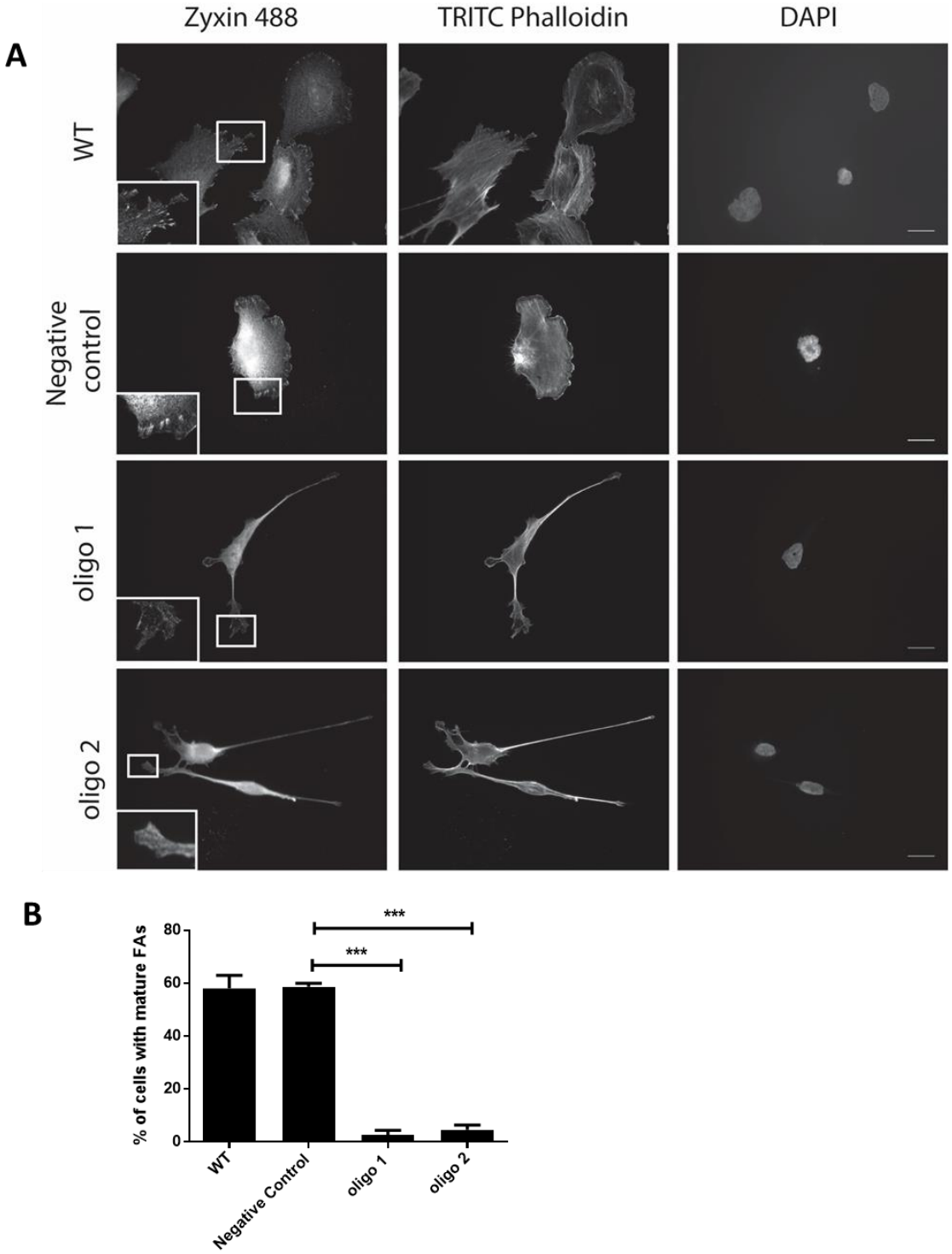

Figure 4.9 Formation of focal adhesions in IQGAP3 depleted BT-549 cells. (A): Control and IQGAP3 knockdown BT-549 cells were seeded on fibronectin and were fixed 96h post transfection. Cells were stained for zyxin (1:400) and anti-rabbit 488 secondary antibody (1:600) as well as TRITC phalloidin. Scale bar corresponds to 10μm. (B): Following imaging cells were scored for mature focal adhesions based on their zyxin staining. Bars represent the mean percentage of cells with focal adhesions and error bars represent the SEM. Statistical analysis involved one way ANOVA followed by Tukey's post hoc testing. Comparisons between the knockdown conditions and the negative control are shown on the graph, (***) = $p \leq 0.001$. There was no significant difference between the WT and the negative control conditions. (N=3).

4.2.6 Invadopodia making ability in IQGAP3 knockdown cells

As well as cell matrix focal adhesions, cancer cells also generate degradation competent adhesions called invadopodia. The significance of invadopodia mediated invasion has been

confirmed *in vitro* and its relevance to cancer metastasis has been validated *in vivo* (Eckert et al., 2011; Leong et al., 2014). IQGAP1 is known to localise at invadopodia and is involved in the delivery of MT1-MMP at the protrusion (Sakurai-Yageta et al., 2008). IQGAP3 has not been implicated in invadopodia dynamics before; therefore in order to test whether IQGAP3 is associated with these protrusions IQGAP3 depleted alongside control MB-231 and BT-549 cells were subjected to the invadopodia assay which had been previously optimised for each cell line (**figures 3.7, 3.8**). Cells were then stained with Phalloidin 488 and scored for the presence of degradation competent invadopodia. Analysis showed that the ability of both MB-231 and BT-549 cells to make invadopodia is almost entirely lost upon IQGAP3 depletion as very few IQGAP3 depleted cells were found positive for actin puncta coinciding with matrix degradation holes (**figures 4.10, 4.11**). Interestingly, IQGAP1 depletion disrupted MT1-MMP localisation at the protrusions as well as matrix degradation without however affecting the formation of invadopodia per se (Sakurai-Yageta et al., 2008). This observation suggests a difference in functionality between IQGAP1 and IQGAP3 as the IQGAP3 depleted cells not only lack matrix degradation mediated holes but also exhibit very little evidence of actin puncta (**figures 4.10, 4.11**).

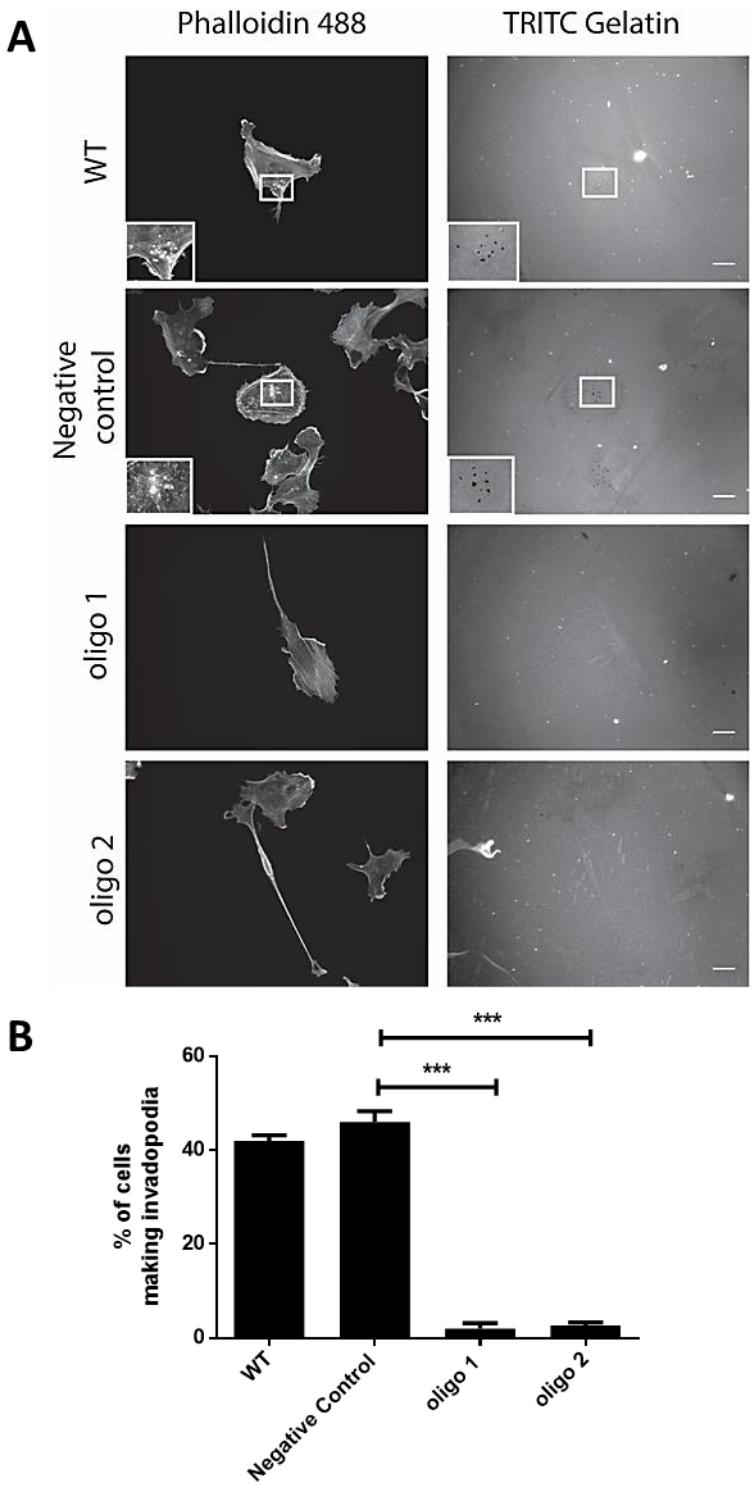

Figure 4.10 Invadopodia Presence in IQGAP3 depleted MB-231 cells. (A): IQGAP3 knockdown and control MB-231 cells were seeded on TRITC gelatin coated coverslips and incubated for 3h. Cells were subsequently stained with Phalloidin 488 and scored for invadopodia presence. Scale bar corresponds to 10μm. (B): Graphical representation of percentage of cells making invadopodia. Bars represent the mean percentage of cells with invadopodia and error bars represent the SEM. Statistical analysis involved one way ANOVA followed by Tukey's post hoc testing. Comparisons between the knockdown conditions and the negative control are shown on the graph, (***) = $p \leq 0.001$. There was no significant difference between the WT and the negative control conditions. (N=3).

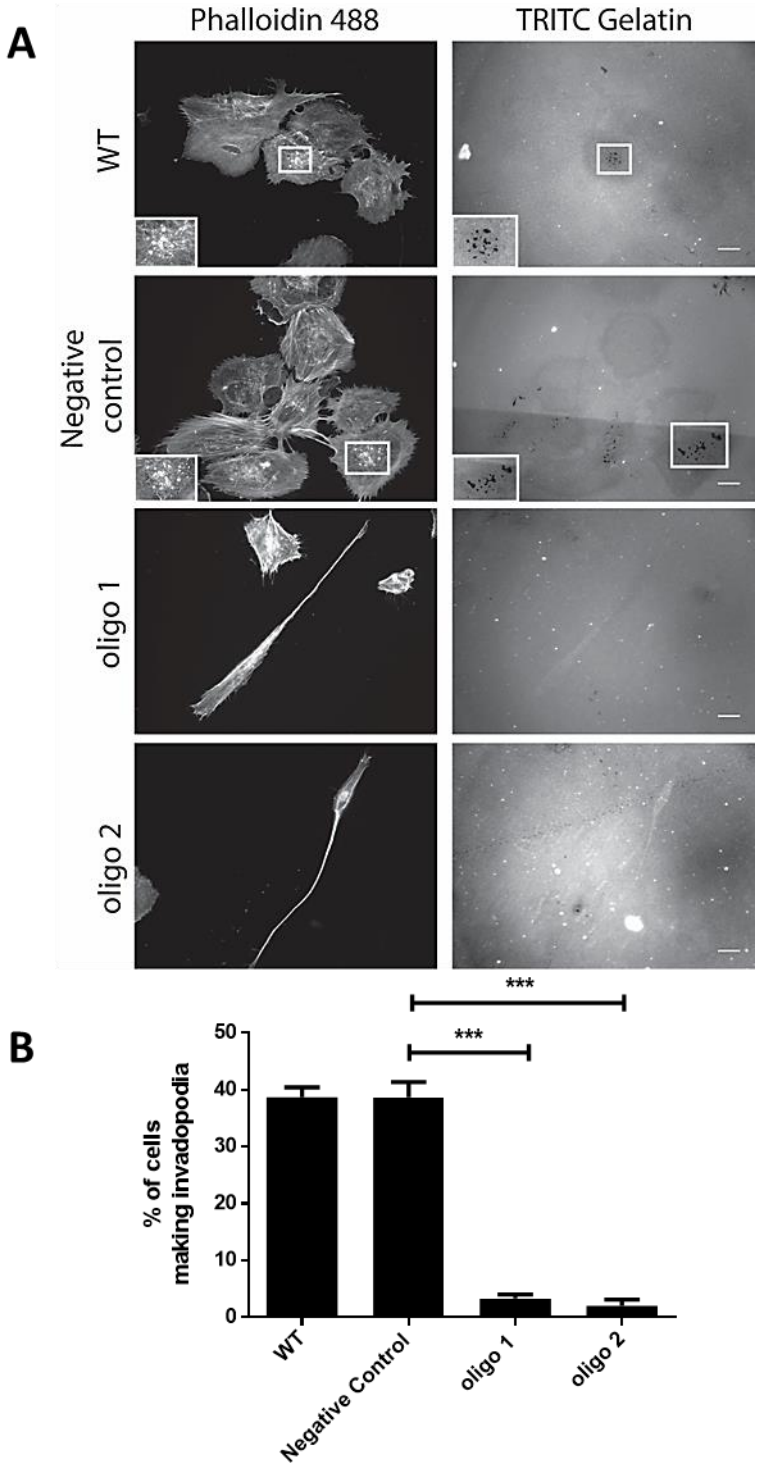

Figure 4.11 Invadopodia Presence in IQGAP3 depleted BT-549 cells. (A): IQGAP3 knockdown and control BT-549 cells were seeded on TRITC gelatin coated coverslips and incubated for 7h. Cells were subsequently stained with Phalloidin 488 and scored for invadopodia presence. Scale bar corresponds to 10μm. (B): Graphical representation of percentage of cells making invadopodia. Bars represent the mean percentage of cells with invadopodia and error bars represent the SEM. Statistical analysis involved one way ANOVA followed by Tukey's post hoc testing. Comparisons between the knockdown conditions and the negative control are shown on the graph, (***) = $p \leq 0.001$. There was no significant difference between the WT and the negative control conditions. (N=3).

4.2.7 Morphology of IQGAP3 overexpressing cells

Cells with reduced IQGAP3 expression display an altered cellular morphology, thus the morphological consequences of IQGAP3 overexpression were also assessed. GFP tagged IQGAP1 and IQGAP3 constructs (**figure 3.1**) were transfected in MB-231 and BT-549 cells. A GFP alone control was also included along with wild-type cells. Transfected cells were then seeded on fibronectin coated coverslips and fixed 48h post transfection. Interestingly, morphological analysis revealed that IQGAP3-GFP MB-231 and BT-549 cells were significantly more elongated their wild-type counterparts (**figure 4.12, 4.13**). IQGAP1-GFP BT-549 cells were found to be significantly more elongated than their wild-type counterparts but less elongated than the IQGAP3-GFP overexpressing cells (**figure 4.13**). However, the elongated phenotype observed following IQGAP3 overexpression was not as dramatic as the one observed in IQGAP3 depleted cells. The quantification of the relative elongation parameter revealed that IQGAP3 depleted cells are more elongated with a mean relative elongation value of 0.8 (**figures 4.4, 4.5**) whereas the IQGAP3 over-expressing cells exhibiting a mean relative elongation value of 0.6 (**figures 4.12, 4.13**). This might suggest that different mechanisms drive the elongated phenotypes observed in IQGAP3 depleted and over-expressing cells.

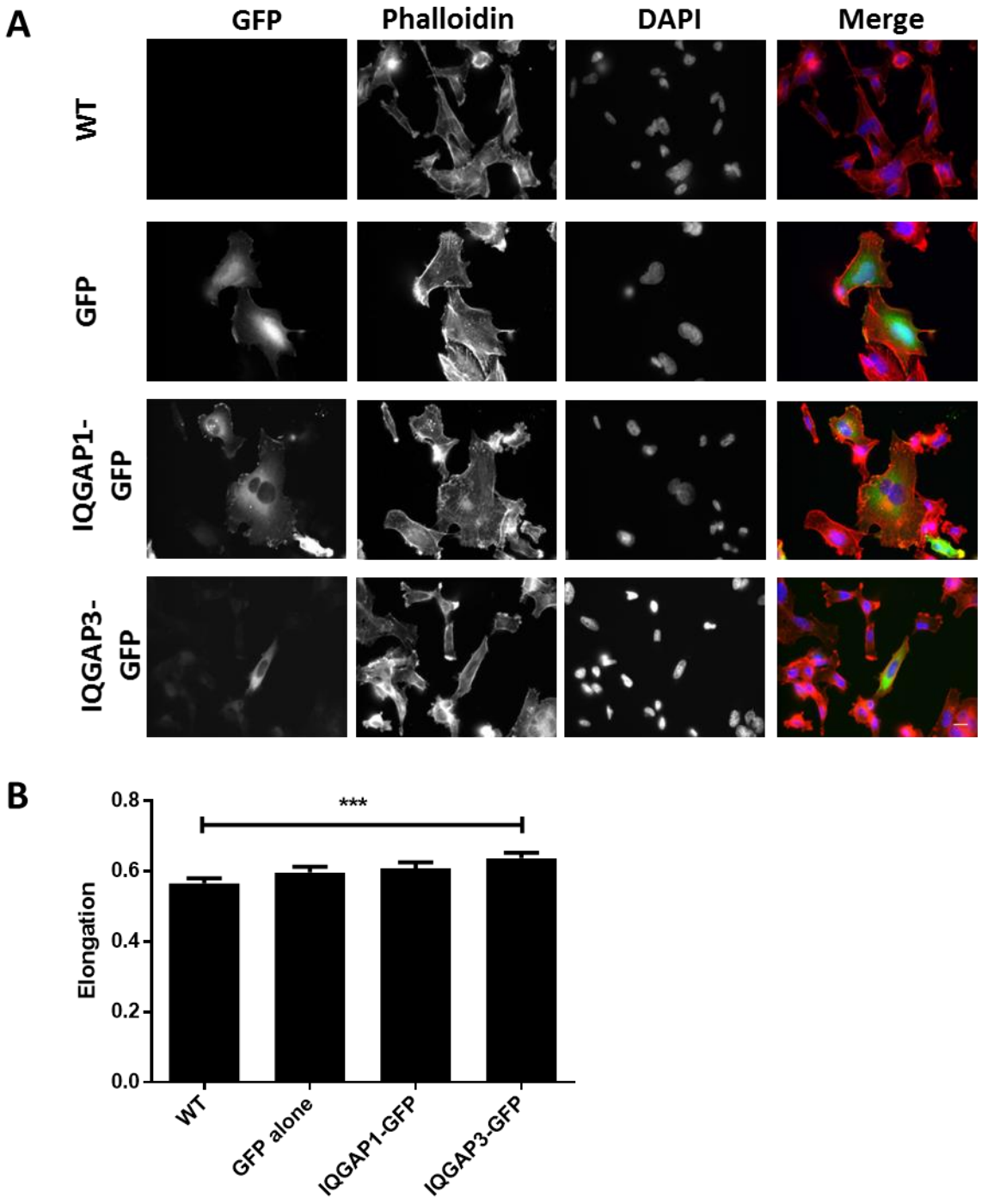

Figure 4.12 Morphology of IQGAP overexpressing MB-231 cells. (A): MB-231 cells were transfected with IQGAP1-GFP or IQGAP3-GFP. A GFP alone and wild-type controls were included in the experiment. Cells were fixed 48h post transfection and stained with TRITC phalloidin and DAPI. IQGAP transfected and control cells were subjected to morphological analysis. Scale bar corresponds to 10μm. (B): Graphical representation of cell elongation index. Bars represent the mean elongation values and error bars represent the SEM. Statistical analysis involved one way ANOVA followed by Tukey's post hoc testing. Comparison between the IQGAP3-GFP and the WT control is indicated on the graph, (***) = $p \leq 0.001$. No other comparisons reached statistical significance (N=3).

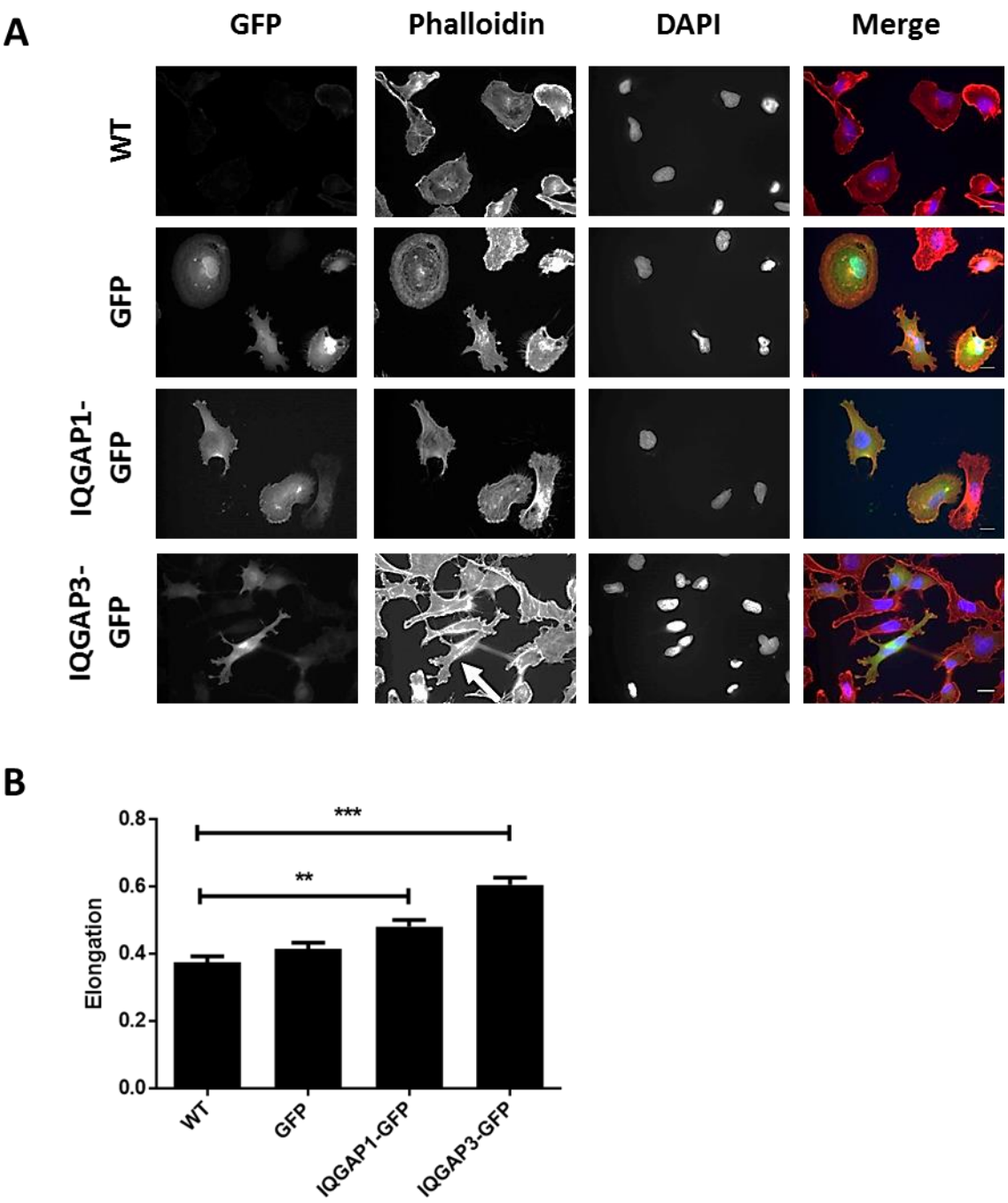

Figure 4.13 Morphology of IQGAP overexpressing BT-549 cells. (A): BT-549 cells were transfected with IQGAP1-GFP or IQGAP3-GFP. A GFP alone and wild-type controls were included in the experiment. Cells were fixed 48h post transfection and stained with TRITC phalloidin and DAPI. IQGAP transfected and control cells were subjected to morphological analysis. Arrow indicates the formation of lamella in the IQGAP3-GFP over-expressing cell. Scale bar corresponds to 10μm. (B): Graphical representation of cell elongation index. Bars represent the mean elongation values and error bars represent the SEM. Statistical analysis involved one way ANOVA followed by Tukey's post hoc testing. Comparisons between the WT control and IQGAP1-GFP as well as the WT control and IQGAP3-GFP are indicated on the graph, (**) = $p \leq 0.01$, (***) = $p \leq 0.001$. No other comparisons reached statistical significance (N=3).

4.2.8 Invadopodia formation in IQGAP3 overexpressing cells.

IQGAP3 depletion inhibited invadopodia formation in MB-231 and BT-549 cells (**figures 4.10, 4.11**). Transient overexpression of IQGAP3 was hence employed to see whether IQGAP3 localises at invadopodia or has an effect in invadopodia mediated degradation thereby supporting a role of IQGAP3 in invadopodia dynamics.

Upon considering the necessary tools for this experiment, it was decided that invadopodia markers other than the actin structure and the resulting degraded gelatin might be needed. Subjecting IQGAP3-GFP overexpressing cells to the invadopodia assay which involves seeding cells on TRITC conjugated gelatin required the detection of an invadopodia marker in the far-red spectrum. Cortactin was decided as the most appropriate candidate since it has been widely used in the literature as a defining marker of invadopodia presence (Foxall et al., 2016). An immunofluorescence staining protocol for cortactin using a secondary antibody emitting in the far-red area of the wavelength spectrum was thus optimised and established for both cell lines. The immunofluorescence cortactin staining was deemed successful when the cortactin signal appeared to co-localise with actin puncta as well as degradation areas (**figure 4.14**).

The assessment of IQGAP3-GFP overexpression in invadopodia dynamics was performed on the BT-549 cells alone. The low transfection efficiency of IQGAP3-GFP in MB-231 cells together with the fact that only a fraction of the cell population makes invadopodia rendered the experiment non feasible in MB-231 cells. BT-549 cells over-expressing IQGAP3-GFP or GFP alone along with wild-type cells were seeded on TRITC gelatin and were fixed following a 7h incubation. Cells were subsequently stained for cortactin as an indication of invadopodia presence. Morphological analysis revealed that IQGAP3 overexpressing cells retain their elongated shape when seeded on gelatin (**figure 4.15A, 4.15B**). Therefore, this effect is not specific to fibronectin coating. Furthermore, upon scoring cells for invadopodia presence it was discovered that the ability of IQGAP3-GFP over-expressing cells to make invadopodia is almost entirely lost as deduced by the absence of actin puncta and matrix degradation mediated holes (**figure 4.15C**). Thus localisation of IQGAP3-GFP at invadopodia was not possible. Again, considering the well described role of IQGAP1 in invadopodia mediated degradation (Sakurai-Yageta et al., 2008), IQGAP3 is thought to affect invadopodia dynamics via an entirely different mechanism.

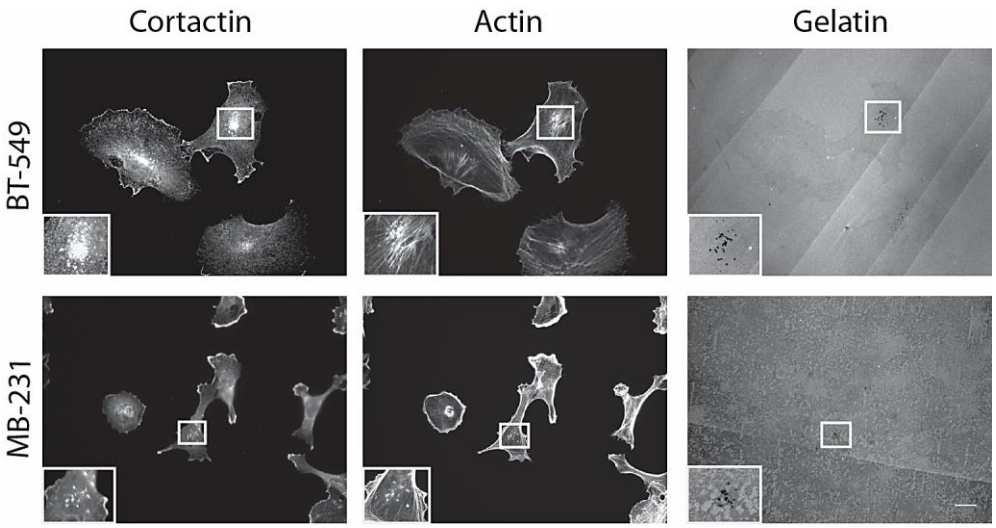

Figure 4.14 Optimisation of cortactin immunofluorescence staining. Cells were seeded on TRITC gelatin and were incubated for 7h in the case of BT-549 cells and 3h in the case of MB-231. Cells were subsequently fixed and stained with cortactin (1:50) followed by alexafluor anti-mouse 647 secondary (1:400) antibody and Phalloidin 488. Scale bar corresponds to 10μm.

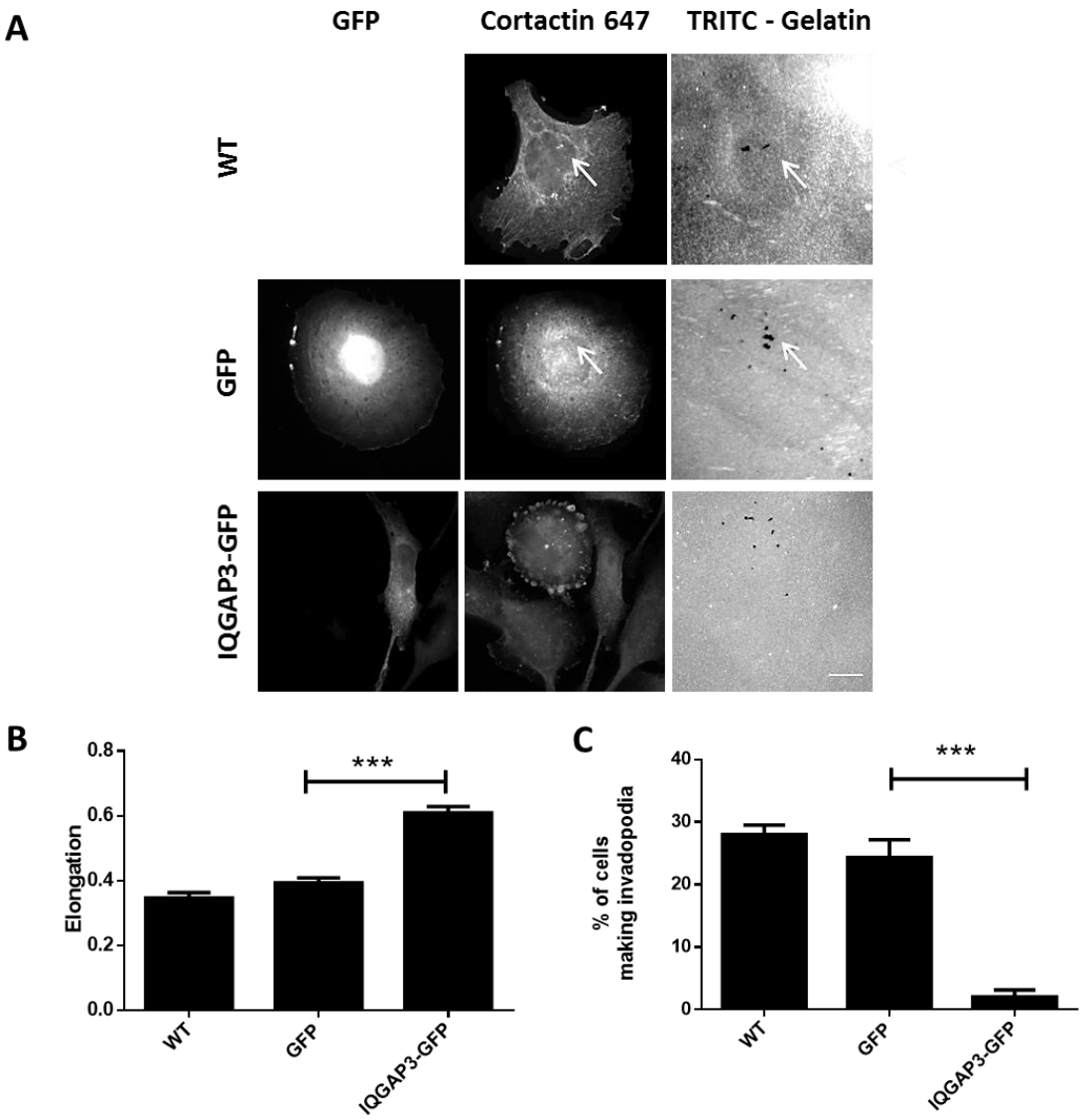

Figure 4.15 Invadopodia formation in IQGAP3-GFP overexpressing BT-549 cells. (A): IQGAP3-GFP overexpressing cells alongside GFP alone and wild-type cells were seeded on TRITC gelatin coated coverslips and were incubated for 7h. Cells were then stained for cortactin and imaged. Scale bar corresponds to 10μm. (B): Graphical representation of the elongation index for each condition. Bars represent the mean elongation values and error bars represent the SEM. Statistical analysis involved one way ANOVA followed by Tukey's post hoc testing. Comparisons between IQGAP3-GFP and the GFP alone control is shown on the graph, (***) = $p \leq 0.001$. There was no significant difference between the WT and the GFP alone control conditions. (N=3). (C): Cells were scored for invadopodia formation for each condition. Bars represent the mean percentage of cells with invadopodia and error bars represent the SEM. Statistical analysis involved one way ANOVA followed by Tukey's post hoc testing. Comparisons between IQGAP3-GFP and the GFP alone control is shown on the graph, (***) = $p \leq 0.001$. There was no significant difference between the WT and the GFP alone control conditions. (N=3).

4.2.9 Effect of modulating IQGAP3 expression in cytokinesis

IQGAP1 as well as IQGAP3 have been reported to have an important role in cytokinesis. IQGAP3 in particular has been shown to control RhoA localisation by uniquely interacting with anillin (Adachi et al., 2014). Diminishing either of the two IQGAPs conferred an increase in binucleate Hela cells suggesting that IQGAP depletion interferes with successful completion of cytokinesis (Adachi et al., 2014). This effect has only been reported in Hela cells which is a widely used cell line in mammalian cytokinesis studies. Consequently, the effect of inhibiting IQGAP3 expression in cytokinesis was examined in the triple negative breast cancer cell lines. Additionally, the effect of IQGAP3 overexpression in cytokinesis was also assessed. The incidence of binucleated cells as revealed by the DAPI stain was recorded for IQGAP3 depleted and overexpressing as well as control MB-231 and BT-549 cells. In contrast to studies in Hela cells, loss of IQGAP3 did not confer an increase in binucleate cells in either MB-231 or BT-549 cells (**figure 4.16A, 4.16C**). Interestingly though, IQGAP3-GFP overexpression conferred a significant increase in binucleated cells in both MB-231 and BT-549 cell populations while IQGAP1-GFP overexpression conferred a significant increase only in binucleated MB-231 cells (**figure 4.16B, 4.16D**).

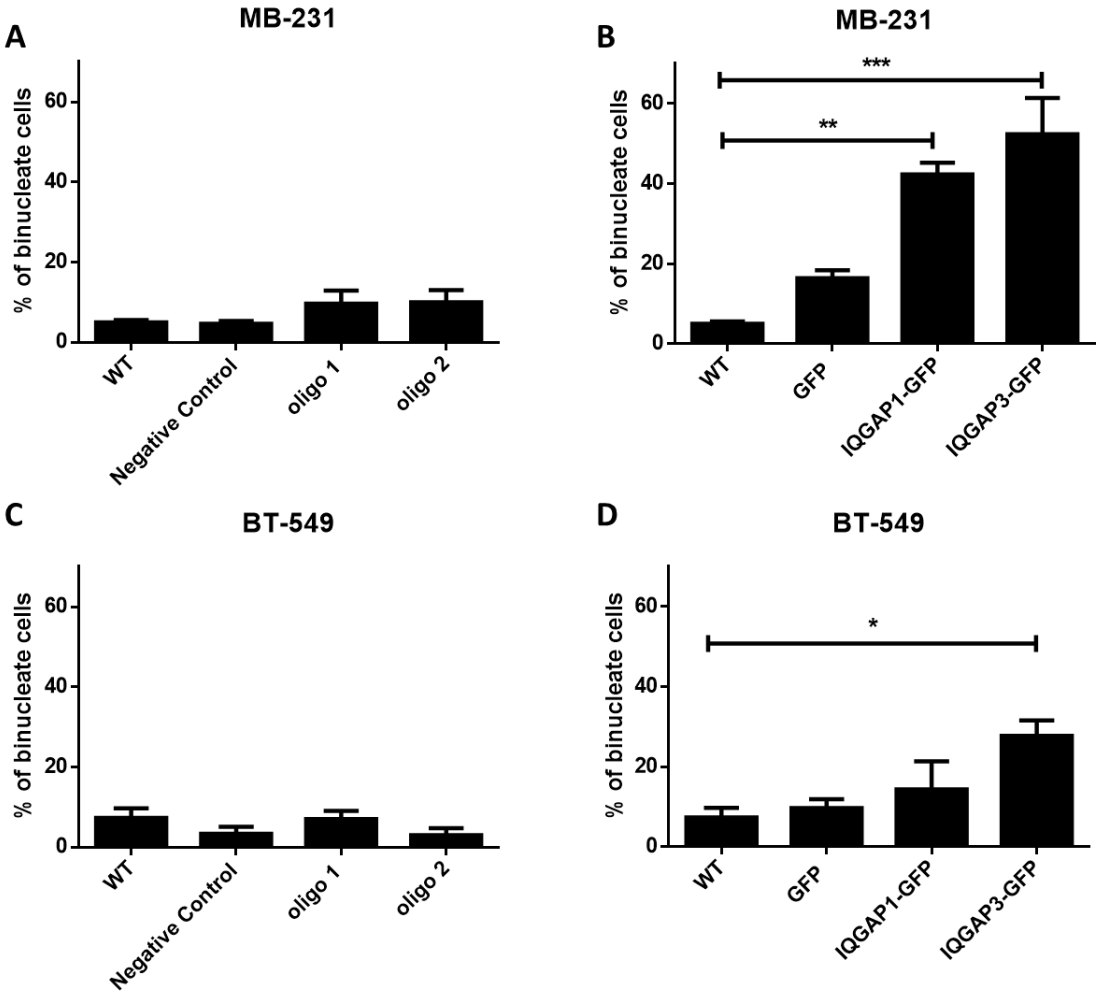

Figure 4.16 Binucleate cells following modulation of IQGAP3 expression. (A): Percentage of binucleate MB-231 cells in knockdown and control conditions. Statistical analysis involved one way ANOVA testing, (non-significant $p > 0.05$). (B): Percentage of binucleate cells overexpressing IQGAP1-GFP, IQGAP3-GFP as well as control MB-231 cells. Statistical analysis involved one way ANOVA followed by Tukey's post hoc testing. Comparisons between the WT control and IQGAP1-GFP as well as the WT control and IQGAP3-GFP are shown on the graph, (**) = $p \leq 0.01$, (***) = $p \leq 0.001$. There was no significant difference between the WT and the GFP alone control conditions. (N=3). (C): Percentage of binucleate BT-549 cells in knockdown and control conditions. Statistical analysis involved one way ANOVA testing, (non-significant $p > 0.05$). (D): Percentage of binucleate overexpressing IQGAP1-GFP, IQGAP3-GFP as well as control BT-549 cells. Statistical analysis involved one way ANOVA followed by Tukey's post hoc testing. Comparison between the WT control and IQGAP3-GFP are shown on the graph, (*) = $p \leq 0.05$. No other comparison reached statistical significance. (N=3). Bars represent the mean percentage of binucleate cells and error bars represent the SEM.

4.3 Discussion

This chapter investigates cellular behaviour following the modulation of IQGAP3 expression levels. After validating two siRNA sequences that can effectively diminish IQGAP3 expression the effect of IQGAP3 depletion in cell proliferation was primarily validated. Consistent with previous published work (Hu et al., 2016; Xu et al., 2016; Yang et al., 2014), the MTT assays performed revealed that cell proliferation is reduced upon IQGAP3 depletion (**figure 4.3**). Work on the role of IQGAP in skin homeostasis suggested that a very robust knockdown may be needed to elicit IQGAP3 depletion mediated effects but at the same time the proliferation arrest may render several experimental assays unsuitable (Monteleon et al., 2015). The morphology, migration and invasion assays in this study are proliferation independent.

IQGAP3 depletion leads to a hyper-elongated morphology in our triple negative breast cancer cell lines (**figures 4.4, 4.5**). Elongated cells feature a mesenchymal type of migration, dynamic turnover of focal adhesions and extension of a single leading cell edge via Rac activity (Friedl and Wolf, 2010). However, IQGAP3 normally binds and maintains Rac in its GTP bound activated state thereby promoting Rac activity (Wang et al., 2007). Loss of IQGAP3 would thus imply loss of Rac activity and ultimately lack of a single elongating leading cell edge. Therefore, the observed elongated morphology induced from IQGAP3 depletion is unlikely to be a result of Rac activity. Meanwhile, the imaged IQGAP3 knockdown cells as well as the time-lapse videos suggested that the elongated phenotype was likely to be a result of loss of tail retraction rather a hyper-extended leading cell edge. Tail retraction is a result of actomyosin contractility which is regulated by Rho (Friedl and Wolf, 2009). Additionally, IQGAP3 depleted cells exhibited a dramatic loss of mature focal adhesions (**figures 4.8, 4.9**) whose formation is also under the regulation of Rho (Chrzanowska-Wodnicka and Burridge, 1996; Ridley and Hall, 1992). Hence, IQGAP3 was thought to be implicated in maintaining Rho activity which was disrupted once IQGAP3 expression was lost.

Interestingly, knockdown of RhoA conferred the same elongated phenotype in MB-231 cells as well as in prostate cancer cell lines PC3 and DU145 (Vega et al., 2011). These cells also exhibited reduced speed similarly to the IQGAP3 depleted MB-231 and BT-549 cells. Furthermore, the authors observed that RhoA knockdown cells extended towards opposing directions thereby affecting overall displacement (Vega et al., 2011). In fact, this is a feature that was also sometimes

observed in the triple negative breast cancer cell lines upon loss of IQGAP3 expression. This might suggest that IQGAP3 depletion could elicit the effects of RhoA depletion which agrees with the hypothesis proposing that IQGAP3 is involved in the regulation of Rho and actomyosin contractility.

Meanwhile, overexpression of IQGAP3-GFP also mediated an elongated phenotype in both MB-231 and BT-549 cells (**figures 4.12, 4.13**). Nonetheless, the IQGAP3 overexpressing cells were notably less elongated as revealed by the quantified relative elongation parameter (**figures 4.5, 4.13**). Consequently, the elongated phenotypes resulting from both knockdown and overexpression of IQGAP3 are most likely results of entirely different signalling pathways. Interestingly, it has been suggested that expression levels of IQGAP1 dictate which pathway the protein is going to scaffold; IQGAP1 depletion or overexpression inhibit ERK activity while overexpression of IQGAP1 activates Akt (Choi and Anderson, 2017). A similar mechanism could be in place for IQGAP3; optimal levels of IQGAP3 might maintain Rho activity and actomyosin contractility while over-expressed IQGAP3 could be switching to enhancing Rac1 and Cdc42 activity.

Nonetheless, the effect of IQGAP3 overexpression in cell morphology has not been directly described before. Upon IQGAP3 knockdown in neuronal cells, axonal extension is lost (Wang et al., 2007) and thus it can be deduced that IQGAP3 supports cell elongation. Consistent with this hypothesis, IQGAP3 is also involved in localising APC at the leading cell edge (Caro-Gonzalez et al., 2012). The interaction of IQGAP1 to APC has similarly been described as important for directional cell migration (Watanabe et al., 2004). Hence, it is perhaps not surprising that IQGAP1-GFP also induced an elongating effect in BT-549 cells (**figure 4.13**) considering the well described role of IQGAP1 in directional cell migration and its localisation at the leading cell edge (M. Fukata et al., 2001; Watanabe et al., 2004). Furthermore, both IQGAPs act as scaffolds and stabilise Rac1 activity which in turn regulates the formation of lamellipodia during cell migration (Smith et al., 2015). Hence, the resulting elongated phenotype upon IQGAP overexpression agrees with previously published findings and thus it can be argued that IQGAP1 and IQGAP3 appear to be functioning in parallel in this case, contributing to increased Rac activity and directional cell migration (Caro-Gonzalez et al., 2012; Fukata et al., 2001; Smith et al., 2015; Watanabe et al., 2004) .

Nonetheless, there is also evidence suggesting that loss of IQGAP1 activity elicits its morphological and migrational consequences in an entirely different way compared to what is

presented in this chapter regarding the effects of IQGAP3 depletion. Multiple cell edges and loss of directionality were observed following transfection of a mutant IQGAP1 construct deficient of the PIP2 binding site in MEFs as well as transfection of an IQGAP1 mutant deficient of the Rac1/Cdc42 binding site in Vero cells (Choi et al., 2013; Watanabe et al., 2004).

Additionally, it was observed that the elongated IQGAP3 depleted cells also lacked mature focal adhesions (**figures 4.8, 4.9**). It has previously been reported that IQGAP1 is associated with focal adhesion dynamics. Indeed IQGAP1 stimulated PDGF induced focal adhesion formation in vascular smooth muscle cells by binding PDGF receptor- β and promoting its auto-phosphorylation (Kohno et al., 2013). Another study has suggested that HECTD1 ensures efficient formation of mature focal adhesions by marking IQGAP1 for ubiquitination while overexpression of IQGAP1-GFP significantly inhibited the formation of focal adhesions in MEFs (Shen et al., 2016). Even though it appears as though the data regarding the association of IQGAP1 with focal adhesions are conflicting; it can be argued that IQGAP1 and IQGAP3 are associated with focal adhesion dynamics even though the mechanisms involved remain unknown. This chapter showed that IQGAP3 depletion dramatically reduced invadopodia formation in MB-231 and BT-549 cells (**figures 4.10, 4.11**).This might suggest that IQGAP1 and IQGAP3 function in the same pathway considering the role of IQGAP1 in delivering MT1-MMP to the protrusions (Sakurai-Yageta et al., 2008). However, reducing IQGAP1 expression had an effect in the invadopodia mediated degradation rather than the formation of the protrusion (Sakurai-Yageta et al., 2008) whereas loss of IQGAP3 expression eliminated invadopodia entirely as measured by the loss of actin puncta and not just degradation mediated matrix holes.

Nonetheless, the dramatic loss of invadopodia upon diminishing IQGAP3 expression does not necessarily mean that IQGAP3 is actively involved in invadopodia dynamics as this observed phenotype could also result from impaired RhoA activity and actomyosin contractility. In fact, work on melanoma cells has highlighted that the coordinated activation and inactivation of RhoA is crucial for the invadopodia lifecycle; with RhoA activity being important for invadopodia formation while RhoA inactivation allows the maturation of the protrusion (Nicholas et al., 2016). Furthermore, inhibition of either myosin II or ROCK led to loss of invadopodia mediated matrix degradation in breast cancer CA1D cells. However, the actual actin protrusions remained but appeared smaller (Alexander et al., 2008). Interestingly, diminishing ROCK1 expression decreased the number of invadopodia protrusions while diminishing ROCK2 expression reduced

invadopodia mediated matrix degradation but did not affect the number of invadopodia in SCC-61 cells (Jerrell and Parekh, 2016).

Meanwhile, overexpression of IQGAP3-GFP also eliminated invadopodia formation and activity. At the same time, IQGAP3 overexpressing triple negative breast cancer cells retained their very elongated morphology on gelatin which agrees with results outlined in chapter 3 where it was deduced that a rounded morphology is more permissive to the formation of invadopodia than an elongated cell morphology (**figure 3.9**). Consequently, by subjecting IQGAP3 knockdown and over-expressing cells to the invadopodia assay it has not been possible to pinpoint a potential mechanism via which IQGAP3 is associated with invadopodia dynamics. Nonetheless, this mechanism is arguably different to the one employed by IQGAP1. It can be postulated that excess IQGAP3 sequesters away crucial invadopodia components ultimately disabling the formation of the protrusion. Considering that IQGAP1 has over 100 known binding partners including cortactin (Hedman et al., 2015), it would not be surprising if IQGAP3 were able to interact with crucial invadopodia components too. Alternatively, it is likely that IQGAP3 is associated with invadopodia by dictating a balanced RhoA activity (Nicholas et al., 2016) and regulating actomyosin contractility which has previously been described as important for invadopodia dynamics (Jerrell and Parekh, 2016).

Ultimately, this chapter suggests that IQGAP3 depletion and overexpression can lead to the same phenotypical effects such as an elongated morphology and loss of invadopodia capacity. Again, as suggested by Choi and Anderson, the activation of the responsible pathway may be dependent on expression levels (Choi and Anderson, 2017); optimal levels of IQGAP3 might maintain morphological integrity and invadopodia capacity while any variation in the IQGAP3 expression levels can induce a switch in the activated pathway and disrupt these features.

Furthermore, IQGAP3 is known to regulate RhoA localisation at the cleavage furrow via a unique interaction to anillin during cytokinesis (Adachi et al., 2014). This suggests that IQGAP3 might be involved in regulating contractility without directly binding to Rho (Adachi et al., 2014; Wang et al., 2007). IQGAP1 localises at the cell cortex throughout mitosis while IQGAP3 specifically localises at the cleavage furrow from metaphase until telophase (Adachi et al., 2014). Knockdown of either IQGAP1 or IQGAP3 affected the localisation of RhoA at the cleavage furrow suggesting that IQGAPs are involved in the formation of the contractile ring during cytokinesis by regulating the recruitment of RhoA (Adachi et al., 2014). However, reduction of IQGAP3 levels in MB-231 and BT-549 cells had no effect in the incidence of binucleated cells. In contrast to IQGAP3 depletion,

overexpression of IQGAP3-GFP significantly increased binucleate cells in both cell lines, while overexpression of IQGAP1-GFP had the same effect in MB-231 cells (**figure 4.16**). Perhaps, poor spatiotemporal regulation of IQGAPs induced by overexpression may interfere with contractility and thus be the reason behind failed cytokinesis.

Overall, evidence yielding from this chapter supports the hypothesis that IQGAP3 might be involved in the regulation of actomyosin contractility. The hyper-elongated morphology accompanied by loss of mature focal adhesions, migratory ability and formation of invadopodia that is observed following depletion of IQGAP3 expression may thus be a result of interfering with actomyosin contractility and not a consequence of disrupting each individual process. Nonetheless, IQGAP3 has not been implicated with actomyosin contractility before. In fact both IQGAP1 and IQGAP3 have traditionally been known to bind and act as scaffolds for Rac1 and Cdc42 and not Rho (Adachi et al., 2014; Kuroda et al., 1996; Wang et al., 2007). Interestingly though, a study employing immunoprecipitation experiments in HEK293T cells showed that IQGAP1 directly interacts with RhoA and RhoC and that the binding to RhoA is enhanced when RhoA is GTP-bound and prenylated (Casteel et al., 2012). More recently, it has also been reported that IQGAP1 binds RhoA in human airway smooth muscle cells and inhibits RhoA activity thereby reducing contractility (Bhattacharya et al., 2014). However, IQGAP3 has never been shown to bind Rho despite well designed immuno-precipitation experiments (Adachi et al., 2014; Wang et al., 2007). Furthermore, if the phenotypes emerging from IQGAP3 depletion are in fact a consequence of disrupted contractility then this would mean that IQGAP3 promotes contractility related pathways. Thus it might be speculated that IQGAP1 and IQGAP3 mediate opposing effects in cell contractility. IQGAPs have been previously reported to have opposing function, given that IQGAP2 is reported to have tumour suppressive action in hepatocellular carcinoma (Schmidt et al., 2008) while IQGAP1 has been extensively described to promote carcinogenesis (White et al., 2009). Ultimately, differential functionality exhibited by IQGAP1 and IQGAP3 in triple negative breast cancer cell motility could also explain that IQGAP3 mRNA levels and not those of IQGAP1 have been found to be elevated in triple negative tumours.

4.4 Future work

This chapter described the phenotypes that arise from diminishing and overexpressing IQGAP3. It can be argued that the observed elongated cells lacking mature focal adhesions that have lost the ability to move and make invadopodia may be a result of impaired actomyosin contractility caused by IQGAP3 depletion. It would be interesting to assess the effect of diminishing IQGAP1 in the triple negative breast cancer cell lines and make a thorough and systematic comparison between IQGAP1 and IQGAP3 depletion in the cell motility phenotypes outlined in this chapter. This could potentially further support the argument that IQGAP3 possesses unique functionality in triple negative breast cancer. Moreover, an inducible knockdown system effectively reducing IQGAP3 expression on demand could allow experimenting with IQGAP3 depletion in more long-term *in vitro* assays such as the spheroid invasion assay (Nicholas et al., 2016) which can validate the role of IQGAP3 in triple negative breast cancer cell invasion. Additionally, monitoring IQGAP overexpressing cells by time-lapse microscopy would further elucidate whether IQGAP1 and IQGAP3 can have complementary activities in cell migration. This however was deemed an unfeasible experiment given the low transfection efficiency of IQGAP3.

The next chapter aims to provide a potential mechanism via which IQGAP3 is implicated in actomyosin contractility and confirm that IQGAP3 has the capacity to contribute to triple negative breast cancer cell motility.

Chapter 5

Investigation of IQGAP3 interacting partners

Chapter 5 : Investigation of IQGAP3 interacting partners

5.1 Introduction

Results outlined in chapter 4 showed that IQGAP3 depletion conferred cytoskeletal changes leading to a very elongated cell shape accompanied by loss of cell migration and invasion properties. Cytoskeletal dynamics are widely known to be under the regulation of the Rho GTPases (Hall, 1998). The conferred elongated morphology pointed towards the loss of cell contraction and tail retraction which is coordinated by Rho (Poincloux et al., 2011; Ridley, 2001). RhoA mediates actomyosin contractility by signalling via Rho kinase (ROCK) which in turn regulates the phosphorylation of myosin regulatory light chain (regulatory MLC) in two ways; by inhibiting MLC phosphatase and by directly phosphorylating regulatory MLC (Amano et al., 2010; Katoh et al., 2001; Kimura et al., 1996). Indeed, phosphorylated myosin II stimulated neurite retraction in N1E-115 neuroblastoma cells following Rho-ROCK activity (Amano et al., 1998). The loss of phosphorylated MLC could thus explain the lack of tail retraction in IQGAP3 depleted triple negative breast cancer cells. Interestingly, IQGAP1 has been shown to bind myosin essential light chain (essential MLC) via one of its IQ motifs in a yeast two hybrid assay (Weissbach et al., 1998). More recent work employing native gel electrophoresis showed that in contrast to IQGAP2, IQGAP1 but also IQGAP3 interact with essential MLC (Atcheson et al., 2011; Pathmanathan et al., 2008). It is postulated that there is a functional difference between these interactions as the interaction of IQGAP3 with essential MLC is likely to be more transient as suggested by the less distinct gel shift observed (Atcheson et al., 2011). IQGAP3 is thus associated with a crucial contractility effector which further supports the hypothesis that IQGAP3 might be involved in the regulation of triple negative breast cancer cell contractility.

Recent work in my lab has revealed a functional complex of PAK6 and Filamin-A upstream of Rho-ROCK which is able to elicit morphological changes and drive a more contractile phenotype in MB-231 cells (personal communication). In fact, similarly to IQGAP3, loss of PAK6 also led to an elongated morphology in MB-231 cells (personal communication) ultimately suggesting that IQGAP3 depletion might phenocopy the effect of reduced expression levels of PAK6. This observation sparked the investigation of whether IQGAP3 is part of the same pathway.

IQGAP3 has not been shown to interact with any member of the PAK family. Interestingly though, IQGAP1 is reported to associate with PAK6 in breast cancer MCF7 cells (Kaur et al., 2008) while

the same association disrupts cell junctions in response to HGF in prostate cancer DU145 cells (Fram et al., 2014). PAK6 is a group II PAK that has traditionally been thought to be a Cdc42 effector (Schrantz et al., 2004) and is known to bind the androgen and oestrogen receptors (AR and ERα) (Lee et al., 2002). It is thus not surprising that PAK6 expression has been validated in prostate and breast cancer cell lines (Kaur et al., 2008) . Similarly to IQGAP3, PAK6 expression is highly expressed in the brain and testis (Kaur et al., 2008; White et al., 2009). Furthermore, PAK6 induced neurite outgrowth in mouse striatum *in vivo* (Civiero et al., 2015) while IQGAP3 was shown to regulate neurite outgrowth of PC12 cells *in vitro* (Wang et al., 2007). It is thus likely that there is a potential synergy between IQGAP3 and PAK6.

Filamin-A was first isolated from chicken embryo gizzard cells where it was found to be arranged similarly to myosin (Wang et al., 1975). Since then, Filamin-A has been found to be a potent actin filament cross-linker (Flanagan et al., 2001). Filamin-A has also been reported to influence cell spreading by interacting with p190RhoGAP and thus regulating Rho activity in human melanoma cells(Mammoto et al., 2007). Additionally, Filamin-A deficient melanoma cells were less contractile than Filamin-A repleted cells as shown by traction force microscopy (Kasza et al., 2009). Interestingly, Filamin-A complexes with IQGAP1 upon β1 integrin activation and together they regulate directional cell migration by modulating Rac1 activity (Jacquemet et al., 2013). Meanwhile, Filamin-A overexpression has been marked in breast tumours and associated with disease progression and metastasis (Tian et al., 2013). The implication of Filamin-A with aggressive breast cancer together with the fact that it interacts with IQGAP1 further supported the investigation of a potential interaction of Filamin-A with IQGAP3.

Hence, the work outlined in this chapter aims to provide evidence suggesting that IQGAP3 is implicated in contractility related pathways thereby being able to modulate triple negative breast cancer cell morphology as part of a complex with PAK6 and Filamin-A.

5.2 Results

5.2.1 Effect of IQGAP3 depletion in myosin light chain activation

IQGAP3 has been reported to bind the essential MLC but the functional significance of this interaction remains unknown (Atcheson et al., 2011). In order to test the hypothesis that IQGAP3 is involved in the regulation of actomyosin contractility, the effect of IQGAP3 depletion was examined on phosphorylated levels of regulatory MLC. Regulatory MLC phosphorylation on Ser19 marks the activation of MLC which is then able to associate with actin and relay cell contraction (Katoh et al., 2001). Control and IQGAP3 depleted MB-231 and BT-549 cells were lysed 96h post transfection and were subjected to western blotting in order to assess the levels of phosphorylated MLC. Indeed, levels of phosphorylated MLC were significantly reduced by both oligonucleotides in both MB-231 and BT-549 cells (**figures 5.1, 5.2**). This finding suggests that IQGAP3 expression levels can have a profound effect on the activity of myosin light chain and thus the formation of contractile actomyosin bundles.

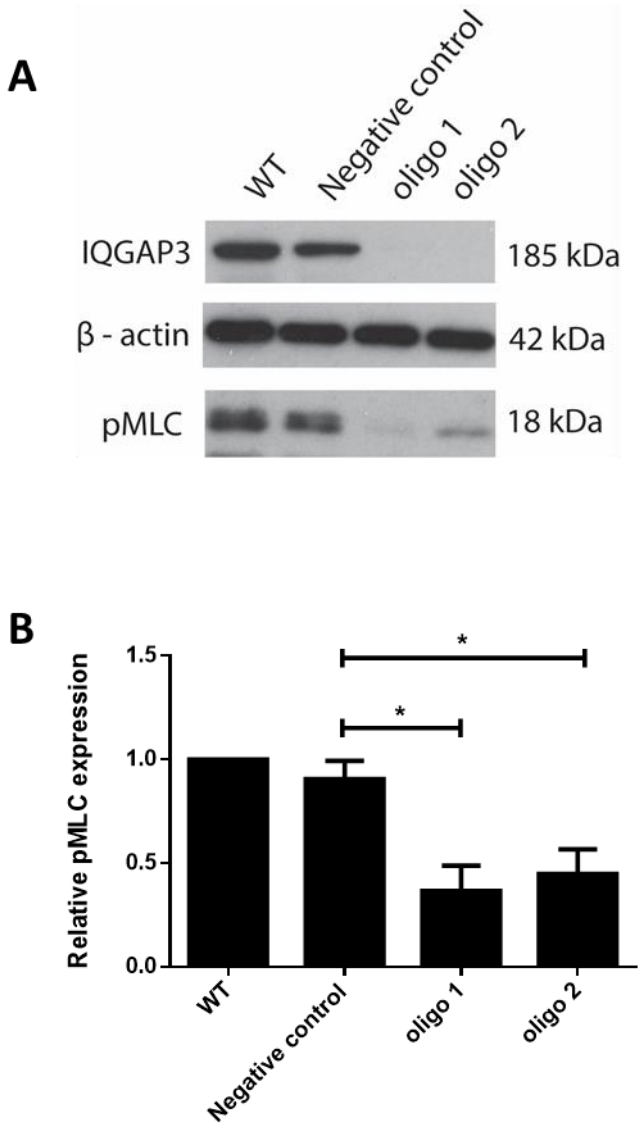

Figure 5.1 Effect of IQGAP3 depletion on phosphorylated MLC in MB-231 cells. (A): Control and IQGAP3 knockdown MB-231 cells were lysed 96h post transfection and were subjected to western blotting. Samples were probed for IQGAP3 (185kDa) and phospho – MLC (18kDa). β-actin was used as a loading control (42kDa). (B): Levels of phospho-MLC were quantified by densitometric analysis on ImageJ and were normalised against the loading control, background noise and wild-type levels. Bars represent the mean relative pMLC expression and error bars represent the SEM. Statistical analysis involved one way ANOVA followed by Tukey's post hoc testing. Comparisons between knockdown conditions and the negative control are indicated on the graph, (*) = $p \leq 0.05$. There was no significant difference between the WT and the negative control conditions (N=3).

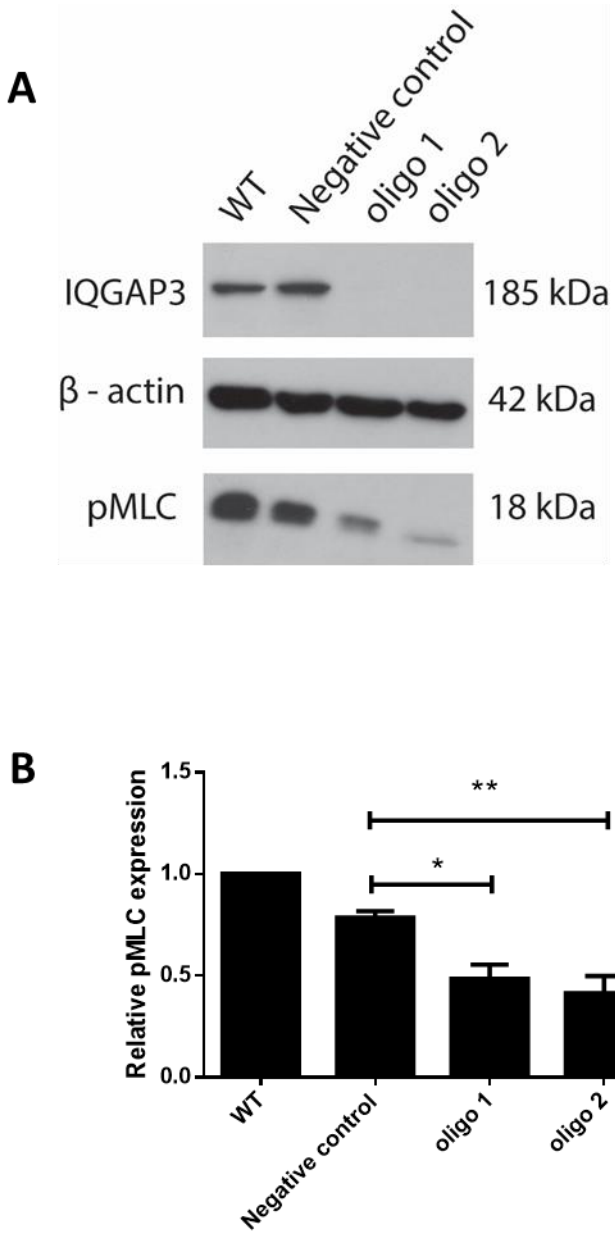

Figure 5.2 Effect of IQGAP3 depletion on phosphorylated MLC in BT-549 cells. (A): Control and IQGAP3 knockdown BT-549 cells were lysed 96h post transfection and were subjected to western blotting. Samples were probed for IQGAP3 (185kDa) and phospho – MLC (18kDa). β-actin was used as a loading control (42kDa). (B): Levels of phospho-MLC were quantified by densitometric analysis on ImageJ and were normalised against the loading control, background noise and wild-type levels. Bars represent the mean relative pMLC expression and error bars represent the SEM. Statistical analysis involved one way ANOVA followed by Tukey's post hoc testing. Comparisons between knockdown conditions and the negative control are indicated on the graph, (**) = $p \leq 0.01$, (*) = $p \leq 0.05$. There was no significant difference between the WT and the negative control conditions (N=3).

5.2.2 Effect of RhoA activation in cell morphology of IQGAP3 depleted cells

Rho-ROCK signalling primarily coordinates cell contractility by regulating the phosphorylation of MLC (Katoh et al., 2001; Kimura et al., 1996). Having established that diminished IQGAP3 reduces levels of activated MLC, the association of IQGAP3 within the Rho-ROCK signalling was then sought to be validated. In order to confirm that IQGAP3 depletion disrupts Rho-ROCK signalling and ultimately phosphorylation of MCL, it was postulated that re-activation of RhoA in IQGAP3 depleted cells would rescue the morphological phenotype caused by reduced levels of IQGAP3. Lysophosphatidic acid (LPA) is a bioactive phospholipid acting on G-protein coupled receptors on the cell membrane to induce RhoA activation (Kranenburg et al., 1999). LPA treatment ultimately leads to increased actomyosin contractility which morphologically translates to cell rounding and neurite retraction in N1E-115 neuronal cells (Kranenburg et al., 1999). Treating IQGAP3 depleted cells with LPA was hence employed as a means of re-introducing RhoA activity and cell contraction. 10μM of LPA for 30 min was determined as an optimal concentration and duration of treatment based on a study employing MB-231 cells to assess the effect of LPA on cell migration (Du et al., 2010). The control conditions of this experiment included cells transfected with negative siRNA control as well as cells transfected with oligo 2 which conferred the most robust reduction of IQGAP3 levels and the most pronounced morphological phenotype (**figures 4.1, 4.4**). LPA was dissolved in PBS containing 0.1% fatty acid free BSA hence IQGAP3 depleted cells treated with PBS containing 0.1% fatty acid free BSA alone were also employed as a technical control. Following LPA treatment cells were fixed and stained with TRITC phalloidin to mark the actin cytoskeleton. Morphological analysis of the imaged cells revealed that LPA treatment specifically rescued and reversed the elongated shape of both IQGAP3 depleted MB-231 and BT-549 cells (**figures 5.3, 5.4**) which is consistent with previous findings reporting cell retraction and ultimately cell rounding following LPA treatment (Kranenburg et al., 1999). In fact, LPA treated IQGAP3 depleted MB-231 cells were even found to be significantly rounder than the cells transfected with negative siRNA control suggesting a dramatic rise in contractility (**figure 5.3**). These findings suggested that IQGAP3 promotes actomyosin contractility by regulating RhoA – ROCK signalling hence the loss of RhoA activity and contractility upon IQGAP3 depletion. Consistently, the re-activation of RhoA in IQGAP3 depleted cells restored contractility and rescued the morphological defect in the triple negative breast cancer cells. However, the results do not suggest that IQGAP3 is implicated in LPA signalling; RhoA

activity is driven by multiple G-protein coupled receptors which are activated by physiological cues (Yu and Brown, 2015) therefore, IQGAP3 could be part of many pathways.

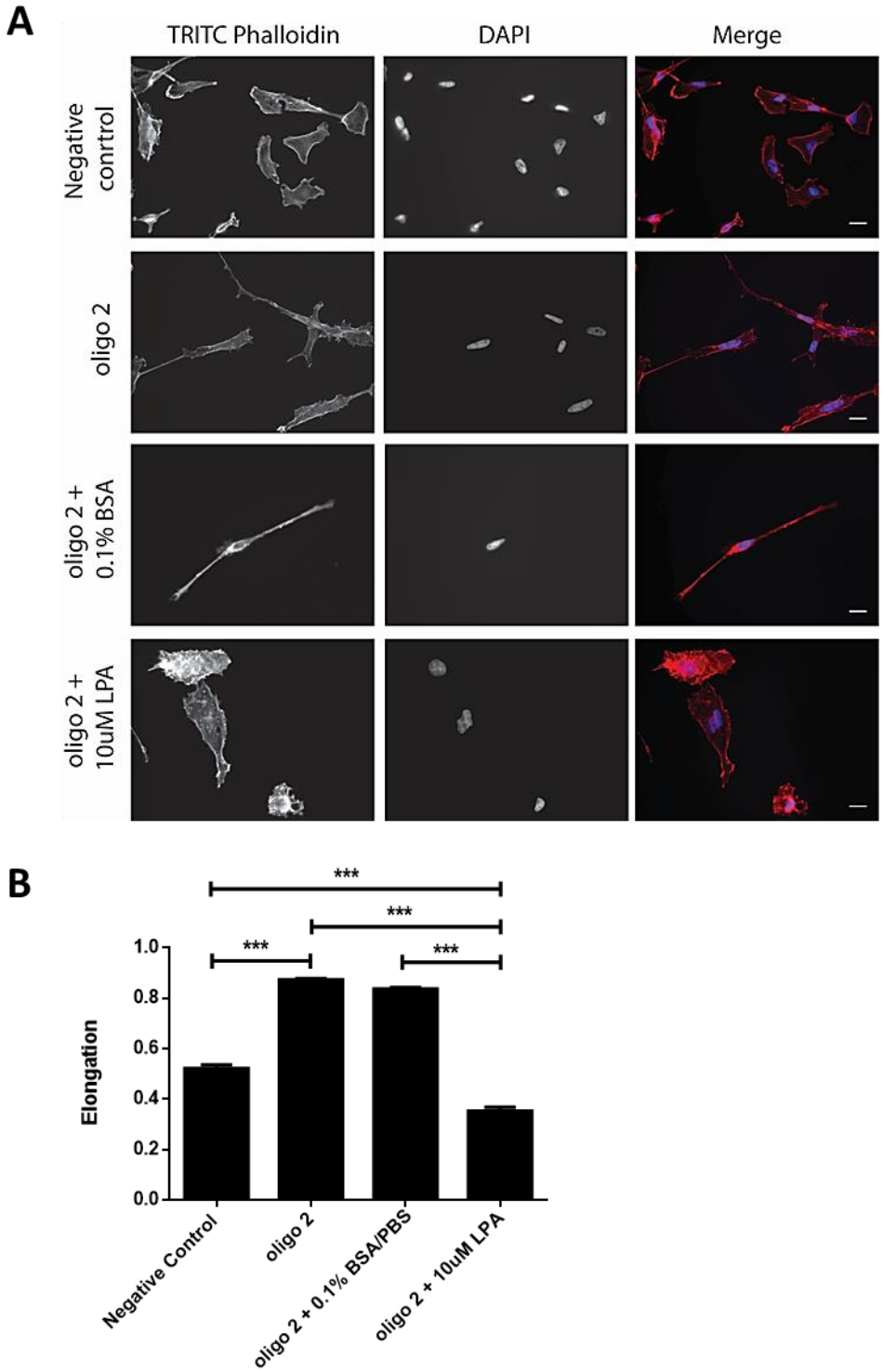

Figure 5.3 Effect of LPA treatment in the cell morphology of IQGAP3 depleted MB-231 cells. (A) : Negative siRNA control, oligo 2 mediated IQGAP3 knockdown, as well as oligo 2 mediated IQGAP3 knockdown with or without 10μM of LPA were fixed 96h post transfection and stained with TRITC-phalloidin and DAPI. Scale bar corresponds to 10μm. (B): Imaged cells were subjected to morphological analysis and their elongation parameter was determined. Bars represent the mean elongation values and error bars represent the SEM. Statistical analysis involved one way ANOVA followed by Tukey's post hoc testing. Statistically significant comparisons are indicated on the graph, (***) = $p \leq 0.001$. There was no significant difference between the oligo 2 and the oligo 2 +0.1% BSA/PBS conditions (N=3).

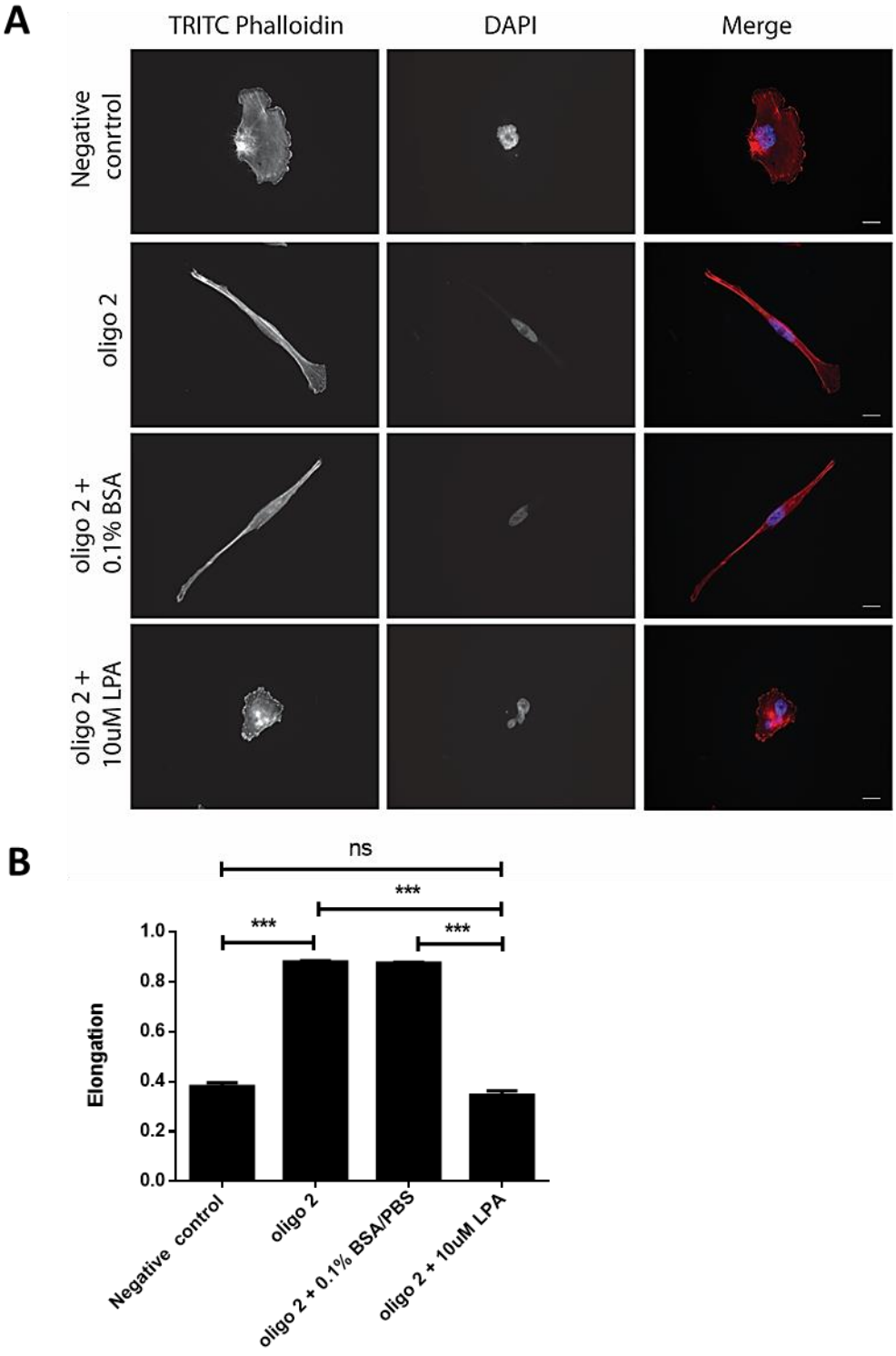

Figure 5.4 Effect of LPA treatment in the cell morphology of IQGAP3 depleted BT-549 cells. (A): Negative siRNA control, oligo 2 mediated IQGAP3 knockdown, as well as oligo 2 mediated IQGAP3 knockdown with or without 10μM of LPA were fixed 96h post transfection and stained with TRITC-phalloidin and DAPI. Scale bar corresponds to 10μm. (B): Imaged cells were subjected to morphological analysis and their elongation parameter was determined. Bars represent the mean elongation values and error bars represent the SEM. Statistical analysis involved one way ANOVA followed by Tukey's post hoc testing. Comparisons are indicated on the graph, (***) = $p \leq 0.001$, (ns) = non-significant. There was no significant difference between the oligo 2 and the oligo 2 +0.1% BSA/PBS conditions (N=3).

5.2.3 IQGAP3 and PAK6 can be found in the same complex

The investigation of the potential interaction between IQGAP3 and PAK6 was prompted by evidence derived from unpublished data from our lab as well as the literature. PAK6 has also been found to function upstream of Rho regulating breast cancer cell contractility while PAK6 depletion also conferred very elongated MB-231 cells (personal communication). Furthermore, IQGAP1 has already been shown to associate with PAK6 thereby providing a link between the two protein families (Fram et al., 2014) In order to test whether IQGAP3 can be found in a complex with PAK6, immunoprecipitation experiments were carried out employing the GFP-TRAP system which provides specific and robust detection of protein interactions. IQGAP3-GFP and PAK6-myc were overexpressed in HEK-293 cells which deliver high levels of expressed protein thus enabling the detection of potential interactions. Lysates of IQGAP3-GFP and PAK6-myc overexpressing cells were mixed together and incubated with the GFP-TRAP beads so that proteins found in a complex with IQGAP3-GFP can be isolated. Co-transfecting IQGAP3-GFP and PAK6-myc was avoided as the efficiency of IQGAP3-GFP overexpression was significantly hindered when co-transfection of the two constructs was attempted. The experiment included an IQGAP3-GFP alone positive control as well as PAK6-myc alone negative control. Samples were then subjected to western blotting and were probed for GFP to ensure that the GFP-TRAP beads have successfully pulled down IQGAP3-GFP. Samples were also probed for myc to assess whether PAK6-myc is found in a complex with IQGAP3-GFP. Indeed, the results of the immunoprecipitation experiment confirmed that PAK6 can be detected in a complex with IQGAP3 (**figure 5.5**). This is a novel complex that has never been described in any cell type before.

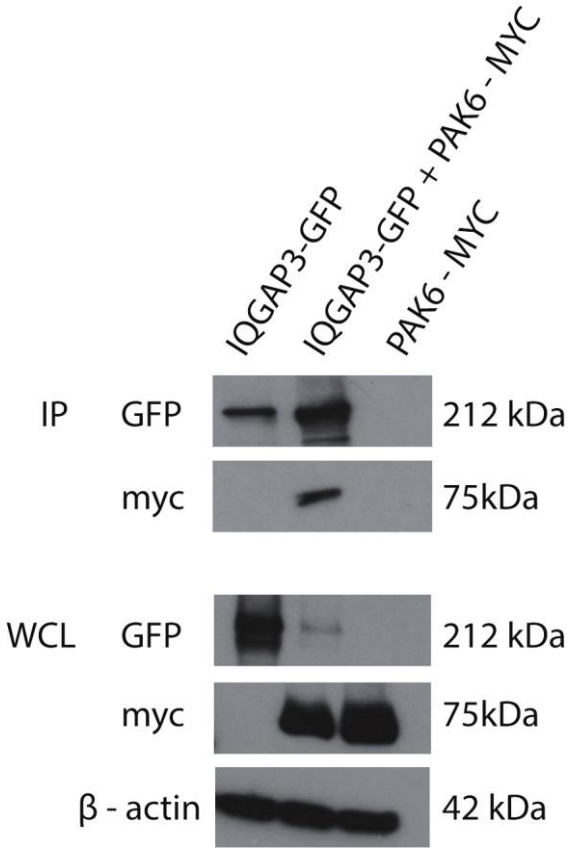

Figure 5.5 Co- immunoprecipitation of IQGAP3 with PAK6 in HEK-293 cells. IQGAP3-GFP and PAK6-myc were transfected in HEK-293 cells. Cells were lysed and lysates were mixed together. An IQGAP3-GFP overexpressing sample was used as technical positive control while a PAK6-myc alone over-expressing sample was used as a negative control. Samples were subjected to the GFP-TRAP immunoprecipitation assay followed by western blotting. IP samples were probed for GFP to validate the pull-down of IQGAP3-GFP (212kDa) and for myc to check whether PAK6-myc is bound to IQGAP3-GFP (75kDa). The whole cell lysates were probed for GFP and myc to validate that the constructs have been adequately over-expressed. β-actin was used a loading control (N=3)

5.2.4 IQGAP3 and PAK1 can be found in the same complex

IQGAP1 has only been known to associate with PAK6 out of the six members of the PAK family (Fram et al., 2014) despite the fact that PAK1 is a far more extensively studied effector of the Rho GTPases (BISHOP and HALL, 2000) This observation together with the establishment of the novel association between IQGAP3 and PAK6 sparked the question of whether IQGAP3 is preferentially coupled with PAK6 (or group II PAKs) as opposed to PAK1. This was addressed by another immunoprecipitation experiment carried out in the same manner as the one that confirmed the interaction between IQGAP3 and PAK6. In this case, IQGAP3-GFP and PAK1-myc were transfected in HEK-293 cells separately and lysates were mixed together in order to be incubated with the GFP-TRAP beads. An IQGAP3-GFP alone sample and a PAK1-myc alone sample were included in the experiment as controls. Samples were subjected to western blotting and probed for GFP to validate the pull-down of IQGAP3-GFP. Samples were also probed for myc to check for the potential interaction between IQGAP3 and PAK1. Indeed, the results of the experiment showed that IQGAP3 can also be found in a complex with PAK1 (**figure 5.6**). This also constitutes a novel association that has never been reported before but whether it is relevant to the implication of IQGAP3 with the regulation of actomyosin contractility of triple negative breast cancer cells is unknown. Nonetheless, IQGAP3 is shown here to be able to be part of the same complex with both group I and group II PAK members (**figures 5.5, 5.6**) suggesting that IQGAP3 could have a role in potentiating the varied functionality of PAK proteins.

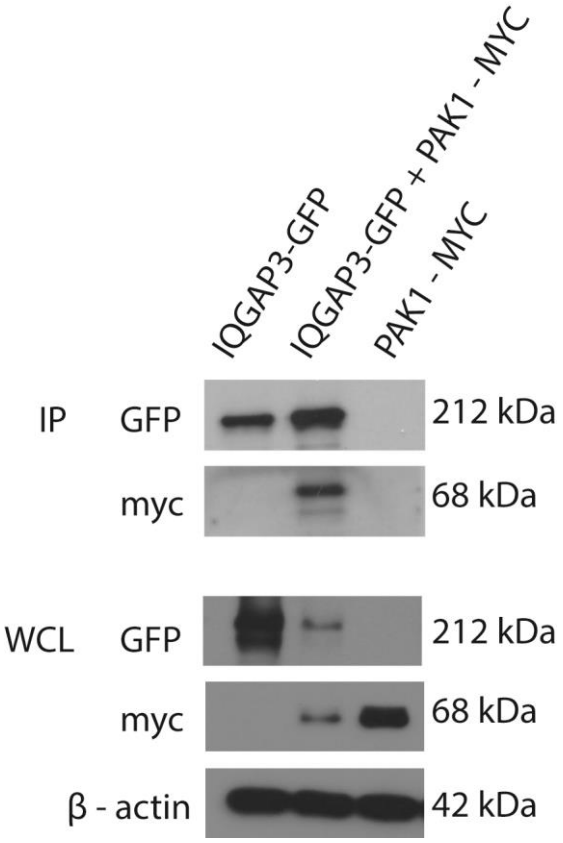

Figure 5.6 Co- immunoprecipitation of IQGAP3 with PAK1 in HEK-293 cells. IQGAP3-GFP and PAK1-myc were transfected in HEK-293 cells. Cells were lysed and lysates were mixed together. An IQGAP3-GFP over-expressing sample was used as technical positive control while a PAK1-myc alone over-expressing sample was used as a negative control. Samples were subjected to the GFP-TRAP immunoprecipitation assay followed by western blotting. IP samples were probed for GFP to validate the pull-down of IQGAP3-GFP (212kDa) and for myc to check whether PAK1-myc is bound to IQGAP3-GFP (75kDa). The whole cell lysates were probed for GFP and myc to validate that the constructs have been adequately over-expressed. β-actin was used a loading control (N=3)

5.2.5 Endogenous IQGAP3 associates with PAK6 in BT-549 cells

In order to further validate the significance of a complex containing IQGAP3 and PAK6 in triple negative breast cancer, another immunoprecipitation experiment was employed, this time in BT-549 cells. This cell line was chosen instead of MB-231 cells as it delivers higher expression levels of proteins when subjected to transient overexpression. PAK6-GFP was thus overexpressed in BT-549 cells and a GFP alone overexpression was used a negative control. Lysates of the two conditions were prepared and incubated with the GFP TRAP beads to pull down PAK6-GFP. Samples were then subjected to western blotting where a GFP probe confirmed that GFP tagged PAK6 had been bound to the beads. Samples were then probed for IQGAP3 which ultimately confirmed that endogenous levels of IQGAP3 interact with overexpressed levels of PAK6-GFP in BT-549 cells (**figure 5.7**). This finding reinforced the hypothesis that a protein complex containing PAK6 and IQGAP3 is relevant and important in triple negative breast cancer. Technical difficulties did not allow the validation of the association between endogenous levels of IQGAP3 and PAK1 in BT-549 cells although such complex cannot be ruled out.

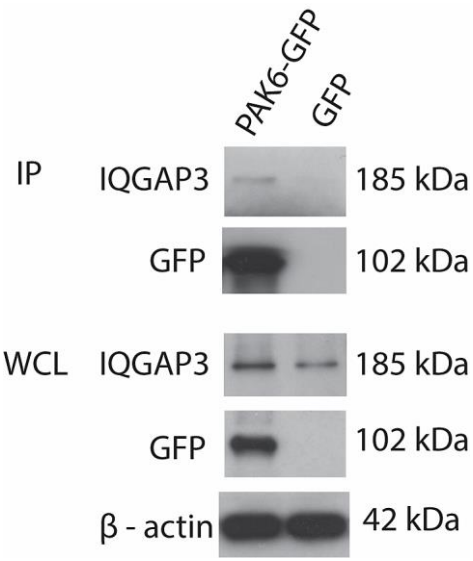

Figure 5.7 Co-immunoprecipitation of IQGAP3 with PAK6 in BT-549 cells. PAK6-GFP and GFP alone were over-expressed in BT-549 cells. Lysates were then subjected to the GFP-TRAP immunoprecipitation assay followed by western blotting. IP samples were probed for GFP to validate the pull-down of PAK6-GFP (102kDa) and for IQGAP3 to check whether endogenous IQGAP3 is bound to PAK6-GFP (185kDa). The whole cell lysates were probed for GFP and IQGAP3 to validate expression of PAK6-GFP and IQGAP3. β-actin was used a loading control (N=3).

5.2.6 Endogenous Filamin-A associates with PAK6 in BT-549 cells

As mentioned before, unpublished data generated in our lab revealed a complex of PAK6 and Filamin-A being able to influence morphological changes through Rho signalling in MB-231 cells (personal communication). In order to validate the importance of this complex, binding of PAK6 with Filamin-A was sought to be confirmed in BT-549 cells. Once again, PAK6-GFP was over-expressed in BT-549 cells while a GFP alone overexpression was included as a negative control. Lysates of the two conditions were prepared and incubated with the GFP TRAP beads to pull down PAK6-GFP. Samples were then subjected to western blotting where a GFP probe confirmed that PAK6-GFP had been bound to the beads. Samples were subsequently probed for Filamin-A which ultimately confirmed that endogenous levels of Filamin-A associate with overexpressed levels of PAK6-GFP in BT-549 cells (**figure 5.8**).

5.2.7 Endogenous Filamin-A associates with IQGAP3 in BT-549 cells

Unpublished data suggesting that IQGAP3 depletion phenocopies PAK6 depletion in modulating cell morphology together with the newly established complexes of IQGAP3 and PAK6 as well as Filamin-A and PAK6 in BT-549 cells, suggested that IQGAP3 could also be part of the PAK6:Filamin-A complex influencing cytoskeletal dynamics. To address this, another immunoprecipitation experiment was employed aiming to detect a potential link between IQGAP3 and Filamin-A. For this experiment, IQGAP3-GFP and GFP alone were overexpressed in BT-549 cells. Lysates for each condition were prepared and were subsequently incubated with GFP-TRAP beads in order to capture any proteins coupled to GFP-tagged IQGAP3. This was followed by western blotting where probing for GFP confirmed that IQGAP3-GFP had been successfully pulled down with the beads. Probing for Filamin-A detected that endogenous Filamin-A was found in a complex with overexpressing IQGAP3 in BT-549 cells (**figure 5.9**). This complex has not been reported before; nonetheless, it may come as no surprise considering that IQGAP1 has been reported to bind Filamin-A and coordinate directional cell migration (Jacquemet et al., 2013).

.

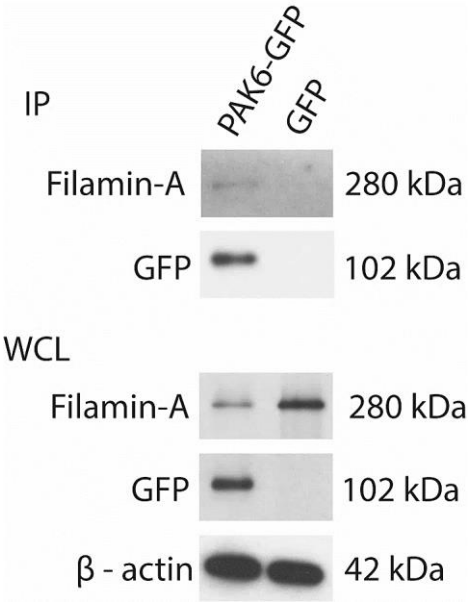

Figure 5.8 Co-immunoprecipitation of Filamin-A with PAK6 in BT-549 cells. PAK6-GFP and GFP alone were overexpressed in BT-549 cells. Lysates were then subjected to the GFP-TRAP immunoprecipitation assay followed by western blotting. IP samples were probed for GFP to validate the pull-down of PAK6-GFP (102kDa) and for Filamin-A to check whether endogenous Filamin-A is bound to PAK6-GFP (280kDa). The whole cell lysates were probed for GFP and Filamin-A to validate expression of PAK6-GFP and Filamin-A. β-actin was used a loading control (N=3).

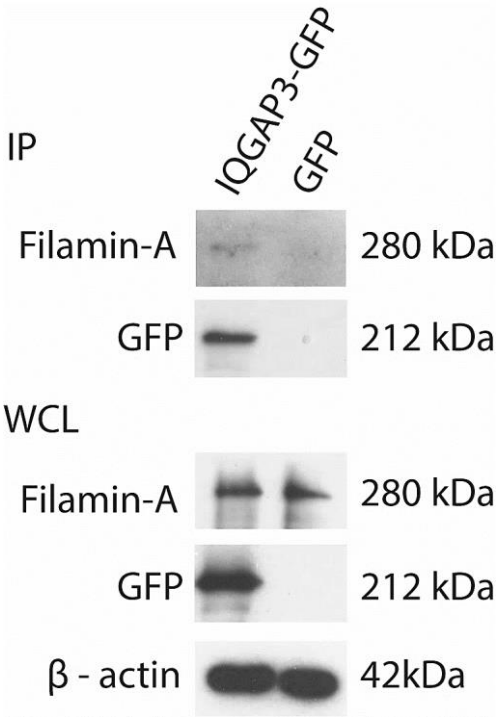

Figure 5.9 Co-immunoprecipitation of Filamin-A with IQGAP3 in BT-549 cells. IQGAP3-GFP and GFP alone were over-expressed in BT-549 cells. Lysates were then subjected to the GFP-TRAP immunoprecipitation assay followed by western blotting. IP samples were probed for GFP to validate the pull-down of IQGAP3-GFP (212kDa) and for Filamin-A to check whether endogenous Filamin-A is bound to IQGAP3-GFP (280kDa). The whole cell lysates were probed for GFP and Filamin-A to validate expression of IQGAP3-GFP and Filamin-A. β-actin was used a loading control (N=3).

5.2.8 Proximity Ligation Assay illuminates binding of IQGAP3 and PAK6

Considering the newly found complex of IQGAP3 and PAK6 as well as their common phenotypic consequences, the relationship between IQGAP3 and PAK6 was sought to be further explored. This was primarily approached by a proximity ligation assay (PLA). This assay allows the detection of protein interactions by giving rise to a single immunofluorescent spot every time two proteins of interest are found in close proximity implying interaction (Söderberg et al., 2006). This is an elegant system as it not only offers opportunities for the quantification of interactions of interest, it can also provide information regarding the localisation of the interaction under investigation as it is performed in intact fixed cells.

The first step of the PLA involves fixing and probing cells with primary antibodies of different species optimised for immunofluorescence. It thus became clear that the IQGAP3 antibody used in western blotting throughout the course of this study needed to be optimised for immuno-fluorescent staining in order to be used in subsequent proximity ligation assays. In order to check whether the IQGAP3 antibody worked in immunofluorescence staining, IQGAP3-GFP was overexpressed in BT-549 cells seeded on fibronectin coated coverslips. Cells were subsequently fixed and stained with the IQGAP3 antibody followed by the anti-rabbit 568 secondary antibody and phalloidin 647 to mark the actin cytoskeleton. This approach allowed the identification of IQGAP3-GFP overexpressing cells by the GFP signal which could then be compared to the 568 signal derived from the IQGAP3 immunofluorescence staining. This method revealed that the IQGAP3 antibody was able to detect overexpressing IQGAP3 when used at 1:50 concentration while endogenous levels could not be detected under the tested protocol (**figure 5.10**).

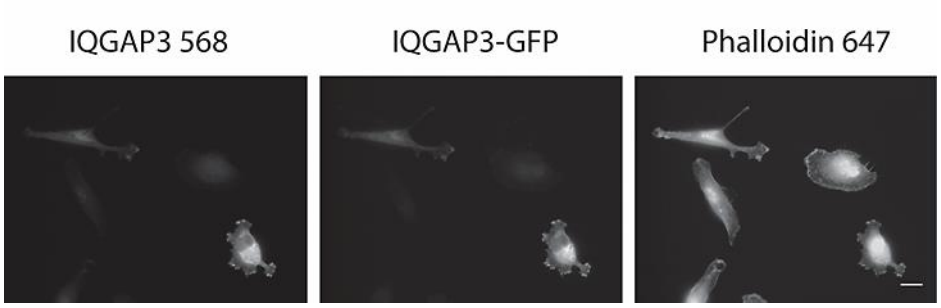

Figure 5.10 Validation of the IQGAP3 antibody (Sigma) in immunofluorescence staining. BT-549 cells were transfected with IQGAP3-GFP. Cells were fixed 48h post transfection and stained with IQGAP3 (Sigma, 1:50) for 2h. Cells were subsequently incubated with anti-rabbit 568 secondary antibody was used at 1:400 and Phalloidin 647 for 1h. Scale bar corresponds to 10μm.

After establishing that the IQGAP3 antibody detects overexpressed IQGAP3 by immunofluorescent staining it became clear that an antibody detecting PAK6 expression in fixed cells was necessary in order to proceed to proximity ligation assays assessing the interaction between IQGAP3 and PAK. However, currently there are no PAK antibodies suitable for detecting PAK expression by means of immunofluorescent staining. Hence, it became clear that in order to explore the interaction between IQGAP3 and PAK6 using a proximity ligation assay, overexpressing IQGAP3 and PAK6 labelled with a non-fluorophore tag would need to be employed. Indeed, co-transfecting IQGAP3-HA and myc tagged PAK6 constructs in BT-549 cells was deemed optimal as this would allow staining with previously optimised rabbit raised IQGAP3 and mouse raised c-myc antibodies. The interaction of IQGAP3 and PAK1 was sought to be similarly tested by co-transfecting IQGAP3-HA and PAK1-myc in order to assess whether IQGAP3 exhibits preferential binding with either PAK1 or PAK6. BT-549 cells transfected with IQGAP3-HA alone but otherwise treated exactly the same as the experimental conditions acted as a negative control to account for non-specific PLA signal. Traditional immunofluorescent staining was also performed alongside the PLA in order to confirm efficient overexpression of transfected constructs.

Following co-transfection of IQGAP3-HA with either PAK6-myc or PAK1-myc, BT-549 cells were fixed and stained for IQGAP3 (red) and c-myc (green) as well as phalloidin to visualise the actin cytoskeleton. This proved that cells had been successfully transfected and thus the PLA signal could be trusted (**figure 5.11**).

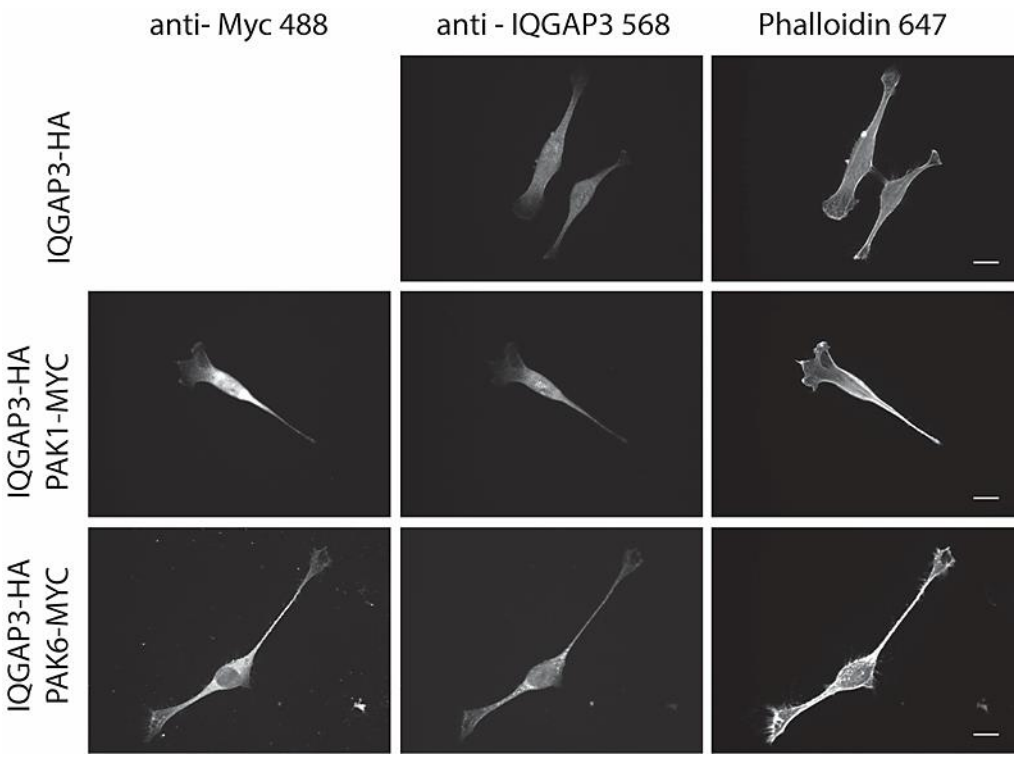

Figure 5.11 BT-549 cells co-transfected with IQGAP3-HA and PAK-myc. BT-549 cells were transfected with IQGAP3-HA and either PAK1-myc or PAK6-myc. Cells transfected with IQGAP3-HA alone were used as a control. Cells were fixed 48h post transfection and stained with anti- IQGAP3 (1:50) and anti – c-myc (1:100) for 2h followed by anti-mouse 488, anti-rabbit 568 and phalloidin 647 for 1h. Scale bar corresponds to 10μm

Having established that the transfected constructs had been effectively over-expressed in BT-549 cells from the traditionally stained controls (**figure 5.11**), the PLA signal for each condition could be analysed. The PLA signal was individually quantified for each imaged cell using particle analysis on ImageJ while the area of each cell was also obtained. This allowed to calculate the PLA signal relative to the cell area in order to account for potential cell area differences across different conditions. The results of the PLA indicated that the mean PLA signal exhibited by IQGAP3:PAK6 complex was significantly higher compared to the one of IQGAP3:PAK1 as well as the IQGAP3-HA negative control (**figure 5.12**). This suggests that IQGAP3 preferentially associates with PAK6 in BT-549 cells (**figure 5.12**). Consistent with this result, overexpressed PAK6-GFP pulled down endogenous IQGAP3 (**figure 5.7**) while technical difficulties prevented the validation of the IQGAP3:PAK1 complex by means of immunoprecipitation in the BT-549 cells.

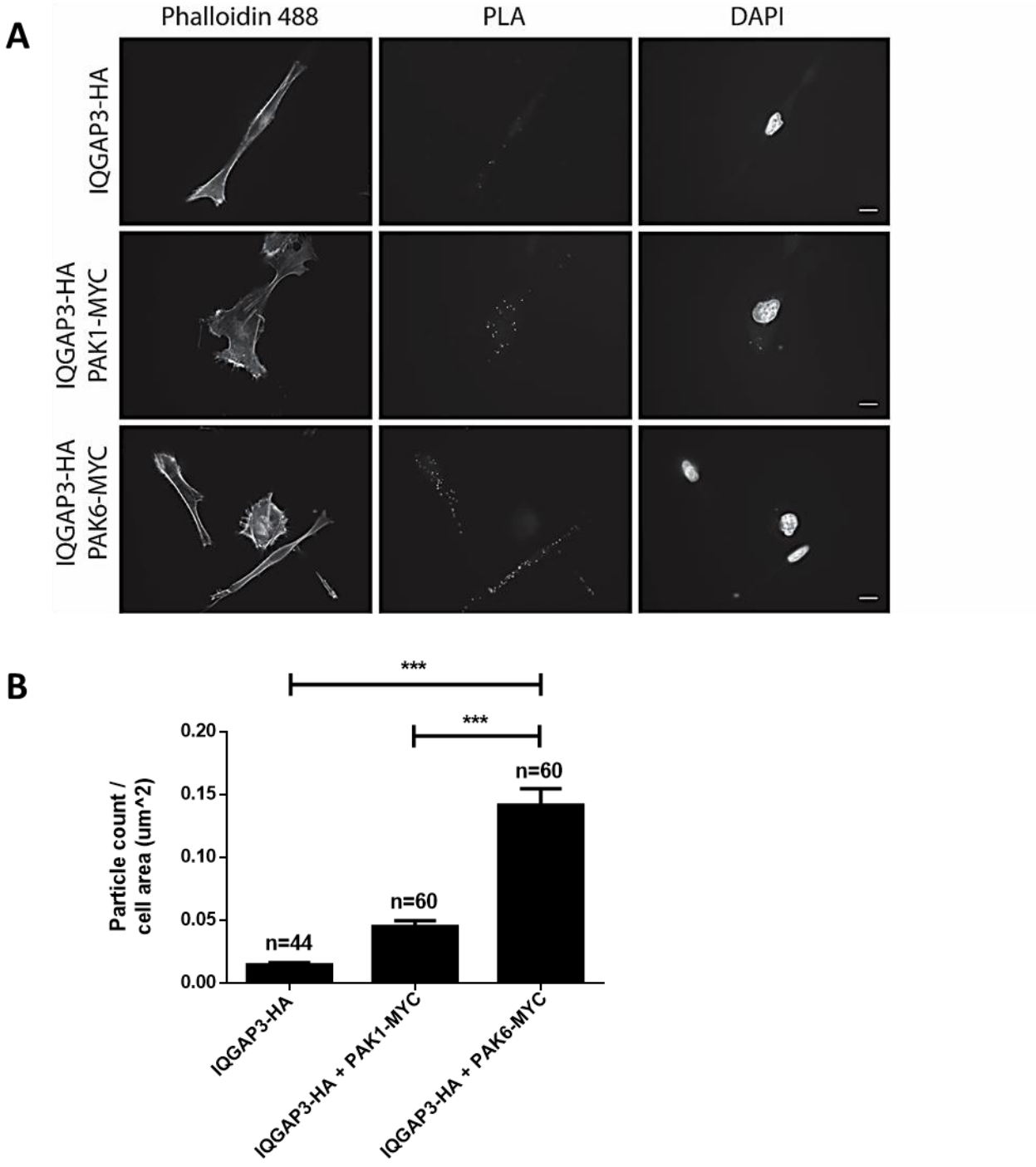

Figure 5.12 Proximity Ligation Assay detecting interactions of IQGAP3-HA with either PAK1-myc or PAK6-myc in BT-549 cells. (A): BT-549 cells were co-transfected with IQGAP3-HA and PAK1-myc or PAK6 myc. Overexpression of IQGAP3-HA alone was included as a control. Cells were stained with IQGAP3 (rabbit, 1:50) and c-myc (mouse 1:100) for 2 h and were subsequently subjected to the PLA assay (red) as well as stained with Phalloidin 488. Scale bar corresponds to 10μm (B): The quantification of the PLA signal and the cell area of each cell were obtained on ImageJ and results were presented as a ratio of PLA spots over cell area. Bars represent the mean relative particle count and error bars represent the SEM. The total number of cells analysed for each condition over 3 independent experiments are noted on the graph. Statistical analysis involved one way ANOVA followed by Tukey's post hoc testing. Statistically significant comparisons are indicated on the graph, (***) = $p \leq 0.001$. There was no significant difference between IQGAP3-HA and the IQGAP3-HA + PAK1-myc conditions (N=3).

5.2.9 Functional significance of the interaction between IQGAP3 and PAK6

Having confirmed the complex of IQGAP3 and PAK6 by both immunoprecipitation experiments and a proximity ligation assay in the BT-549 cells, the functional value of this relationship was sought to be tested in the context of cell morphology. It is already established that depletion of either IQGAP3 (**figure 4.5**) or PAK6 (personal communication) leads to an elongated morphology in breast cancer cells. Both IQGAP3 and PAK6 have independently been suggested to function upstream of Rho–ROCK influencing cell contractility and cell morphology (**figures 5.1 – 5.4,** personal communication). To further explore whether IQGAP3 and PAK6 function as a regulatory complex in mediating cell morphology changes, the effect of overexpressing PAK6 in IQGAP3 depleted cells was sought to be assessed. Indeed, IQGAP3 depleted BT-549 cells seeded on fibronectin coated coverslips were subjected to transient overexpression of PAK6-GFP or GFP alone as a negative control. Cells were fixed 96h post IQGAP3 knockdown and stained with TRITC-Phalloidin to visualise the actin cytoskeleton. IQGAP3 depleted cells transfected with PAK6-GFP remained significantly more elongated than cells transfected with negative siRNA control. However, they were also found to be significantly rounder than IQGAP3 depleted cells and IQGAP3 depleted cells transfected with GFP alone (**figure 5.13**). Consequently, overexpression of PAK6-GFP and not GFP alone partially rescued the elongated phenotype caused by IQGAP3 depletion ultimately suggesting that IQGAP3 is important in potentiating PAK6 activity upstream of Rho in triple negative breast cancer cells (**figure 5.13**).

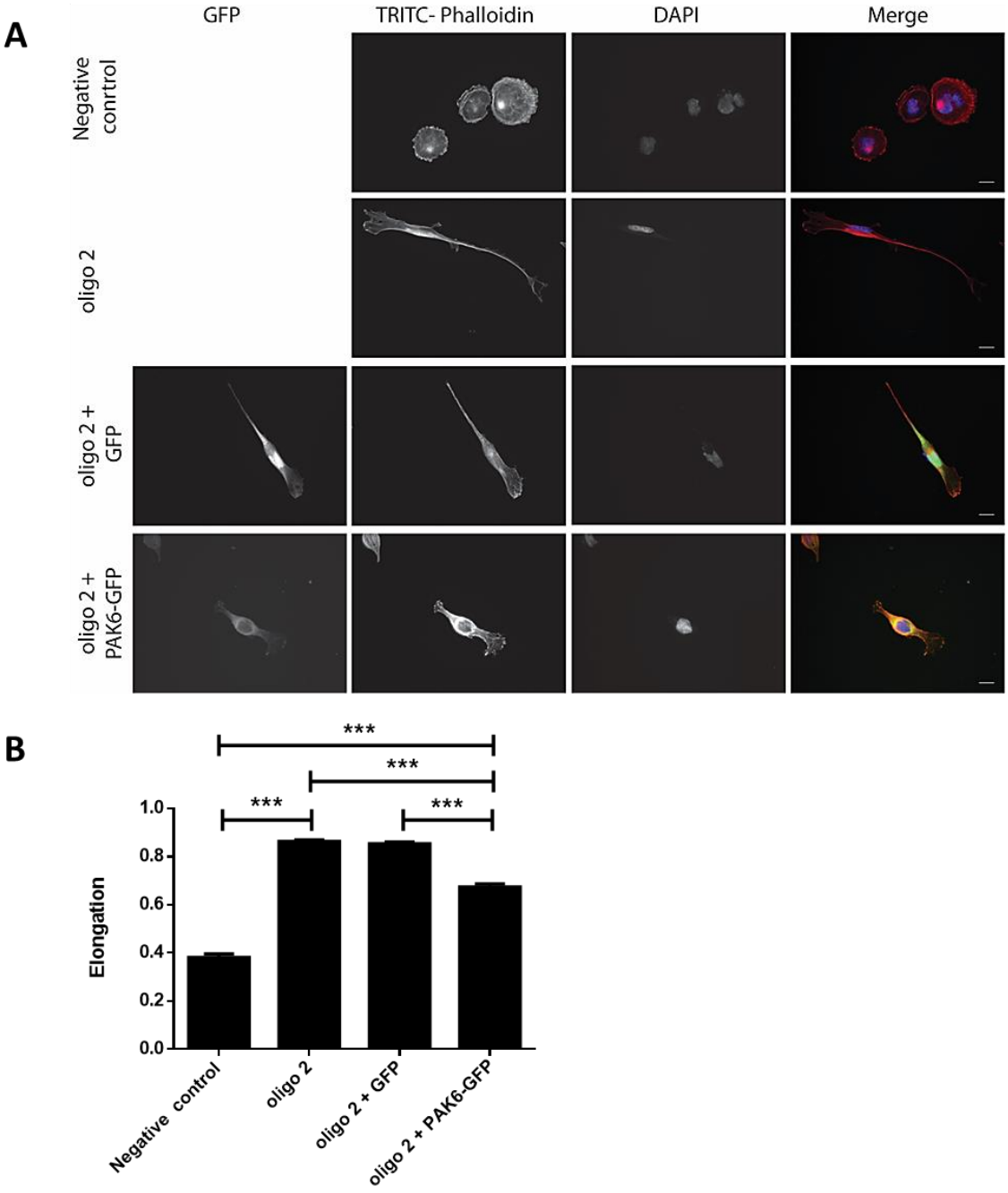

Figure 5.13 Partial phenotypic rescue of IQGAP3 depletion mediated morphology by overexpression of PAK6. (A): BT-549 cells were subjected to IQGAP3 knockdown and subsequent overexpression of PAK6-GFP or GFP alone. Cells were fixed 96h post siRNA transfection and stained with TRITC-Phalloidin and DAPI. Scale bar corresponds to 10μm. (B): Morphological analysis of imaged cells was performed on ImageJ and the elongation parameter was obtained. Bars represent the mean elongation values and error bars represent the SEM. Statistical analysis involved one way ANOVA followed by Tukey's post hoc testing. Statistically significant comparisons are indicated on the graph, (***) = $p \leq 0.001$. There was no significant difference between the oligo 2 and the oligo 2 + GFP conditions (N=3).

5.3 Discussion

This chapter identified potential mechanisms and protein interactions via which IQGAP3 might be influencing cell morphology. Indeed, IQGAP3 depletion significantly reduced levels of phosphorylated MLC in both MB-231 and BT-549 cells. LPA induced - RhoA activation in IQGAP3 depleted cells rescued the defective morphology suggesting that IQGAP3 promotes actomyosin contractility. IQGAP3 was found to associate with PAK1 and PAK6 in HEK-293 cells but the significance of the relationship between IQGAP3 and PAK6 was further highlighted by performing additional immunoprecipitation experiments and the proximity ligation assay on BT-549 cells. IQGAP3 was also found to form a complex with Filamin-A, a known actin filament cross-linker previously found to associate with PAK6 and coordinate cell morphology (personal communication). Ultimately, by investigating the functional aspect of the relationship between IQGAP3 and PAK6 it was revealed that overexpression of PAK6 in IQGAP3 depleted cells partially rescued the elongated phenotype suggesting that Rho activity had been restored.

A reduction in phosphorylation levels of regulatory MLC upon IQGAP3 depletion established IQGAP3 as a regulatory element of actomyosin contractility. It is unlikely that this is a result of reduced total levels of regulatory MLC as it is a very stable molecule with a longer half-life than the course of the experiment (Zak, 1977). IQGAP3 has previously been reported to interact with essential MLC but the functional significance of this interaction is unknown (Atcheson et al., 2011). It can be argued that the interaction between IQGAP3 and essential MLC creates a conformational change that in turn promotes phosphorylation of the regulatory MLC and/or the association of myosin with actin filaments. The implication of IQGAP3 in actomyosin contractility also supports the argument that the elongated cell morphology conferred by diminished levels of IQGAP3 is a direct result of disrupted actomyosin contractility and loss of cell contraction. Interestingly, PAK1 which is a novel binding partner of IQGAP3 (**figure 5.6**) has been shown to phosphorylate myosin light chain kinase (MLCK) and thus inhibit its activity as well as reduce phosphorylated levels of MLC in Hela cells (Sanders et al., 1999). In contrast to this early finding, PAK1 depletion reduced levels of pMLC in T47D breast cancer cells (Coniglio et al., 2008). This chapter reported binding of IQGAP3 with PAK1 (**figure 5.6)** as well as attenuated myosin light chain activation upon IQGAP3 depletion (**figure 5.1**). These observations, together with the previously shown interaction of IQGAP3 with essential MLC (Atcheson et al., 2011), might

suggest that IQGAP3 could also display scaffolding activity in the regulation of PAK1 mediated regulatory MLC phosphorylation.

The morphological rescue of IQGAP3 depleted cells mediated by treating them with LPA highlighted the fact that loss of IQGAP3 disrupted RhoA activity. Interestingly, it is widely accepted that IQGAP3 does not directly interact with RhoA (Adachi et al., 2014; Wang et al., 2007). At the same time, IQGAP3 has been known to bind Rac1 and Cdc42 and act as their effector stabilising their activated state (Wang et al., 2007; Smith et al., 2015). Together these observations suggest that IQGAP3 adopts different mechanisms in mediating the effects of the small Rho GTPases.
Interestingly, protein levels of RhoA have been found to be significantly increased in invasive breast cancers compared to normal tissue (del Pulgar et al., 2005). Consistent with this finding, RhoA depletion in MB-231 cells inhibited invasion through a 3D matrigel matrix while cells notably remained atop the matrix spreading elongated protrusions (Poincloux et al., 2011) in a similar fashion as the IQGAP3 depleted MB-231 cells (**figure 4.4**). Furthermore, ROCK1 and ROCK2 were found to be over-expressed in advanced breast tumours compared to early stage breast cancer (Liu et al., 2009) . Meanwhile, the use of MB-231 cells in a mouse orthotopic mouse model engrafted with human bone showed that pharmacological inhibition of ROCK by Y27632 reduced metastases to engrafted human bone and the mouse skeleton (Liu et al., 2009).
Consistent with morphological evidence presented in this thesis, treating MB-231 cells with 50 μM of Fasudil, a known ROCK inhibitor, induced cell elongation while the administration of Fasudil in a mouse orthotopic model injected with MB-231 decreased the number of tumour bearing mice (Ying et al., 2006). Overall, there is compelling evidence suggesting that IQGAP3 depletion phenocopies the disruption of Rho-ROCK signalling in breast cancer cells while the use of LPA as a means of re-establishing Rho activity confirms that IQGAP3 lies upstream of Rho influencing Rho activity and cell contraction in breast cancer cells.

IQGAP3 was found to associate with both PAK1 and PAK6 which has never been described before (**figure 5.5, 5.6**). This chapter suggests that the IQGAP3:PAK6 association is a much more frequent event than the IQGAP3:PAK1 association in BT-549 cells based on the results obtained from the PLA (**figure 5.12**). At the same time, the partial morphological rescue of IQGAP3 depleted cells by overexpressing PAK6 further highlighted the physiological significance of the complex as it suggests that IQGAP3 recruits PAK6 and maintains PAK6 induced RhoA activity,

ultimately achieving cell contraction and tail retraction. Interestingly, previous work from our lab focusing on the invadopodia life-cycle in melanoma cells has revealed that RhoA activity is specifically coordinated by PAK4 (a group II PAK like PAK6) and not PAK1 (Nicholas et al., 2016). Nonetheless, the PLA results did not reveal a particular cell location where the IQGAP3:PAK6 complex might be more active as the signal was scattered throughout the cell area (**figure 5.12**). Therefore, the complex is likely influencing global cell contraction rather than tail retraction specifically.

At the same time, no morphological defect was observed in PAK1 depleted MB-231 cells suggesting that loss of PAK1 does not phenocopy the loss of either IQGAP3 or PAK6 (Dart et al., 2015). Hence, the complex containing IQGAP3 and PAK1 is less likely to integrate in a common signalling pathway influencing cell morphology. However, It can be argued that similarly to IQGAP1 (Choi and Anderson, 2017) expression levels of IQGAP3 could also be dictating different interacting partners and integration in different signalling pathways. Based on this assumption and results outlined in this chapter, endogenous IQGAP3 might interact with PAK6 and promote cell contractility while overexpressed IQGAP3 might potentiate the interaction with PAK1 and become implicated in an entirely different pathway.

This chapter also revealed the association between IQGAP3 and Filamin-A. Interestingly, Filamin-A deficient neutrophils exhibited a tail retraction defect which was caused from the fact that Filamin-A regulates RhoA activity and actomyosin contractility at the neutrophil uropod (Sun et al., 2013). Furthermore, Filamin-A recruited FilGAP that in turn supressed Rac activity in response to phosphorylation by ROCK thereby contributing to the antagonistic actions of Rac and Rho and promoting cell polarity (Ohta et al., 2006). Filamin-A is thus implicated in the coordination of RhoA activity and cell morphology. Consequently, the novel relationship between IQGAP3 and Filamin-A further supports the possibility that IQGAP3 complexes with PAK6 and Filamin-A thus integrating with contractility pathways previously reported in my lab (personal communication).

Despite evidence presented here, supporting the functional significance of IQGAP3:PAK6 in maintaining RhoA activity, IQGAP3 could be influencing RhoA activity via different mechanisms. A complex of IQGAP1 and Filamin-A is reported to be recruited at integrin activation sites in the cell periphery during cell spreading on fibronectin. IQGAP1 then recruits and couples to RacGAP1 which locally deactivates Rac1 thereby ensuring balanced cell protrusion and directional cell migration of human osteosarcoma U2OS cells (Jacquemet et al., 2013). Furthermore, integrin trafficking in human ovarian cancer A2780 cells migrating in 3D induced the phosphorylation of

RacGAP1 which is recruited by IQGAP1 at the tips of invasive protrusions termed as pseudopods. There, RacGAP1 locally suppressed Rac1 allowing RhoA activity to be increased and promote pseudopod extension and invasion ((Jacquemet et al., 2013b). Interestingly, this describes a migration mode where RhoA activity induced cell elongation (Jacquemet et al., 2013a). IQGAP3 could also be implicated in deactivating Rac1 thus allowing the coordinated activation of RhoA. Results presented in this chapter as well as the literature highlight the fact that IQGAP1 and IQGAP3 share Filamin-A as a binding partner (**figure 5.9**), (Jacquemet et al., 2013b). It would thus not be surprising if IQGAP3 were able to bind RacGAP1 and elicit the deactivation of Rac1. However, no morphological defects were reported for IQGAP1 depleted MB-231 cells (Sakurai-Yageta et al., 2008) which suggests that the mechanism via which IQGAP3 integrates with contractility pathways is not shared by IQGAP1.

Ultimately, this chapter yielded novel IQGAP3 binding partners via which IQGAP3 might be influencing cell morphology. It also presented the prospect of IQGAP3 influencing Rho activity despite being known to act as a scaffold for Rac1 and Cdc42 thus expanding the cellular processes IQGAP3 might be involved with.

5.4 Future work

This chapter sought to expose a functional IQGAP3:PAK6:Filamin-A complex able to regulate actomyosin contractility. A closer examination of the cell areas where this complex becomes active would point to mechanisms via which this complex elicits its morphological effects. The association between IQGAP3 and PAK6 can be further investigated by using domain mutants of either proteins to provide more structural and entirely novel evidence on the interaction between IQGAP3 and PAKs. The elucidation of specific IQGAP3 domains in motility pathways could trigger the investigation of whether they have therapeutic value. Indeed, IQGAP1 domains have been considered as pharmacological targets with the WW domain showing particular promise when administered systemically in a mouse model of pancreatic cancer (Jameson et al., 2013). A similar approach could thus be employed for IQGAP3. Furthermore, looking into the effects of IQGAP3 depletion in the Rho-ROCK signalling would further support the argument that IQGAP3 is able to influence Rho activity as this would provide concrete evidence that IQGAP3 does not only mediate the effects of Rac1 and Cdc42. This could be approached by measuring levels of active RhoA following manipulation of IQGAP3 levels either by western blotting or by FRET microscopy using a RhoA biosensor (Fritz et al., 2013).

It would also be interesting to further explore the relationship between IQGAP3 and novel binding partner Filamin-A by assessing whether one precedes and recruits the other similarly to the relationship of IQGAP1 and Filamin-A (Jacquemet et al., 2013b). The localisation of Filamin-A could be primarily assessed in a background of IQGAP3 depletion to check whether IQGAP3 acts like IQGAP1 in terms of recruiting Filamin-A at particular cellular sites (Jacquemet et al., 2013b). Finally, it would be interesting to see whether Filamin-A overexpression rescues the defective morphology of IQGAP3 depleted cells similarly to PAK6.

Chapter 6

Concluding remarks

Chapter 6 : Concluding Remarks

Triple negative breast cancer is the most lethal form of the disease due to its aggressive and metastatic behaviour as well as high rates of relapse (Dent et al., 2009). Additionally, TNBC patients cannot benefit from the targeted therapies that have significantly improved outcomes in ER and HER2 positive breast cancers ultimately relying on standard chemotherapy regimens (Reis-Filho and Tutt, 2008). Nonetheless, TNBC comprises a wide range of tumours whose common characteristic remains the lack of hormone and HER2 positive amplification; hence the need to elucidate and therapeutically target the signalling pathways that drive the invasive phenotype of these tumours is highlighted (Hudis and Gianni, 2011). Indeed, genetic profiling has revealed specific subtypes within the triple negative spectrum based on specific expression patterns; basal-like tumours exhibit an upregulation of proliferation and growth factor signalling pathways while the mesenchymal-like type is enriched with pathways enabling cell motility such as the regulation of cytoskeletal dynamics by the Rho GTPases (Lehmann et al., 2011a).

This study originated from a tissue micro-array performed at the Breast Cancer Now Unit of Guy's Hospital that revealed the specific upregulation of IQGAP3 mRNA levels in triple negative tumours compared to other types of the disease as well as normal tissue (de Rinaldis et al., 2013). Little is known about IQGAP3 compared to the earlier discovered IQGAP1 and IQGAP2 (White et al., 2009). However, considering the scaffolding activity of IQGAP3 for the Rho GTPases Rac1 and Cdc42 as well as the actin cytoskeleton, this study asked the question of whether IQGAP3 could be contributing to the necessary cytoskeletal rearrangements that would explain the invasive phenotype of triple negative tumours.

At first, suitable cell models exhibiting the motile phenotype of TNBC were sought to be established, paying particular attention to cell morphology and the ability of cells to migrate in 2D as well as make invadopodia. Presence of invadopodia was chosen as an indication of invasive potential as these protrusions have been heavily associated with cancer cell intravasation while IQGAP1 has been implicated with invadopodia mediated matrix degradation (Gligorijevic et al., 2012; Sakurai-Yageta et al., 2008). Initially, IQGAP3 protein expression was detected across a panel of triple negative lines including the MCF10A cell line as a near normal representative. Even though mRNA levels of IQGAP3 had been measured in triple negative cell lines and tumours before (de Rinaldis et al., 2013), protein expression had not been previously reported. Interestingly, near normal MCF10A cells displayed lower IQGAP3 expression levels than most

triple negative cell lines whereas no triple negative line exhibited higher levels of IQGAP1 than the near normal representative (**figures 3.2, 3.3**). Additionally, the high IQGAP3 expressing MB-231 and MB-436 (**figure 3.2**) cells also exhibited an elongated morphology which is associated with EMT and tumour progression (Kalluri and Weinberg, 2009). Nonetheless, IQGAP3 expression did not correlate with either cell morphology, migration or invadopodia capacity across the cell line panel. Interestingly, based on the cell lines assessed in this study, invadopodia capacity did not predict invasive potential as non invadopodia making MB-436 and HCC38 have been shown to be invasive in other *in vitro* and *in vivo* settings (Iida et al., 2012; Thompson et al., 1992). Systematic analysis revealed that a rounder morphology is more permissive of invadopodia formation in breast cancer cells (**figures 3.9, 3.10**) ultimately suggesting that there may be a cross-talk between invadopodia formation and cell morphology.

Notably, IQGAP3 depleted MB-231 and BT-549 triple negative breast cancer cells displayed a very elongated phenotype along with reduced cell speed, and formation of mature focal adhesions and invadopodia. The mechanisms involved in conferring these features appear to be unique to IQGAP3 as no morphological defect was reported in IQGAP1 depleted MB-231 cells (Sakurai-Yageta et al., 2008). Additionally, IQGAP1 depleted MB-231 cells retain their actin rich invadopodia structure but exhibit diminished matrix degradation (Sakurai-Yageta et al., 2008) whereas IQGAP3 depletion eliminates the entire invadopodia structure (**figure 4.10, 4.11**). Moreover, the loss of invadopodia capacity in the IQGAP3 depleted cells is in agreement with the fact that a rounded morphology was found to be more permissive of invadopodia formation.

Unexpectedly, IQGAP3 overexpression also conferred cell elongation and loss of invadopodia capacity, even though the morphological defect was less pronounced than the one observed in IQGAP3 depleted cells (**figures 4.12, 4.13, 4.15**). Ultimately, this meant that depletion and overexpression of IQGAP3 had similar phenotypic results. This could be explained by an observation previously made for IQGAP1 (Choi and Anderson, 2017). IQGAP1 expression levels have been observed to dictate which signalling pathways IQGAP1 scaffolds; IQGAP1 acts as a scaffold for both the MAPK cascade and the PI3K-Akt pathway. Depletion or overexpression of IQGAP1 disrupted ERK activation while overexpression of IQGAP1 was only found to promote activation of Akt (Choi and Anderson, 2017). In a similar fashion, endogenous IQGAP3 levels could be supporting normal morphological integrity and invadopodia formation while any variation of IQGAP3 expression levels could be driving the activation of other pathways disrupting these normal processes. More specifically, IQGAP3 overexpression could be prolonging the activated

state of Rac1 and Cdc42 ultimately contributing to actin polymerisation and cell elongation via enhanced formation of lamellipodia (**figure 6.1**).

In contrast, the time-lapse movies of IQGAP3 depleted cells indicated that cells had lost the ability to retract their tail and thus move forward suggesting a defect in cell contractility. Additionally, RhoA depleted MB-231 cells were also reported to exhibit the same elongated phenotype as well as reduced migration (Vega et al., 2011). In fact, RhoA depleted cells were observed to extend towards opposite directions ultimately not moving at all (Vega et al., 2011) which was a feature that was sometimes observed in IQGAP3 depleted cells too. Together these observations lead to the hypothesis that IQGAP3 depletion is phenocopying RhoA depletion and is thus interfering with cell contractility.

To test this hypothesis, levels of phosphorylated regulatory MLC were assessed in IQGAP3 depleted cells in order to examine whether IQGAP3 has a direct effect on cell contractility. Activation of regulatory MLC was found to be attenuated in IQGAP3 depleted cells which further supported the fact that cell contractility is disrupted upon loss of IQGAP3 (**figures 5.1, 5.2**). This is particularly interesting as the interaction between IQGAP3 and essential MLC has previously been reported (Atcheson et al., 2011). Ultimately, this suggests that IQGAP3 might promote actomyosin contractility by interacting with essential MLC thereby creating a conformational change that enables phosphorylation of regulatory MLC and/or the association of myosin with actin filaments.

Additionally, IQGAP3 depleted cells were also treated with LPA to re-activate RhoA. LPA treatment rescued the elongated phenotype and restored contractility ultimately suggesting that IQGAP3 can also impact RhoA activity (**5.3, 5.4**). It can thus be postulated that IQGAP3 can contribute to the regulation of cell contractility by being active both upstream and downstream of RhoA. The concept of IQGAP3 scaffolding different parts of the same pathway is not novel as it has also been previously described to scaffold for the MAPK cascade by interacting with both Ras (Nojima et al., 2008) and ERK (Yang et al., 2014).

This finding is particularly important because IQGAP3 had so far only been reported to act as a scaffold for Rac1 and Cdc42 while the absence of direct interaction between IQGAP3 and Rho has been repeatedly shown (Adachi et al., 2014; Wang et al., 2007; White et al., 2009). This suggests that IQGAP3 is able to promote RhoA activity indirectly. Meanwhile, IQGAP1 has been suggested to directly act as a scaffold for RhoA and p190-RhoGAP ultimately promoting downregulation of RhoA activity and airway smooth muscle relaxation (Bhattacharya et al., 2014).

At the same time, IQGAP1 has also been shown to indirectly promote RhoA activity by inhibiting Rac activation via RacGAP1 (Jacquemet et al., 2013a). It becomes obvious that IQGAPs can potentially influence Rho activity via multiple pathways. Nonetheless, the morphological defect resulting from disruption of contractility in IQGAP3 depleted triple negative breast cancer cells is likely to be driven by mechanisms unique to IQGAP3 as no morphological defect was reported in IQGAP1 depleted MB-231 cells (Sakurai-Yageta et al., 2008). Ultimately, it can be postulated that despite the high homology and similar scaffolding activity shared by IQGAPs, fine-tuned spatiotemporal regulation as well as the potential of multiple binding partners (Hedman et al., 2015) allow them to also possess unique functionality that is likely to be tissue specific.

The disruption of actomyosin contractility in invasive breast tumours such as the ones that fall under the triple negative spectrum is an exciting therapeutic opportunity as expression levels of RhoA as well as ROCK1 and ROCK2 have been found to be higher in advanced tumours compared to early stage disease and normal tissue (del Pulgar et al., 2005; Liu et al., 2009). Additionally, the amoeboid type of migration which is characterised by increased RhoA activity and cell contractility, (Sahai and Marshall, 2003) is also observed at the invasive front of multiple tumour types including the one of the breast (Gao et al., 2017). High actomyosin contractility is hence likely to contribute to the aggressive behaviour of triple negative tumours. Nonetheless, inhibition of ROCK has yielded contradictory results as a therapeutic approach for cancer perhaps due to the intrinsic cell plasticity of certain cell types (Wei et al., 2015).

Therapeutic targeting of IQGAPs has only recently been explored and presents promise especially in cases where resistance has developed to other targeted therapies or where kinase targeting has non-specific effects (Kumar et al., 2008; Sanchez-Laorden et al., 2013). The use of IQGAP1 domains as potential therapeutic agents have shown promise by competing with the targeted pathway of interest (Jameson et al., 2013; Monteleon et al., 2015). The same concept could thus be applied in the case of IQGAP3 in the attempt to downregulate cell contractility in TNBC. In fact, IQGAP3 expression is much more tissue specific than IQGAP1 which reduces the chance of side effects (White et al., 2009). At the same time, similarly to IQGAP1, IQGAP3 is likely to have multiple binding partners (Hedman et al., 2015). This implies that IQGAP3 might be involved in many different signalling pathways and thus the possibility of off target effects upon therapeutic targeting cannot be ruled out.

Moreover, considering the unique morphological defect observed in IQGAP3 depleted TNBC cells as well as the potential implication of high actomyosin contractility in the metastatic behaviour of

TNBC, the mechanisms via which IQGAP3 is promoting actomyosin contractility in TNBC cells are most likely specific to IQGAP3. This could explain why IQGAP3 mRNA levels were found to be upregulated in triple negative tumours compared to other types of breast cancer and normal tissue (de Rinaldis et al., 2013).

In the attempt to provide a mechanism via which IQGAP3 is able to influence RhoA activity, this study revealed novel complexes containing IQGAP3 and PAK6 (**figure 5.7)** as well as IQGAP3 and Filamin-A (**figure 5.9**). Filamin-A has been shown to regulate RhoA activity and tail retraction in neutrophils (Sun et al., 2013) while unpublished work from my lab has previously revealed a role of PAK6:Filamin-A complex in influencing contractility and cell morphology. In fact, depletion of PAK6 also induced elongation in MB-231 cells (personal communication). It can thus be deduced that both IQGAP3 and PAK6 depletion mimic loss of RhoA in conferring morphological consequences (Vega et al., 2011). This thesis hence proposed that IQGAP3 could act as a scaffold for this functional complex in order to potentiate RhoA activity. In agreement with this argument was the fact that overexpression of PAK6-GFP in IQGAP3 depleted BT-549 cells partially rescued the defective elongated phenotype (**figure 5.13).** Contrary to what is presented in this thesis, it was recently suggested that PAK6 inhibits cell contraction by mediating RhoD induced inhibition of RhoC (Durkin et al., 2017). Even though this seems to be directly contradicting the work presented here, it merely adds to the complexity of the cross-talk between Rho GTPases and their spatiotemporal regulation mediated by GEFs and GAPs. PAK6 could in fact be inhibiting RhoC mediated cell contraction but promoting RhoA mediated cell contraction. The action of PAK6 could also be different in the context of cancer cell migration as described in this thesis and viral infection which is the biological process involved in Durkin *et al*.

In conclusion, this thesis provided evidence suggesting that IQGAP3 is directly influencing actomyosin contractility by regulating the activation of myosin light chain. Additionally, this thesis proposed that IQGAP3 can be found as part of complexes with PAK6 and Filamin-A which might contribute to the regulation of RhoA activity and cell contractility ultimately coordinating cell morphology and efficient cell migration in TNBC cells. Without the scaffolding activity of IQGAP3, the spatial regulation, recruitment and perhaps activation of PAK6 and Filamin-A could be disrupted, resulting in attenuated actomyosin contractility and subsequently defective cell morphology and migration as shown in the proposed model (**figure 6.1**).

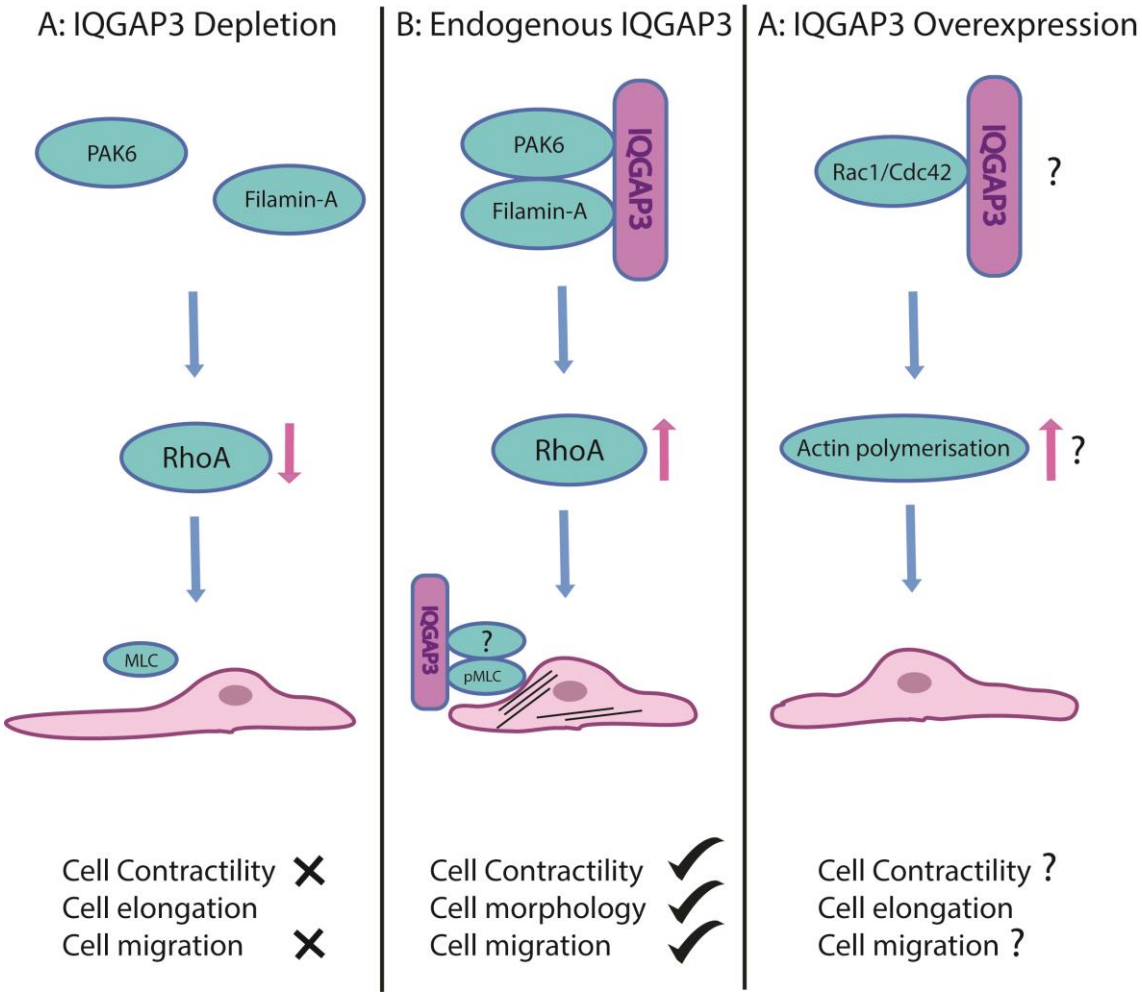

Figure 6.1 Proposed model of IQGAP3 action. (A): Upon IQGAP3 depletion, PAK6 and Filamin-A are not recruited to induce RhoA activity and therefore actomyosin contractility is disrupted Additionally, IQGAP3 no longer scaffolds essential MLC which attenuates the phosphorylation of regulatory MLC. Ultimately, cells become hyper-elongated while contractility and cell migration is diminished. (B): Endogenous levels of IQGAP3 form complexes with PAK6 and Filamin-A which are postulated to induce RhoA activity thereby increasing actomyosin contractility. IQGAP3 also interacts with essential MLC which is most likely supporting the phosphorylation of regulatory MLC and/or the association of myosin with actin filaments. As a result, cells are contractile, maintain morphological integrity and are capable of forward moving. (C): IQGAP3 overexpression is likely promoting the activation of other signalling pathways. Considering that IQGAP3 is primarily scaffolding the activity of Rac1 and Cdc42, it is possible that overexpression of IQGAP3 is prolonging the activated state of these Rho GTPases. Consequently, this contributes to increased actin polymerisation and cell elongation.

References

Abel, A., Schuldt, K., Rajasekaran, K., Hwang, D., Riese, M., Rao, S., Thakar, M., Malarkannan, S., 2015. IQGAP1: Insights into the function of a molecular puppeteer. Mol Immunol 65, 336–349.

Adachi, M., Kawasaki, A., Nojima, H., Nishida, E., Tsukita, S., 2014. Involvement of IQGAP family proteins in the regulation of mammalian cell cytokinesis. Genes Cells 19, 803–820.

Alexander, N., Branch, K., Parekh, A., Clark, E., Iwueke, I., Guelcher, S., Weaver, A., 2008. Extracellular Matrix Rigidity Promotes Invadopodia Activity. Curr Biol 18, 1295–1299.

Althuis, M., Fergenbaum, J., Garcia-Closas, M., Brinton, L., Madigan, P., Sherman, M., 2004. Etiology of hormone receptor-defined breast cancer: a systematic review of the literature. Cancer Epidemiology Biomarkers Prev Publ Am Assoc Cancer Res Cosponsored Am Soc Prev Oncol 13, 1558–68.

Amano, M., Chihara, K., Nakamura, N., Fukata, Y., Yano, T., Shibata, M., Ikebe, M., Kaibuchi, K., 1998. Myosin II activation promotes neurite retraction during the action of Rho and Rho- kinase. Genes Cells 3, 177–188.

Amano, M., Ito, M., Kimura, K., Fukata, Y., Chihara, K., Nakano, T., Matsuura, Y., Kaibuchi, K., 1996. Phosphorylation and Activation of Myosin by Rho-associated Kinase (Rho-kinase). J Biol Chem 271, 20246–20249.

Amano, M., Nakayama, M., Kaibuchi, K., 2010. Rho- kinase/ROCK: A key regulator of the cytoskeleton and cell polarity. Cytoskeleton 67, 545–554.

Anders, C., Carey, L., 2009. Biology, Metastatic Patterns, and Treatment of Patients with Triple-Negative Breast Cancer. Clin Breast Cancer 9, S73–S81.

Arias- Romero, L., Chernoff, J., 2008. A tale of two Paks. Biol Cell 100, 97–108.

Atcheson, E., Hamilton, E., Pathmanathan, S., Greer, B., Harriott, P., Timson, D., 2011. IQ-motif selectivity in human IQGAP2 and IQGAP3: binding of calmodulin and myosin essential light chain. Bioscience Rep 31, 371–379.

Ayala, I., Baldassarre, M., Giacchetti, G., Caldieri, G., Tetè, S., Luini, A., Buccione, R., 2008. Multiple regulatory inputs converge on cortactin to control invadopodia biogenesis and extracellular matrix degradation. Journal of cell science 121, 369–78.

Bae, Y., Kim, A., Kim, M., Choi, J., Kang, S., Lee, S., 2013. Fibronectin expression in carcinoma cells correlates with tumor aggressiveness and poor clinical outcome in patients with invasive breast cancer. Human Pathology 44, 2028–2037.

Bardwell, J., Lagunes, L., Zebarjedi, R., Bardwell, L., 2017. The WW domain of the scaffolding protein IQGAP1 is neither necessary nor sufficient for binding to the MAPKs ERK1 and ERK2. J Biol Chem 292, 8750–8761.

Bashour, A.-M., Fullerton, A., Hart, M., Bloom, G., 1997. IQGAP1, a Rac- and Cdc42-binding Protein, Directly Binds and Cross-links Microfilaments. J Cell Biology 137, 1555–1566.

Beaty, B., Sharma, V., Bravo-Cordero, J., Simpson, M., Eddy, R., Koleske, A., Condeelis, J., 2013. β1 integrin regulates Arg to promote invadopodial maturation and matrix degradation. Mol Biol Cell 24, 1661–1675.

Bedolla, R.G., Wang, Y., Asuncion, A., Chamie, K., Siddiqui, S., Mudryj, M.M., Prihoda, T.J., Siddiqui, J., Chinnaiyan, A.M., Mehra, R., de Vere White, R.W., Ghosh, P.M., 2009. Nuclear versus cytoplasmic localization of filamin A in prostate cancer: immunohistochemical correlation with metastases. Clin. Cancer Res. 15, 788–96.

Bhattacharya, M., Sundaram, A., Kudo, M., Farmer, J., Ganesan, P., Khalifeh-Soltani, A., Arjomandi, M., Atabai, K., Huang, X., Sheppard, D., 2014. IQGAP1-dependent scaffold suppresses RhoA and inhibits airway smooth muscle contraction. J Clin Invest 124, 4895–4898.

BISHOP, A., HALL, A., 2000. Rho GTPases and their effector proteins. Biochem J 348, 241–255.

Bissell, M., Hines, W., 2011. Why don't we get more cancer? A proposed role of the microenvironment in restraining cancer progression. Nature Medicine 17, 320–329.

Blanchoin, L., Boujemaa-Paterski, R., Sykes, C., Plastino, J., 2014. Actin Dynamics, Architecture, and Mechanics in Cell Motility. Physiol Rev 94, 235–263.

Bokoch, G., 2003. Biology of the p21 activated kinases. Annu Rev Biochem 72, 743–781.

Bokoch, G., Wang, Y., Bohl, B., Sells, M., Quilliam, L., Knaus, U., 1996. Interaction of the Nck Adapter Protein with p21-activated Kinase (PAK1). J Biol Chem 271, 25746–25749.

Bravo-Cordero, J., Oser, M., Chen, X., Eddy, R., Hodgson, L., Condeelis, J., 2011. A Novel Spatiotemporal RhoC Activation Pathway Locally Regulates Cofilin Activity at Invadopodia. Curr Biol 21, 635–644.

Briggs, M., Sacks, D., 2003. IQGAP proteins are integral components of cytoskeletal regulation. Embo Rep 4, 571–574.

Brill, Li, Lyman, Church, Wasmuth, Weissbach, Bernards, Snijders, 1996. The Ras GTPase-activating-protein-related human protein IQGAP2 harbors a potential actin binding domain and interacts with calmodulin and Rho family GTPases. Mol Cell Biol 16, 4869–4878.

Brown, M., Sacks, D., 2006. IQGAP1 in cellular signaling: bridging the GAP. Trends Cell Biol 16, 242–249.

Burridge, K., Wittchen, E., 2013. The tension mounts: Stress fibers as force-generating mechanotransducers. J Cell Biology 200, 9–19.

Byrne, K., Monsefi, N., Dawson, J., Degasperi, A., Bukowski-Wills, J.-C., Volinsky, N., Dobrzyński, M., Birtwistle, M., Tsyganov, M., Kiyatkin, A., Kida, K., Finch, A., Carragher, N., Kolch, W., Nguyen, L., von Kriegsheim, A., Kholodenko, B., 2016. Bistability in the Rac1, PAK, and RhoA Signaling Network Drives Actin Cytoskeleton Dynamics and Cell Motility Switches. Cell Syst 2, 38–48.

Cailleau, R., Olivé, M., Cruciger, Q., 1978. Long-term human breast carcinoma cell lines of metastatic origin: Preliminary characterization. Vitro 14, 911–915.

Caro-Gonzalez, H., Nejsum, L., Siemers, K., Shaler, T., Nelson, J., Barth, A., 2012. Mitogen-activated protein kinase (MAPK/ERK) regulates adenomatous polyposis coli during growth-factor-induced cell extension. J Cell Sci 125, 1247–1258.

Carr, H., Zuo, Y., Oh, W., Frost, J., 2013. Regulation of Focal Adhesion Kinase Activation, Breast Cancer Cell Motility, and Amoeboid Invasion by the RhoA Guanine Nucleotide Exchange Factor Net1. Mol Cell Biol 33, 2773–2786.

Carter, J., Douglass, L., Deddens, J., Colligan, B., Bhatt, T., Pemberton, J., Konicek, S., Hom, J., Marshall, M., Graff, J., 2004. Pak-1 Expression Increases with Progression of Colorectal Carcinomas to Metastasis. Clin Cancer Res 10, 3448–3456.

Casteel, D., Turner, S., Schwappacher, R., Rangaswami, H., Su-Yuo, J., Zhuang, S., Boss, G., Pilz, R., 2012. Rho Isoform-specific Interaction with IQGAP1 Promotes Breast Cancer Cell Proliferation and Migration. J Biol Chem 287, 38367–38378.

Chan, K., Cortesio, C., Huttenlocher, A., 2009. FAK alters invadopodia and focal adhesion composition and dynamics to regulate breast cancer invasion. The Journal of Cell Biology 185, 357–370.

Cheung, K., Gabrielson, E., Werb, Z., Ewald, A., 2013. Collective Invasion in Breast Cancer Requires a Conserved Basal Epithelial Program. Cell 155, 1639–1651.

Chew, Masaracchia, Goeckeler, Wysolmerski, 1998. Phosphorylation of non-muscle myosin II regulatory light chain by p21-activated kinase (gamma-PAK). J Muscle Res Cell M 19, 839–54.

Ching, Y.-P., Leong, V., Wong, C.-M., Kung, H.-F., 2003. Identification of an Autoinhibitory Domain of p21-activated Protein Kinase 5. J Biol Chem 278, 33621–33624.

Choi, S., Anderson, R., 2017. And Akt- ion! IQGAP1 in control of signaling pathways. Embo J 36, 967–969.

Choi, S., Hedman, A., Sayedyahossein, S., Thapa, N., Sacks, D., Anderson, R., 2016. Agonist-stimulated phosphatidylinositol-3,4,5-trisphosphate generation by scaffolded phosphoinositide kinases. Nat Cell Biol 18, 1324–1335.

Choi, S., Thapa, N., Hedman, A., Li, Z., Sacks, D., Anderson, R., 2013. IQGAP1 is a novel phosphatidylinositol 4,5 bisphosphate effector in regulation of directional cell migration. Embo J 32, 2617–2630.

Chrzanowska-Wodnicka, Burridge, 1996. Rho-stimulated contractility drives the formation of stress fibers and focal adhesions. J Cell Biology 133, 1403–15.

Civiero, L., Cirnaru, M., Beilina, A., Rodella, U., Russo, I., Belluzzi, E., Lobbestael, E., Reyniers, L., Hondhamuni, G., Lewis, P., den Haute, C., Baekelandt, V., Bandopadhyay, R., Bubacco, L., Piccoli, G., Cookson, M., Taymans, J., Greggio, E., 2015. Leucine- rich repeat kinase 2 interacts with p21- activated kinase 6 to control neurite complexity in mammalian brain. J Neurochem 135, 1242–1256.

Clark, A., Vignjevic, D., 2015. Modes of cancer cell invasion and the role of the microenvironment. Current Opinion in Cell Biology 36, 13–22.

Clark, E., Whigham, A., Yarbrough, W., Weaver, A., 2007. Cortactin is an essential regulator of matrix metalloproteinase secretion and extracellular matrix degradation in invadopodia. Cancer research 67, 4227–35.

Coniglio, S., Zavarella, S., Symons, M., 2008. Pak1 and Pak2 Mediate Tumor Cell Invasion through Distinct Signaling Mechanisms. Mol Cell Biol 28, 4162–4172.

Crimaldi, L., Courtneidge, S., Gimona, M., 2009. Tks5 recruits AFAP-110, p190RhoGAP, and cortactin for podosome formation. Exp Cell Res 315, 2581–2592.

Cunningham, C.C., Gorlin, J.B., Kwiatkowski, D.J., Hartwig, J.H., Janmey, P.A., Byers, H.R., Stossel, T.P., 1992. Actin-binding protein requirement for cortical stability and efficient locomotion. Science 255, 325–7.

Dart, A., Box, G., Court, W., Gale, M., Brown, J., Pinder, S., Eccles, S., Wells, C., 2015. PAK4 promotes kinase-independent stabilization of RhoU to modulate cell adhesion. J Cell Biology 211, 863–879.

De Rinaldis, E., Gazinska, P., Mera, A., Modrusan, Z., Fedorowicz, G., Burford, B., Gillett, C., Marra, P., Grigoriadis, A., Dornan, D., Holmberg, L., Pinder, S., Tutt, A., 2013. Integrated genomic analysis of triple-negative breast cancers reveals novel microRNAs associated with clinical and molecular phenotypes and sheds light on the pathways they control. Bmc Genomics 14, 643.

Del Pulgar, T., Benitah, S., Valerón, P., Espina, C., Lacal, J., 2005. Rho GTPase expression in tumourigenesis: Evidence for a significant link. Bioessays 27, 602–613.

Delorme-Walker, V., Peterson, J., Chernoff, J., Waterman, C., Danuser, G., DerMardirossian, C., Bokoch, G., 2011. Pak1 regulates focal adhesion strength, myosin IIA distribution, and actin dynamics to optimize cell migration. J Cell Biology 193, 1289–1303.

Dent, R., Hanna, W., Trudeau, M., Rawlinson, E., Sun, P., Narod, S., 2009. Pattern of metastatic spread in triple-negative breast cancer. Breast Cancer Res Tr 115, 423–428.

DerMardirossian, C., Bokoch, G., 2005. GDIs: central regulatory molecules in Rho GTPase activation. Trends Cell Biol 15, 356–363.

Du, J., Sun, C., Hu, Z., Yang, Y., Zhu, Y., Zheng, D., Gu, L., Lu, X., 2010. Lysophosphatidic Acid Induces MDA-MB-231 Breast Cancer Cells Migration through Activation of PI3K/PAK1/ERK Signaling. Plos One 5, e15940.

Durkin, C., Leite, F., Cordeiro, J., Handa, Y., Arakawa, Y., Valderrama, F., Way, M., 2017. RhoD Inhibits RhoC-ROCK-Dependent Cell Contraction via PAK6. Dev Cell 41, 315–329.e7.

Eckert, M., Lwin, T., Chang, A., Kim, J., Danis, E., Ohno-Machado, L., Yang, J., 2011. Twist1-Induced Invadopodia Formation Promotes Tumor Metastasis. Cancer Cell 19, 372–386.

Edwards, D., Sanders, L., Bokoch, G., Gill, G., 1999. Activation of LIM-kinase by Pak1 couples Rac/Cdc42 GTPase signalling to actin cytoskeletal dynamics. Nat Cell Biol 1, 253–259.

Eguiara, A., Holgado, O., Beloqui, I., Abalde, L., Sanchez, Y., Callol, C., Martin, A., 2011. Xenografts in zebrafish embryos as a rapid functional assay for breast cancer stem-like cell identification. Cell cycle (Georgetown, Tex.) 10, 3751–7.

Etienne-Manneville, S., Hall, A., 2001. Integrin-Mediated Activation of Cdc42 Controls Cell Polarity in Migrating Astrocytes through PKCζ. Cell 106, 489–498.

Fackler, O., Grosse, R., 2008. Cell motility through plasma membrane blebbing. J Cell Biology 181, 879–884.

Fang, X., Zhang, B., Thisse, B., Bloom, G., Thisse, C., 2015. IQGAP3 is essential for cell proliferation and motility during zebrafish embryonic development. Cytoskeleton 72, 422–433.

Flanagan, L., Chou, J., Falet, H., Neujahr, R., Hartwig, J., Stossel, T., 2001. Filamin A, the Arp2/3 complex, and the morphology and function of cortical actin filaments in human melanoma cells. J Cell Biology 155, 511–518.

Foulkes, W., Smith, I., Reis-Filho, J., 2010. Triple-Negative Breast Cancer. New Engl J Medicine 363, 1938–1948.

Foxall, E., Pipili, A., Jones, G., Wells, C., 2016. Significance of Kinase Activity in the Dynamic Invadosome. European Journal of Cell Biology.

Fram, S., King, H., Sacks, D., Wells, C., 2014. A PAK6–IQGAP1 complex promotes disassembly of cell–cell adhesions. Cell Mol Life Sci 71, 2759–2773.

Friedl, P., 2004. Prespecification and plasticity: shifting mechanisms of cell migration. Curr Opin Cell Biol 16, 14–23.

Friedl, P., Alexander, S., 2011. Cancer Invasion and the Microenvironment: Plasticity and Reciprocity. Cell 147, 992–1009.

Friedl, P., Locker, J., Sahai, E., Segall, J., 2012. Classifying collective cancer cell invasion. Nat Cell Biol 14, 777–783.

Friedl, P., Wolf, K., 2003. Tumour-cell invasion and migration: diversity and escape mechanisms. Nat Rev Cancer 3, 362–374.

Friedl, P., Wolf, K., 2009. Proteolytic interstitial cell migration: a five-step process. Cancer and Metastasis Reviews 28, 129–135.

Friedl, P., Wolf, K., 2010. Plasticity of cell migration: a multiscale tuning model. The Journal of Cell Biology 188, 11–19.

Fritz, R., Letzelter, M., Reimann, A., Martin, K., Fusco, L., Ritsma, L., Ponsioen, B., Fluri, E., Schulte-Merker, S., van Rheenen, J., Pertz, O., 2013. A Versatile Toolkit to Produce Sensitive FRET Biosensors to Visualize Signaling in Time and Space. Sci Signal 6, rs12–rs12.

Fukata, M., Watanabe, T., Noritake, J., Nakagawa, M., Yamaga, M., Kuroda, S., Matsuura, Y., Iwamatsu, A., Perez, F., Kaibuchi, K., 2001. Rac1 and Cdc42 Capture Microtubules through IQGAP1 and CLIP-170. Cell 109, 873–85.

Fukata, Y., Amano, M., Kaibuchi, K., 2001. Rho-Rho-kinase pathway in smooth muscle contraction and cytoskeletal reorganization of non-muscle cells. Trends Pharmacol. Sci. 22, 32–9.

Gao, Y., Wang, Z., Hao, Q., Li, W., Xu, Y., Zhang, J., Zhang, W., Wang, S., Liu, S., Li, M., Xue, X., Zhang, W., Zhang, C., Zhang, Y., 2017. Loss of ERα induces amoeboid-like migration of breast cancer cells by downregulating vinculin. Nat Commun 8, 14483.

Gardel, Nakamura, Hartwig, Crocker, Stossel, Weitz, 2006. Prestressed F-actin networks cross-linked by hinged filamins replicate mechanical properties of cells. P Natl Acad Sci Usa 103, 1762–1767.

Gazdar, A., Kurvari, V., Virmani, A., Gollahon, L., Sakaguchi, M., Westerfield, M., Kodagoda, D., Stasny, V., Cunningham, T., Wistuba, I., Tomlinson, G., Tonk, V., Ashfaq, R., Leitch, M., Minna, J., Shay, J., 1998. Characterization of paired tumor and non- tumor cell lines established from patients with breast cancer. Int J Cancer 78, 766–774.

Gligorijevic, B., Wyckoff, J., Yamaguchi, H., Wang, Y., Roussos, E., Condeelis, J., 2012. N-WASP-mediated invadopodium formation is involved in intravasation and lung metastasis of mammary tumors. Journal of cell science 125, 724–34.

Goc, A., Al-Azayzih, A., Abdalla, M., Al-Husein, B., Kavuri, S., Lee, J., Moses, K., Somanath, P.R., 2013. P21 activated kinase-1 (Pak1) promotes prostate tumor growth and microinvasion via inhibition of transforming growth factor β expression and enhanced matrix metalloproteinase 9 secretion. J. Biol. Chem. 288, 3025–35.

Ha, B., Davis, M., Chen, C., Lou, H., Gao, J., Zhang, R., Krauthammer, M., Halaban, R., Schlessinger, J., Turk, B., Boggon, T., 2012. Type II p21-activated kinases (PAKs) are regulated by an autoinhibitory pseudosubstrate. Proc National Acad Sci 109, 16107–16112.

Hall, A., 1998. Rho GTPases and the Actin Cytoskeleton. Science 279, 509–514.

Hashim, N., Nicholas, N., Dart, A., Kiriakidis, S., Paleolog, E., Wells, C., 2013. Hypoxia-induced invadopodia formation: a role for β-PIX. Open Biology 3, 120159.

Hayat, M., Howlader, N., Reichman, M., Edwards, B., 2007. Cancer Statistics, Trends, and Multiple Primary Cancer Analyses from the Surveillance, Epidemiology, and End Results (SEER) Program. Oncol 12, 20–37.

Hedman, A.C., Smith, J.M., Sacks, D.B., 2015. The biology of IQGAP proteins: beyond the cytoskeleton. EMBO Rep. 16, 427–46.

Hetmanski, J., Schwartz, J.-M., Caswell, P., 2016a. Modelling GTPase dynamics to understand RhoA-driven cancer cell invasion. Biochem Soc T 44, 1695–1700.

Hetmanski, J., Zindy, E., Schwartz, J.-M., Caswell, P., 2016b. A MAPK-Driven Feedback Loop Suppresses Rac Activity to Promote RhoA-Driven Cancer Cell Invasion. Plos Comput Biol 12, e1004909.

Hirata, B., Oda, J., Guembarovski, R., Ariza, C., de Oliveira, C., Watanabe, M., 2014. Molecular Markers for Breast Cancer: Prediction on Tumor Behavior. Dis Markers 2014, 513158.

Ho, Y.-D., Joyal, J., Li, Z., Sacks, D., 1999. IQGAP1 Integrates Ca2+/Calmodulin and Cdc42 Signaling. J Biol Chem 274, 464–470.

Holliday, D., Speirs, V., 2011. Choosing the right cell line for breast cancer research. Breast Cancer Res 13, 215.

Holm, C., Rayala, S., Jirström, K., Stål, O., Kumar, R., Landberg, G., 2006. Association Between Pak1 Expression and Subcellular Localization and Tamoxifen Resistance in Breast Cancer Patients. Jnci J National Cancer Inst 98, 671–680.

Hoshino, D., Branch, K., Weaver, A., 2013. Signaling inputs to invadopodia and podosomes. J Cell Sci 126, 2979–2989.

Hu, B., Shi, B., Jarzynka, M., Yiin, J.-J., D'Souza-Schorey, C., Cheng, S.-Y., 2009. ADP-Ribosylation Factor 6 Regulates Glioma Cell Invasion through the IQ-Domain GTPase-Activating Protein 1-Rac1–Mediated Pathway. Cancer Res 69, 794–801.

Hu, G., Xu, Y., Chen, W., Wang, J., Zhao, C., Wang, M., 2016. RNA Interference of IQ Motif Containing GTPase-Activating Protein 3 (IQGAP3) Inhibits Cell Proliferation and Invasion in Breast Carcinoma Cells. Oncol Res Featur Preclin Clin Cancer Ther 24, 455–461(7).

Hudis, C., Gianni, L., 2011. Triple-Negative Breast Cancer: An Unmet Medical Need. Oncol 16, 1–11.

Huttenlocher, A., Horwitz, A., 2011. Integrins in Cell Migration. Csh Perspect Biol 3, a005074.

Huynh, N., Liu, K., Baldwin, G., He, H., 2010. P21-activated kinase 1 stimulates colon cancer cell growth and migration/invasion via ERK- and AKT-dependent pathways. Biochimica Et Biophysica Acta Bba - Mol Cell Res 1803, 1106–1113.

Iida, J., Dorchak, J., Lehman, J., Clancy, R., Luo, C., Chen, Y., Somiari, S., Ellsworth, R., Hu, H., Mural, R., Shriver, C., 2012. FH535 Inhibited Migration and Growth of Breast Cancer Cells. PLoS ONE 7, e44418.

Iorns, E., Drews-Elger, K., Ward, T.M., Dean, S., Clarke, J., Berry, D., El Ashry, D., Lippman, M., 2012. A new mouse model for the study of human breast cancer metastasis. PLoS ONE 7, e47995.

Jacquemet, G., Green, D., Bridgewater, R., von Kriegsheim, A., Humphries, M., Norman, J., Caswell, P., 2013a. RCP-driven α5β1 recycling suppresses Rac and promotes RhoA activity via the RacGAP1–IQGAP1 complex. J Cell Biology 202, 917–935.

Jacquemet, G., Morgan, M., Byron, A., Humphries, J., Choi, C., Chen, C., Caswell, P., Humphries, M., 2013b. Rac1 is deactivated at integrin activation sites through an IQGAP1–filamin-A–RacGAP1 pathway. J Cell Sci 126, 4121–4135.

Jaffer, Z., Chernoff, J., 2002. p21-Activated kinases: three more join the Pak. Int J Biochem Cell Biology 34, 713–717.

Jameson, K., Mazur, P., Zehnder, A., Zhang, J., Zarnegar, B., Sage, J., Khavari, P., 2013. IQGAP1 scaffold-kinase interaction blockade selectively targets RAS-MAP kinase-driven tumors. Nat Med 19, 626–630.

Jemal, A., Siegel, R., Xu, J., Ward, E., 2010. Cancer Statistics, 2010. Ca Cancer J Clin 60, 277–300.

Jerrell, R., Parekh, A., 2016. Matrix rigidity differentially regulates invadopodia activity through ROCK1 and ROCK2. Biomaterials 84, 119–129.

Kalluri, R., Weinberg, R., 2009. The basics of epithelial-mesenchymal transition. Journal of Clinical Investigation 119, 1420–1428.

Kassianidou, E., Kumar, S., 2015. A biomechanical perspective on stress fiber structure and function. Biochimica Et Biophysica Acta Bba - Mol Cell Res 1853, 3065–3074.

Kasza, K.E., Nakamura, Hu, Kollmannsberger, Bonakdar, Fabry, Stossel, T.P., Wang, Weitz, D.A., 2009. Filamin A Is Essential for Active Cell Stiffening but not Passive Stiffening under External Force. Biophys J 96, 4326–4335.

Katoh, K., Kano, Y., Amano, M., Onishi, H., Kaibuchi, K., Fujiwara, K., 2001. Rho-Kinase–Mediated Contraction of Isolated Stress Fibers. J Cell Biology 153, 569–584.

Kaur, R., Liu, X., Gjoerup, O., Zhang, A., Yuan, X., Balk, S., Schneider, M., Lu, M., 2005. Activation of p21-activated Kinase 6 by MAP Kinase Kinase 6 and p38 MAP Kinase. J Biol Chem 280, 3323–3330.

Kaur, R., Yuan, X., Lu, M.L., Balk, S.P., 2008. Increased PAK6 expression in prostate cancer and identification of PAK6 associated proteins. Prostate 68, 1510–6.

Kenny, P., Lee, G., Myers, C., Neve, R., Semeiks, J., Spellman, P., Lorenz, K., Lee, E., Barcellos-Hoff, M., Petersen, O., Gray, J., Bissell, M., 2007. The morphologies of breast cancer cell lines in three- dimensional assays correlate with their profiles of gene expression. Mol Oncol 1, 84–96.

Kessenbrock, K., Plaks, V., Werb, Z., 2010. Matrix Metalloproteinases: Regulators of the Tumor Microenvironment. Cell 141, 52–67.

Kimura, Ito, Amano, Chihara, Fukata, Nakafuku, Yamamori, Feng, Nakano, Okawa, Iwamatsu, Kaibuchi, 1996. Regulation of Myosin Phosphatase by Rho and Rho-Associated Kinase (Rho-Kinase). Science 273, 245–248.

King, H., Nicholas, N., Wells, C., 2014. International Review of Cell and Molecular Biology, International review of cell and molecular biology. sciencedirect.

Kohno, T., Urao, N., Ashino, T., Sudhahar, V., Inomata, H., Yamaoka-Tojo, M., McKinney, R., Fukai, T., Ushio-Fukai, M., 2013. IQGAP1 links PDGF receptor-β signal to focal adhesions involved in vascular smooth muscle cell migration: role in neointimal formation after vascular injury. Am J Physiology - Cell Physiology 305, C591–C600.

Krakhmal, Zavyalova, Denisov, Vtorushin, Perelmuter, 2015. Cancer Invasion: Patterns and Mechanisms. Acta Naturae 7, 17–28.

Kranenburg, O., Poland, M., van Horck, F., Drechsel, D., Hall, A., Moolenaar, W., 1999. Activation of RhoA by Lysophosphatidic Acid and Gα12/13 Subunits in Neuronal Cells: Induction of Neurite Retraction. Mol Biol Cell 10, 1851–1857.

Kumar, N., Afeyan, R., Kim, H.-D., Lauffenburger, D., 2008. Multipathway Model Enables Prediction of Kinase Inhibitor Cross-Talk Effects on Migration of Her2-Overexpressing Mammary Epithelial Cells. Mol Pharmacol 73, 1668–1678.

Kurella, V., Richard, J., Parke, C., LeCour, L., Bellamy, H., Worthylake, D., 2009. Crystal Structure of the GTPase-activating Protein-related Domain from IQGAP1. J Biol Chem 284, 14857–14865.

Kuroda, S., Fukata, M., Kobayashi, K., Nakafuku, M., Nomura, N., Iwamatsu, A., Kaibuchi, K., 1996. Identification of IQGAP as a Putative Target for the Small GTPases, Cdc42 and Rac1. J Biol Chem 271, 23363–23367.

Lagoutte, E., Villeneuve, C., Lafanechère, L., Wells, C., Jones, G., Chavrier, P., Rossé, C., 2016. LIMK Regulates Tumor-Cell Invasion and Matrix Degradation Through Tyrosine Phosphorylation of MT1-MMP. Sci Reports 6, 24925.

Lamouille, S., Xu, J., Derynck, R., 2014. Molecular mechanisms of epithelial–mesenchymal transition. Nature Reviews Molecular Cell Biology 15, 178–196.

Lauffenburger, D., Horwitz, A., 1996. Cell Migration: A Physically Integrated Molecular Process. Cell 84, 359–369.

Lee, S., Ramos, S., Ko, A., Masiello, D., Swanson, K., Lu, M., Balk, S., 2002. AR and ER interaction with a p21-activated kinase (PAK6). Mol Endocrinol Baltim Md 16, 85–99.

Lehmann, B., Bauer, J., Chen, X., Sanders, M., Chakravarthy, B., Shyr, Y., Pietenpol, J., 2011a. Identification of human triple-negative breast cancer subtypes and preclinical models for selection of targeted therapies. Journal of Clinical Investigation 121, 2750–2767.

Lehmann, B., Bauer, J., Chen, X., Sanders, M., Chakravarthy, B., Shyr, Y., Pietenpol, J., 2011b. Identification of human triple-negative breast cancer subtypes and preclinical models for selection of targeted therapies. J Clin Invest 121, 2750–2767.

Leong, H., Robertson, A., Stoletov, K., Leith, S., Chin, C., Chien, A., Hague, N., Ablack, A., Carmine-Simmen, K., McPherson, V., Postenka, C., Turley, E., Courtneidge, S., Chambers, A., Lewis, J., 2014. Invadopodia Are Required for Cancer Cell Extravasation and Are a Therapeutic Target for Metastasis. Cell Reports 8, 1558–1570.

Li, A., Dawson, J.C., Forero-Vargas, M., Spence, H.J., Yu, X., König, I., Anderson, K., Machesky, L.M., 2010. The actin-bundling protein fascin stabilizes actin in invadopodia and potentiates protrusive invasion. Current biology : CB 20, 339–45.

Li, L., Lu, Y., Stemmer, P., Chen, F., 2015. Filamin A phosphorylation by Akt promotes cell migration in response to arsenic. Oncotarget 6, 12009–12019.

Li, Z., Kim, S., Higgins, J., Brenner, M., Sacks, D., 1999. IQGAP1 and Calmodulin Modulate E-cadherin Function. J Biol Chem 274, 37885–37892.

Li, Z., Zhang, H., Lundin, L., Thullberg, M., Liu, Y., Wang, Y., Claesson-Welsh, L., Strömblad, S., 2010. p21-activated Kinase 4 Phosphorylation of Integrin β5 Ser-759 and Ser-762 Regulates Cell Migration. J Biol Chem 285, 23699–23710.

Liedtke, C., Mazouni, C., Hess, K., André, F., Tordai, A., Mejia, J., Symmans, F., Gonzalez-Angulo, A., Hennessy, B., Green, M., Cristofanilli, M., Hortobagyi, G., Pusztai, L., 2008. Response to Neoadjuvant Therapy and Long-Term Survival in Patients With Triple-Negative Breast Cancer. J Clin Oncol 26, 1275–1281.

Littlewood-Evans, Bilbe, Bowler, Farley, Wlodarski, Kokubo, Inaoka, Sloane, Evans, Gallagher, 1997. The osteoclast-associated protease cathepsin K is expressed in human breast carcinoma. Cancer Res 57, 5386–90.

Liu, S., Goldstein, R., Scepansky, E., Rosenblatt, M., 2009. Inhibition of Rho-Associated Kinase Signaling Prevents Breast Cancer Metastasis to Human Bone. Cancer Res 69, 8742–8751.

Lock, F., Ryan, K., Poulter, N., Parsons, M., Hotchin, N., 2012. Differential Regulation of Adhesion Complex Turnover by ROCK1 and ROCK2. Plos One 7, e31423.

Logue, J., Whiting, J., Tunquist, B., Langeberg, L., Scott, J., 2011. Anchored Protein Kinase A Recruitment of Active Rac GTPase. J Biological Chem 286, 22113–22121.

Lohmer, L., Kelley, L., Hagedorn, E., Sherwood, D., 2014. Invadopodia and basement membrane invasion in vivo. Cell Adhesion Migr 8, 246–55.

Lorusso, G., Rüegg, C., 2012. New insights into the mechanisms of organ-specific breast cancer metastasis. Semin Cancer Biol 22, 226–233.

Loy, Sim, Yong, 2003. Filamin-A fragment localizes to the nucleus to regulate androgen receptor and coactivator functions. Proc National Acad Sci 100, 4562–4567.

Lucas, Salimath, Slomiany, Rosenzweig, 2010. Regulation of invasive behavior by vascular endothelial growth factor is HEF1-dependent. Oncogene 29, 4449–4459.

Lämmermann, T., Sixt, M., 2009. Mechanical modes of “amoeboid” cell migration. Curr Opin Cell Biol 21, 636–644.

Ma, L., Rohatgi, R., Kirschner, M., 1998. The Arp2/3 complex mediates actin polymerization induced by the small GTP-binding protein Cdc42. Proc National Acad Sci 95, 15362–15367.

MacPherson, M., Fagerholm, S., 2010. Filamin and filamin-binding proteins in integrin-regulation and adhesion. Focus on: “FilaminA is required for vimentin-mediated cell adhesion and spreading”. Am J Physiology - Cell Physiology 298, C206–C208.

Mader, C., Oser, M., Magalhaes, M., Bravo-Cordero, J., Condeelis, J., Koleske, A., Gil-Henn, H., 2011. An EGFR-Src-Arg-cortactin pathway mediates functional maturation of invadopodia and breast cancer cell invasion. Cancer research 71, 1730–41.

Mammoto, A., Huang, S., Ingber, D., 2007. Filamin links cell shape and cytoskeletal structure to Rho regulation by controlling accumulation of p190RhoGAP in lipid rafts. J Cell Sci 120, 456–467.

Mandal, S., Johnson, K., Wheelock, M., 2008. TGF-β induces formation of F-actin cores and matrix degradation in human breast cancer cells via distinct signaling pathways. Exp Cell Res 314, 3478–3493.

Manser, E., Leung, T., Salihuddin, H., Zhao, Z., Lim, L., 1994. A brain serine/threonine protein kinase activated by Cdc42 and Rac1. Nature 367, 40–46.

Manser, E., Loo, T.-H., Koh, C.-G., Zhao, Z.-S., Chen, X.-Q., Tan, L., Tan, I., Leung, T., Lim, L., 1998. PAK Kinases Are Directly Coupled to the PIX Family of Nucleotide Exchange Factors. Mol Cell 1, 183–192.

Mataraza, J., Li, Z., Jeong, H.-W., Brown, M., Sacks, D., 2007. Multiple proteins mediate IQGAP1-stimulated cell migration. Cell Signal 19, 1857–1865.

Mataraza, J.M., Briggs, M.W., Li, Z., Entwistle, A., Ridley, A.J., Sacks, D.B., 2003. IQGAP1 promotes cell motility and invasion. J. Biol. Chem. 278, 41237–45.

Matsunaga, H., Kubota, K., Inoue, T., Isono, F., Ando, O., 2014. IQGAP1 selectively interacts with K-Ras but not with H-Ras and modulates K-Ras function. Biochem Bioph Res Co 444, 360–364.

Mattila, P., Lappalainen, P., 2008. Filopodia: molecular architecture and cellular functions. Nat Rev Mol Cell Bio 9, 446–454.

Monteiro, P., Rossé, C., Castro-Castro, A., Irondelle, M., Lagoutte, E., Paul-Gilloteaux, P., Desnos, C., Formstecher, E., Darchen, F., Perrais, D., Gautreau, A., Hertzog, M., Chavrier, P., 2013. Endosomal WASH and exocyst complexes control exocytosis of MT1-MMP at invadopodia. The Journal of Cell Biology 203, 1063–1079.

Monteleon, C., McNeal, A., Duperret, E., Oh, S., Schapira, E., Ridky, T., 2015. IQGAP1 and IQGAP3 Serve Individually Essential Roles in Normal Epidermal Homeostasis and Tumor Progression. J Invest Dermatol 135, 2258–2265.

Moshfegh, Y., Bravo-Cordero, J., Miskolci, V., Condeelis, J., Hodgson, L., 2015. A Trio–Rac1–Pak1 signalling axis drives invadopodia disassembly. Nat Cell Biol 16, 571–583.

Mullins, D., Heuser, J., Pollard, T., 1998. The interaction of Arp2/3 complex with actin: Nucleation, high affinity pointed end capping, and formation of branching networks of filaments. Proc National Acad Sci 95, 6181–6186.

Murphy, D., Courtneidge, S., 2011. The “ins” and “outs” of podosomes and invadopodia: characteristics, formation and function. Nat Rev Mol Cell Bio 12, 413–426.

Murrell, M., Oakes, P., Lenz, M., Gardel, M., 2015. Forcing cells into shape: the mechanics of actomyosin contractility. Nat Rev Mol Cell Bio 16, 486–498.

Nakamura, F., Osborn, T., Hartemink, C., Hartwig, J., Stossel, T., 2007. Structural basis of filamin A functions. J Cell Biology 179, 1011–1025.

Nakamura, F., Stossel, T., Hartwig, J., 2011. The filamins: organizers of cell structure and function. Cell Adhesion Migr 5, 160–9.

Nayal, A., Webb, D., Brown, C., Schaefer, E., Vicente-Manzanares, M., Horwitz, A., 2006. Paxillin phosphorylation at Ser273 localizes a GIT1–PIX–PAK complex and regulates adhesion and protrusion dynamics. J Cell Biology 173, 587–589.

Nicholas, N., Pipili, A., Lesjak, M., Ameer-Beg, S., Geh, J., Healy, C., Ross, A., Parsons, M., Nestle, F., Lacy, K., Wells, C., 2016. PAK4 suppresses PDZ-RhoGEF activity to drive invadopodia maturation in melanoma cells. Oncotarget 7, 70881–70897.

Nielsen, T., Hsu, F., Jensen, K., Cheang, M., Karaca, G., Hu, Z., Hernandez-Boussard, T., Livasy, C., Cowan, D., Dressler, L., Akslen, L., Ragaz, J., Gown, A., Gilks, B., van de Rijn, M., Perou, C., 2004. Immunohistochemical and Clinical Characterization of the Basal-Like Subtype of Invasive Breast Carcinoma. Clin Cancer Res 10, 5367–5374.

Nobes, C., Hall, A., 1995. Rho, Rac, and Cdc42 GTPases regulate the assembly of multimolecular focal complexes associated with actin stress fibers, lamellipodia, and filopodia. Cell 81, 53–62.

Nojima, H., Adachi, M., Matsui, T., Okawa, K., Tsukita, S., Tsukita, S., 2008. IQGAP3 regulates cell proliferation through the Ras/ERK signalling cascade. Nat Cell Biol 10, 971–978.

Nouri, K., Timson, D., Ahmadian, M., 2017. New model for the interaction of IQGAP1 with CDC42 and RAC1. Small Gtpases 0.

Ohashi, K., Nagata, K., Maekawa, M., Ishizaki, T., Narumiya, S., Mizuno, K., 2000. Rho-associated Kinase ROCK Activates LIM-kinase 1 by Phosphorylation at Threonine 508 within the Activation Loop. J Biol Chem 275, 3577–3582.

Ohta, Y., Hartwig, J., Stossel, T., 2006. FilGAP, a Rho- and ROCK-regulated GAP for Rac binds filamin A to control actin remodelling. Nat Cell Biol 8, 803–814.

Ohta, Y., Suzuki, N., Nakamura, S., Hartwig, J.H., Stossel, T.P., 1999. The small GTPase RalA targets filamin to induce filopodia. Proc. Natl. Acad. Sci. U.S.A. 96, 2122–8.

Olson, M., Sahai, E., 2009. The actin cytoskeleton in cancer cell motility. Clin Exp Metastasis 26, 273–287.

Ong, C., Gierke, S., Pitt, C., Sagolla, M., Cheng, C., Zhou, W., Jubb, A., Strickland, L., Schmidt, M., Duron, S., Campbell, D., Zheng, W., Dehdashti, S., Shen, M., Yang, N., Behnke, M., Huang, W., McKew, J., Chernoff, J., Forrest, W., Haverty, P., Chin, S.-F., Rakha, E., Green, A., Ellis, I., Caldas, C., O'Brien, T., Friedman, L., Koeppen, H., Rudolph, J., Hoeflich, K., 2015. Small molecule inhibition of group I p21-activated kinases in breast cancer induces apoptosis and potentiates the activity of microtubule stabilizing agents. Breast Cancer Res 17, 1–12.

Orgaz, J., Pandya, P., Dalmeida, R., Karagiannis, P., Sanchez-Laorden, B., Viros, A., Albrengues, J., Nestle, F., Ridley, A., Gaggioli, C., Marais, R., Karagiannis, S., Sanz-Moreno, V., 2014. Diverse matrix metalloproteinase functions regulate cancer amoeboid migration. Nat Commun 5, 4255.

Oser, M., Yamaguchi, H., Mader, C., Bravo-Cordero, J.J., Arias, M., Chen, X., DesMarais, V., van Rheenen, J., Koleske, A., Condeelis, J., 2009. Cortactin regulates cofilin and N-WASp activities to control the stages of invadopodium assembly and maturation. J Cell Biology 186, 571–587.

Palmer, T., Ashby, W., Lewis, J., Zijlstra, A., 2011. Targeting tumor cell motility to prevent metastasis. Adv Drug Deliver Rev 63, 568–581.

Parri, M., Chiarugi, P., 2010. Rac and Rho GTPases in cancer cell motility control. Cell Commun Signal 8, 1–14.

Parrini, M., 2012. Untangling the complexity of PAK1 dynamics. Cell Logist 2, 78–83.

Pathmanathan, S., Elliott, S., McSwiggen, S., Greer, B., Harriott, P., Irvine, B., Timson, D., 2008. IQ motif selectivity in human IQGAP1: binding of myosin essential light chain and S100B. Mol Cell Biochem 318, 43–51.

Pathmanathan, S., Hamilton, E., Atcheson, E., Timson, D., 2011. The interaction of IQGAPs with calmodulin-like proteins. Biochem Soc T 39, 694–699.

Patsialou, A., Bravo-Cordero, J., Wang, Y., Entenberg, D., Liu, H., Clarke, M., Condeelis, J., 2013. Intravital multiphoton imaging reveals multicellular streaming as a crucial component of in vivo cell migration in human breast tumors. Intravital 2, e25294.

Petrie, R., Yamada, K., 2012. At the leading edge of three-dimensional cell migration. J Cell Sci 125, 5917–5926.

Poincloux, R., Collin, O., Lizárraga, F., Romao, M., Debray, M., Piel, M., Chavrier, P., 2011. Contractility of the cell rear drives invasion of breast tumor cells in 3D Matrigel. Proceedings of the National Academy of Sciences 108, 1943–1948.

Pollard, 1986. Rate constants for the reactions of ATP- and ADP-actin with the ends of actin filaments. J Cell Biology 103, 2747–2754.

Puto, L., Pestonjamasp, K., King, C., Bokoch, G., 2003. p21-activated Kinase 1 (PAK1) Interacts with the Grb2 Adapter Protein to Couple to Growth Factor Signaling. J Biol Chem 278, 9388–9393.

Qian, E.-N., Han, S.-Y., Ding, S.-Z., Lv, X., 2016. Expression and diagnostic value of CCT3 and IQGAP3 in hepatocellular carcinoma. Cancer Cell Int 16, 55.

Rajadurai, C., Havrylov, S., Zaoui, K., Vaillancourt, R., Stuible, M., Naujokas, M., Zuo, D., Tremblay, M., Park, M., 2012. Met receptor tyrosine kinase signals through a cortactin–Gab1 scaffold complex, to mediate invadopodia. J Cell Sci 125, 2940–2953.

Rane, C., Minden, A., 2014. P21 activated kinases: structure, regulation, and functions. Small Gtpases 5, e28003.

Razinia, Z., Mäkelä, T., Ylänne, J., Calderwood, D., 2012. Filamins in Mechanosensing and Signaling. Annu Rev Biophys 41, 227–246.

Reis- Filho, Tutt, 2008. Triple negative tumours: a critical review. Histopathology 52, 108–118.

Ren, J.-G., Li, Z., Crimmins, D., Sacks, D., 2005. Self-association of IQGAP1 CHARACTERIZATION AND FUNCTIONAL SEQUELAE. J Biol Chem 280, 34548–34557.

Ren, J.-G., Li, Z., Sacks, D., 2007. IQGAP1 modulates activation of B-Raf. Proc National Acad Sci 104, 10465–10469.

Ridley, 2001. Rho GTPases and cell migration. J Cell Sci 114, 2713–22.

Ridley, A., 1999. Stress fibres take shape. Nat Cell Biol 1, E64–E66.

Ridley, A., Paterson, H., Johnston, C., Diekmann, D., Hall, A., 1992. The small GTP-binding protein rac regulates growth factor-induced membrane ruffling. Cell 70, 401–410.

Ridley, A.J., Hall, 1992. The small GTP-binding protein rho regulates the assembly of focal adhesions and actin stress fibers in response to growth factors. Trends Cell Biol 2, 324.

Ridley, A.J., Schwartz, M.A., Burridge, K., Firtel, R.A., Ginsberg, M.H., Borisy, G., Parsons, J.T., Horwitz, A.R., 2003. Cell migration: integrating signals from front to back. Science 302, 1704–9.

Rojas, K., Stuckey, A., 2016. Breast Cancer Epidemiology and Risk Factors. Clin Obstet Gynecol 59, 651.

Rossé, C., Lodillinsky, C., Fuhrmann, L., Nourieh, M., Monteiro, P., Irondelle, M., Lagoutte, E., Vacher, S., Waharte, F., Paul-Gilloteaux, P., Romao, M., Sengmanivong, L., Linch, M., van Lint, J., Raposo, G., Vincent-Salomon, A., Bièche, I., Parker, P., Chavrier, P., 2014. Control of MT1-MMP transport by atypical PKC during breast-cancer progression. Proc National Acad Sci 111, E1872–E1879.

Rottner, Hall, Small, J.V., 1999. Interplay between Rac and Rho in the control of substrate contact dynamics. Curr Biol 9, 640–S1.

Roy, M., Li, Z., Sacks, D., 2004. IQGAP1 Binds ERK2 and Modulates Its Activity. J Biol Chem 279, 17329–17337.

Roy, M., Li, Z., Sacks, D., 2005. IQGAP1 Is a Scaffold for Mitogen-Activated Protein Kinase Signaling. Mol Cell Biol 25, 7940–7952.

Sahai, E., Garcia-Medina, R., Pouysségur, J., Vial, E., 2007. Smurf1 regulates tumor cell plasticity and motility through degradation of RhoA leading to localized inhibition of contractility. J Cell Biology 176, 35–42.

Sahai, E., Marshall, C., 2003. Differing modes of tumour cell invasion have distinct requirements for Rho/ROCK signalling and extracellular proteolysis. Nat Cell Biol 5, 711–719.

Sakurai-Yageta, M., Recchi, C., Dez, G., Sibarita, J.-B., Daviet, L., Camonis, J., D'Souza-Schorey, C., Chavrier, P., 2008. The interaction of IQGAP1 with the exocyst complex is required for tumor cell invasion downstream of Cdc42 and RhoA. The Journal of Cell Biology 181, 985–998.

Sanchez-Laorden, B., Viros, A., Marais, R., 2013. Mind the IQGAP. Cancer Cell 23, 715–717.

Sanders, L., Matsumura, F., Bokoch, G., de Lanerolle, P., 1999. Inhibition of Myosin Light Chain Kinase by p21-Activated Kinase. Science 283, 2083–2085.

Sanz-Moreno, V., Gadea, G., Ahn, J., Paterson, H., Marra, P., Pinner, S., Sahai, E., Marshall, C., 2007. Rac Activation and Inactivation Control Plasticity of Tumor Cell Movement. Cell 135, 510–23.

Savoy, R.M., Ghosh, P.M., 2013. The dual role of filamin A in cancer: can't live with (too much of) it, can't live without it. Endocr. Relat. Cancer 20, R341–56.

Sbroggiò, M., Carnevale, D., Bertero, A., Cifelli, G., Blasio, E., Mascio, G., Hirsch, E., Bahou, W., Turco, E., Silengo, L., Brancaccio, M., Lembo, G., Tarone, G., 2011. IQGAP1 regulates ERK1/2 and AKT signalling in the heart and sustains functional remodelling upon pressure overload. Cardiovasc Res 91, 456–464.

Schmidt, V., Chiariello, C., Capilla, E., Miller, F., Bahou, W., 2008. Development of Hepatocellular Carcinoma in Iqgap2-Deficient Mice Is IQGAP1 Dependent. Mol Cell Biol 28, 1489–1502.

Schmidt, V., Scudder, L., Devoe, C., Bernards, A., Cupit, L., Bahou, W., 2003. IQGAP2 functions as a GTP-dependent effector protein in thrombin-induced platelet cytoskeletal reorganization. Blood 101, 3021–3028.

Schoumacher, M., Goldman, R., Louvard, D., Vignjevic, D., 2010. Actin, microtubules, and vimentin intermediate filaments cooperate for elongation of invadopodia. J Cell Biology 189, 541–556.

Schrantz, N., da Correia, J., Fowler, B., Ge, Q., Sun, Z., Bokoch, G., 2004. Mechanism of p21-activated Kinase 6-mediated Inhibition of Androgen Receptor Signaling. J Biol Chem 279, 1922–1931.

Seals, D., Azucena, E., Pass, I., Tesfay, L., Gordon, R., Woodrow, M., Resau, J., Courtneidge, S., 2005. The adaptor protein Tks5/Fish is required for podosome formation and function, and for the protease-driven invasion of cancer cells. Cancer Cell 7, 155–165.

Sells, M., Knaus, U., Bagrodia, S., Ambrose, D., Bokoch, G., Chernoff, J., 1997. Human p21-activated kinase (Pak1) regulates actin organization in mammalian cells. Curr Biol 7, 202–210.

Shen, X., Jia, Z., D'Alonzo, D., Wang, X., Bruder, E., Emch, F., Geyter, C., Zhang, H., 2016. HECTD1 controls the protein level of IQGAP1 to regulate the dynamics of adhesive structures. Cell Commun Signal 15, 2.

Shifrin, Y., Arora, P., Ohta, Y., Calderwood, D., McCulloch, C., 2009. The Role of FilGAP-Filamin A Interactions in Mechanoprotection. Mol Biol Cell 20, 1269–1279.

Smith, J., Hedman, A., Sacks, D., 2015. IQGAPs choreograph cellular signaling from the membrane to the nucleus. Trends Cell Biol 25, 171–184.

Smith, S., Jaffer, Z., Chernoff, J., Ridley, A., 2008. PAK1-mediated activation of ERK1/2 regulates lamellipodial dynamics. J Cell Sci 121, 3729–3736.

Soule, Maloney, Wolman, Peterson, Brenz, McGrath, Russo, Pauley, Jones, Brooks, 1990. Isolation and characterization of a spontaneously immortalized human breast epithelial cell line, MCF-10. Cancer Res 50, 6075–86.

Spuul, P., Ciufici, P., Veillat, V., Leclercq, A., Daubon, T., Kramer, I., Génot, E., 2014. Importance of RhoGTPases in formation, characteristics, and functions of invadosomes. Small Gtpases 5, e28195.

Stagg, J., Allard, B., 2013. Immunotherapeutic approaches in triple-negative breast cancer: latest research and clinical prospects. Ther Adv Medical Oncol 5, 169–181.

Stossel, T., Condeelis, J., Cooley, L., Hartwig, J., Noegel, A., Schleicher, M., Shapiro, S., 2001. Filamins as integrators of cell mechanics and signalling. Nat Rev Mol Cell Bio 2, 138–145.

Sun, C., Forster, C., Nakamura, F., Glogauer, M., 2013. Filamin-A Regulates Neutrophil Uropod Retraction through RhoA during Chemotaxis. Plos One 8, e79009.

Swart-Mataraza, J., Li, Z., Sacks, D., 2002. IQGAP1 Is a Component of Cdc42 Signaling to the Cytoskeleton. J Biol Chem 277, 24753–24763.

Söderberg, O., Gullberg, M., Jarvius, M., Ridderstråle, K., Leuchowius, K.-J., Jarvius, J., Wester, K., Hydbring, P., Bahram, F., Larsson, L.-G., Landegren, U., 2006. Direct observation of individual endogenous protein complexes in situ by proximity ligation. Nat Methods 3, 995–1000.

Takkunen, M., Hukkanen, M., Liljeström, M., Grenman, R., Virtanen, I., 2010. Podosome- like structures of non- invasive carcinoma cells are replaced in epithelial- mesenchymal transition by actin comet- embedded invadopodia. J Cell Mol Med 14, 1569–1593.

Tate, C., Rhodes, L., Segar, C., Driver, J., Pounder, N., Burow, M., Collins-Burow, B., 2012. Targeting triple-negative breast cancer cells with the histone deacetylase inhibitor panobinostat. Breast Cancer Res 14, 1–15.

Tehrani, S., Tomasevic, N., Weed, S., Sakowicz, R., Cooper, J., 2007. Src phosphorylation of cortactin enhances actin assembly. Proceedings of the National Academy of Sciences of the United States of America 104, 11933–8.

Thiery, J., 2002. Epithelial–mesenchymal transitions in tumour progression. Nat Rev Cancer 2, 442–454.

Thiery, J., Acloque, H., Huang, R., Nieto, A., 2009. Epithelial-Mesenchymal Transitions in Development and Disease. Cell 139, 871–890.

Thompson, E., Newgreen, D., Tarin, D., 2005. Carcinoma Invasion and Metastasis: A Role for Epithelial-Mesenchymal Transition? Cancer Res 65, 5991–5995.

Thompson, E., Paik, S., Brünner, N., Sommers, C., Zugmaier, G., Clarke, R., Shima, T., Torri, J., Donahue, S., Lippman, M., Martin, G., Dickson, R., 1992. Association of increased basement membrane invasiveness with absence of estrogen receptor and expression of vimentin in human breast cancer cell lines. Journal of Cellular Physiology 150, 534–544.

Tian, H.-M., Liu, X.-H., Han, W., Zhao, L.-L.,, Yuan, C.-J., 2013. Differential expression of filamin A and its clinical significance in breast cancer. Oncol Lett 6, 681–686.

Tolias, K., Hartwig, J., Ishihara, H., Shibasaki, Y., Cantley, L., Carpenter, C., 2000. Type Iα phosphatidylinositol-4-phosphate 5-kinase mediates Rac-dependent actin assembly. Curr Biol 10, 153–156.

Tominaga, T., Sahai, E., Chardin, P., McCormick, F., Courtneidge, S., Alberts, A., 2000. Diaphanous-Related Formins Bridge Rho GTPase and Src Tyrosine Kinase Signaling. Mol Cell 5, 13–25.

Vadlamudi, R., Li, F., Adam, L., Nguyen, D., Ohta, Y., Stossel, T., Kumar, R., 2002. Filamin is essential in actin cytoskeletal assembly mediated by p21-activated kinase 1. Nat Cell Biol 4, 681–690.

Valastyan, S., Weinberg, R., 2011. Tumor Metastasis: Molecular Insights and Evolving Paradigms. Cell 147, 275–292.

Van der Flier, A., Sonnenberg, A., 2001. Structural and functional aspects of filamins. Biochimica Et Biophysica Acta Bba - Mol Cell Res 1538, 99–117.

Vega, F., Fruhwirth, G., Ng, T., Ridley, A., 2011. RhoA and RhoC have distinct roles in migration and invasion by acting through different targets. J Cell Biology 193, 655–665.

Vega, F., Ridley, A., 2008. Rho GTPases in cancer cell biology. Febs Lett 582, 2093–2101.

Velkova, A., Carvalho, M., Johnson, J., Tavtigian, S., Monteiro, A., 2010. Identification of Filamin A as a BRCA1-interacting protein required for efficient DNA repair. Cell Cycle Georget Tex 9, 1421–33.

Vicente-Manzanares, M., Koach, M., Whitmore, L., Lamers, M., Horwitz, A., 2008. Segregation and activation of myosin IIB creates a rear in migrating cells. J Cell Biology 183, 543–554.

Vicente-Manzanares, M., Ma, X., Adelstein, R., Horwitz, A., 2009. Non-muscle myosin II takes centre stage in cell adhesion and migration. Nat Rev Mol Cell Bio 10, 778–790.

Wang, Ash, Singer, 1975. Filamin, a new high-molecular-weight protein found in smooth muscle and non-muscle cells. Proc National Acad Sci 72, 4483–4486.

Wang, H., Huo, R., Xu, M., Lu, L., Xu, Z., Li, J., Zhou, Z., Sha, J., 2009. Cloning and Characterization of a Novel Transcript Variant of IQGAP2 in Human Testis. Dna Sequence 15, 319–325.

Wang, R., Mazumdar, A., Vadlamudi, R., Kumar, R., 2002. P21- activated kinase- 1 phosphorylates and transactivates estrogen receptor- α and promotes hyperplasia in mammary epithelium. Embo J 21, 5437–5447.

Wang, R.-A., Zhang, Balasenthil, Medina, Kumar, 2005. PAK1 hyperactivation is sufficient for mammary gland tumor formation. Oncogene 25, 2931–2936.

Wang, S., Watanabe, T., Noritake, J., Fukata, M., Yoshimura, T., Itoh, N., Harada, T., Nakagawa, M., Matsuura, Y., Arimura, N., Kaibuchi, K., 2007. IQGAP3, a novel effector of Rac1 and Cdc42, regulates neurite outgrowth. J Cell Sci 120, 567–577.

Watanabe, T., Wang, S., Noritake, J., Sato, K., Fukata, M., Takefuji, M., Nakagawa, M., Izumi, N., Akiyama, T., Kaibuchi, K., 2004. Interaction with IQGAP1 Links APC to Rac1, Cdc42, and Actin Filaments during Cell Polarization and Migration. Dev Cell 7, 871–883.

Weissbach, L., Bernards, A., Herion, D., 1998. Binding of Myosin Essential Light Chain to the Cytoskeleton-Associated Protein IQGAP1. Biochem Bioph Res Co 251, 269–276.

Wen, X., Li, X., Liao, B., Liu, Y., Wu, J., Yuan, X., Ouyang, B., Sun, Q., Gao, X., 2009. Knockdown of p21-activated Kinase 6 Inhibits Prostate Cancer Growth and Enhances Chemosensitivity to Docetaxel. Urology 73, 1407–1411.

Wennerberg, K., Ellerbroek, S., Liu, R.-Y., Karnoub, A., Burridge, K., Der, C., 2002. RhoG Signals in Parallel with Rac1 and Cdc42. J Biol Chem 277, 47810–47817.

Whale, Dart, Holt, Jones, Wells, 2012. PAK4 kinase activity and somatic mutation promote carcinoma cell motility and influence inhibitor sensitivity. Oncogene 32, 2114–2120.

White, C., Brown, M., Sacks, D., 2009. IQGAPs in cancer: A family of scaffold proteins underlying tumorigenesis. Febs Lett 583, 1817–1824.

Wolf, K., Wu, Y., Liu, Y., Geiger, J., Tam, E., Overall, C., Stack, S., Friedl, P., 2007. Multi-step pericellular proteolysis controls the transition from individual to collective cancer cell invasion. Nature Cell Biology 9, 893–904.

Wu, K., Zhang, X., Li, F., Xiao, D., Hou, Y., Zhu, S., Liu, D., Ye, X., Ye, M., Yang, J., Shao, L., Pan, H., Lu, N., Yu, Y., Liu, L., Li, J., Huang, L., Tang, H., Deng, Q., Zheng, Y., Peng, L., Liu, G., Gu, X., He, P., Gu, Y., Lin, W., He, H., Xie, G., Liang, H., An, N., Wang, H., Teixeira, M., Vieira, J., Liang, W., Zhao, X., Peng, Z., Mu, F., Zhang, X., Xu, X., Yang, H., Kristiansen, K., Wang, J., Zhong, N., Wang, J., Pan-Hammarström, Q., He, J., 2015. Frequent alterations in cytoskeleton remodelling genes in primary and metastatic lung adenocarcinomas. Nat Commun 6, 10131.

Wyckoff, J., Pinner, S., Gschmeissner, S., Condeelis, J., Sahai, E., 2006. ROCK- and Myosin-Dependent Matrix Deformation Enables Protease-Independent Tumor-Cell Invasion In Vivo. Curr Biol 16, 1515–1523.

Xu, J., Prosperi, J., Choudhury, N., Olopade, O., Goss, K., 2015. β-Catenin Is Required for the Tumorigenic Behavior of Triple-Negative Breast Cancer Cells. Plos One 10, e0117097.

Xu, W., Xu, B., Yao, Y., Yu, X., Cao, H., Zhang, J., Liu, J., Sheng, H., 2016. Overexpression and biological function of IQGAP3 in human pancreatic cancer. Am J Transl Res 8, 5421–5432.

Yamaguchi, H., Lorenz, M., Kempiak, S., Sarmiento, C., Coniglio, S., Symons, M., Segall, J., Eddy, R., Miki, H., Takenawa, T., Condeelis, J., 2005. Molecular mechanisms of invadopodium formation. J Cell Biology 168, 441–452.

Yamaguchi, H., Yoshida, S., Muroi, E., Yoshida, N., Kawamura, M., Kouchi, Z., Nakamura, Y., Sakai, R., Fukami, K., 2011. Phosphoinositide 3-kinase signaling pathway mediated by p110α regulates invadopodia formation. J Cell Biology 193, 1275–1288.

Yang, F., Li, X., Sharma, M., Zarnegar, M., Lim, B., Sun, Z., 2001. Androgen Receptor Specifically Interacts with a Novel p21-activated Kinase, PAK6. J Biol Chem 276, 15345–15353.

Yang, Y., Zhao, W., Xu, Q.-W., Wang, X.-S., Zhang, Y., Zhang, J., 2014. IQGAP3 Promotes EGFR-ERK Signaling and the Growth and Metastasis of Lung Cancer Cells. Plos One 9, e97578.

Ying, H., Biroc, S., Li, W., Alicke, B., Xuan, J.-A., Pagila, R., Ohashi, Y., Okada, T., Kamata, Y., Dinter, H., 2006. The Rho kinase inhibitor fasudil inhibits tumor progression in human and rat tumor models. Mol Cancer Ther 5, 2158–2164.

Yousef, E., Tahir, M., St-Pierre, Y., Gaboury, L., 2014. MMP-9 expression varies according to molecular subtypes of breast cancer. Bmc Cancer 14, 1–12.

Yu, O., Brown, J., 2015. G Protein–Coupled Receptor and RhoA-Stimulated Transcriptional Responses: Links to Inflammation, Differentiation, and Cell Proliferation. Mol Pharmacol 88, 171–180.

Yue, J., Huhn, S., Shen, Z., 2013. Complex roles of filamin-A mediated cytoskeleton network in cancer progression. Cell Biosci 3, 1–12.

Zaidel-Bar, R., Ballestrem, C., Kam, Z., Geiger, B., 2003. Early molecular events in the assembly of matrix adhesions at the leading edge of migrating cells. J Cell Sci 116, 4605–4613.

Zak, 1977. Metabolism of myofibrillar proteins in the normal and hypertrophic heart. Basic Res Cardiol 72, 235–240.

Zenke, F., King, C., Bohl, B., Bokoch, G., 1999. Identification of a Central Phosphorylation Site in p21-activated Kinase Regulating Autoinhibition and Kinase Activity. J Biol Chem 274, 32565–32573.

Zhang, M., Siedow, M., Saia, G., Chakravarti, A., 2010. Inhibition of p21- activated kinase 6 (PAK6) increases radiosensitivity of prostate cancer cells. Prostate 70, 807–816.

Zhao, Z., Manser, E., Loo, T.-H., Lim, L., 2000. Coupling of PAK-Interacting Exchange Factor PIX to GIT1 Promotes Focal Complex Disassembly. Mol Cell Biol 20, 6354–6363.

Zhong, Z., Yeow, W.-S., Zou, C., Wassell, R., Wang, C., Pestell, R., Quong, J., Quong, A., 2010. Cyclin D1/Cyclin-Dependent Kinase 4 Interacts with Filamin A and Affects the Migration and Invasion Potential of Breast Cancer Cells. Cancer Res 70, 2105–2114.